Examining the context of cytochrome P450 27C1-mediated retinoid desaturation in the skin

By

Sarah M. Glass

Dissertation

Submitted to the Faculty of the

Graduate School of Vanderbilt University

in partial fulfillment of the requirements

for the degree of

DOCTOR OF PHILOSOPHY

in

Biochemistry

December 18, 2021

Nashville, Tennessee

Approved:

Martin Egli, Ph.D., Chair

Manuel Ascano, Ph.D.

Ambra Pozzi, Ph.D.

Kevin Schey, Ph.D.

F. Peter Guengerich, Ph.D., Advisor

ACKNOWLEDGEMENTS

I would first like to thank my past and present advisors, Dr. Laura Furge and Dr. Fred Guengerich. I consider myself extremely lucky to have had my first experience with scientific research in Dr. Furge's lab. My interest in biochemistry and enzymology (of cytochrome P450s in particular) stem from my experiences in her lab. The skills and knowledge that I gained from my time there were fundamental to my development as a scientist and have helped me greatly in my thesis work. Dr. Guengerich has also been an excellent mentor to me. Time in his lab has helped me learn how to think critically about research and develop as an independent scientist. I am especially grateful for his continued support of my thesis project, even as components of my research have changed direction.

During my time in the Guengerich lab, I have worked alongside many great scientists who have provided both guidance and friendship. I am especially grateful for the company of Dr. Michael Reddish, Dr. Stella Child, Kevin McCarty, and Dr. Hannah Wapshott-Stehli. I also would like to thank Kathy Trisler who provided help and support throughout my time in the lab along with past and present research assistants, Thanh Phan, Clay Wilkey, Jesse Chapman, and Lucy Lui, for keeping the lab stocked with proteins and other supplies.

I also thank my dissertation committee members, Dr. Martin Egli, Dr. Manuel Ascano, Dr. Kevin Schey, and Dr. Ambra Pozzi, for their input and guidance with my project.

I am also grateful for Dr. Beth Bowman, Carolyn Berry, and Patty Mueller. Whether it be registering me for classes or just being there for me to talk to, they always provided the support I needed.

For my thesis project, I received help from scientists at Vanderbilt University and other institutions. In the Vanderbilt Mass Spectrometry Research Center, Dr. Wade Calcutt helped with

small molecule analysis and proteomics was performed by Dr. Kristie Rose. Dr. Manuel Chiusa and Dr. Corina Borza of Dr. Ambra Pozzi's lab in the Vanderbilt University Medical Center assisted me with tissue and primary cell culture work, and Dr. Ambra Pozzi helped perform tissue immunofluorescence. Plasmids for protein expression were provided by Dr. Richard Auchus from the University of Michigan, Dr. Nina Isoherranen from the University of Washington, and Dr. Marcin Golczak from Case Western Reserve University. Dr. Mrinal Sarkar and Dr. Johann Gudjonsson from the Skin Biology and Disease Resource-Based Center at the University of Michigan provided N/TERT-2G cells and Samantha Lisy of Dr. Manuel Ascano's lab at Vanderbilt University cultured these cells for my experiments. Dr. Jennifer Schafer of the Vanderbilt Cell Imaging Shared Resource Core assisted with microscopy and imaging of cells.

Lastly, I would also like to acknowledge funding from the National Institutes of Health (R01 GM118122, T32 ES007028, and F31 AR077386).

TABLE OF CONTENTS

LIST OF TABLES

LIST OF FIGURES

LIST OF ABBREVIATIONS

5-IAF	5-Iodoacetamidofluorescein
ABC	Ammonium bicarbonate
Acrylodan	Acrylodan-2-dimethylaminonapthalene
ADH	Alcohol dehydrogenase
AdR	NADPH-adrenodoxin reductase
Adx	Adrenodoxin
APCI	Atmospheric-pressure chemical ionization
atRA	All-*trans* retinoic acid
atRAL	All-*trans* retinal
atROL	All-*trans* retinol
b_5	Cytochrome b_5
BCA	Bicinchoninic acid
BHT	Butylated hydroxytoluene
BPE	Bovine pituitary extract
BSA	Bovine serum albumin
CHAPS	3-((3-Cholamidopropyl) dimethylammonio)-1-propanesulfonate
CID	Collision induced dissociation
CRABP	Cellular retinoic acid binding protein
CRBP	Cellular retinol binding protein
CYP	Cytochrome P450
DAPI	4′,6-Diamidino-2-phenylindole
DDA	Data-dependent analysis

ddRA	3,4-Dehydroretinoic acid
ddRAL	3,4-Dehydroretinal
ddROL	3,4-Dehydroretinol
DEAE	Diethylaminoethyl
DIA	Data-independent analysis
DLPC	1,2-Dilauroyl-*sn*-glycero-3-phosphocholine
DMSO	Dimethylsulfoxide
DTT	Dithiothreitol
EDTA	Ethylenediaminetetraacetic acid
EDC	1-Ethyl-3-(3-dimethylaminopropyl)carbodiimide hydrochloride
EGF	Epidermal growth factor
ESI	Electrospray ionization
FABP	Fatty acid binding protein
FASP	Filter aided sample preparation
FDR	False discovery rate
HEPES	4-(2-Hydroxyethyl)-1-piperazineethanesulfonic acid
HLM	Human liver microsomes
HPLC	High-performance liquid chromatography
HRMS	High resolution mass spectrometry
IAA	Iodoacetamide
IAEDANS	5-((((2-Iodoacetyl)amino)ethyl)amino)naphthalene-1-sulfonic acid
iLBP	Intracellular lipid-binding protein
IPTG	Isopropylthio-β-galactoside

IR	Infrared
IPTG	Isopropyl β-D-1-thiogalactopyranoside
KO	Knock-out
LB	Luria-Bertani
LRAT	Lecithin retinol acyltransferase
MES	2-(N-morpholino)ethanesulfonic acid
MMTS	Methyl methanethiosulfonate
MOPS	3-(N-morpholino)propanesulfonic acid
MRM	Multiple reaction monitoring
MS	Mass spectrometry
MST	Microscale thermophoresis
MWCO	Molecular weight cut-off
NADPH	β-Nicotinamide adenine dinucleotide 2′-phosphate
NHEK	Normal human epidermal keratinocytes
Ni-NTA	Nickel-nitrilotriacetic Acid
OD	Optical density
P450	Cytochrome P450
PBS	Phosphate-buffered saline
PCR	Polymerase chain reaction
PMSF	Phenylmethylsufonyl fluoride
POR	NADPH-cytochrome P450 reductase
PRM	Parallel reaction monitoring
QconCAT	Quantification concatemer

RALDH	Retinaldehyde dehydrogenase
RAR	Retinoic acid receptor
RARE	RAR elements
RBP	Retinol binding protein
RDH	Retinol dehydrogenase
RE	Retinyl ester
REH	Retinyl ester hydrolase
RXR	Retinoid-X receptor
RXRE	Retinoid X response elements
SCC	Squamous cell carcinoma cell line
SDS	Sodium dodecyl sulfate
SDS-PAGE	Sodium dodecyl sulfate polyacrylamide gel electrophoresis
SEC	Size exclusion chromatography
SPR	Surface plasmon resonance
Sulfo-NHS	*N*-hydroxysulfosuccinimide
TEAB	Triethylammonium bicarbonate
TB	Terrific broth
TBME	*Tert*-butyl methyl ether
TCEP	Tris(2-carboxyethyl)phosphine
UPLC	Ultra-performance liquid chromatography
WT	Wild-type

Chapter 1. Introduction

1.1 Overview of retinoids

The term "retinoids" refers to natural forms of vitamin A as well as synthetic analogues. The endogenous retinoids, retinol (vitamin A alcohol), retinaldehyde (vitamin A aldehyde), and retinoic acid (vitamin A acid), are similar in structure, containing a β-ionone ring, an unsaturated isoprenoid side chain, and a variable polar/acidic terminal group. The isoprenoid side chain can exist in a variety of geometric conformations, the predominant being all-*trans*, with smaller amounts of 9-*cis*, 11-*cis*, and 13-*cis*. Fatty acids can also be attached to retinol, forming retinyl esters. β-carotene (provitamin A) can be converted to retinal or retinoic acid in the body. The major vitamin A vitamers are shown in Figure 1.

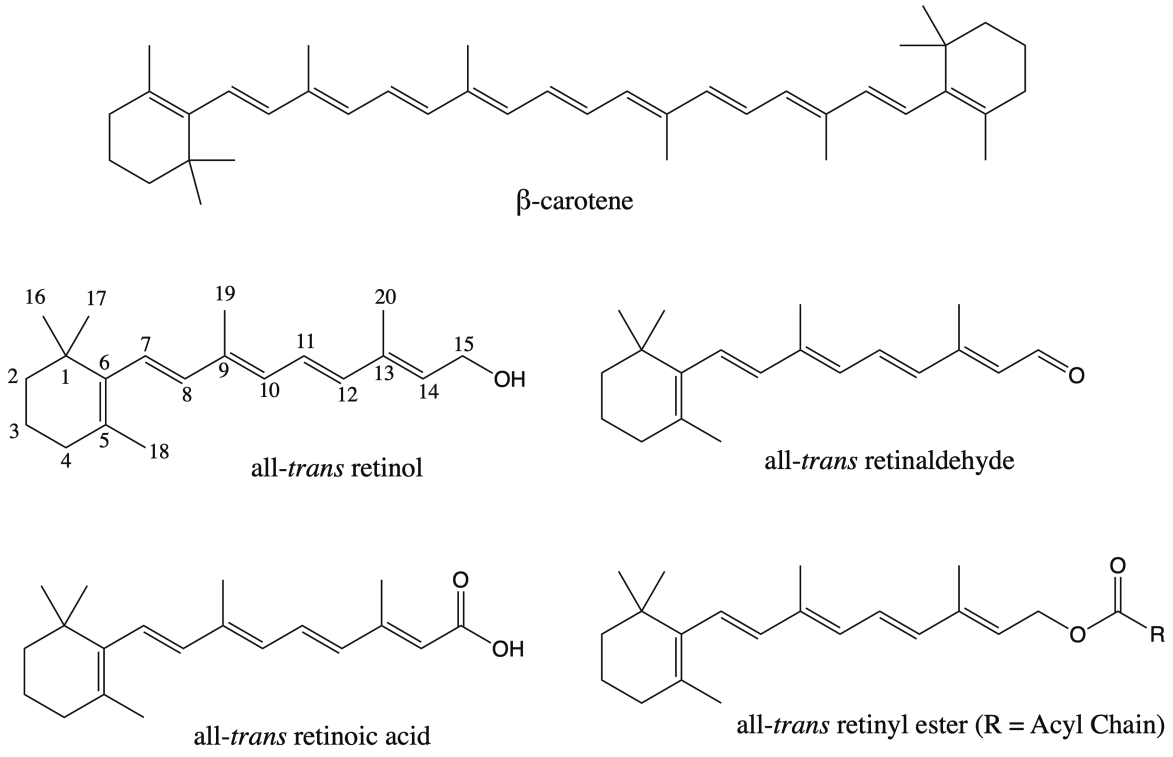

Figure 1. Structure of endogenous vitamin A related molecules. IUPAC numbering of retinoids is shown on the all-*trans* retinol structure (1).

Retinoid synthesis does not occur *de novo* in humans or any animal species. Retinoids are generated from dietary intake of carotenoid- or vitamin A-containing plants, animal products, and fortified foods. Mechanisms of absorption have been thoroughly reviewed (2) and are not the focus of this work. To briefly summarize the predominant mechanism, dietary vitamin A is esterified in the intestine (3) and transported to the liver as part of chylomicrons/chylomicron remnants (4). Retinyl esters can be hydrolyzed to retinol which binds to retinol binding protein (RBP) and is then secreted into the plasma (concentration 2 μM) (5,6). Retinyl esters and retinol are also primarily stored in the liver (50-80% of total body concentration) (7). Retinol-RBP associates with transthyretin in the plasma (8) and is transported to a variety of target cells.

Retinoids are important to a variety of aspects of human physiology (reviewed in (9)) including reproduction and development, immunity, vision, and maintenance of epithelial surfaces. Outside of the role of retinal in vision, retinoic acid is the predominant biologically active form of retinoids. Retinoic acid mediates retinoid function through binding to retinoic acid receptors (RARs) or retinoid-X receptors (RXRs). There are three isotypes of each of these: α, β, and ɣ. These nuclear receptors can function as homodimers or heterodimers and bind to DNA sequences called RAR elements (RAREs) or retinoid X response elements (RXREs) in promoter regions of target genes. Retinoic acid has been shown to affect the expression of over 500 genes, though some of these are indirectly affected (10). Unless stated otherwise, all information presented below is pertaining to humans.

1.2 Retinoids in the skin

1.2.1 Human skin anatomy

The functions of retinoids in human skin have been studied since 1925 (11). While some generalizations about retinoids in the skin can be made, retinoid function and metabolism can vary depending on the region of the skin or cell type in question. The skin is made up of three layers: the epidermis, the dermis, and the hypodermis (Figure 2). The epidermis is predominately made up of keratinocytes (>80-95%), but there are also melanocytes, Langerhans' cells, and Merkel cells. Keratinocytes produce keratin, the major structural protein of the skin, and are responsible for the formation of the epidermal water barrier along with the regulation of calcium absorption. Melanocytes primarily produce melanin, which leads to skin pigmentation. Langerhans' cells are dendritic cells, and they have a role in antigen presentation. Merkel cells interact with free nerve endings within the skin and serve as a sensor for touch. Additionally, cells within the epidermis are organized into five layers: the stratum basale, stratum spinosum, stratum granulosum, stratum lucidum, and stratum corneum (listed from deepest layer to most superficial). The stratum basale contains active stem cells, Merkel cells, proliferating keratinocytes, and melanocytes and is attached to the basement membrane above the dermis. The stratum spinosum is approximately 8-10 cell layers, and contains polyhedral keratinocytes that are joined together with desmosomes along with Langerhans' cells. The stratum granulosum is 3-5 cell layers and contains keratinocytes that contain keratohyalin granules which function to bind keratin filaments together. Keratinocytes within the stratum granulosum and more superficial layers secrete lamellar bodies, which form the protective lipid envelope barrier of the skin. The stratum lucidum is 2-3 cell layers found in thicker skin regions (i.e., palms of hands, soles of feet) and is associated with the production of eleidin, a precursor to keratin. The stratum corneum is 20-30 cell layers and is made up of keratin and dead

keratinocytes (anucleate squamous cells). A calcium gradient within the epidermis promotes the differentiation of keratinocytes as they move up through the layers of the epidermis (12). Many proteins required for keratinocyte differentiation (i.e., keratins, involucrin, filaggrin, etc.) are transcriptionally regulated by changes in calcium levels (13). A basement membrane (or basal lamina) separates the epidermis from the dermis. This is stabilizing extracellular matrix structure that acts as a diffusion barrier. The dermis is a connective tissue below the epidermis consisting of primarily fibroblasts that contains sweat glands, hair follicles, blood vessels, and sensory neurons. Fibroblasts generate and maintain the connective tissue and extracellular matrix within the dermis through the production of laminin, fibronectin, and collagens. Finally, the hypodermis is the deepest layer of the skin, and it contains adipocytes that store fats along with blood vessels and nerves. Specific differences in retinoid metabolism and function that have been described will be noted in the following sections.

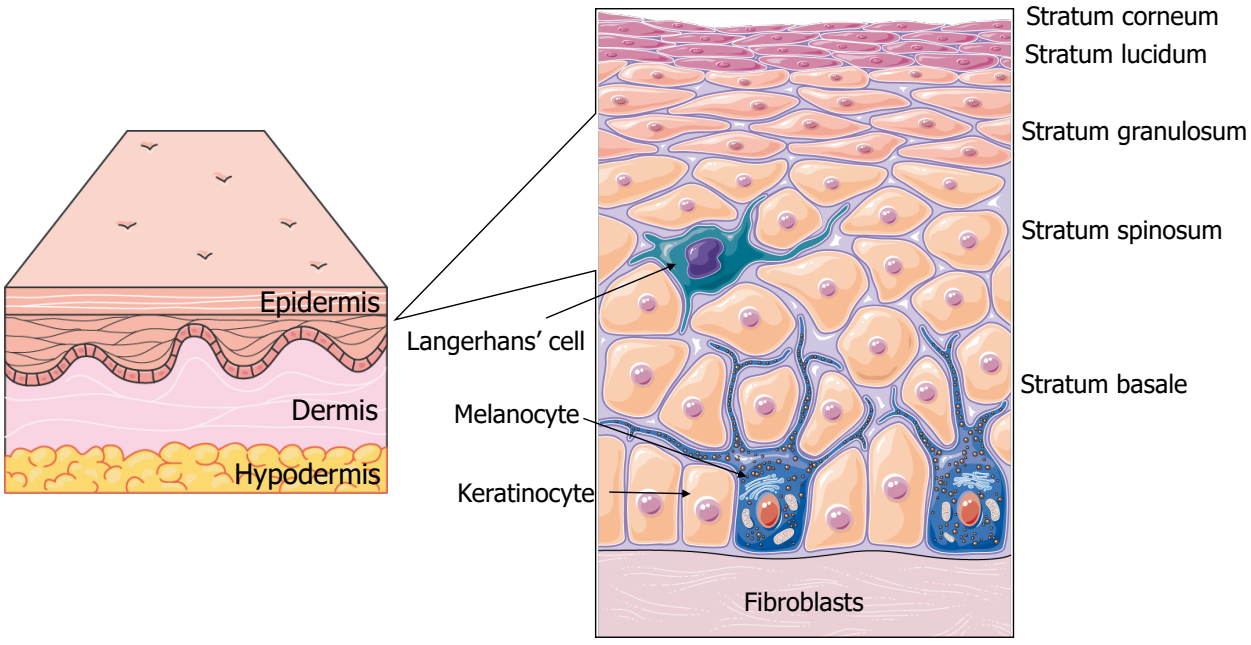

Figure 2. Anatomy of human skin. Images are modified from Servier Medical Art.

1.2.2 Retinoid biosynthesis

Retinol from the plasma is taken up into the cell through the STRA6 receptor (14). Retinoids can also be applied topically and absorbed into the skin (15) and β-carotene can also serve as a precursor for vitamin A formation (16). The conversion of retinol to biologically-active retinoic acid is a two-step process. Alcohol dehydrogenases and short-chain dehydrogenases catalyze the reversible conversion of retinol and retinaldehyde and then retinaldehyde dehydrogenases metabolize retinaldehyde to retinoic acid (17). Retinoid metabolism within the cell is summarized in Figure 3. Little is known about the isomerization of retinoids – there is some evidence for both nonenzymatic and enzymatic contributions (e.g. (18,19)). All-*trans* retinoids are thought to be the most stable isomer in keratinocytes (20).

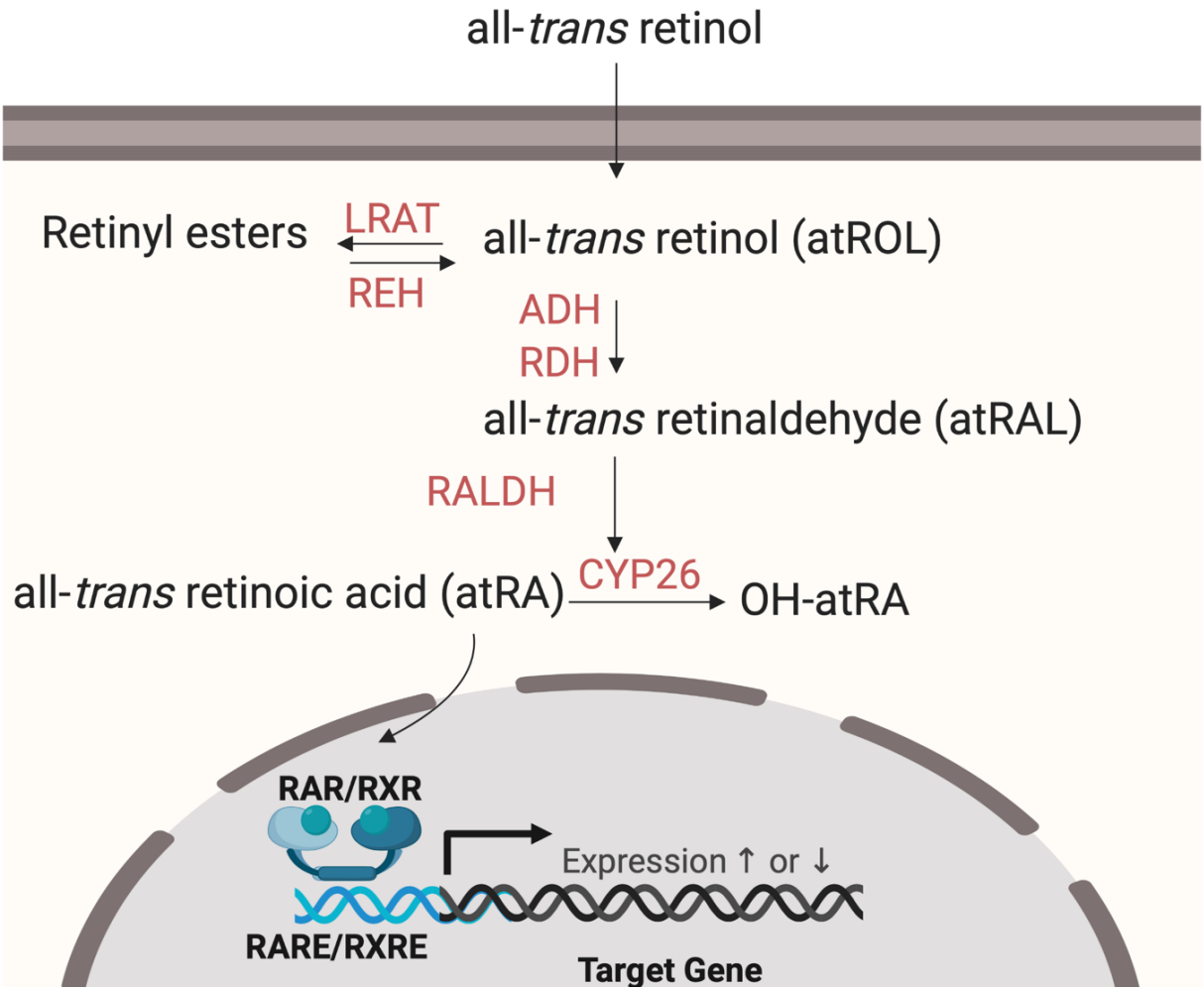

Figure 3. Overview of retinoid metabolism in the skin. The all-*trans* retinoid metabolic pathways are adapted from Roos *et al* (20). ADH, alcohol dehydrogenase; CYP26; cytochrome P450 26 family; LRAT, lecithin retinol acyltransferase; RALDH, retinaldehyde dehydrogenase; RAR/RXR, retinoic acid/retinoid X receptor; RARE/RXRE, retinoic acid/retinoid X responsive element; RDH, retinol dehydrogenase; RE, retinyl ester; REH, retinyl ester hydrolase. Created with BioRender.com.

Once within the cell, retinoids are bound to cellular retinol binding proteins (CRBPs) and cellular retinoic acid binding proteins (CRABPs). CRBPs bind retinol and retinaldehyde and CRABPs bind retinoic acid. Humans have four CRBP and two CRABP proteins with varying binding affinities and tissue distribution (21). The predominant binding proteins in the skin are CRBP-1 and CRABP-2. CRABP-1 is expressed in low concentrations or is not detected (22,23).

This may be due to keratinocytes and fibroblasts both expressing CRABP-2, while CRABP-1 is primarily expressed in melanocytes which are less prevalent in the skin (24). In total, there is 3 pmol/mg protein of CRABP and 1 pmol/mg of CRBP in the epidermis (25). The dermis does not have consistent expression of CRABP but contains a similar amount of CRBP as the epidermis (25). CRBPs facilitate the metabolism and action of retinoids within the cell, delivering them to specific enzymes for metabolism or receptors (21). Additionally, the ratio of apo-CRBP (without retinoid bound) to holo-CRBP (with retinoid bound) has been shown to regulate retinoid metabolism within the cell (21).

1.2.3 Retinoid catabolism

All-*trans* retinoic acid is the primary active retinoid within the skin. Retinoic acid can be further metabolized to biologically inactive monooxygenated products, most notably at the 4-position (4-hydroxy and 4-oxo retinoic acid). In keratinocytes, these products do not bind to RAR/RXR and can be rapidly excreted from the cell (unpublished observations stated in (20)). This activity is mediated by cytochrome P450 enzymes, specifically the CYP26 family – 26A1, 26B1, and 26C1 (26,27). P450 26A1 is expressed in basal keratinocytes (28), P450 26B1 is expressed in fibroblasts (29), and P450 26C1 has been detected in a keratinocyte cell line (30). Holo-CRABPs deliver retinoic acid to the members of the CYP26 family for metabolism (31,32). Catabolism of retinoids *in vivo* may be inhibited by excess apo-CRABPs, as activity of the CYP26 family is inhibited by apo-CRABP *in vitro* (31,32).

1.2.4 Retinoid storage

While retinoids cannot be made *de novo*, they can be stored at relatively high levels within the body (33). Lecithin:retinol acyltransferase (LRAT) and acyl-CoA: retinol acyltransferase (ARAT) transfer long-chain fatty acyl groups to retinol, forming retinyl esters (34,35). Many fatty acids can be utilized, including palmitic, stearic, oleic, and linoleic acids. In the skin, retinyl esterification occurs in basal keratinocytes 4-fold more than keratinocytes in the upper layers (34). Retinyl esters can be hydrolyzed by retinyl ester hydrolases (REHs) to generate free retinol. The amount of retinyl esters is regulated by feedback inhibition – increased concentrations of unesterified retinoids within the cells stimulates esterification and retinoid depletion stimulates retinyl ester hydrolysis (34,36). The ratio of apo:holo-CRBP also affects the activity of LRAT and REH – LRAT is inhibited by excess apo-CRBP-1 (37) and the activity of REH is stimulated (38), leading to an overall increase in the amount of available all-*trans* retinol. This apo:holo-CRBP regulation is thought to provide a mechanism to control retinoid availability within the cell (21).

1.2.5 Retinoid function

Overall, retinoids in the skin regulate cell apoptosis, differentiation, and proliferation. Most retinoid function is associated with alterations to gene expression mediated by retinoic acid receptors. Specific retinoid functions in multiple cell types of the skin have been described. In keratinocytes, retinoids promote proliferation and inhibit terminal differentiation (39). RAR-RXR heterodimers are the major contributors to RARE binding in keratinocytes (40). Retinoic acid suppresses the expression of proteins required for the differentiated keratinocyte phenotype such as keratins, involucrin, and protein required for cornification (39). The increased proliferation caused by retinoids results in epidermal thickening (hyperplasia) due to the increased number of

keratinocyte cell layers within the stratum spinosum and stratum granulosum (41). Retinoids also can reduce melanin production in melanocytes, reducing hyperpigmentation (42). In fibroblasts of the dermis, collagen synthesis is promoted and levels of degrading matrix metalloproteinases are decreased (43).

Because of their function, many retinoid-based therapies exist for a variety of conditions including psoriasis, cancers, acne, ichthyoses, keratodermas, and skin aging (44-46). From 1990-2004, 41.5 million patients were prescribed topical retinoids (47) and some retinoids are also available over the counter. These retinoid therapies are utilized to either modulate the metabolism of endogenous retinoids by interacting with metabolic enzymes or binding proteins or to directly activate retinoid receptors and cause changes in gene expression. Understanding both the activity and metabolism of endogenous retinoids is therefore not only important from a basic human physiology standpoint, but also for drug development.

1.3 3,4-Dehydroretinoids

The functional significance and metabolism of some endogenous retinoids, especially 3,4-dehydroretinoids, is not well understood. All-*trans*-3,4-dehydroretinoids (also referred to as vitamin A2 or 3,4-didehydroretinoids) represent a parallel pathway to the all-*trans* retinoids in the skin. These retinoids were first discovered in human skin in 1980 (48). Overall, 3,4-dehydroretinoids constitute about 20% of the retinoids present in the epidermis, and levels are consistent across tested skin from different regions of the body and between sexes (16). Very few studies have reported the presence of 3,4-dehydroretinoids in human tissue outside of the skin. Levels of retinoids were assessed in human embryos and fetuses and one unidentified retinoid, later confirmed to be 3,4-dehydroretinol, was present in all samples (but not quantified) (49,50).

3,4-dehydroretinyl ester was also identified as a minor component in a human liver sample (51). The lack of 3,4-dehydoretinoids reported in other tissues does not necessarily indicate that they are definitively not present there. Total quantification of the range of endogenous retinoids is technically challenging, given the wide range of concentrations present *in vivo*, presence of multiple geometric isomers, and requirements of extraction, among other issues (52). What is currently known about the biosynthesis and function 3,4-dehydroretinoids in humans is exclusively from studies focused on the skin.

1.3.1 3,4-Dehydroretinoid biosynthesis

Due to the lack of 3,4-dehydroretinol in plasma (16), 3,4-dehydroretinol is thought to be formed locally in the skin from all-*trans* retinol, specifically in the epidermis (53). Three major cell types from the skin – keratinocytes, melanocytes, and fibroblasts – were tested for their ability to convert all-*trans* retinol to 3,4-dehydroretinol, and only keratinocytes had significant activity (54). Melanocytes appear to also produce 3,4-dehydroretinoids, though at a lower rate (54,55). 3,4-Dehydroretinol formation was increased in differentiated keratinocytes (54). Of the all-*trans* retinoids, only all-*trans* retinol seems to serve as a precursor for 3,4-dehydroretinoids as all-*trans* retinoic acid does not get converted to 3,4-dehydroretinoic acid in cells or when applied topically to the skin (56). While many studies have investigated the biosynthesis of 3,4-dehydroretinol in the skin, the enzyme responsible for catalyzing the reaction was never identified. The conversion of all-*trans* retinoids to 3,4-dehydroretinoids does not appear to be reversible (36).

Presumably the metabolism of 3,4-dehydroretinoids (esterification and oxidation) involves the same or similar enzymes as the all-*trans* retinoid pathway, though this has not been extensively investigated. 3,4-Dehydroretinoids bind to cellular retinoid binding proteins with similar affinities

to all-*trans* retinoids (57,58), and so binding proteins likely facilitate their metabolism and function as well. Retinol dehydrogenase 10 can give rise to both all-*trans* retinoic acid and 3,4-dehydroretinoic acid (59). 3,4-Dehydroretinaldehyde can be metabolized to 3,4-dehydroretinoic acid in a variety of species, though sometimes with variable efficiency in comparison with the corresponding all-*trans* retinaldehyde (60,61). 3,4-Dehydroretinol can be esterified for storage. The susceptibility of 3,4-dehydroretinoic acid to catabolism by the CYP26 family is unknown (only 3,4-dehydroretinol has been tested as a potential substrate (32)).

1.3.2 3,4-Dehydroretinoid function

The biological activities of retinoic acids are generally tied to their ability to bind RARs/RXRs. 3,4-dehydroretinoic acid can bind to RAR α, β, and ɣ with nanomolar affinity, similar to all-*trans* retinoic acid (56). Reports about the interaction with 3,4-dehydroretinoic acid and RXRs are somewhat mixed. One study found that, like the retinoic acid counterparts, 3,4-dehydroretinoic acid does not bind to RXRs, but the 9-*cis* form does (62). A later study showed that 3,4-dehydroretinoic acid could bind to RXRα (though with low affinity) and was able to activate transcription mediated by RXRα homodimers and RARβ -RXRα heterodimers 2-3 times more than all-*trans* retinoic acid (63).

Few differences in dehydroretinoid function have been described. 3,4-Dehydroretinoic acid and all-*trans* retinoic acid are equally potent in inhibition of terminal differentiation in keratinocytes (56). In an array analysis focused on genes related to congenital ichthyosis, no differentially regulated genes were found when comparing all-*trans* retinoic acid and 3,4-dehydroretinoic acid (64). Some differences in p53 regulated transcription were observed when comparing all-*trans* retinoic acid and 3,4-dehydroretinoic acid: 3,4-dehydroretinoic acid does not

significantly increase transcription of Fas ligand-TNF superfamily, member 6 (FASLG), BCL2-related protein A1 (BCL2A1), or estrogen receptor 1 (ESR1) while all-*trans* retinoic acid does (65). No studies have performed RNA sequencing to assess the full transcriptome changes with 3,4-dehydroretinoid treatment, so there may be differentially regulated genes that have not been identified.

One proposed function of 3,4-dehydroretinoids is in the cellular response to UV exposure. Multiple groups have illustrated that 3,4-dehydroretinoids are more stable than their all-*trans* retinoid counterparts when exposed to UV (65,66). UVA and UVB also promote dehydroretinol biosynthesis (65). Dehydroretinoids also reduce UVA/B driven apoptosis more effectively than all-*trans* retinoids, potentially due to differences in gene regulation identified in the same study (i.e. Fas ligand) (65).

1.3.3 Association of 3,4-dehydroretinoids with skin malignancies

When 3,4-dehydroretinol was first identified in human tissue, it was in a study assessing retinoid levels in psoriasis skin in comparison to a healthy control (48). There was a marked increase in one retinoid, 3,4-dehydroretinol. The concentration of 3,4-dehydroretinol was later found to be increased in several other skin diseases – often ones associated with hyperproliferation. Studies of skin disorders that have measured levels of all-*trans* retinol and 3,4-dehydroretinol are summarized in Table 1. The mechanisms or consequences of these changes within the skin are not known. Also of note, retinoids commonly prescribed for acne and other skin conditions lead to decreases in 3,4-dehydroretinol levels (67). Identifying and understanding more about the enzyme that catalyzes the formation of 3,4-dehydroretinoids may provide insight into the potential cause of these changes in retinoid levels with different diseases and treatments.

Table 1. Concentrations of all-*trans* retinol and 3,4-dehydroretinol in the skin in patients with a variety of skin conditions vs. healthy controls.

Skin condition		Retinol	Dehydroretinol	Source
Seborrheic keratosis	Involved	86%	174%	(68)
Actinic keratosis	Involved	39% ($p < 0.001$)	206% ($p < 0.005$)	(68)
Basal cell carcinoma	Involved	141% ($p < 0.05$)	517% ($p < 0.001$)	(68)
	Involved	88%	127%	(69)
Squamous cell carcinoma	Involved	172% ($p < 0.05$)	611% ($p < 0.01$)	(69)
Keratoacanthoma	Involved	235% ($p < 0.05$)	667% ($p < 0.01$)	(69)
Plaque psoriasis	Uninvolved	88% (N.S.)	134% (N.S.)	(70)
	Involved	97% (N.S.)	339% ($p < 0.01$)	(70)
Darier's disease	Uninvolved	133% ($p < 0.05$)	109% (N.S.)	(71)
	Involved	128% ($p < 0.05$)	356% ($p < 0.001$)	(71)
Acne vulgaris	Uninvolved	76% ($p < 0.05$)	100% (N.S.)	(72)
	Involved	73% ($p < 0.05$)	221% ($p < 0.05$)	(72)
Atopic dermatitis	Uninvolved	96% (N.S.)	169% ($p < 0.05$)	(72)
	Involved	52% ($p < 0.05$)	264% ($p < 0.01$)	(72)
Ichthyosis vulgaris	Uninvolved	126% (N.S.)	203% ($p < 0.05$)	(72)
	Involved	98% (N.S.)	136% (N.S.)	(72)
Lichen planus	Uninvolved	96% (N.S.)	133% (N.S.)	(72)
	Involved	151% ($p < 0.05$)	574% ($p < 0.01$)	(72)
Uraemic pruritus	N.D.	258% ($p < 0.01$)	67% ($p < 0.05$)	(73)

Statistical significance vs. healthy control was determined in each study and is shown along with the percentage of retinoid in the disease conditions vs. controls. N.S. = not statistically significant in study. N.D. = not described.

1.3.4-Dehydroretinoids in other species

This work focuses on 3,4-dehydroretinoids in human skin, though they are present in other species. Given that information from other species may provide insights into the potential function and formation of dehydroretinoids in humans, a summary on work with other species is provided below.

The first characterized function of dehydroretinoids was in chromophore switching, a phenomenon described in the 19th century (74,75). It is estimated that approximately 25% of all vertebrate species utilize 3,4-dehydroretinoid based visual pigments called porphyropsins

(reviewed in (76)). Outside of a couple terrestrial lizards, this seems to be exclusive to aquatic vertebrates - specifically fish, amphibians, and aquatic reptiles. The utilization of these chromophores allows the species to see longer wavelength light. Studies have also illustrated other potential functions for dehydroretinoids in the eyes of geckos, where crystallins bound to dehydroretinoids may protect the retina from UV damage (77).

While 3,4-dehydroretinoids can serve similar physiological functions as all-*trans* retinoids in animals (78,79), little to no 3,4-dehydroretinoids are usually detected if the animals are not fed a 3,4-dehydroretinoid rich diet (80-82). 3,4-Dehydroretinoid formation in mice can occur through a different mechanism than what has been described in human skin (where all-*trans* retinol serves as a precursor), as 3'-hydroxy-3,4-dehydro-β-carotene (anhydrolutein) leads to the formation of 3,4-dehydroretinol (83).

3,4-Dehydroretinol and 3,4-dehydroretinoic acid have been found in chick embryos in specific tissues and have morphogenic properties (84,85). Additionally, 3,4-dehydroretinoids have been detected in the eggs of fish, amphibians, and reptiles (86). As discussed above, 3,4-dehydroretinol was also found in human fetuses and embryos (49,50). The biological importance of 3,4-dehydroretinoids in human embryos and fetal development is unknown, but the presence of these retinoids in a variety of species raises an interesting possibility of a shared function in development.

1.4 Cytochrome P450 27C1

In 2015, cytochrome P450 (CYP or P450) 27C1 was identified as the enzyme responsible for mediating the chromophore switch phenomenon in fish and amphibians, catalyzing the desaturation of all-*trans* retinoids to 3,4-dehydroretinoids (87). It was then determined that purified

recombinant human P450 27C1 also performed the same reactions *in vitro* (Figure 4) (88). Of note, mice and rats lack the gene for Cyp27c1 due to chromosomal rearrangement (89) and no publications describe the presence of clinically-relevant P450 27C1 variants.

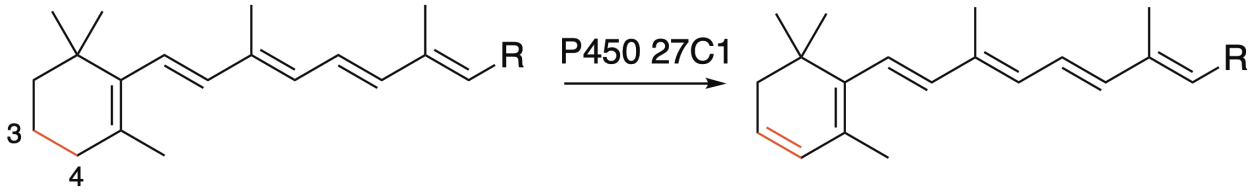

Figure 4. 3,4-Desaturation of all-trans retinoids by P450 27C1. Minor 3- and 4- hydroxylation products are also formed. Substrates: R = CH_2OH, all-trans retinol (vitamin A); R=CHO, all-trans retinaldehyde (vitamin A aldehyde); R = COOH, all-trans retinoic acid (vitamin A acid).

The Guengerich lab has utilized purified recombinant P450 27C1 (90) to extensively characterize components of the catalytic mechanism. All three of the unesterified all-*trans* retinoids - retinol, retinaldehyde, and retinoic acid – are bound by P450 27C1 with nanomolar to low micromolar affinities (88). P450 27C1 forms 3,4-dehydroretinoids from each of these all-trans retinoids efficiently (88), along with minor amounts of 3- and 4-hydroxyretinoids (91). Catalytic activity is dependent on the mitochondrial P450 redox partners NADPH-adrenodoxin reductase (AdR) and adrenodoxin (Adx) (88). Reduction of P450 27C1 by Adx and hydrogen abstraction contributes to rate limitation for catalysis and mechanisms for desaturation have also been proposed (91).

Given what is known about 3,4-dehydroretinoids in the skin, the expression of P450 27C1 in the skin was also investigated (91). Of the three tissues tested (skin, kidney, and liver), only skin showed the presence of P450 27C1 at the protein level (Figure 5). Two proteoforms of P450 27C1 were noted, with one likely being the full-length sequence and one being post-mitochondrial

membrane insertion/cleavage based on sequence information and proteomic analyses (91). Previous studies have detected P450 27C1 mRNA in liver, kidney, pancreas, lung, ovary, adrenal, thyroid, salivary gland, mammary gland, and several fetal tissues (90). The Human Protein Atlas (http://www.proteinatlas.org) also shows RNA distribution in many tissues, with enhanced expression in the skin (92). Given the localization of P450 27C1, it is likely the previously unidentified retinoid desaturase in the skin, though this has not been explicitly proven. The biological function of P450 27C1 in the skin is unknown.

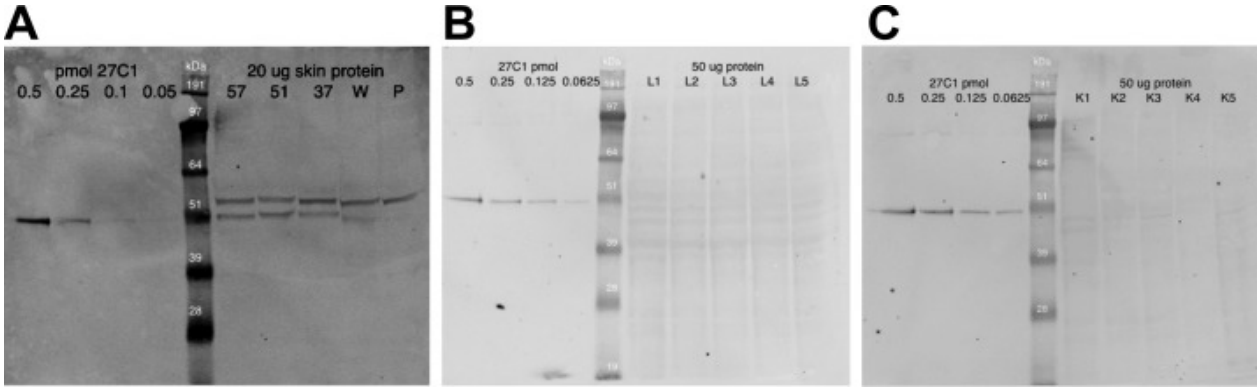

Figure 5. Immunoblot analysis of P450 27C1 expression. Samples from five homogenates of human skin (*A*), liver (*B*), and kidney (*C*) are shown in the rightmost lanes of each blot. Purified recombinant P450 27C1 is shown in the left four lanes. Protein amounts are indicated above the lanes. Figure from (91).

1.5 Cytochrome P450s

Cytochrome P450 27C1 is part of the cytochrome P450 superfamily of heme-containing monooxygenases. Cytochrome P450s were discovered in 1962 and were named for their maximal absorbance at 450 nm when the iron in the heme is reduced and bound to carbon monoxide (93). The general reaction scheme for P450s is shown below:

$$RH + NADPH + O_2 + H^+ \longrightarrow ROH + NADP^+ + H_2O$$

Scheme 1. General reaction scheme for cytochrome P450 enzymes. RH corresponds to the substrate which is oxidized to form ROH.

P450s are present in all domains of life and humans have 57 P450s. P450s nomenclature utilizes a three-part naming system: the first is a number corresponding to the family (40% sequence identity), the second is a letter corresponding to the subfamily (55% identity), and the third is a number corresponding to the specific enzyme (94). Human cytochrome P450s oxidize a variety of endogenous and exogenous small molecules, including steroids, xenobiotics, eicosanoids, fatty acids, and vitamins. The human P450s organized by substrate class are shown in Table 2.

Table 2. Human cytochrome P450s organized by substrate class.

Steroids	Xenobiotics	Fatty Acids	Eicosanoids	Vitamins	Unknown
1B1	1A1	2J2	2U1	2R1	2A7
7A1	1A2	2S1	4F2	24A1	4X1
7B1	2A6	2U1	4F3	26B1	20A1
8B1	2A13	4A11	4F8	26C1	
11A1	2B6	4A22	5A1	27B1	
11B1	2C8	4B1	8A1	27C1	
11B2	2C9	4F11			
17A1	2C18	4F12			
19A1	2C19	4F22			
21A2	2D6	4V2			
27A1	2E1	4Z1			
39A1	2F1				
46A1	2W1				
51A1	3A4				
	3A5				
	3A7				
	3A43				

Table shows assignments as listed in (95).

Cytochrome P450 enzymes can also be stratified based on required redox partners. P450 oxidation requires the donation of two electrons. There are two systems of proteins that can provide these electrons to human P450s, depending on their subcellular localization: the microsomal NADPH-cytochrome P450 reductase (POR) and cytochrome b_5 (b_5) system and the mitochondrial AdR and Adx system. POR and AdR are flavoproteins that transfer electrons from NADPH. POR can directly transfer electrons to microsomal P450s, or to b_5, a small hemoprotein, which can then transfer the electron to the P450. AdR transfers electrons to Adx, a small, ~12 kDa, [2Fe-2S] cluster protein which can then subsequently transfer electrons to the mitochondrial P450s. Redox partner proteins are thought to primarily interact with P450s through electrostatic interactions (96). Of the 57 human P450 enzymes, seven (P450s 11A1, 11B1, 11B2, 24A1, 27A1, 27B1, and 27C1) are intrinsically mitochondrial and utilize the AdR and Adx proteins for electron transfer (97). The involvement of these mitochondrial redox partner proteins in the P450 catalytic cycle is illustrated in Figure 6. Outside of their role as electron donors, numerous studies have suggested that these proteins may also be allosteric effectors of P450 activity (98-105). Whether or not Adx is an allosteric effector of P450 27C1 activity is unknown.

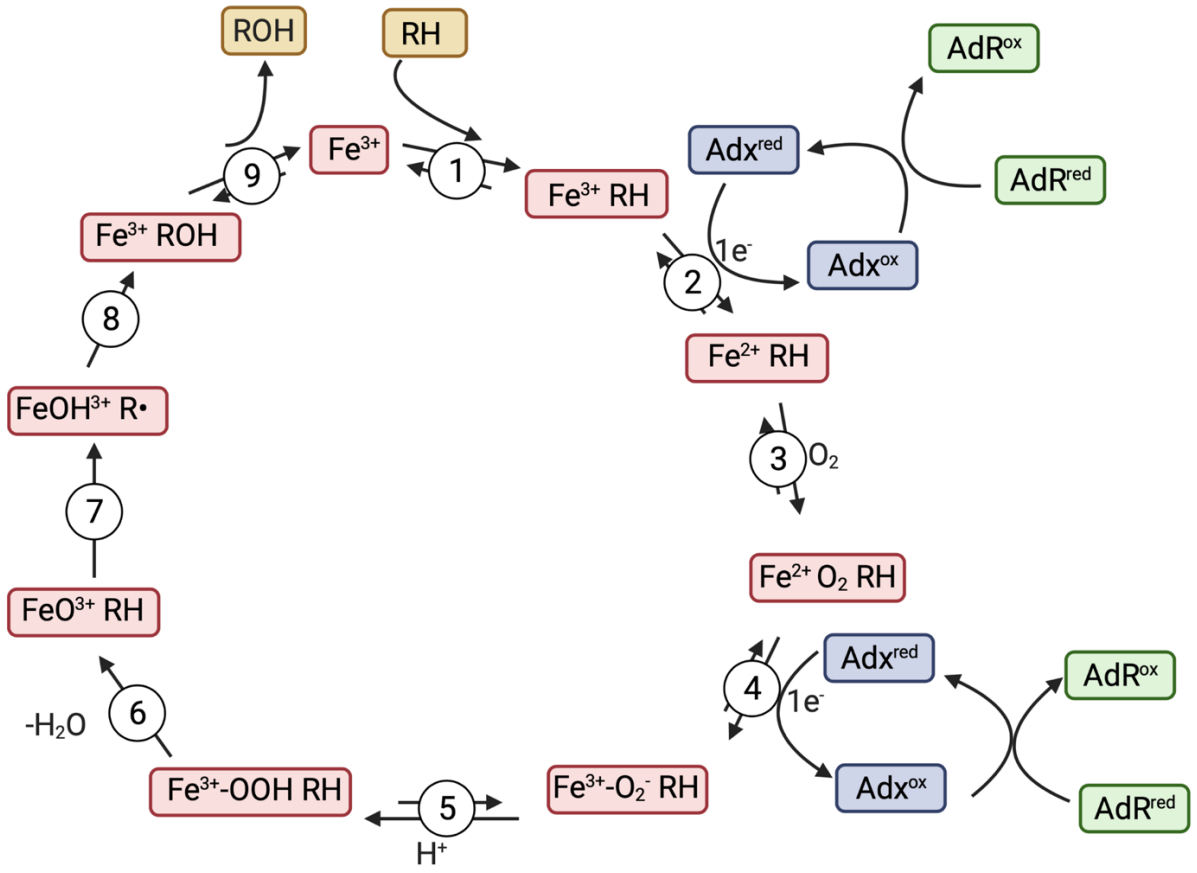

Figure 6. Mitochondrial P450 catalytic cycle. Figure adapted from (91). Created with BioRender.com.

1.6 Existing support of P450 27C1 as the retinoid desaturase in human skin

While P450 27C1 was not initially identified as the retinoid desaturase in the skin, studies assessing the biosynthesis of 3,4-dehydroretinoids present multiple points of supporting evidence towards this hypothesis:

1. The localization of 3,4-dehydroretinoid production to the skin matches P450 27C1 protein expression (91).
2. Fractions generated by differential centrifugation of sonically disrupted cells were assayed for conversion of all-*trans* retinol to 3,4-dehydroretinol and fractions containing

mitochondria showed this activity (106). No activity was observed in the microsomal fraction. This supports the enzyme being a mitochondrial P450 specifically. This work ends up attributing the activity to the plasma membrane based on a protocol for generating plasma membrane ghosts (107), but this method utilizes hypotonic conditions which have been criticized due to potential mitochondrial lysis (108).

3. 3,4-Dehydroretinol formation is inhibited following ketoconazole treatment, a general P450 inhibitor (67). This was initially thought to be due feedback regulation from changes in all-*trans* retinoic acid concentrations (through CYP26 inhibition), but it also supports desaturation being P450 mediated.
4. 3,4-Dehydroretinoid formation is supported by NADPH and not other cofactors (65). Cytochrome P450 enzymes are supported by redox partner proteins that utilize NADPH.

1.7 Research objectives

Given the characteristics of the previously unidentified retinoid desaturase in the skin and what is known about P450 27C1, I hypothesize that P450 27C1 is the enzyme responsible for the formation of 3,4-dehydroretinoids from all-*trans* retinoids in keratinocytes. The overall goal of my dissertation research is to provide a better understanding of the function and homeostasis of dehydroretinoids in the skin through additional characterization of P450 27C1. Towards that end, I have utilized a combination of biochemical, analytical, and molecular biology tools to address specific questions related to P450 27C1. Each of the of the following points constitutes a chapter in this thesis:

1. Where within the skin is P450 27C1 localized? What concentration of P450 27C1 and P450 redox partner proteins are present in the skin? (Chapter 3)

2. Is adrenodoxin an allosteric effector of P450 27C1 retinoid desaturation? How do Adx and P450 27C1 interact? (Chapter 4)
3. Is P450 27C1 able to interact with cellular retinoid binding proteins to receive its substrates? (Chapter 5)
4. What is the function of P450 27C1 and 3,4-dehydroretinoids in keratinocytes? (Chapter 6)

Chapter 2. Materials and Methods

2.1 Materials and Reagents

2.1.1 Retinoids

All-*trans* retinol (atROL), all-*trans* retinal (atRAL), and all-*trans* retinoic acid (atRA) were purchased from Sigma-Aldrich (St. Louis, MO) or Toronto Research Laboratories (Toronto, ON, CA). 3-Dehydro retinal (ddRAL), 3-dehydro retinol (ddROL), 4-hydroxy-all-*trans* retinoic acid, 4-oxo-all-*trans* retinoic acid, and all-*trans* retinoic acid-d_5 were purchased from Toronto Research Laboratories. 3-Dehydro retinoic acid (ddRA) was purchased from Santa Cruz Biochemical (Dallas, TX). All retinoid stocks were prepared fresh in absolute ethanol and kept in amber glass. Stock concentrations were determined spectrophotometrically based on extinction coefficients for each retinoid in ethanol (extinction coefficients listed in Table A1, see representative spectra in Figure 7) (109). Hamilton glass syringes were used to prepare retinoid solutions. Solid stocks were stored under argon at -80 ºC once opened.

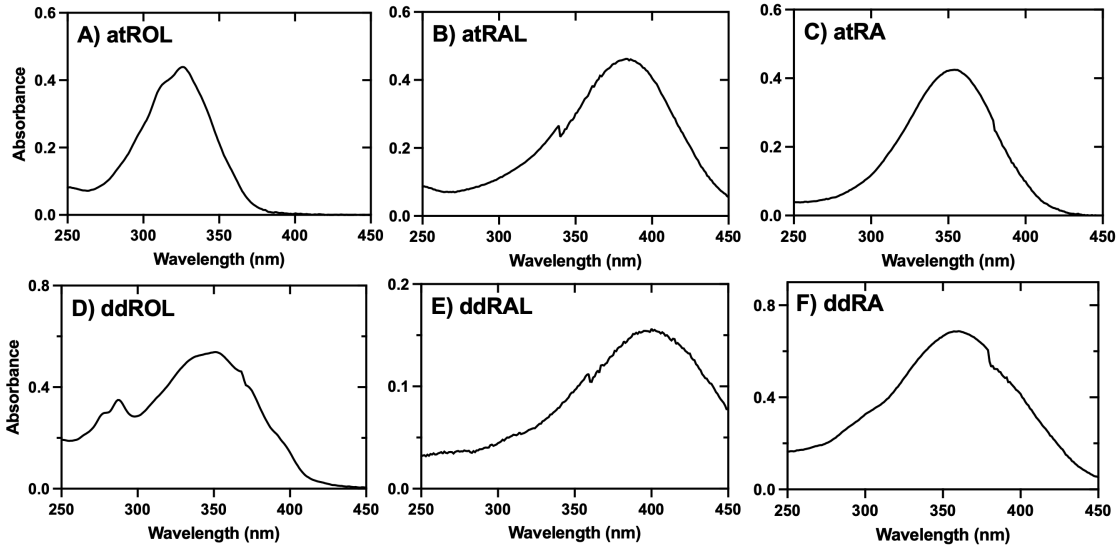

Figure 7. Representative UV-vis spectra of retinoids. *A*, all-*trans* retinol; *B*, all-*trans* retinaldehyde; *C*, all-*trans* retinoic acid; *D,* 3,4-dehydroretinol; *E*, 3,4-dehydroretinaldehyde; *F*, 3,4-dehydroretinoic acid were recorded in ethanol.

2.1.2 Antibodies

P450 27C1 antibodies were raised in rabbits by Cocalico Biologicals (Stevens, PA) and the antibody was purified from sera by affinity chromatography utilizing purified recombinant P450 27C1 (rabbit number 497) (91). The goat anti-rabbit IgG 800CW near-infrared (IR) dye was from LI-COR. Alexa Fluor 555-conjugated goat anti-rabbit IgG was from Invitrogen (now Thermo Fisher Scientific).

2.1.3 Human skin samples

All tissue samples were obtained with the approval of the Vanderbilt Institutional Review Board, which considers these studies exempt. Two human skin samples, from the abdominal area of two adult females (sample HS#1 and HS#2) were obtained from excess tissue in breast free-flap surgery. The other five skin samples termed P, 37, 51, and 57 were banked from a previous study (91). For HS#1 and HS#2, the epidermis was separated from the dermis by dispase II digestion (for isolation of cells) or by scraping (for immunoblotting).

2.1.4 Other materials

BL21 (DE3) Gold *Escherichia coli* competent cells were from Agilent (Santa Clara, CA). Dermal cell basal media and keratinocyte growth kit were from ATCC (Manassas, VA). 2× Laemmli sample buffer was from Bio-Rad (Hercules, CA). $^{13}C_6$-L-Arginine and $^{13}C_6$-L-lysine were from Cambridge Isotope Laboratories (Tewksbury, MA). Human liver microsomes (HLM, 150 donors pooled, mixed gender) were purchased from Corning (Corning, NY). Glycerol was from Fisher Scientific (now Thermo Fisher Scientific, Waltham, MA). Thrombin, Sephadex G-75 resin, and HiTrap desalting columns were from GE Life Sciences (now Cytiva, Marlborough,

MA). EpiLife medium, EpiLife defined growth supplement, keratinocyte SFM, basal medium, bovine pituitary extract (BPE), human recombinant epidermal growth factor (EGF), and dispase II were from Gibco (now Thermo Fisher Scientific). NuPAGE 4-12% and 10% Bis-Tris gels, Simply Blue SafeStain, NuPAGE MES and MOPS SDS running buffer, 4× NuPAGE LDS sample buffer, 6-acrylodan-2-dimethylaminonapthalene (acrylodan), 5-((((2-iodoacetyl)amino)ethyl)amino)naphthalene-1-sulfonic acid (IAEDANS), Alexa Fluor 488 C_5 maleimide, MAX Efficiency DH5α *E. coli* competent cells, and SyPro Ruby blot stain were from Invitrogen (now Thermo Fisher Scientific). Nitrocellulose membrane and Odyssey blocking buffer (PBS) (now Intercept blocking buffer) was from LI-COR Biosciences (Lincoln, NE). Monolith Protein Labeling Kit RED NHS 2nd Generation was from NanoTemper (Munich, Germany). NdeI, HindIII-HF, Phusion High-Fidelity DNA Polymerase, and T4 DNA Ligase were from New England Biolabs (Ipswich, MA). The BCA protein assay kit was from Pierce (now Thermo Fisher Scientifc). Trypsin and trypsin/Lys-C mix was from Promega (Madison, WI). S-Trap micro kits were from Protifi (Famingdale, NY). cOmplete, mini, EDTA-free protease inhibitor cocktail tablets were from Roche (now Millipore Sigma). Nickel-nitrilotriacetic acid agarose (Ni-NTA), QIAquick Gel Extraction Kit, and QIAquick PCR Purification Kit was from Qiagen (Germantown, MD). Dialysis tubing was from Spectrum Spectra/Por (New Brunswick, NJ). 1-Ethyl-3-(3-dimethylaminopropyl)carbodiimide hydrochloride (EDC), *N*-hydroxysulfosuccinimide (Sulfo-NHS), and Zeba Spin Desalting Columns were from Thermo Scientific (now Thermo Fisher Scientific). Amicon Ultra Centrifugal Filters, β-nicotinamide adenine dinucleotide 2′-phosphate (NADPH), L-α-dilauroyl-*sn*-glycero-3-phosphocholine (DLPC), isopropyl β-D-1-thiogalactopyranoside (IPTG), ammonium bicarbonate (ABC), iodoacetamide (IAA), urea, M9

minimal salts, high-performance liquid chromatography (HPLC) grade solvents, and all other reagents were from Millipore Sigma/Sigma-Aldrich (St. Louis, MO).

2.2 Recombinant proteins

2.2.1 P450 27C1

2.2.1.1 Expression

P450 27C1 was expressed and purified similarly to previously described with the following specifications (construct #3, N-terminus modified, residues 3-60 deleted with expression optimized sequence) (90). The amino acid sequence of the P450 27C1 construct is shown in Table A2. DH5α Max Efficiency *E. coli* competent cells were transformed with the P450 27C1 and pGro (GroEL/ES) plasmids and grown on Difco Luria-Bertani (LB) agar plates containing ampicillin (100 µg/ml) and kanamycin (50 µg/ml). An individual colony was used to inoculate LB broth (100 ml) containing ampicillin (100 µg/ml) and kanamycin (50 µg/ml) in a 250-ml Erlenmeyer flask. The solution was incubated overnight at 37 ºC and 220 rpm. Overnight culture (5 ml) was used to inoculate TB media bulk culture (500 ml) containing ampicillin (100 µg/ml), kanamycin (50 µg/ml), trace elements (0.025% v/v), and glycerol (0.4% v/v) in a 2.8-liter Fernbach flask. Bulk LB cultures were incubated at 37 ºC and 250 rpm until they reached an OD_{600} of 0.6. At this point, expression of P450 27C1 was induced by addition of IPTG (1 mM, final). Expression of GroEL/ES was induced by the addition of solid L-(+)-arabinose (4 g/liter). 5-Aminolevulinic acid hydrochloride (1 mM, final) was also added at the time of induction to promote heme synthesis. Flasks were incubated at 27 °C and 190 rpm for 40 h. Cells were pelleted by centrifugation at 5,000 × g, 4 ºC for 20 min and stored at -80 ºC.

2.2.1.2 Purification

Cell pellets were thawed on ice, resuspended in 2× TES (15 ml/g pellet; 150 mM Tris HCl buffer (pH 7.4) containing 0.5 M sucrose and 0.1 mM EDTA), lysozyme (60 µl of 50 mg/ml solution/g pellet), and water (15 ml/g pellet), and stirred at 4 ºC for 30 min. This solution was centrifuged at 5,000 × g (4 ºC) for 20 min and the supernatant was discarded to isolate spheroplasts. Spheroplasts were resuspended in sonication buffer (300 mM potassium phosphate (pH 7.4), 20% glycerol (v/v), 6 mM magnesium acetate) with protease inhibitor tablets and phenylmethylsulfonyl fluoride (PMSF; 1 mM, final) and sonicated with a 3/8-inch tip on a Branson Digital Sonifier Model 450 (VWR, Radnor, PA) at 80% power in 30 s bursts on ice for 5-6 cycles. The solution was centrifuged at 10,000 × g (4 ºC) for 20 minutes, and the supernatant was centrifuged again at 100,000 × g (4 ºC) for 1.5 h. The pellets were resuspended in 100 ml of solubilization buffer (300 mM potassium phosphate (pH 7.4), 20% glycerol (v/v), 1.5% CHAPS (w/v)) by stirring overnight at 4 ºC. This solubilized solution was centrifuged at 100,000 × g, 4 ºC for 30 min. The supernatant was loaded onto a 2.5-cm diameter open-bed glass column containing 10 ml Ni-NTA agarose resin equilibrated with 300 mM potassium phosphate buffer (pH 7.4) containing 20% glycerol (v/v) and 10 mM imidazole using a peristaltic pump. The column was then washed with 20 column volumes of wash buffer 1 (300 mM potassium phosphate (pH 7.4) containing 20% glycerol (v/v), 0.5% CHAPS (w/v), and 20 mM imidazole), and 5 column volumes of wash buffer 2 (300 mM potassium phosphate (pH 7.4) containing 20% glycerol (v/v), and 50 mM imidazole). Proteins were eluted in 25 4-ml fractions using elution buffer (300 mM potassium phosphate (pH 7.4) containing 20% glycerol (v/v) and 300 mM imidazole). Fractions were pooled and EDTA was added (1 mM final) before dialysis against 100 mM potassium phosphate (pH 7.4) containing 20% glycerol (v/v) and 0.1 mM EDTA (3 times, 100× volume). The concentration of the final dialyzed protein was

determined by method of Omura and Sato (110), and the yield was ~85 nmol/liter bulk culture. Final protein purity was assessed by SDS-PAGE (Figure 8).

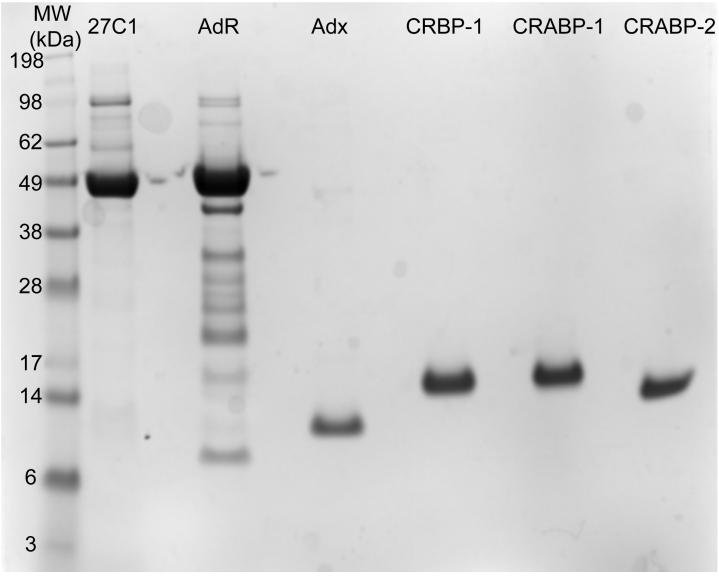

Figure 8. SDS-PAGE of purified recombinant proteins. Each lane contained 100 pmol of each of the following proteins: human P450 27C1, bovine adrenodoxin (Adx), bovine adrenodoxin reductase (AdR), and human CRBP-1, CRABP-1, and CRABP-2. Proteins are stained with SimplyBlue SafeStain.

2.2.2 Redox partners

2.2.2.1 Expression and purification

Bovine adrenodoxin (Adx) and NADPH-adrenodoxin reductase (AdR) were expressed in *E. coli* and purified as described previously (111,112). The amino acid sequence of bovine Adx is shown in Figure A1. Final protein purity was assessed by SDS-PAGE (Figure 8).

The plasmid containing human Adx (pLW01) was a gift from Dr. Richard Auchus (University of Michigan) (113), and the protein was expressed and purified according to a similar method as bovine Adx, with some modifications. The amino acid sequence of human Adx is shown in Table A2 and Figure A1 (comparison with bovine Adx). Briefly, the plasmid was transformed

into *E. coli* BL21 cells and plated on LB_{amp} agar. A single colony was inoculated into 50 ml of Luria-Bertani (LB) media containing 100 µg/ml ampicillin and incubated overnight at 37 °C with shaking at 220 rpm. This pre-culture was used to inoculate bulk culture media at a 1:100 v/v dilution (500 ml Terrific Broth (TB) containing ampicillin (100 µg/ml). The cultures were incubated at 37 °C and 200 rpm until the OD reached approximately 0.6 (~5 h), at which point isopropyl β-D-1-thiogalactopyranoside (IPTG, 0.4 mM) and trace elements (0.025% v/v) were added, and the temperature and speed were reduced to 26 °C and 150 rpm, respectively. The cell pellet was harvested by centrifugation (3000 × g for 10 min) after a further 24 h of growth. The pelleted cells were resuspended in 100 mM potassium phosphate (pH 7.4) buffer containing 20% glycerol (v/v) and 0.1 mM DTT and sonicated for 8 × 30 s at 70% amplitude. The sonicated cells were then centrifuged at 100,000 × *g* for 1 h at 4 °C. The supernatant was loaded onto a DEAE-Sepharose column (2.5 × 10 cm), equilibrated with 50 mM potassium phosphate buffer (pH 7.4) containing 0.1 mM DTT. The column was washed with the same buffer, and the protein was eluted using a linear gradient of KCl (0-200 mM). The fractions containing Adx (as identified by A_{414} measurements and SDS-PAGE) were pooled, concentrated by centrifugal filtration, and loaded onto a Sephadex G-75 column (2.5 cm × 100 cm) equilibrated with 10 mM potassium phosphate (pH 7.4) containing EDTA (0.1 mM). The fractions containing Adx (based on A_{414} measurements) were combined and purity > 95% was confirmed by SDS-PAGE. The total yield was 2,000 nmol of Adx from 3 liters of culture, which was then aliquoted and stored at -80 °C. The final purity of human Adx by SDS-PAGE is shown in Figure 9.

2.2.2.2 Fluorescently labeled Adx

Human Adx was labeled with three different cysteine-reactive fluorescent dyes. Stocks of the fluorescent dyes were made in CH_3CN (acrylodan) or DMSO (IAEDANS, Alexa Fluor 488 C_5 maleimide). Human Adx (100 μM) was incubated with 10-fold molar excess dye in 100 mM potassium phosphate (pH 7.4) for 20 h at 4 °C in a black microcentrifuge tube. The final concentration of organic solvent was < 10% (v/v). Zeba Spin Desalting Columns were used according to the manufacturer's instructions to remove excess dye. Spectra of the final purified, labeled proteins were recorded using a NanoDrop spectrophotometer (Thermo Fisher Scientific) The concentration of labeled Adx was calculated by measuring the absorbance and using ε_{493} = 72,000 M^{-1} cm^{-1} for Alexa Fluor 488. Fluorescence spectra of each labeled Adx preparation were recorded using an OLIS DM-45 spectrofluorometer (On-Line Instrument Systems, Athens, GA). The extent of labeling was calculated by dividing this concentration by the calculated concentration of Adx based on ε_{414} = 9,800 M^{-1} cm^{-1} (114). The A_{414} from Alexa Fluor 488 is only ~2% of the A_{493}; this was not corrected for in calculation of the Adx concentration. The purity of Alexa Fluor 488-Adx and unlabeled Adx was assessed by SDS-PAGE (Figure 9).

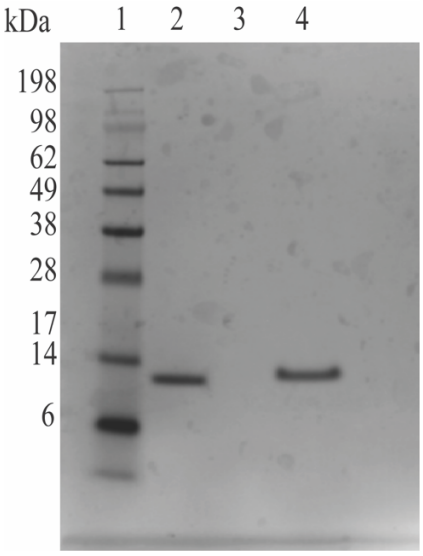

Figure 9. SDS-PAGE of human Adx. Proteins were separated on a NuPAGE 10% Bis-Tris gel with MES running buffer and then stained with SimplyBlue SafeStain. Lane 1, SeeBlue Plus2 pre-stained protein ladder; Lane 2: Adx (unlabeled); Lane 3: blank; Lane 4: Alexa Fluor 488-Adx.

2.2.3 Retinoid-binding proteins

2.2.3.1 Expression

The plasmid for human CRBP-1 (pD441 plasmid with a 6-His C-terminal tag) was obtained from Dr. Marcin Golczak (Case Western Reserve University). The vectors for CRABP-1 and CRABP-2 (pET28a- vectors with 6-His N-terminal tag, removable by thrombin cleavage) were obtained from Dr. Nina Isoherranen (University of Washington). Vectors for the CRABP mutants, CRABP-1 E75Q/K81P/E102K and CRABP-2 Q75E/P81K/K102E, were prepared by site-directed mutagenesis by GeneScript (Piscataway, NJ). Final protein construct sequences are listed in Table A3. Expression and purification are based on the methods in Silvaroli *et al.* and Zhong *et al*., with the following modifications (32,115). Mutant CRABP proteins were prepared the same as described for wild-type proteins. Retinoid-binding proteins were transformed into *E. coli* strain BL21 (DE3) Gold (Agilent) and grown on Difco LB agar plates containing kanamycin (20 µg/ml). An individual colony was used to inoculate 100 ml of LB broth containing kanamycin (50 µg/ml)

in a 250-ml Erlenmeyer flask. The solution was incubated overnight at 37 ºC with shaking at 220 rpm. Overnight culture (5 ml) was used to inoculate LB media bulk culture (500 ml) containing kanamycin (50 µg/ml) in a 2.8-liter Fernbach flask. Bulk LB cultures were incubated at 37 ºC and 250 rpm. When the bulk culture reached an OD_{600} of 0.6, expression of retinoid-binding proteins was induced with either 0.5 mM (CRBP-1) or 1 mM (CRABP-1, CRABP-2) IPTG. After 2 (CRABP-1, CRABP-2) or 4 (CRBP-1) h, cells were pelleted by centrifugation at 5,000 × g for 15 min at 4 ºC. Pellets were stored at -80 ºC until workup.

2.2.3.2 CRBP-1 Purification

Cells from bulk cultures (3 liters) were thawed on ice and resuspended in 120 ml of lysis buffer (20 mM Tris HCl buffer (pH 7.4) containing 500 mM NaCl and 5 mM imidazole) with lysozyme (1 mg/ml). Resuspended pellets were incubated with stirring for 30 min at 4 ºC and then sonicated on ice using a 3/8-inch tip on a Branson Digital Sonifier Model 450 (VWR), set at 80% power for 3 cycles of 30 s with 1-min intermissions. The solution was then centrifuged at 15,000 × g for 30 min at 4 ºC. The supernatant was applied to a 2.5-cm diameter open-bed glass column containing 10 ml of Ni-NTA-agarose resin equilibrated in lysis buffer by peristaltic pump with a flow rate of 2 ml/min. The resin was then washed with 5 column volumes of lysis buffer, 5 column volumes of wash buffer (20 mM Tris HCl buffer (pH 7.4) containing 500 mM NaCl and 30 mM imidazole), and then proteins were eluted into 40 1-ml fractions with 4 column volumes of elution buffer (20 mM Tris HCl buffer (pH 7.4) containing 500 mM NaCl and 250 mM imidazole). Aliquots of each fraction were analyzed on a NuPAGE 10% Bis-Tris SDS-PAGE gel with MES running buffer to identify fractions that contained CRBP-1 (16 kDa band) (Figure 8). Fractions containing purified CRBP-1 were pooled, concentrated, and buffer-exchanged into storage buffer

(20 mM Tris HCl (pH 8.0) containing 10% glycerol (v/v)) using an Amicon Ultra 3K centrifugal filter device. The final CRBP-1 concentration was calculated using the molar extinction coefficient of $\varepsilon_{280} = 26{,}470\ M^{-1}\ cm^{-1}$. The yield was ~500 nmol/liter of bulk culture. Proteins were aliquoted and stored at -80 ºC.

2.2.3.3 CRABP-1 and CRABP-2 Purification

The harvest and Ni-NTA purification of the CRABPs were similar to CRBP-1, with the following exceptions: 50 ml of lysis buffer (for 3 liters bulk culture) was used and PMSF (1 mM) and EDTA-free protease inhibitor tablets (2 mini-tablets, Roche) were added, sonication was done at 75% power for 5 rounds of 10 s with 30 s intermissions, and centrifugation was done at 20,000 × g. Fractions containing CRABPs were pooled and dialyzed 4 times (3,000 MWCO tubing) against 50 volumes of 20 mM Tris HCl buffer (pH 7.4) containing 500 mM NaCl to remove imidazole. CRABP-1 and CRABP-2 (~17 kDa) were located using SDS-PAGE. Mutant CRABP proteins were prepared as described for wild-type proteins. The concentrations of CRABPs were calculated based on molar extinction coefficients of $\varepsilon_{280} = 20{,}970\ M^{-1}cm^{-1}$ and $\varepsilon_{280} = 19{,}480\ M^{-1}cm^{-1}$ for CRABP-1 and CRABP-2, respectively. The yields were ~2,000 nmol/liter bulk culture for both wild-type proteins. The yields for the mutant proteins were 500 nmol/liter (CRABP-1 Q75E/P81K/K102E) and 1,400 nmol/liter (CRABP-2 E75Q/K81P/E102K). Proteins were stored at -80 ºC with 10% glycerol (v/v) prior to thrombin digestion.

Stored CRABPs were thawed on ice and incubated with bovine thrombin overnight at 4 ºC (0.03 U per 10 µg of CRABP). Thrombin digestion was monitored and verified by SDS-PAGE. Approximately 500 ml of Sephadex G-75 was prepared in a 2.5 cm × 100 cm open-bed glass column. A peristaltic pump was used to maintain a flow rate of ~0.4-0.6 ml/min. The column was

washed with 1 column volume of HEDK buffer (10 mM HEPES (pH 8.0) containing 100 mM KCl, 0.1 mM EDTA, and 0.5 mM DTT). The thrombin-digested CRABPs were loaded onto the column and eluted in ~15 ml fractions over 1 column volume with HEDK buffer. Aliquots of each fraction were placed into a 96-well UV-Star microplate (Greiner Bio-One, Monroe, NC) and analyzed for A_{280} using a BioTek plate reader (now part of Agilent Technologies). Fractions containing protein by this measurement were analyzed using a NuPAGE 10% Bis-Tris SDS-PAGE gel with MES running buffer to identify fractions that contained the thrombin-cleaved CRABP products (~16 kDa and 15 kDa, for CRABP-1 and 2, respectively, Figure 8). Fractions containing CRABPs were pooled and concentrated using an Amicon Ultra 3K MWCO centrifugal device. The final CRABP-1 concentration was calculated using the molar extinction coefficient of ε_{280} = 20,970 M^{-1} cm^{-1}. The yield was ~500 nmol/liter bulk culture (~25% recovery). The final CRABP-2 concentration was calculated using the molar extinction coefficient of ε_{280} = 19,480 M^{-1} cm^{-1}. The yield was ~2,200 nmol/liter bulk culture (~100% recovery). The yield for the mutant proteins was 370 nmol/liter (~77% yield, CRABP-1 Q75E/P81K/K102E) and 1,000 nmol/liter (~70% yield, CRABP-2 E75Q/K81P/E102K). Proteins were aliquoted and stored at -80 ºC with 10% glycerol (v/v) added.

2.2.3.4 Preparation of holo-CRBPs

Holo-CRBPs were prepared immediately before assays by incubating apo-CRBPs with a 2.5-fold molar excess of retinoid for 30 min on ice (<2% ethanol final, v/v) in 50 mM potassium phosphate (pH 7.4) buffer containing 25 mM NaCl. The CRBP-retinoid solution was then centrifuged at 25,000 × g for 20 min at 4 ºC. The supernatant was applied to a 5 ml HiTrap Desalting column with a syringe, according to manufacturer's instructions. Absorbance spectra of

purified holo-CRBPs were recorded from 220-500 nm to ensure retinoid-binding (representative spectra in Figure 10). The concentration of each holo-CRBP was calculated using previously determined extinction coefficients (see Table A1).

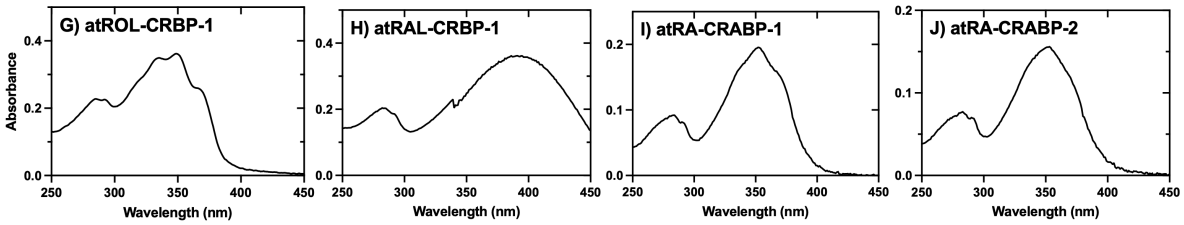

Figure 10. Representative UV-vis spectra of holo-cellular retinoid binding proteins. *G,* atROL-CRBP-1; *H*, atRAL-CRBP-1; *I*, atRA-CRABP-1; *J*, atRA-CRABP-2 were recorded after desalting in 50 mM potassium phosphate (pH 7.4) buffer containing 25 mM NaCl.

2.2.4 QconCAT

2.2.4.1 Design

Candidate peptides were identified by performing LC-MS/MS analysis of in-gel trypsin digested purified P450 27C1, AdR, Adx, POR, and b_5 (see details below). Peptides were selected based on the following qualifications: 1) unique in the human proteome, 2) no detected missed cleavages, 3) predicted to ionize efficiently and have missed cleavage by CONSeQuence software (116), 4) no known sequence variants or post-translational modifications, 5) intensity, 6) detection in whole tissue homogenate. Based on these criteria, two peptides per protein were chosen for generation of the QconCAT polypeptide. Peptides were concatenated along with a small N-terminal peptide added for protection, a modified Glu-Fibrinopeptide B for quantification of the QconCAT, and a C-terminal His-tag for purification as previously described by Russel *et al.* (117) (Figure 11). The QconCAT was also designed to include peptides for quantification of adrenal P450s (11A1, 11B1, 11B2, 17A1, and 21A2) through the same selection procedure.

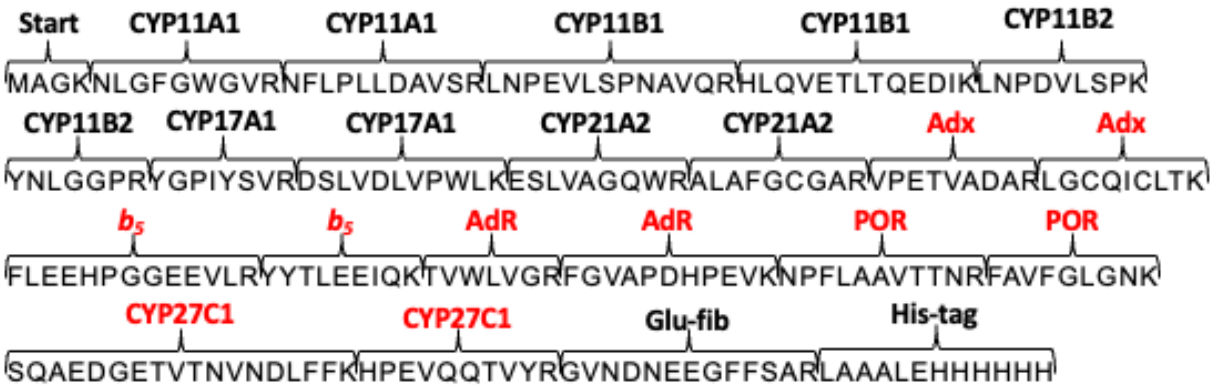

Figure 11. QconCAT polypeptide construct. Sequence is annotated with peptide origin. A modified Glu-fib peptide is included for quantification of the QconCAT and the construct contains a His-tag for purification. The QconCAT construct is 28 kDa.

This amino acid sequence was used as an input for codon optimization for expression in *E. coli*. NdeI and HindIII restriction sites were avoided in codon optimization, and then these sites were added to the ends of the optimized cDNA. The full sequence was ordered from Integrated DNA Technologies (Coralville, IA) and is shown in Table A4 along with forward and reverse primers for PCR (TAAGCACATATGATGGC and TGCTTAAAGCTTTCAATG). The QconCAT gene was amplified by PCR using these primers and Phusion High-Fidelity DNA Polymerase in an Applied Biosciences Verti 96-Well Thermal Cycler (now Thermo Fisher Scientific) according to manufacturer's instructions. Initial denaturation for PCR was performed at 98 °C for 30 s, cycles had denaturation at 98 °C for 10 s, annealing at 48 °C for 30 s, and extension at 60 °C for 3 min, and final extension was performed at 72 °C for 30 min. Amplified PCR product was isolated with a QIAquick PCR purification kit. A double restriction digest with NdeI and HindIII-HF was performed with the amplified QconCAT gene and the pCWOri+ plasmid. Digested products were separated by agarose gel and isolated with a QIAquick gel

extraction kit. Ligation was performed with T4 DNA ligase according to manufacturer's instructions and was then transformed into DH5α Max Efficiency *E. coli* competent cells. Single colonies were isolated from LB_{amp} plates and plasmids were verified by restriction digest and sequencing (GenHunter, Nashville, TN).

2.2.4.2 Expression

The QconCAT plasmid was transformed into BL21-Gold (DE3) *E. coli* and plated on LB_{amp} agar. Initial expression tests were performed in LB media to ensure construct expression before proceeding with minimal media expression. A single colony was used to inoculate a minimal media overnight culture with ampicillin (100 µg/ml) which was incubated overnight at 37 °C with shaking at 220 rpm. Minimal media was sterile filtered and contained 1× M9 salts, 1 mM $MgSO_4$, 0.2% (w/v) glucose, 0.1 mM $CaCl_2$, (5×10^{-5}) % thiamine, 5 µM $ZnCl_2$, and 0.1 mg of each amino acid. Overnight culture (5 ml) was used to inoculate 100 ml of minimal media with ampicillin (100 µg/ml) in a 250 ml Erlenmeyer flask. The 100 ml culture was incubated at 37 °C at 200 rpm until the OD_{600} = 0.6. Expression of the QconCAT was induced with IPTG (1 mM, final) and additional $ZnCl_2$ was added (10 µM, final). After 24 h, cells were pelleted by centrifugation at 4 °C, 5000 × g for 10 min and then frozen at -80 °C. The QconCAT was expressed with $^{13}C_6$-lysine and $^{13}C_6$-arginine or with all light amino acids.

Note: Addition of $ZnCl_2$ was found to be necessary. Expression in minimal media leads to overexpression of ZinT (formerly known as YodA), which has a native N-terminal His-tag and an apparent M_r of 28 kDa on SDS-PAGE (same as the QconCAT construct). Addition of $ZnCl_2$ prevents ZinT from binding to the Ni-NTA resin in the purification steps. This protocol for ZinT removal was provided by Dr. Jens Meiler's group (Vanderbilt University).

2.2.4.3 Purification

Pelleted cells were resuspended in TES (50 ml) with 3.75 mg of lysozyme and protease inhibitors (1 mini cOmplete EDTA-free protease inhibitor cocktail tablet) and then incubated with stirring at 4 °C for 30 min. This solution was centrifugated at 4 °C, 5,000 × g for 30 min and then the supernatant was discarded. The pellet was resuspended in 5 ml of sonication buffer (50 mM HEPES (pH 7.4), 500 mM NaCl, 1% CHAPS sodium (w/v), with a mini protease inhibitor tablet) and then sonicated with a ¼" tip for 5 × 30 s at 50% amplitude. Spheroblasts were pelleted by centrifugation at 4 °C, 1,000 × g for 20 min and then supernatant was carefully removed. This supernatant was centrifuged at 4 °C, 100,000 × g for 1 h. The pellet was then resuspended in 2 ml of binding buffer (20 mM potassium phosphate (pH 7.4), 500 mM NaCl, 6 M guanidine hydrochloride, 2 mM imidazole) using a Teflon-glass homogenizer following by stirring at room temperature for 1 h. This solution was centrifuged again at 4 °C, 100,000 × g for 15 min. Proteomic analysis was performed to identify the solubilized high-speed spin pellet as the localization of the QconCAT. This solution (2 ml) was rolled with 1 ml of Ni-NTA resin in binding buffer overnight at 4 °C.

The resin was poured into an open-bed glass column and then washed with binding buffer until the A_{280} = 0. Consecutive washes were performed with 10, 25, and 35 mM imidazole containing buffers (composition otherwise the same as binding buffer) until A_{280} = 0. Proteins were then eluted into ten 1 ml fractions with buffer containing 300 mM imidazole. To identify fractions containing the QconCAT, aliquots were taken from each step of the purification and proteins were precipitated overnight at -20 °C with 10× volume of 100% ethanol to remove guanidine hydrochloride. Proteins were pelleted by centrifugation at 4 °C, 15,000 × g for 15 min and then

washed with 90% ethanol. Samples were dried and then resuspended in LDS buffer by sonication before analyzing with SDS-PAGE.

Fractions containing the QconCAT were pooled and dialyzed using Spectra/Por 6-8000 MWCO membrane against >100× volume of 20 mM potassium phosphate (pH 7.4), 500 mM NaCl three times to remove guanidine hydrochloride. QconCAT quantification was estimated by SDS-PAGE SimplyBlue SafeStain staining in comparison with a BSA standard curve. By this method, the yield was ~1 nmol of QconCAT (from 100 ml of minimal media culture).

2.3 Catalytic Assays

2.3.1 Steady-state kinetics of P450 27C1 retinoid metabolism with CRBPs

Incubations for P450 27C1 desaturation reactions were done similarly as previously described, with the following specifications (88,91). Reactions were done in amber vials and contained 0.02 µM human P450 27C1, 5 µM bovine Adx, 0.2 µM bovine AdR, 16 µM L-α-dilauryl-*sn*-glycero-3-phosphocholine (DLPC), and 1 mM NADPH in 50 mM potassium phosphate buffer (pH 7.4). Samples were preincubated at 37 °C for 5 min in a shaking water bath prior to the addition of retinoid (100% ethanol stock) or holo-CRBP to initiate the reaction (0-4 µM, final). The final reaction volume was 500 µl (≤1% ethanol, final, v/v). One minute after initiation, reactions were quenched by vortex mixing with 1 ml *tert*-butyl methyl ether (TBME) containing 20 µM butylated hydroxytoluene (BHT) and were then placed on ice. An aliquot (0.7 ml) of the top layer was removed and transferred to a 1.5-ml amber vial. Samples were dried under N_2 and resuspended in 50 µl ethanol and 50 µl of water (50% (v/v) ethanol, final) for UPLC-UV analysis. Experiments were performed in duplicate.

Peak areas were transformed to moles using an external standard curve prepared for each dehydroretinoid product. Data was analyzed with hyperbolic fits solving for k_{cat} and k_{cat}/K_m (k_{sp}) directly (118) (see Eq. 1, Eq. 2) in Prism software (GraphPad, San Diego, CA).

$$v_0 = \frac{k_{sp}[S]}{1+\frac{k_{sp}[S]}{k_{cat}}} \qquad \text{Eq. 1}$$

$$k_{sp} = \frac{k_{cat}}{K_m} \qquad \text{Eq. 2}$$

Results from holo-CRBP assays were compared with the calculated kinetics of product formation under the assumption that P450 27C1 is only able to metabolize free retinoid in solution. The amount of free retinoid ($[R]_f$) in solution was calculated using the quadratic binding equation (Eq. 3), as reported in Nelson *et al.* (31), where $[CRBP]_T$ is the total amount of binding protein, $[R]_T$ is the total amount of retinoid in the reaction, and the K_d is the binding affinity for the retinoid to the binding protein. The K_d values used for calculations were those previously reported (Table A5). Calculated free retinoid concentrations were input into Eq. 1 to determine product formation.

$$[R]_f = \frac{\sqrt{([CRBP]_T-[R]_T+K_d)^2+4K_d[R]_T}-([CRBP]_T-[R]_T+K_d)}{2} \qquad \text{Eq. 3}$$

2.3.2 Isotope dilution channeling experiments

Reactions were performed as described above with the following specifications: reactions were initiated by the simultaneous addition of free all-*trans* retinoic acid (d_5, 10 μM) and holo-CRABP-1 or holo-CRABP-2 (d_0, 10 μM) and reaction times ranged from 30s-180s. An additional 1 μM concentration of the respective apo-CRABP was added to the holo-CRABP preparation to ensure that no free d_0-all-*trans* retinoic acid was added to the reaction. Reactions were performed with free d_0- and d_5-all-*trans* retinoic acid to determine how much the reaction rate was altered by the presence of the isotope labels (4,4,18,18,18-d_5-all-*trans* retinoic acid, positions labeled in Fig.

2). A small change in catalytic rate has previously been observed with the P450 27C1 desaturation of 4,4-d_2-all-*trans* retinol (91). The other deuterium labels are not likely to lead to catalytic rate changes, given that P450 27C1 does not oxidize the 18-position. Experiments were performed in duplicate.

Relative product formation was calculated by dividing the product peak area with the sum of the substrate and product peak areas. Product formation from the d_5-all-*trans* retinoic acid was corrected by dividing the value by the fraction of d_5/d_0 product formation in control incubations with free retinoids.

2.3.3 Effects of excess apo-CRBP

Reactions were performed as described above with the following differences: 0-2.5 μM apo-CRBP (up to 5× the concentration of retinoid) was added and the reaction was initiated with a 0.5 μM concentration of free retinoid or holo-CRBP. Experiments were performed in duplicate. Sample analysis was performed as described above. Relative product formation was calculated by dividing the product peak area by the sum of the substrate and product peak areas. Percent activity was calculated relative to a reaction that did not contain apo-CRBP.

K_i values were calculated in GraphPad Prism using the Morrison quadratic equation (Eq. 4). In this equation, y is the activity, v_0 is the activity in the absence of inhibitor, E_t is the concentration of enzyme, x is the concentration of inhibitor, S is the concentration of substrate, K_i is the inhibition constant, and K_m is the Michaelis-Menten constant determined in an experiment without the competitor (excess apo-CRBP). Values for E_t, S, and K_m were all fixed during fitting.

$$y = v_0 * \frac{1-\sqrt{([E_t]+x+K_i\left(1+\frac{[S]}{K_m}\right)-(([E_t]+x+K_i\left(1+\frac{[S]}{K_m}\right))^2-4[E_t]*x}}{2[E_t]} \qquad \text{Eq. 4}$$

2.3.4 Adx dependence

For comparison of bovine and human Adx, assays were performed as described above, but with varying concentrations of Adx (0-100 μM), 0.5 μM all-*trans* retinol, and the reaction initiation with NADPH (1.5 mM).

For comparison of unlabeled human Adx and Alexa Fluor 488-labeled Adx, assays were performed with varying concentrations of Adx (0-10 μM), 0.5 μM all-*trans* retinol, and the reaction was initiated with NADPH (1 mM).

2.3.5 Dehydroretinoid synthesis in N/TERT cell lysates

Assays for *in vitro* dehydroretinoid formation with cultured human keratinocyte cell lysates were performed similarly as previously described (65). N/TERT-2G keratinocytes grown to near confluence were harvested by trypsinization and resuspended in PBS (pH 7.4) with 280 mM sucrose, 10% glycerol. Solutions were sonicated at 12% amplitude for 12 × 0.5 s pulses. Protein concentrations were determined via BCA assay. Incubations were performed with 0.02 mg protein, 2 mM $CaCl_2$, 1.5 mM $MgCl_2$, and 2 mM NADPH in 100 mM Tris HCl (pH 7.4). The final reaction volume was 200 μl. Samples pre-equilibrated at 37 °C for 5 min in a shaking water bath before being initiated with 10 μM all-*trans* retinol. A control was also done with addition of ethanol only. Reactions were also performed in the presence of 10 μM ketoconazole to assess potential inhibition of 3,4-dehydroretinoid production. After 1 hr, reactions were quenched by vortexing with 1 ml of TBME containing 20 μM BHT and then being placed on ice. Reactions were performed with all N/TERT-2G cell lines in singlet. To facilitate separation of the aqueous and organic layer, samples

were centrifuged at 1,000 × g for 3 min. An aliquot of the upper layer (0.7 ml) was removed and dried under N_2. Samples were frozen at -80 °C for up to 2 days before analysis.

Dried extracts were resuspended in 230 µl of 100% ethanol and 20 µl of 6 M KOH by vortexing. Samples were sealed and heated at 55 °C for 30 min to hydrolyze retinyl esters. Water (100 µl) was added and then samples were chilled on ice for 2 min. This was extracted two times with 1 ml of hexane. Layers were separated by centrifugation as described above. Extractions were pooled and evaporated under N_2 before being resuspended in 50 µl 100% ethanol and then 50 µl of water. To the remaining ethanolic KOH mixture, 119 µl of 1 M HCl was added to acidify the sample for retrieval of the retinoid acids. This acidified solution was extracted with 2 ml of hexane, and an aliquot of the hexane layer was evaporated under N_2 and resuspended as described above.

2.3.6 3,4-Dehydroretinoic acid metabolism in human liver microsomes

The potential for 3,4-dehydroretinoic acid catabolism was assessed in assays with HLMs. Reactions contained 0.2 mg HLM and 2 mM NADPH in 100 mM potassium phosphate buffer (pH 7.4). The final reaction volume was 500 µl. Reactions were performed at 37 °C as described above and were initiated with 5 µM of all-*trans* retinoic acid or 3,4-dehydroretinoic acid. Reactions were also performed in the presence of 10 µM ketoconazole (a general P450 inhibitor) or R115866 (a CYP26-specific inhibitor). Control incubations without NADPH or without retinoid were also done. After 30 min, reactions were quenched, extracted, and resuspended as described above.

2.4 Ligand Binding Studies

2.4.1 Retinoid binding/transfer rates to P450 27C1

To estimate apparent k_{on} values, P450 27C1 (1 μM, final) was mixed with each retinoid substrate (1 μM, final, free retinoid or holo-CRBP) in 200 mM potassium phosphate buffer (pH 7.4). Assays with free retinoid included Adx (15 μM, final). Measurements were made at 23 °C using an OLIS RSM-1000 stopped-flow spectrophotometer (On-Line Instrument Systems, Athens, GA). The settings and instrument configurations were: wavelength range: 330-535 nm; slit widths: 1.24 mm; pathlength: 20 mm; gratings: 400 lines/mm, 500 nm blaze. For free substrates, spectra were recorded for 4 s after mixing (1000 spectra/s). For holo-CRBPs, spectra were recorded over a longer period (1000 s with 2 spectra/s). Absorbance readings at 390 and 420 nm were extracted from the spectra and then ΔA_{390}-A_{420} was calculated at each time point. Traces were averaged using the OLIS GlobalWorks software. Absorbance differences were corrected to make the initial A_{390}-A_{420} value 0. Mixing transients were fit by nonlinear regression in GraphPad Prism as reported previously with Eq. 5 (104). Pre-trigger data is shown (pre-zero time data), but is not used for fitting. In this equation y is the observed absorbance difference, A is a scaling constant, C_0 is the initial concentration of the enzyme/substrate, k is the binding rate constant, and x is time.

$$y = A * \left(\frac{-[C_0]}{[C_0]*k*x+1} + [C_0]\right) \qquad \text{Eq. 5}$$

To determine if the rate of retinoid transfer from holo-CRBPs was dependent on the P450 27C1 concentration, holo-CRABPs (1 μM, with 0.1 μM excess apo-protein) were mixed with varying amounts of P450 27C1 (1-5 μM) in the presence of Adx (15 μM) in 200 mM potassium phosphate buffer (pH 7.4). Measurements were made at 23 °C using an OLIS computerized HP 8452 Diode Array. Spectra were recorded from 350 to 500 nm for 1000 s with 1 s integration time.

Absorbance readings at 390 and 420 nm were extracted from the spectra and ΔA_{390}-A_{420} was calculated at each time point using the OLIS GlobalWorks software. Absorbance differences were corrected to make the initial value zero. Binding constants were calculated in GraphPad Prism using a modified single-exponential one-phase association equation (Eq. 6) or a bi-exponential two-phase association equation (Eq. 7). In these equations, y is the measured absorbance difference, y_{max} is the plateau value, $span_{fast}$ and $span_{slow}$ are the percentages accounted for by each exponential component multiplied by y_{max}, k is the binding rate constant, and x is time.

$$y = y_{max}(1 - e^{-kx}) \quad \text{Eq. 6}$$

$$y = span_{fast}\left(1 - e^{-k_{fast}x}\right) + span_{slow}(1 - e^{-k_{slow}x}) \quad \text{Eq. 7}$$

2.4.2 Equilibrium retinoid binding titrations with Adx

All-*trans* retinol (0-1.04 μM) was titrated into P450 27C1 (90 nM) in 200 mM potassium phosphate buffer (pH 7.4) in the presence of varying concentrations of Adx (0-1.8 μM). To enable absorbance measurements at this low P450 27C1 concentration, titrations were performed in a 10-cm cell (25 mL solution) (Starna Cells, catalog # 34-Q-100). The final volume of ethanol in the titration was <0.05 % (v/v). Spectra were recorded with an OLIS Cary-14 spectrophotometer from 350-500 nm. Titrations were performed by Stephany N. Webb. The reference spectrum (with no substrate) was subtracted from each titration spectrum. ΔA_{390}-A_{420} was calculated at each concentration, with the substrate-free value corrected to 0. The plot of absorbance difference versus substrate concentration was fit in Prism software (GraphPad, San Diego, CA) using the quadratic equation (Eq. 8), In this equation, ΔA_{max} is the extrapolated absorbance difference at an

infinite ligand concentration, E_T is the concentration of P450 27C1, X is the concentration of all-*trans* retinol, and K_d is the dissociation constant.

$$\Delta A = \Delta A_{max} \frac{(E_T+K_d+X)+\sqrt{(E_T+K_d+X)^2-4E_TX}}{2E_T} \qquad \text{Eq. 8}$$

2.5 Protein-Protein Binding Studies

2.5.1 Microscale thermophoresis

Binding affinity of Adx (human and bovine) for bovine AdR and human P450 27C1 was studied using a Monolith NT.115 Microscale Thermophoresis (MST) system (NanoTemper Technologies GmbH) in the Vanderbilt Structural Biology Core Facility. Either human or bovine Adx was labeled using a NanoTemper Monolith Protein Labeling Kit RED NHS 2nd Generation, which reacts with amine groups in a protein sample to label the protein with a fluorescent dye (RED) (proprietary). The kit labeling instructions were modified because initial attempts at labeling resulted in a degree of labeling of ~10%. By increasing the dye-protein incubation time from 30 min to 2 h and increasing the dye:protein ratio from 3.3 to 10, the extent of labeling was increased to ~50%, as determined by UV-visible absorbance measurements at 650 and 280 nm.

MST samples contained 20 nM either RED-labeled bovine Adx or RED-labeled human Adx, 100 mM potassium phosphate buffer (pH 7.4), 0.05% Tween 20 (v/v), and various concentrations of either bovine AdR or P450 (100 pM to 39 μM). Samples were loaded into the standard Monolith NT.115 capillaries and tested by MST analysis at 25 °C. The results were analyzed by plotting the baseline-corrected normalized fluorescence (ΔF_{norm} [%]) versus enzyme concentration. Data from two or three independently pipetted experiments were analyzed using a single site binding model, and the resultant K_d values were averaged with error propagated through

the averaging. MST experiments were performed by Ian Barckhausen and data analysis was performed by Dr. Michael Reddish.

2.5.2 Adx binding fluorescence titrations

P450 27C1 (0-290 nM) or AdR (0-502 nM) was titrated into a solution of Alexa Fluor 488-Adx (50 nM) in potassium phosphate buffer (50, 100, or 200 mM, pH 7.4). Titrations were performed in a semi-micro 1-cm quartz cell with clear windows (Starna Cells, Atascadero, CA, catalog # 29F-Q-10) in an OLIS DM-45 spectrofluorometer with 1.24 mm slits and an integration time of 0.1 s with 493 nm excitation and emission spectra recorded from 500-600 nm. To determine potential effects of P450 substrate binding on Adx binding affinity, titrations were also performed with P450 27C1 incubated with an equal molar concentration of all-*trans* retinol. Titrations were performed in triplicate by Stephany N. Webb. The fluorescence at the emission maximum was normalized and plotted against the concentration of P450 or AdR and fit with a quadratic binding equation in GraphPad Prism (San Diego, CA) to calculate the K_d value. This is shown in Eq. 8 (but with absorbance). Application here utilizes the following as parameters: ΔF_{max} is the extrapolated fluorescence difference at an infinite ligand (P450 27C1 or AdR) concentration, E_T is the concentration of Adx, X is the concentration of P450 27C1 or AdR, and K_d is the dissociation constant.

For normalization, the minimum emission value during the titration was subtracted from the emission value at each point, and then this value was divided by the range in emission values observed in the titration. Preliminary titrations were also performed with P450 27C1 and the acrylodan- (excitation 391 nm; emission 450-700 nm) and IAEDANS-Adx (excitation 337 nm; emission 350-600 nm).

2.5.3 Crosslinking

EDC (2 mM) and Sulfo-NHS (5 mM) was added to Adx (40 μM), Alexa Fluor 488-Adx (40 μM), or CRABPs (20 μM) in 100 mM potassium phosphate buffer (pH 7.4) and incubated at 23 °C with shaking for 15 min. EDC and Sulfo-NHS solutions were made in water immediately before addition. P450 27C1 (2 μM) was added to the reaction (final volume 20 μl) and the samples were incubated for 2 h at 23 °C with shaking before quenching with an equal volume of 2× Laemmeli buffer (with β-mercaptoethanol). The samples were heated at 90 °C for 10 min and then loaded onto a NuPAGE 4-12% Bis-Tris SDS-PAGE gel with MOPS running buffer. The gel was stained with SimplyBlue SafeStain.

2.6 Proteomic analysis

2.6.1 Sample preparation

2.6.1.1 In-gel

Purified recombinant proteins (for selecting peptides for the QconCAT), skin homogenates or cell lysates (50 μg), or the QconCAT were separated by SDS-PAGE. In the comparison of sample workup methods, the QconCAT (2 pmol) and skin homogenate (50 μg) was combined and run briefly on SDS-PAGE for in-gel clean-up. The excised gel pieces were destained, reduced, and alkylated as previously described (119). Regions of interest were excised from SDS-PAGE and cut into small, ~1 mm cubes and incubated with 100 mM ABC, 30% CH_3CN for 30 min with shaking for destaining. Samples were reduced with 10 mM DTT in 100 mM ABC for 30 min at 55 °C and then alkylated with 55 mM IAA in 100 mM ABC for 30 min at room-temperature in the dark. Gel pieces were shrunk by shaking with CH_3CN between treatments and for storage at -

20 °C until digestion. Digestion was performed with trypsin (0.01 µg/µl) or trypsin/Lys-C (0.01 µg/µl) in 10 mM ABC at 37 °C overnight. Peptides were extracted from gel pieces with 66% CH_3CN, 5% HCO_2H. This solution was dried with a SpeedVac with heating and resuspended in 0.1% HCO_2H.

Adx-P450 27C1 cross-links and Alexa Fluor 488-labeled Adx samples were worked up similarly. After destaining, reduction, and alkylation, samples were submitted to Kristie Rose in the Vanderbilt Mass Spectrometry Research Center who performed a digestion with trypsin (0.2 µg) at 37 °C for 16 h, extractions (two with 0.1% CF_3CO_2H, 60% CH_3CN, and one with 0.1% CF_3CO_2H, 80% CH_3CN), and resuspension in 0.2% HCO_2H.

2.6.1.2 Filter aided sample preparation

Filtered aided sample preparation (FASP) was performed similarly to previously described (120). A sample of skin homogenate (50 µg) and QconCAT (2 pmol) was made up with 1% SDS and 0.1 M DTT (30 µl, final) and heated at 95 °C for 5 min. This sample along with 200 µl of 8 M urea, 50 mM ABC was loaded onto a pre-washed 10,000 MWCO centrifugal filter (0.5 ml). The sample was vortexed and centrifuged at 14,000 × g for 20 min. An additional 200 µl of 8 M urea, 50 mM ABC was added and the centrifugation was repeated. The flow through was discarded. Alkylation was performed in the filter unit with 100 µl of 15 mM IAA in 8 M urea, 50 mM ABC in the dark at room temperature for 20 min. This solution was centrifuged at 14,000 × g for 20 mins, and then 100 µl of 8 M urea, 50 mM ABC was used to wash two times, with centrifugation in between rinses. To remove urea, two additional washes were performed with 100 µl of 50 mM ABC. The filter unit was transferred to a new collection tube, and 120 µl of 50 mM ABC with 1 µg of trypsin/Lys-C was added to the filter (1:50 protease:protein ratio). Digestion was performed

overnight at 37 °C in a water bath. To elute peptides, the filter was centrifuged at 14,000 × g for 20 mins. An additional elution was performed by addition of 50 µl of water and repeated centrifugation. Elutions were pooled, dried down, and resuspended as described with the in-gel method.

2.6.1.3 S-Trap

The S-Trap micro sample prep kit from Protofi was utilized according to manufacturer's instructions. Skin homogenate (50 µg) and QconCAT (2 pmol) were combined in 2× lysis buffer (10% sodium dodecyl sulfate (SDS), 100 mM triethylammonium bicarbonate (TEAB) (pH 8.5)) to a final volume of 23 µl. The final SDS concentration of the mix was ~5% (>2% SDS is recommended for good recovery). The sample was reduced by incubating with 1 µl of 120 mM tris(2-carboxyethyl)phosphine (TCEP) at 55 °C for 15 min. Alkylation was performed at room temperature for 10 min with 1 µl of 500 mM methyl methanethiosulfonate (MMTS) in $(CH_3)_2CHOH$. The sample was acidified with 2.5 µl of 27.5% phosphoric acid (final pH < 1). The sample volume at this point is 27.5 µl. Six volumes (165 µl) of binding/wash buffer (100 mM TEAB in 90% CH_3OH) was added to the sample and the sample was applied to an S-Trap micro column and centrifuged at 10,000 × g for 30 s. The S-Trap was washed three times with 150 µl of binding/wash buffer, and the S-Trap unit was rotated 180° between each centrifugation at 10,000 × g for 30 s. Residual buffer was removed by a final 1 min spin at 10,000 × g. Trypsin/Lys-C (5 µg, 1:10 weight:weight ratio to the amount of protein on the column) in 50 mM TEAB (20 µl, final volume) was applied to the column and digestion was performed overnight at 37 °C in a water bath. To elute peptides, the column was consecutively eluted three times with 40 µl each of 50 mM TEAB, then 0.2% HCO_2H, and finally 50% CH_3CN, with centrifugation at 10,000 × g for 1

min between each elution. Elutions were pooled, dried down, and resuspended as described with the in-gel method.

2.6.2 Analysis of P450s and redox partners for QconCAT

For identification of peptides for QconCAT generation, raw data files were analyzed using MyriMatch software version 2.2.140 (121) against the sequences for recombinant proteins. Software settings were: enzyme: trypsin; precursor ion resolution: high; fragmentation mass resolution: low; modifications: methionine oxidation (15.9949 Da, dynamic) and cysteine carbmidomethylation (57.0215 Da, fixed). Spectra were visualized in IDPicker software (122) and the false discovery rate was set to 5%. Results were also analyzed in Skyline (123) to identify peptides unique to the human proteome.

2.6.3 Cross-linking analysis

pLink 2 software (version 2.3.9) (124) was used to identify cross-linked peptides. Software settings were as follows: cross-linker: EDC-DE; enzyme: trypsin; number of missed cleavages: 2; peptide mass: 400-6,000; peptide length: 4-60; precursor tolerance: 20 ppm; fragment tolerance: 20 ppm; fixed modifications: carbamidomethyl [C]; variable modifications: oxidation[M]; filter tolerance: 10 ppm; false discovery rate (FDR): separate FDR < 5% at PSM label. The *E. coli* proteome with the sequences for recombinant human Adx and P450 27C1 was used as a database (with contaminant proteins added by pLink 2). MS/MS spectra were visualized in pLabel version 2.4.1.

2.6.4 Identification of Alexa Fluor 488 Adx labeling site

For identification of the site of the Alexa Fluor 488 label, raw data files were analyzed using MyriMatch software version 2.2.140 (121) against the sequence for recombinant human Adx. Software settings were: enzyme: trypsin; precursor ion resolution: high; fragmentation mass resolution: high; modifications: methionine oxidation (15.9949 Da, dynamic), cysteine carbmidomethylation (57.0215 Da, dynamic), Alexa Fluor 488-cysteine (698.0988 Da, dynamic). The 698.0998 Da modification for the Alexa Fluor 488 represents the predominant charge state of the Alexa Fluor 488 modification (see structure in Figure 28), though others were observed (data not shown). Spectra were visualized in IDPicker software (122) and the false discovery rate was set to 5%.

Formatte

Deleted: I

2.7 Chromatography

2.7.1 UPLC-UV

Aliquots of each sample (20 µl) were analyzed by UPLC with a Waters (Milford, MA) Acquity system on an Acquity BEH octadecylsilane (C_{18}) column (1.7 µm; 2.1 mm × 100 mm) at 40 °C with a flow rate of 0.5 ml/min. Solvent A was 95% H_2O, 4.9% CH_3CN, 0.1% HCO_2H and Solvent B was 95% CH_3CN, 4.9% H_2O, 0.1% HCO_2H (all v/v/v). The solvent gradient used was: 0-0.1 min, 40% A; 5-6 min, 25% A; 6.5-8 min, 0% A; 8.5-10 min, 40% A. Retinoids were identified by co-elution with commercial standards and quantification was based on A_{350} (ddROL), A_{401} (ddRAL), and A_{370} (ddRA) peak areas. Example chromatograms from reactions with all-*trans* retinoids and purified P450 27C1 are shown in Figure 12.

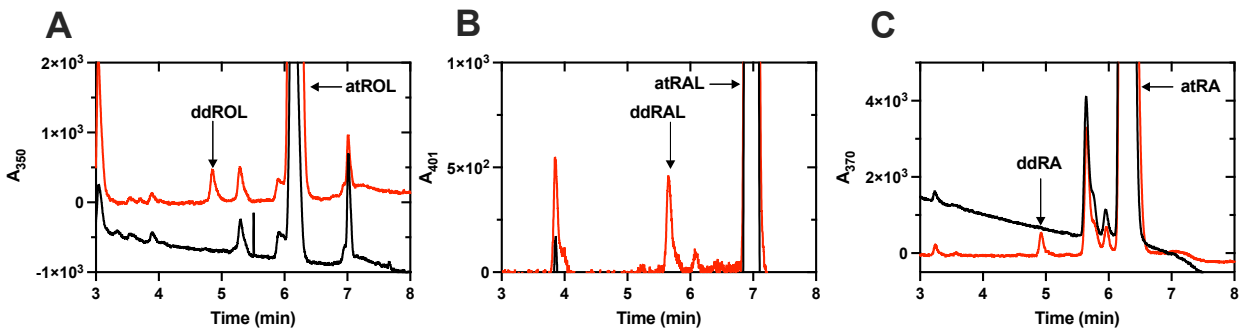

Figure 12. Representative UPLC-UV chromatograms of P450 27C1 incubations with all-*trans* retinoids. Reactions were performed with 4 µM free substrate: *A*, all-*trans* retinol; *B*, all-*trans* retinaldehyde; *C*, all-*trans* retinoic acid in the presence (red) or absence (black) of NADPH.

2.7.2 UPLC-MS/MS

LC-MS/MS analysis was performed with the same chromatography system described above for other catalytic assays. A Thermo LTQ XL-Orbitrap mass spectrometer was operated with atmosphere pressure chemical ionization (APCI) in positive ion mode and 15,000 resolution. The mass spectrometer was tuned with all-*trans* retinoic acid. The tune settings were: sheath gas flow rate, 40; auxiliary gas flow rate, 20; capillary temperature, 275 °C; APCI vaporizer temperature, 400 °C; discharge current, 15 µA; capillary voltage, 2.5 V; tube lens, 45 V. For the MRM mode, the isolation width was 2 *m/z* and the collision energy was 35. Transitions used for quantification are shown in Table 3 and example mass spectra and extracted ion chromatograms (XICs) are shown in Figure 13.

Table 3. Mass spectrometry MRM transitions used in isotope dilution experiments.

Retinoid	MS1		MS2	
	Calculated	**Observed**	**Calculated**	**Observed**
d_0-atRA	301.2168 $C_{20}H_{29}O_2$ $[M+H]^+$	301.2151 (-5.49 ppm)	205.1229 $C_{13}H_{17}O_2$[a]	205.1229 (+0.22 ppm)
d_0-ddRA	299.2011 $C_{20}H_{27}O_2$ $[M+H]^+$	299.1994 (-5.70 ppm)	243.1385 $C_{16}H_{19}O_2$	243.1397 (+4.92 ppm)
d_5-atRA	306.2481 $C_{20}H_{24}D_5O_2$ $[M+H]^+$	306.2493 (+3.79 ppm)	206.1957 $C_{15}H_{16}D_5$	206.1946 (-5.38 ppm)
d_4-ddRA	303.2262 $C_{20}H_{23}D_4O_2$ $[M+H]^+$	N.D.[b]	247.1636 $C_{16}H_{15}D_4O_2$	247.1642 (+2.38 ppm)

[a] A mechanism for the formation of this d_0-all-*trans* retinoic acid fragment has previously been proposed (125).

[b] N.D. = not detected. The parent mass for d_4-ddRA was not consistently observed over baseline with fragmentation.

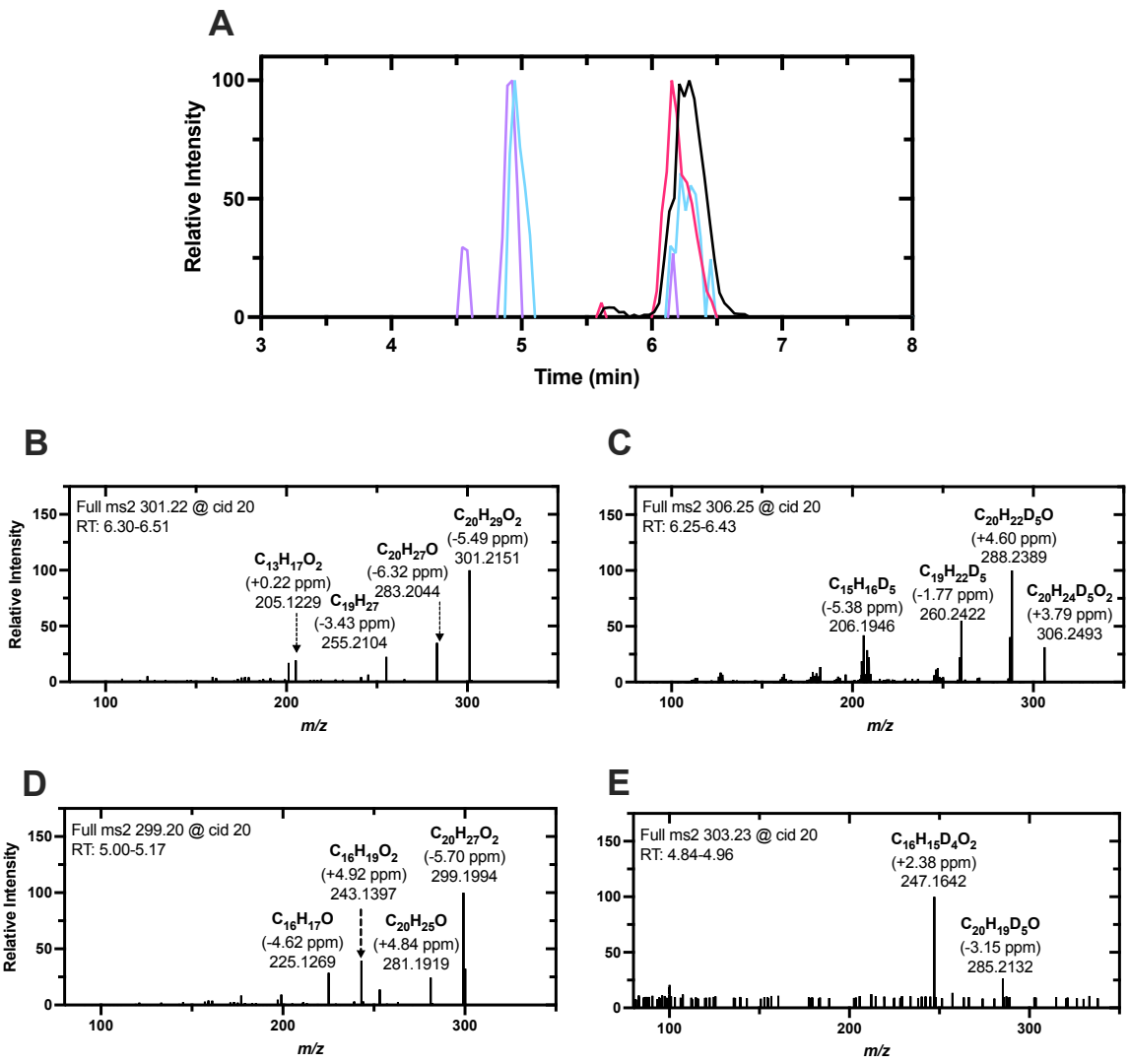

Figure 13. Representative MRM chromatograms and annotated MS/MS spectra of P450 27C1 all-*trans* retinoic acid isotope dilution assays. *A*, MRM chromatogram for transitions listed in Table 3 (d_0-atRA, 301.2>205.1 (—); d_5-atRA 299.2>243.1 (—); d_0-ddRA 306.2>206.1 (—); d_4-ddRA 303.2>247.2 (—)). All are shown with a 10 ppm mass window. Annotated MS/MS spectra for: *B*, d_0-all *trans* retinoic acid; *C*, d_5-all *trans* retinoic acid; *D*, d_0-3,4-dehydroretinoic acid; *E*, d_4-3,4-dehydroretinoic acid. The top three (two for panel *E*) abundant fragments are identified.

Formatte

Deleted:

2.7.3 nanoLC-MS/MS

Peptides were loaded onto a 21.5 cm capillary (360 µm outer diameter, 100 µm inner diameter) octadecylsilane (C18) reversed phase (Jupiter, 3 µm beads, 300 Å, Phenomenex) analytical column using a Dionex Ultimate 3000 nanoLC. The mobile phase solvents consisted of:

solvent A: 0.1% HCO_2H in H_2O; solvent B: 0.1% HCO_2H in CH_3CN (all. v/v). Peptides were eluted with gradient of: 0-2 min, 2% B; 2-73 min, 2-40% B; 73-78 min, 40-95% B; 78-79 min, 95% B; 79-80 min, 95-2% B; 80-90 min, 2% B (all v/v) at a flow rate of 0.35 μL min^{-1}.

For identification of cross-linked peptides and the site of Alexa Fluor 488-Adx modification, a Q-Exactive Plus mass spectrometer was used in positive ion mode for full MS/data-dependent MS2 (Top 15) analysis. The full MS settings were as follows: microscans, 1; resolution, 70,000; AGC target, 3e6; maximum IT, 60 ms; scan range, 375 to 1800 *m/z*. The dd-ms2 settings were: microscans, 1; resolution, 17,500; AGC target, 1e5; maximum IT, 100 ms; loop count, 15; MSX count, 1; TopN, 15; isolation window, 2.0 m/z; scan range, 200 to 2000 *m/z*; (N)CE, 26.

For selection of peptides for QconCAT generation, peptides from purified recombinant proteins were separated with a Thermo EASY-nLC and analyzed on a Thermo LTQ XL-Orbitrap mass spectrometer in positive ion mode for full MS/data-dependent MS2 (Top 5) analysis with a 60-minute gradient.

For comparison of sample preparation methods for absolute quantification analysis, peptides from skin homogenates and the heavy-labeled QconCAT were analyzed on a Q-Exactive Plus mass spectrometer in positive ion mode for full MS/data-dependent MS2 (Top 4) analysis with PRM for peptide masses of interest (precursor masses in Table A6) over a 90-minute gradient.

2.8 Structural modeling

2.8.1 Protein docking

The structure of P450 27C1 has not been experimentally determined. The human P450 27C1 structure was downloaded from the AlphaFold Protein Structure Database (126). The structure in the database was for the full-length protein sequence and the PDB file was modified

to remove the first 63 residues (disordered) to align the sequence with the recombinant protein used in this study. The X-ray crystal structure for human Adx was obtained from the Protein Data Bank (PDB ID: 3P1M (127)). Only chain A was used.

PDB files for each protein were used as inputs to HADDOCK 2.4 (128,129) and the amino acids identified in cross-linking mass spectrometry studies were selected as active residues in the interaction. Given the likely conformational flexibility of Adx Lys-127, this residue and cross-links with it were not listed as active residues in the interaction. Other parameters were kept at the default settings. HADDOCK scoring weighs intermolecular van der Waals energy and empirical desolvation energy (both 1.0 multiplier) more highly than intermolecular electrostatic energy (0.2 multiplier) and interaction restraints (0.1 multiplier). Given that electrostatic interactions between P450s and ferredoxin proteins are generally considered more important than van der Waals forces (96), and the cross-linking data available, preference was given to models with low restraint and electrostatic energies, as opposed to selecting the lowest HADDOCK score model. Heme and the [2Fe-2S] cluster were added into best model from cluster 3 and 4 (prosthetic groups and co-factors are not compatible with docking software, no heme in AlphaFold structure) for measuring distances. All structures were visualized in PyMOL software (130).

2.8.2 Structure comparisons

To identify structural differences that might lead to differences in interaction with P450 27C1, CRABP-1 and CRAPB-2 sequences were aligned in UniProt with Clustal Omega (131). The surface electrostatic potential of holo-CRABP-1 and holo-CRABP-2 was calculated using the APBS plugin (132) in PyMOL (130) using existing x-ray crystallography structures (PDB: 1CBR, 1CBS)(133).

2.9 Tissue Immunofluorescence

HS#1 and HS#2 were embedded in optimal cutting temperature compound and 5 µm frozen sections were made using a cryostat. Slides were thawed and washed in PBS and then blocked with 3% BSA in PBS for 1 hr. Purified rabbit anti-P450 27C1 was used as the primary antibody at a 1:50 dilution in PBS with 3% BSA overnight at 4 °C. Alexa Fluor 555-conjugated goat anti-rabbit IgG was used as the secondary antibody at a 1:400 dilution. Slides were mounted with medium fortified with DAPI for nuclear staining. Dr. Ambra Pozzi assisted with the tissue immunofluorescence, performed imaging, and prepared the figure (Figure 15).

Formatte

Deleted:

2.10 Cell Culture

2.10.1 Primary keratinocytes

Primary cells from HS#1 and HS#2 were isolated from the epidermis (generated with dispase) by trypsin digestion. Cells were grown in EpiLife Medium with EpiLife Defined Growth Supplement (containing bovine serum albumin, bovine transferrin, hydrocortisone, rh IGF-1, prostaglandin E2, and rh EGF) according to Thermo Fisher Scientific recommended handling procedures. Primary epidermis keratinocytes (normal, human, adult) were also obtained from ATCC (PCS-200-011). These keratinocytes were grown in serum-free Dermal Cell Basal Media supplemented with a Keratinocyte Growth Kit (containing bovine pituitary extract, rh TGF-a, L-glutamine, hydrocortisone hemisuccinate, rh insulin, epinephrine, and apo-transferrin) according to ATCC recommended handling procedures. Keratinocytes from ATCC were grown for multiple passages. All cells were grown to near confluence, and then harvested for immunoblotting by scraping in 180 mM Tris HCl (pH 6.8), 2.7% SDS (w/v), 27% glycerol (v/v).

2.10.2 N/TERT keratinocytes

N/TERT-2G immortalized keratinocyte cell lines (134) were provided by Drs. Mrinal K. Sarkar and Johann E. Gudjonsson of the University of Michigan Skin Biology and Disease Resource-based Center. Two homozygous *CYP27C1* knock-out (KO) N/TERT-2G cells lines (termed *CYP27C1* KO #6 and #9) were generated using non-homologous end joining via CRISPR/Cas9 as previously described (135) (sequencing chromatogram in Figure A2). The sgRNA used for KO was CCATCCTTTATGAGAGTCGT (antisense). N/TERT-2G cells were grown in Keratinocyte SFM supplemented with BPE, EGF, $CaCl_2$ (0.3 mM), and penicillin-streptomycin. Cells were subcultured at ~50-60% confluence. Cells were imaged in plastic culture dishes using a Nikon AZ100 upright wide field microscope at 20× magnification in the Cell Imaging Shared Resource with the assistance of Dr. Jenny Schafer to document morphology of cell lines. In some experiments, after cells reached ~50% confluence, they were switched to a media containing 2.0 mM of $CaCl_2$ to stimulate differentiation, and then harvested after 2 or 6 days after treatment. Cells were cultured by Samantha M. Lisy of Dr. Manuel Ascano's lab. Cells were grown to ~90% confluence and then harvested for immunoblotting by scraping in 180 mM Tris HCl (pH 6.8), 2.7% SDS (w/v), 27% glycerol (v/v) or by trypsin digestion and resuspension in PBS (pH 7.4) with 280 mM sucrose, 10% glycerol (v/v) for *in vitro* activity assays.

2.11 Immunoblotting

Immunoblotting of tissue homogenates and cell lysates was carried out as previously described (91). Skin homogenates were prepared as previously described (91). Keratinocyte lysates were prepared in 180 mM Tris HCl (pH 6.8), 2.7% SDS (w/v), 27% glycerol (v/v) with

sonication at 10% intensity for 3 × 10 s. The protein concentration of each sample was measured using a BCA assay. Proteins were separated by SDS-PAGE and then transferred to nitrocellulose membrane. After the membranes were dry, blots were stained with SyPro Ruby Blot Stain for total protein visualization according to manufacturer's instructions and imaged using a PharosFX Plus (Bio-Rad), Typhoon FLA 7000 (GE Healthcare), or ChemiDoc MP (Bio-Rad) imager. The membranes were then blocked with Odyssey blocking buffer (PBS) (or Intercept Blocking Buffer, newer reformulation). P450 27C1 immunoblotting used a 1:200 (v/v) dilution (~1 µg/mL final) of the immunopurified rabbit antiserum (rabbit number 497) and a 1:10,000 (v/v) dilution of goat anti-rabbit IgG 800CW near-infrared (IR) dye for the secondary antibody incubation. Fluorescence signals were detected using a LI-COR Odyssey infrared imaging system (Thermo Fisher Scientific) or a ChemiDoc MP.

Chapter 3. Localization and absolute quantification of P450 27C1 and P450 redox partners

3.1 Introduction

While cytochrome P450s are often expressed in the liver, P450 27C1 appears to be specifically expressed in the skin (91). The localization of P450 27C1 to the skin is consistent with what is known about 3,4-dehydroretinoids. 3,4-Dehydroretinol is thought to be formed within the skin, and not transported there from the liver like all-*trans* retinol, given that it is not detected in the serum (16). The biosynthesis of 3,4-dehydroretinoids is specifically localized to keratinocytes of the epidermis (53,54). In these previous studies, the enzyme responsible for the formation was never identified. If P450 27C1 is this previously unidentified desaturase as hypothesized, it should co-localize with the known areas of 3,4-dehydroretinoid biosynthesis.

While the Guengerich lab previously demonstrated that P450 27C1 is expressed in the skin (91), the localization to a specific layer or cell type is not known. As discussed in Chapter 1, the skin is made up of three main layers, the epidermis, the dermis, and the hypodermis, and there are a variety of different cell types present. The general anatomy of the skin is shown in Figure 2. The layers and cell types within the skin are diverse, with each having a distinct function and difference in protein expression. I hypothesize that P450 27C1 is expressed in keratinocyte of the epidermis, given that this is where 3,4-dehydroretinoids are formed. The localization of P450 27C1 to a specific region of the skin and cell type would provide insight into its function and regulation along with enabling selection of a cellular system to study its biological function (Chapter 6).

Additionally, the quantification of P450 27C1 within the skin is of interest. The Guengerich lab has previously utilized quantitative immunoblotting for measuring the abundance of P450 27C1 in the skin (91). In immunoblotting of skin homogenates, P450 27C1 appeared as two

proteoforms, one with a M_r of ~50 kDa and one of ~55 kDa. Assuming that the antibody binds equally to each proteoform, the total concentration of P450 27C1 ranged from 17-30 pmol/mg protein in the five skin samples tested. Quantitative immunoblotting is not without limitations, outside of its dependence on a quality antibody, minor differences in procedures or materials, transfer efficiencies, and even interoperator variability can lead to irreproducible results (136,137). With the limitations of quantitative immunoblotting in mind, LC-MS/MS based absolute quantification was pursued as an alternative. In bottom-up proteomics studies, protein abundances are inferred from identified peptides (either by spectral counting or peak area). Outside of the benefit of LC-MS/MS being very sensitive (detection in femtomoles vs. the 0.1 picomole limit of detection with P450 27C1 immunoblotting (91)), multiple proteins of interest can be quantified at once utilizing parallel/multiple reaction monitoring (PRM/MRM). P450 27C1 has previously been quantified in the skin, but, to my knowledge, no one has quantified the mitochondrial redox partner proteins AdR and Adx. While *in vitro* catalytic assays with mitochondrial P450s typically utilize a 1:10:1 or similar molar ratio for AdR:Adx:P450, the actual ratios of these proteins is unknown. Determining the concentrations of the redox partner proteins in the skin will enable a better understanding of physiological conditions for mitochondrial P450 catalysis.

Absolute quantification via LC-MS/MS requires a suitable reference standard. In this work, I have generated a quantitative concatemer (QconCAT) for the measurement of select extrahepatic P450s (specifically P450 27C1 of the skin, and steroidogenic P450s of the adrenal gland) and the microsomal and mitochondrial P450 redox partners. The QconCAT technique (Figure 14, protocol in (138)) involves expressing an artificial protein containing proteotypic signature peptides for proteins of interest in *E. coli* with media with isotopically labeled amino acids. The QconCAT can be quantified and then digested and analyzed with the analyte proteins of interest. Ion intensities

(from both unlabeled and heavy-labeled peptides) are measured in LC-MS/MS analysis and are used to calculate the absolute amount of each protein in the sample. This approach has previously been utilized with drug-metabolizing cytochrome P450s (139).

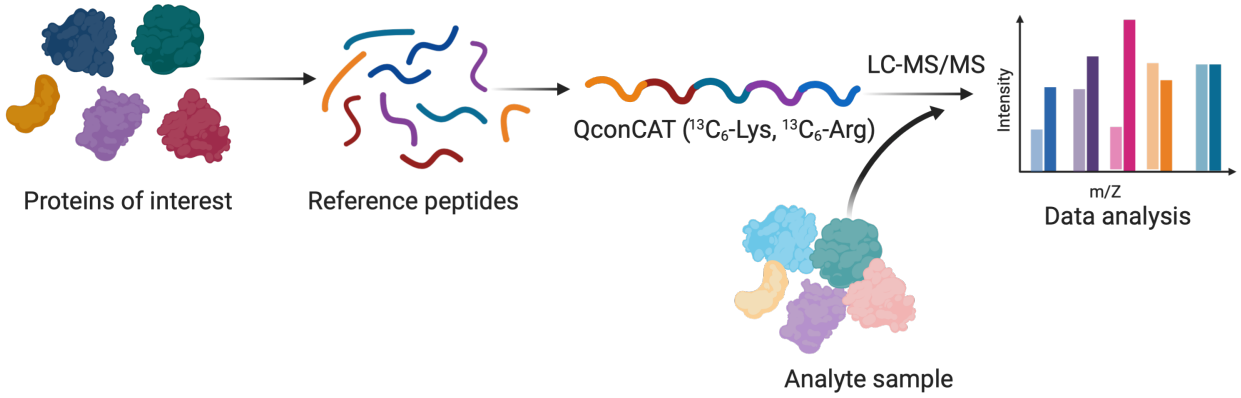

Figure 14. Principle of QconCAT quantification experiment. Proteins of interest (P450 27C1, AdR, Adx, POR, and b_5) are quantified within analyte samples (i.e. skin homogenates). Two signature peptides from each protein are assembled into an artificial QconCAT protein. Purified and quantified heavy-labeled QconCAT is mixed with the analyte samples and digested. The absolute amount of each protein can be determined by comparing heavy:light intensities in MS analysis. Figure created in Biorender.com.

This study utilizes tissue immunofluorescence, primary cell culture, and immunoblotting to localize P450 27C1 to the keratinocytes of the epidermis. Further, P450 27C1 and the P450 redox partners are quantified within the skin and keratinocytes utilizing a targeted LC-MS/MS based approach.

3.2 Results

3.2.1 P450 27C1 is expressed in keratinocytes of the epidermis

The localization of P450 27C1 within the skin was visualized with tissue immunofluorescence (Figure 15). Immunohistochemistry was also attempted but the localization

of P450 27C1 could not be determined given the high background signal in the secondary antibody only control (Figure A3). The DAPI nuclear staining patterns allows for identification of specific regions of the skin. The uppermost layer of the epidermis, the stratum corneum, is made up of dead cells without nuclei, while the deepest layer of the epidermis, the stratum basale, contains proliferating (nucleated) cells. The dermis is predominantly made up of connective tissue and nucleated cells are distributed throughout. P450 27C1 appears to be specifically localized to the basal cell layer of the epidermis, given the increased signal in nucleated cells immediately above the dermis (Figure 15).

Formatte

Deleted:

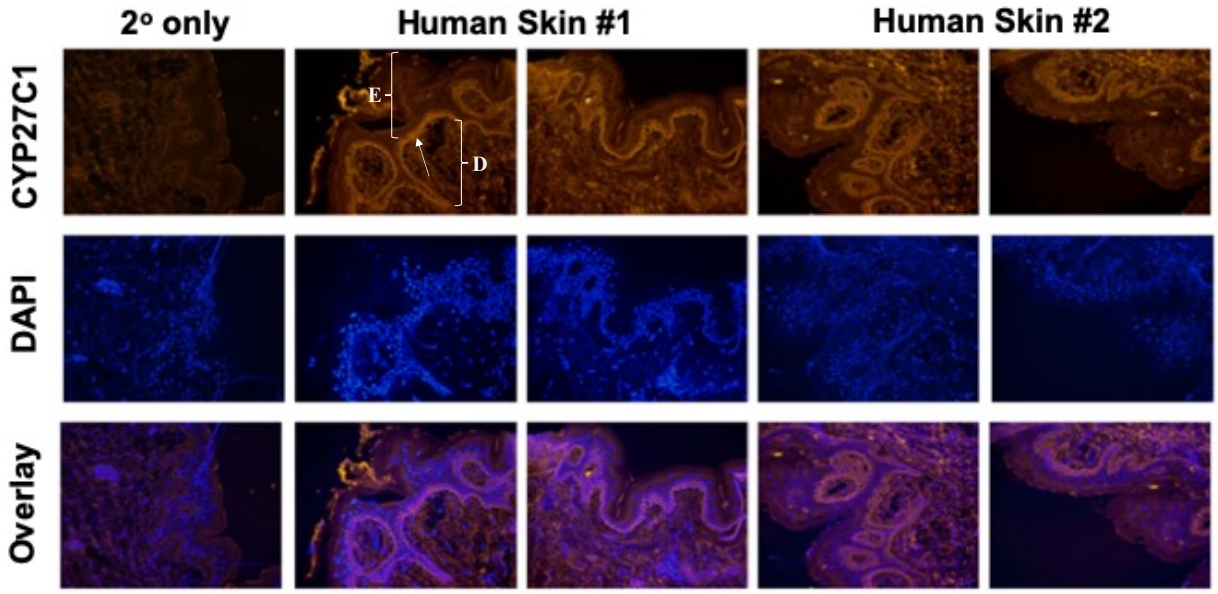

Figure 15. Tissue immunofluorescence analysis of P450 27C1 in the skin. Sections (5 µm) were cut from skin frozen in OCT compound. A 1:50 dilution of rabbit anti-P450 27C1 was used and a 1:400 dilution of goat anti-rabbit Alexa Fluor 555 was used for visualization. Slides were mounted with medium fortified with DAPI for nuclear staining. Top row: Alexa Fluor 555 signal; middle row: DAPI nuclear stain; bottom row: combined images. Secondary antibody only control is shown in the first column. Other columns show two sections from separate donors. For orientation to the skin layers, labels are added with brackets to one panel (E, epidermis; D, dermis) along with an arrow indicating the area of P450 27C1 expression. Imaging and initial figure preparation was performed by Dr. Ambra Pozzi.

Localization of P450 27C1 to the epidermis was verified by performing immunoblotting on separated epidermis and dermis (Figure 16). Immunoreactive bands are only observed in the epidermis homogenate, supporting the localization observed with tissue immunofluorescence. The basal cell layer of the epidermis is comprised mainly of keratinocytes. To directly assess if keratinocytes were expressing P450 27C1, immunoblotting was performed with lysates from keratinocytes isolated from HS#1 and HS#2 samples and primary keratinocytes from ATCC. Immunoreactive bands for P450 27C1 were observed in all primary keratinocyte cell lysates (Figure 16). There were bands observed at both ~50 kDa and ~55 kDa M_r like previous results with human skin, but bands were observed as doublets (two at ~50 and two at ~55 kDa).

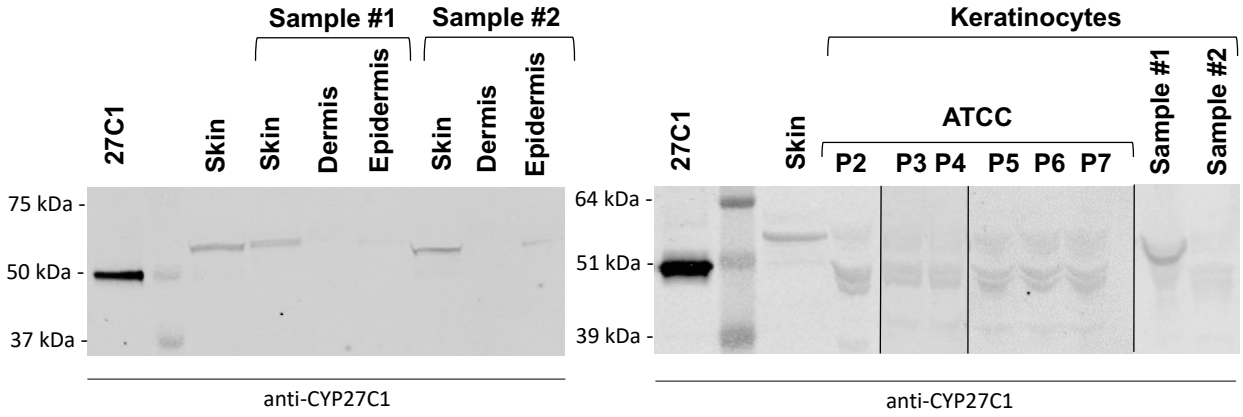

Figure 16. Immunoblotting of P450 27C1 within the skin. *A*, Immunoblot of P450 27C1 in layers of the skin. *B*, Immunoblot of P450 27C1 in primary keratinocyte lysates. Purified recombinant P450 27C1 is shown as a reference. Each lane contains 50 µg of total protein as determined by a BCA assay. Black lines indicate splicing of multiple blots.

3.2.2 QconCAT generation

Unique tryptic peptides from P450 27C1, the P450 redox partners, and adrenal P450s were assembled into a QconCAT (construct in Figure 11). The QconCAT sequence was optimized for expression in *E. coli* and grown in minimal media containing $^{13}C_6$-lysine and $^{13}C_6$-arginine.

Inclusion bodies were isolated, solubilized, and then the QconCAT was purified by Ni-NTA. Purity was assessed by SDS-PAGE (Figure 17*A*) and complete construct was verified by proteomic analysis of in-gel trypsin digested QconCAT (Figure 17*B, C*). The QconCAT was identified with 87% sequence coverage from IDPicker searches of LC-MS/MS data. Identification of peptides at the N- and C-termini indicate complete expression of the construct.

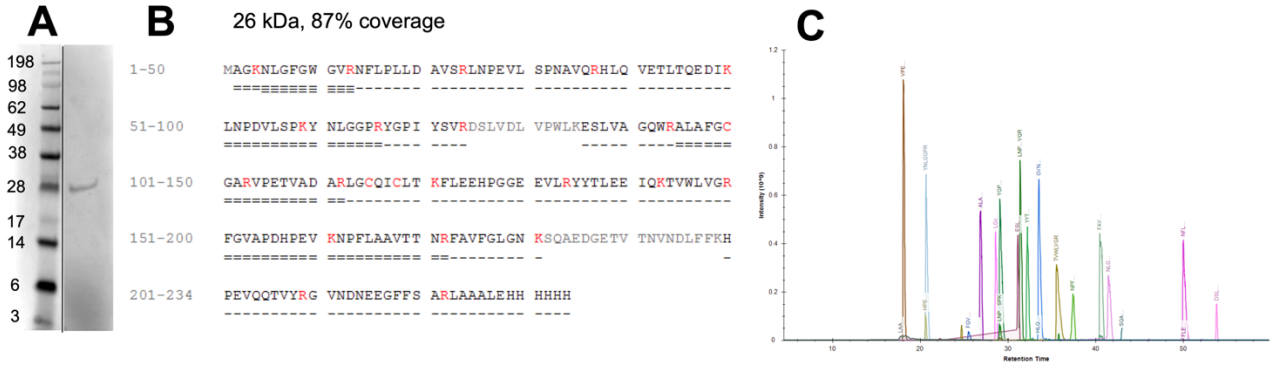

Figure 17. Purification of QconCAT. *A*, SDS-PAGE illustrating purity of heavy QconCAT following Ni-NTA purification from solubilized inclusion bodies and dialysis. *B*, Coverage of heavy QconCAT obtained from IDPicker searches of LC-MS/MS data against the *E. coli* UniProt database with QconCAT sequence. *C*, Example elution profile of QconCAT peptides in Skyline.

High incorporation of the heavy amino acids is necessary for QconCAT generation to minimize signal from light peptides not associated with analyte samples. Labeling efficiencies were calculated from Skyline peak integration of purified heavy QconCAT analyzed by LC-MS/MS. Example peaks are shown in Figure 18*A*. The incorporation efficiency of lysine was 95 ± 3% and arginine was 92 ± 1% (average ± SD across peptides) (Figure 18*B*). These levels are sufficient for quantitative assays.

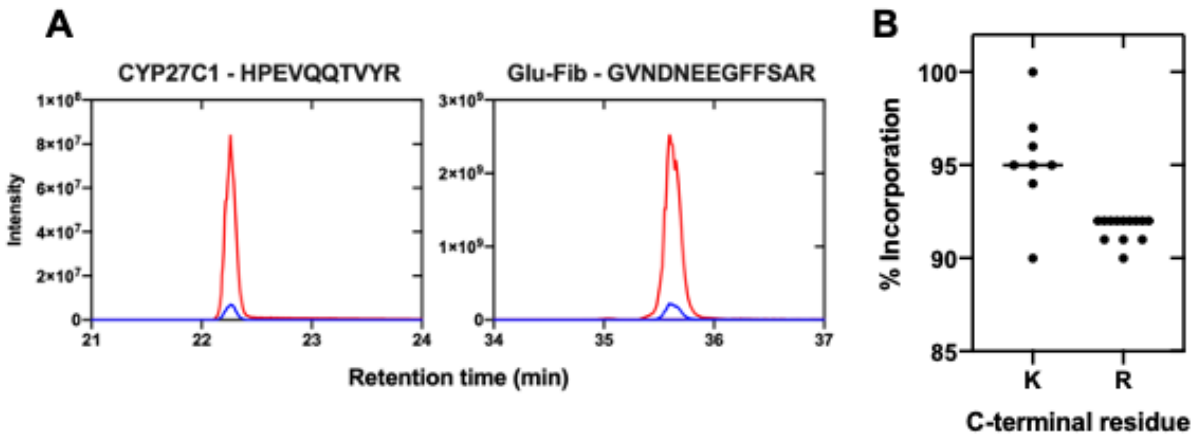

Figure 18. QconCAT $^{13}C_6$-arginine and $^{13}C_6$-lysine incorporation. *A*, Example elution profile of labeled QconCAT peptide HPEVQQTVYR for P450 27C1 and GVNDNEEGFFSAR for the modified Glu-Fibrinopeptide B. *B*, Percentage incorporation of $^{13}C_6$-lysine (K) and $^{13}C_6$-arginine (R) determined from the ratio of peak areas of heavy to light peptides when purified digested heavy QconCAT was analyzed by LC-MS/MS.

The peak intensity from the QconCAT should scale linearly with the amount of QconCAT present. Tryptic peptides profiles were assessed by mixing unlabeled and labeled QconCAT protein in various ratios (10:0, 9:1, 7:3, 5:5, 3:7, 1:9, and 0:10 (v/v)) before in-gel tryptic digestion. Peak intensities from each peptide were analyzed in Skyline. Quantification was as expected from the prepared ratios (Figure 19).

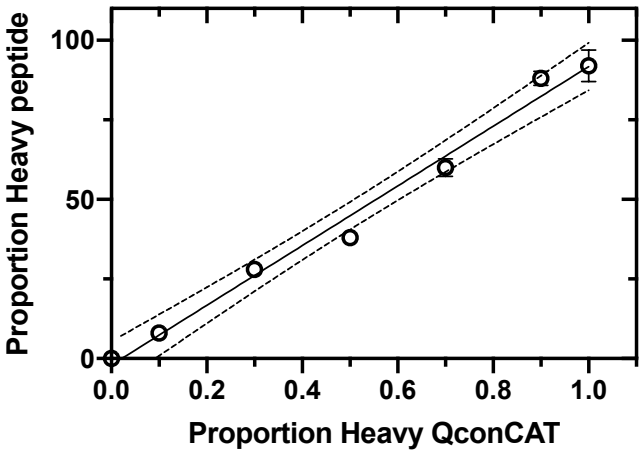

Figure 19. Mixed H/L QconCAT peptide quantification. The measured proportion of the heavy peptide area is plotted relative to the proportion of heavy protein in the mixture (v/v) for the average ± S.D. of 20 peptides. Dotted lines show the 95% confidence limits for the fitted line. Experiment completed in singlet.

3.2.3 Selection of sample preparation method for absolute quantification and validation

To perform accurate quantification, complete digestion of the QconCAT and analyte proteins of interest and recovery of the peptides is essential. Four potential sample preparation methods were tested to determine which resulted in best sample digestion and was most suitable for the detection of analyte proteins of interest: in-gel fractionation, in-gel clean-up, FASP, and S-Trap. A Top 4 DDA with a PRM method was utilized to enable detection of the lower abundance analyte proteins of interest. To determine the total number of proteins and peptides detected in each method, data searching was performed with IDPicker. Quantification of analyte peptides of interest was performed in Skyline. Based on the level of the total ion chromatogram of each sample, the S-Trap method resulted in the highest concentration of peptides (NL 1.28E10 vs. NL low-mid E9 levels with other methods). S-Trap resulted in the highest number of protein and peptide identifications (567 proteins, 1738 peptides) in comparison with in-gel clean-up (162 proteins, 667 peptides), separate analysis of the low and high molecular weight regions from in-

gel fractionation (106 proteins, 305 peptides for low molecular weight; 176 proteins, 733 peptides for high molecular weight), and FASP (273 proteins, 510 peptides). There is high overlap in the proteins identified by each total protein method, though there are still select proteins identified in only one sample preparation method (Figure 20*A*). Given this, it is also important to check for analyte peptides of interest in each sample. Peptides for all the proteins of interest were detected in the S-Trap sample, while less were detected with the FASP and in-gel methods. For the one peptide that was detected in all sample preparation methods (VPETVADAR of Adx), peak areas with the S-Trap were also higher than the other methods (Figure 20*B*).

A

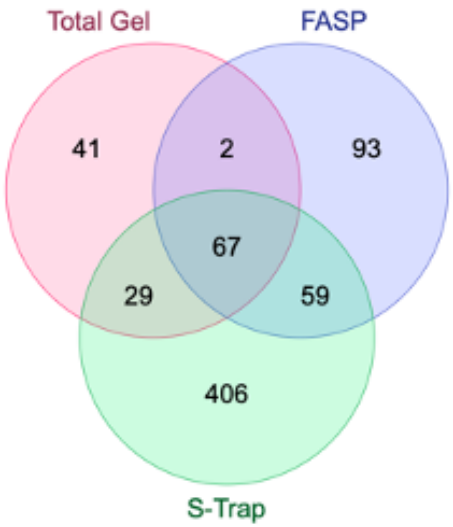

B

Method	Normalized Signal (Area/µg total protein)	
	Light	Heavy
In-gel (total)	1.54E+05	1.91E+06
In-gel (low MW)	2.23E+06	N.A.
FASP	8.64E+06	1.01E+08
S-Trap	1.08E+07	1.12E+08

Figure 20. Comparison of protein identification by sample preparation method. *A*, Overlap between the number of proteins identified in Top 4 analysis of the HS#2 homogenate are illustrated in a Venn diagram with the total gel, S-TRAP, and FASP sample preparation methods. *B*, Comparison of Adx peptide VPETVADAR peak area with gel fractionation (low molecular weight region), total gel, S-TRAP, and FASP methods. Peak areas are normalized to the hypothetical injected total protein amount. N.A. = not applicable - QconCAT was not added to fractioned in-gel samples.

The calculated concentration of P450 27C1 and P450 redox partners within the skin is only accurate if the analyte sample is representative of the tissue. The hypodermis layer was removed before homogenization, so proteomic data (Top 20 analysis of S-Trap preparation) was analyzed for the presence of specific markers of the dermis and layers of the epidermis. The most prevalent proteins (by number of filtered spectra) were keratins and collagens, as expected for skin. Proteins described as specific markers are listed in Table 4 (140,141). Expected markers for the epidermis (stratum basale, stratum spinosum, and stratum granulosum) and dermis were detected. Proteins that have been previously described to have enriched expression in the stratum corneum (CDSN, SERPINB7, KLK5, KLK11, SRPP4, ALOX12B) were not detected.

Table 4. Identification of specific markers of layers and cell types of the skin in HS#2 homogenate.

Localization	Protein(s)	Detected?
Skin Layer		
Epidermis	Keratin, type II cytoskeletal 1 (KRT1)	+
	Keratin, type I cytoskeletal 14 (KRT14)	+
Dermis/Subcutis	Collagen alpha-1(III) chain (COL3A1)	+
Sublayers		
Stratum basale	Keratin, type I cytoskeletal 15 (KRT15)	+
Stratum spinosum	Galectin-7 (LGALS7)	+
Stratum granulosum	Filaggrin (FLG)	+
Stratum corneum	CDSN, SERPINB7, KLK5, KLK11, SPRR4, ALOX12B	-

3.3 Discussion

In tissue immunofluorescence (Figure 15) and immunoblot analysis (Figure 16), P450 27C1 appears to be specifically localized to basal keratinocytes of the epidermis. Localization of P450 27C1 within the skin in tissue immunofluorescence is based on assignment of regions based on DAPI nuclear staining. Assignment could be strengthened by performing immunofluorescence

analysis of other markers (i.e., see layer specific markers in Table 4). The localization of P450 27C1 to the epidermis and keratinocytes specifically is consistent with what is known about 3,4-dehydroretinoid formation within the skin (53,54).

It has previously been shown that 3,4-dehydroretinoid formation is highest in differentiated keratinocytes in culture (54). This is inconsistent with the tissue immunofluorescence results, which show P450 27C1 is expressed in cells within the basal layer of the epidermis. The cells here are proliferating, not differentiating. This may be due to the differences of keratinocytes in culture and keratinocytes *in vivo*. There are well documented differences in keratinocyte retinoid response specifically in culture compared to what occurs *in vivo* (142). For example, retinoids suppress terminal differentiation in culture, but stimulate keratinocyte proliferation *in vivo*. It may be possible that, *in vivo,* P450 27C1 is expressed in basal proliferating keratinocytes but in culture it is expressed in differentiating keratinocytes. Primary keratinocytes in this work were cultured in low calcium media, which results in proliferating keratinocytes. P450 27C1 expression was detected in these keratinocytes (Figure 16), but the possibility for expression to be higher in differentiated keratinocytes cannot be ruled out. This could be addressed by performing immunoblotting with lysates from primary keratinocytes treated with high calcium media.

On a subcellular level, P450 27C1 is thought to be localized to the mitochondria. The localization assignment is based on the requirement of P450 27C1 for the mitochondrial P450 redox partner proteins, AdR and Adx, for catalysis (88) and its amino acid sequence (91). Localization has not been illustrated experimentally. Cell immunofluorescence with primary keratinocytes was attempted to assess this but was inconclusive due to high background signal (data not shown). Localization could also be assessed by immunoblotting subcellular fractions isolated by differential centrifugation. Given the difficulty of growing the large amounts of

primary keratinocytes required for subcellular fractionation, trial transfections of HEK293 cells with *CYP27C1* were performed. Unfortunately, P450 27C1 was not expressed in multiple trials so this approach was not pursued further (data not shown). With optimization, both cell immunofluorescence and immunoblotting of fractions from differential centrifugation could be viable methods to illustrate the subcellular localization of P450 27C1.

Multiple proteoforms of P450 27C1 have been detected in immunoblot analyses (Figure 5, Figure 16). In Ensembl, *CYP27C1* is listed as having two transcripts (splice variants), one of which is 4401 bps and the other is 2092 bps, but both result in 372 residue translated proteins, and no alternative transcript start sites have been annotated (143) (ENSG00000186684). Because of this, the proteoforms observed are likely due to post-translational modification. Mitochondrial P450s are cytoplasmically synthesized and then cleaved when they are inserted into the mitochondrial membrane (97). Based on previous proteomic analysis of human skin, the larger protein is assigned as the full-length sequence and the smaller protein is assigned as an N-terminal truncation, putatively after insertion into the mitochondria (91). There are additional immunoreactive bands detected in primary keratinocytes (Figure 16, more than the usual two detected in skin Figure 5). The identity of these additional bands is unknown. P450 27C1 may have additional post-translational modifications. Mitochondrial proteins have been shown to be phosphorylated, O-glycosylated, acetylated, and succinylated (144). Some P450 enzymes are directed to the mitochondria in response to phosphorylation and phosphorylation has been shown to strengthen interactions between some P450s and Adx (reviewed in (145)). Additional investigation is required to assign identifications and functional relevance to the proteoforms observed in immunoblotting.

A heavy-labeled QconCAT for the quantification of P450 27C1 and the four P450 redox partners, POR, AdR, Adx, and b_5, was successfully expressed and purified (Figure 17, Figure 18).

The failure rate for QconCAT expression is suggested to be around 20% (not including problems with labeling inefficiency) (117). While there are no results for absolute quantification presented here, the development of the QconCAT is still a significant undertaking. The development of this QconCAT will enable future quantification of P450 27C1 and redox partners within the skin, layers of the skin, and in keratinocytes. The abundance of each protein can be calculated using Eq. 9 as previously described (117). In this equation $A_{Protein}$ is the calculated protein abundance in the starting material measured in pmol mg^{-1} total protein, $C_{Glu\text{-}Fib}$ is the concentration of the light Glu-Fib spiked into the resuspension, *H.Glu-Fib/L.Glu-Fib* is the ratio of heavy (QconCAT-derived) Glu-Fib to light Glu-Fib (spiked standard), *L.Peptide/H.Peptide* is the ratio of light (analyte sample-derived) to heavy (QconCAT-derived) peptide, V is the resuspension volume, and $C_{TotalProtein}$ is the amount of protein in the analyte sample utilized for digestion.

$$A_{Protein} = C_{Glu-Fib} \times \frac{H.Glu-Fib}{L.Glu-Fib} \times \frac{L.Peptide}{H.Peptide} \times V \times C_{TotalProtein} \qquad \text{Eq. 9}$$

To my knowledge, the S-Trap has not previously been utilized to assess the skin proteome. Quantification of P450 27C1 in skin homogenates can be compared with results from quantitative immunoblotting (91). Previous quantitative proteomic analyses of the skin are limited. There is one study that has reported a concentration for POR utilizing label-free quantification (4.46 ± 0.77 pmol mg^{-1}) (146). Results from QconCAT analyses can be compared directly with this value. Quantification of the other P450 redox partners proteins within the skin has not been reported to my knowledge. Quantifying these proteins is not only important for determining the physiologically relevant concentrations of redox partners for P450 27C1. Other P450s are expressed in the skin (reviewed in (147)) and these values are also relevant for studies with these enzymes.

3.4 Conclusions

P450 27C1 is localized to basal keratinocytes of the epidermis based on immunofluorescence and immunoblotting analyses. Multiple proteoforms of P450 27C1 are present within the cell, but the identity and function of the individual proteoforms remains unknown. The generation of a QconCAT for detection of P450 27C1 and the P450 redox partners enables absolute quantification of these proteins within the skin.

Chapter 4. Binding of cytochrome P450 27C1, a retinoid desaturase, to its accessory protein adrenodoxin

Portions of this chapter are adapted from "Functional interactions of adrenodoxin with several human mitochondrial cytochrome P450 enzymes" published in *Archives of Biochemistry and Biophysics* and has been reproduced with the permission of the publisher and my co-authors Stella A. Child, Michael J. Reddish, Margo H. Goldfarb, and Ian R. Barckhausen. Other portions of the chapter are from a manuscript currently submitted and in revision with co-author Stephany N. Webb.

Child, S.A., Reddish, M.J., Glass, S.M., Goldfarb, M.H., Barckhausen, I.R., Guengerich, F.P. (2020) "Functional interactions of adrenodoxin with several human mitochondrial P450 enzymes". *Arch. Biochem. Biophys.* **694**, 108596.

Glass, S.M., Webb, S.N., Guengerich, F.P. "Binding of cytochrome P450 27C1, a retinoid desaturase, to its accessory protein adrenodoxin." *Arch. Biochem. Biophys.*(in revision)

4.1 Introduction

P450 oxidation reactions require the donation of two electrons. There are two systems of proteins that can provide these electrons to human P450s, depending on the subcellular localization: the microsomal POR and b_5 system and the mitochondrial AdR and Adx system. AdR is a flavoprotein that transfers electrons from NADPH to Adx, a small, ~12 kDa, [2Fe-2S] cluster protein which can then subsequently transfer electrons to the mitochondrial P450s. Of the 57 human P450 enzymes, seven (P450s 11A1, 11B1, 11B2, 24A1, 27A1, 27B1, and 27C1) are intrinsically mitochondrial and utilize the AdR and Adx proteins for electron transfer (97). The mitochondrial P450s metabolize endogenous substrates throughout the body: P450 11A1 converts cholesterol to pregnenolone, P450 11B1 and 11B2 generate cortisol and aldosterone, P450 24A1 and 27B1 hydroxylate vitamin D_3, P450 27A1 is involved in the biosynthesis of bile acids, and P450 27C1 desaturates retinoids (vitamin A) (88,97,148).

Studies of mitochondrial P450 reactions have utilized a variety of experimental conditions. Many studies with Adx have been and are currently done with the bovine protein, given that this

protein could be isolated before heterologous expression of human Adx was possible (149-153). Some mitochondrial P450s, like 11B2, have had catalytic assays performed with both recombinant human (113,154,155) and bovine (104,156,157) sources of Adx. For steady-state kinetic assays, the Adx:P450 ratio has varied from 8:1 (155) to 60:1 (154) with Adx concentrations ranging from 1 μM (104) to 30 μM (156). Differences in results have been observed across studies, and the contribution of varying Adx constructs and/or concentrations to these discrepancies is unknown.

Both bovine and human Adx are able to interact with human mitochondrial P450s. The interaction between mitochondrial P450s and Adx is dominated by electrostatic interactions (96). Adx is generally thought to bind via its F-helix to the proximal surface of P450s, specifically to positively charged residues of the K-helix. Both of the existing P450-Adx fusion structures (P450s 11A1 (158) and 11B2 (99)), have Adx in this position. Outside of the generally conserved interaction interface, there is variability among the P450s with some having additional identified interactions. Due to the contribution of electrostatic forces to Adx interactions, the interactions between Adx and AdR and mitochondrial P450s are ionic strength dependent (113,153,159).

There are multiple models for the mechanism of electron transfer between the three proteins. The predominant model is the shuttle mechanism, where oxidized Adx binds to AdR, dissociates after being reduced, and then binds to the P450 and transfers the electron (153,160) (Figure 21). There is also a modified shuttle mechanism, where an Adx dimer is involved instead of a monomer (149). The ability of Adx to form functional dimers has been proposed (161,162). A ternary complex has also been proposed, with Adx interacting with both AdR and the P450 (163), as well as a quaternary complex involving two Adx proteins and one AdR and P450 (164). Crosslinking studies with P450 11B1 or 11B2 with Adx describe the interaction of the P450 with a dimer of Adx (113). An Adx dimer has also been proposed to interact with P450 24A1 based on

Formatte

Deleted:

the large binding interface detected by NMR (100). On the other hand, cross-linking studies with P450 11A1 and Adx suggest interaction with a monomer (165). Mechanisms may vary depending on the P450 involved.

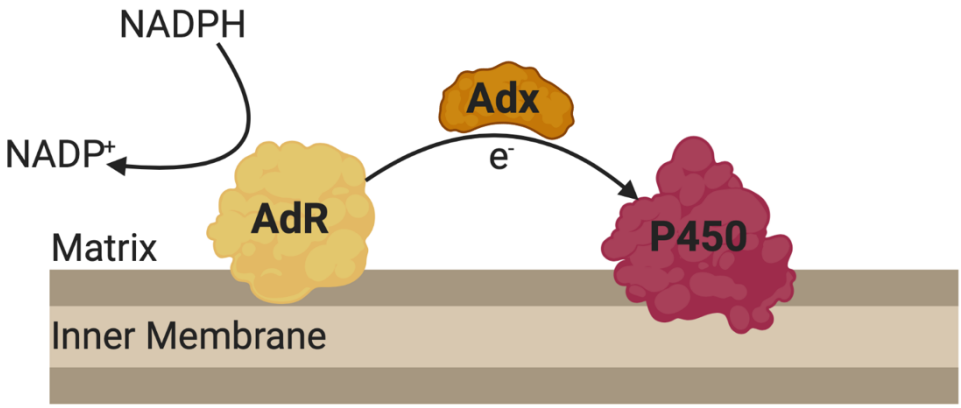

Figure 21. Shuttle mechanism for AdR-Adx mediated electron transfer to mitochondrial P450s. AdR generates electrons from NADPH. Electrons from AdR are transferred to Adx and then to the P450. Figure created in BioRender.com.

P450 redox partners can be allosteric effectors of P450 activity in addition to their roles as electron donors. Perhaps the most well studied example of this is P450 17A1 and b_5, where it has been proposed that b_5 can stimulate the 17,20-lyase reaction by facilitating a conformational change of the P450 (98,101,166). Allosteric stimulation by b_5 has also been observed with many other P450s (reviewed in (103)) and there is also some evidence for allosteric modulation with POR (167,168). In the past decade, there have been multiple reports characterizing the potential allosteric role of Adx with mitochondrial P450s. P450 11B2 substrate binding was promoted by Adx (99,104). In contrast, Adx binding to P450 24A1 reduced substrate binding affinity while stabilizing the enzyme-substrate complex and altering substrate positioning within the active site (100,102,169) and the P450 11A1-Adx fusion protein did not exhibit higher binding affinity for

its substrate, unlike P450 11B2-Adx (99,158). Adx has also been proposed to be an effector for oxygen transfer to P450 27B1 (105). If Adx binding to the P450 affects substrate binding, substrate binding should also affect Adx binding to the P450, as the sum of these binding steps should be energetically equivalent based on the thermodynamic box principle (170). Yablokov *et al.* have reported that the presence of substrate can also modulate the P450-Adx interaction in the cases of P450 11A1, 11B1, and 11B2 and that this effect this is P450- and substrate-specific (171). Mutually facilitated Adx and substrate binding has been observed with P450 11A1 and P450 27B1 (172,173). P450 24A1 ligand interactions can also affect Adx recognition (174).

Overall, work surrounding the nature of interactions between Adx and mitochondrial P450s has pointed to numerous differences depending on the P450 in question. Additionally, direct comparison between some studies is hindered due to lack of knowledge as to how the species or concentration of Adx utilized affects results. In comparison to other mitochondrial P450s, very little is known about the nature of the interaction between P450 27C1 and Adx. P450 27C1 is an all-*trans* retinoid desaturase expressed in the skin (88,91) and is the only human mitochondrial P450 for which there is no structural information describing the interaction with Adx. The Guengerich lab has previously measured the rate of P450 27C1 reduction by Adx (3.6 min^{-1} with substrate present) (91), but additional details about the complex are not known. In this work, the ability of P450 27C1 to interact with bovine and human Adx was assessed along with investigation of the nature of the P450 27C1-Adx complex and potential allosteric effects of Adx binding to P450 27C1.

4.2 Results

4.2.1 P450 27C1 catalytic activity dependence on Adx concentration and construct

Steady-state kinetic measurements were made to compare the effectiveness of human and bovine Adx to support P450 27C1. The concentration of P450 27C1, substrate, and bovine AdR were fixed. The concentration of Adx was varied to examine the concentration-dependence of the observed catalytic rate (Figure 22). The observed reaction rate increased with Adx concentration until a maximal rate was achieved, as expected. This relationship was hyperbolic in nature and data was fit using a typical Michaelis-Menten equation for enzyme kinetics. This application is somewhat unusual, as this equation typically treats the small molecule being oxidized as the substrate in the reactions. In this case, the reduced Adx acts as the rate-limiting co-substrate, so it can be treated as the dependent-substate variable in a Michaelis-Menten analysis. This treatment allows for a comparison of the maximal rate achieved by the enzyme (k_{cat}), the sensitivity of the reaction to Adx concentration ($K_{m,app}$), and the overall efficiency of the reaction with respect to Adx concentration ($k_{cat}/K_{m,app}$). For P450 27C1, the k_{cat} was 0.79 min^{-1}, the $K_{m,app}$ was 1 μM, and the $k_{cat}/K_{m,app}$ was 0.8 $\mu M^{-1}min^{-1}$ with both bovine and human Adx.

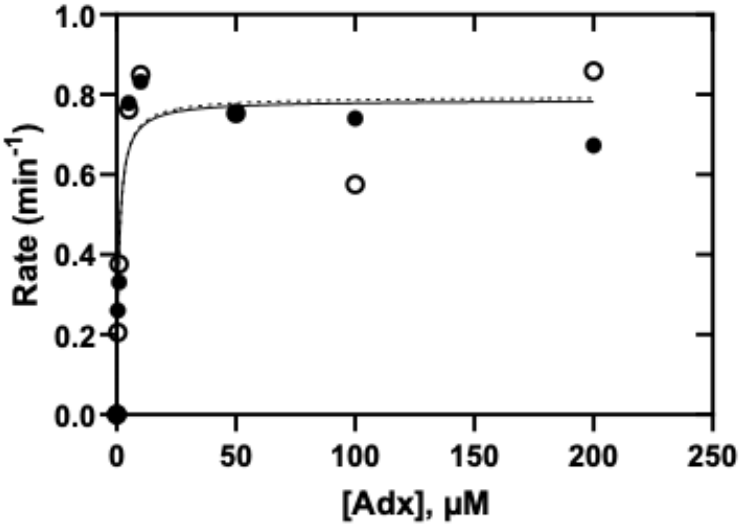

Figure 22. Support of P450 27C1-mediated all-*trans* retinol desaturation by varying concentrations of bovine and human Adx. Bovine (○---○) or human (●—●) Adx (0-200 µM) was utilized in assays for P450 27C1 all-*trans* retinol desaturation. Data are shown as points with hyperbolic fit to the data shown with the lines.

4.2.2 Estimate of P450 27C1-Adx binding affinity by MST

MST was used to measure the dissociation constants (K_d) describing the interaction of both human and bovine Adx with P450 27C1 and bovine AdR. In these experiments, Adx used was labeled with a fluorophore by conjugation of an NHS-ester to a free amine, kept at a constant ratio. The concentration of the enzyme was varied within the experiment. Each MST data set was fit to a single-site binding model assuming a 1:1 stoichiometry (Figure 23). The inter-day amplitudes of isotherms varied significantly so multiple trials were averaged for data analysis. K_d values were averaged between replicates with error propagation. For P450 27C1, binding to bovine Adx was favored 7-fold (30 ± 10 nM vs. 220 ± 70 nM) and for AdR, bovine Adx was favored 4-fold (10 ± 4 nM vs. 40 ± 20 nM).

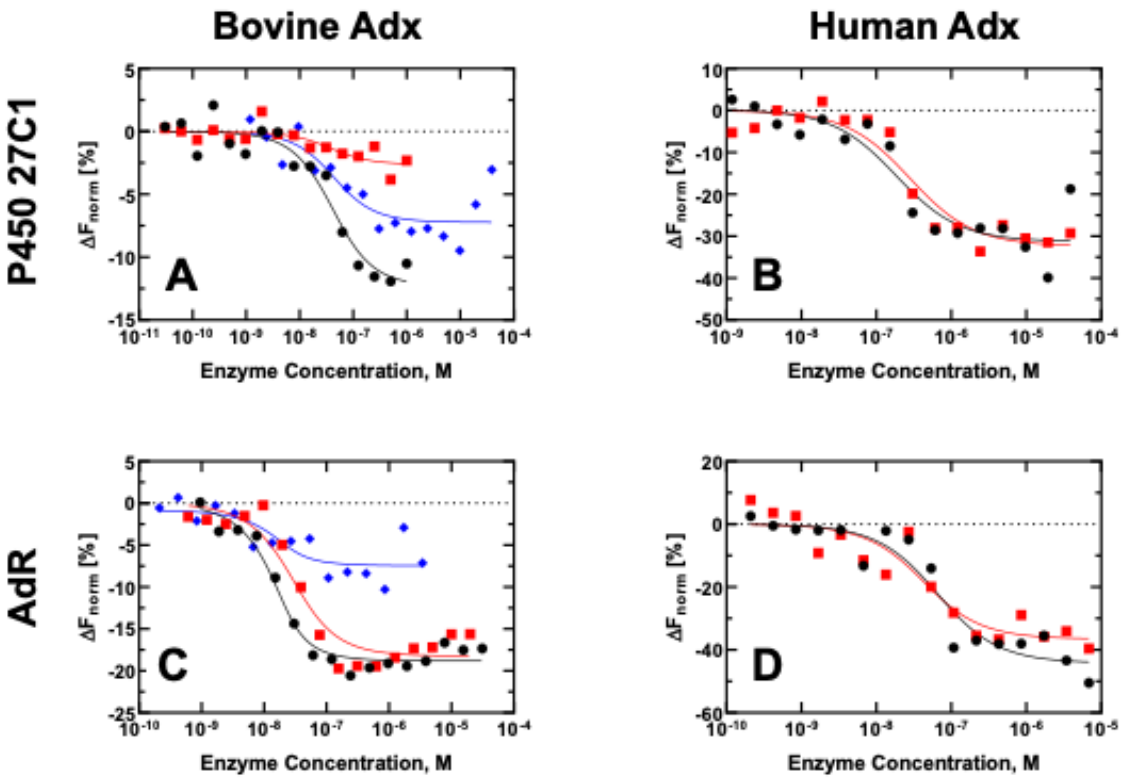

Figure 23. MST data for binding of P450 27C1 and AdR with Adx. Binding of P450 27C1 (*A, B*) and AdR (*C*, *D*) with bovine (*A*, *C*) and human (*B*, *D*) Adx. Each trace, shown with different colors, is a different independently determined experiment. The fit is a modified quadratic based on a single-binding site model, provided by the NanoTemper MST Analysis Software.

4.2.3 Selection of Alexa Fluor 488 for fluorescent-labeling of Adx

As an alternative to MST, fluorescence titrations with labeled Adx were also performed. Given the similarity in catalytic assays results and binding affinity from MST with bovine and human Adx, only human Adx was utilized here. Three cysteine-reactive dyes—acrylodan, IAEDANS, and Alexa Fluor 488 C_5 maleimide—were used to label human Adx. The absorbance and fluorescence properties of each dye-Adx conjugate were assessed. All three dye-Adx conjugates displayed the expected fluorescence spectrum based on known properties of the dye, indicating successful labeling (Alexa Fluor 488-Adx in Figure 24, other data not shown). Only the Alexa Fluor 488-Adx resulted in clear changes in the emission spectra upon P450 27C1 binding

(Figure 24, other data not shown), so this dye conjugate was utilized for further studies. Coupling of Alexa Fluor 488 with Adx was also efficient, with ≥ 93% labeling.

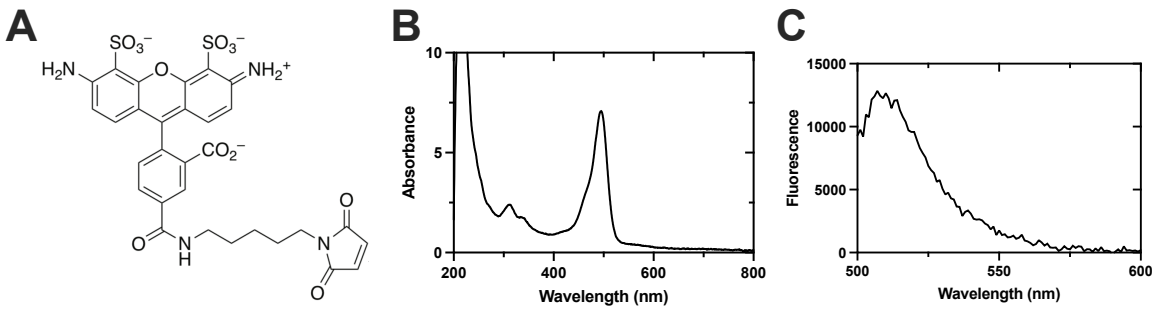

Figure 24. Spectral properties of Alexa Flour 488-Adx. *A*, Dye structure; *B*, dye-Adx absorbance spectrum (87 µM Alexa Fluor 488-Adx, NanoDrop); *C*, dye-Adx fluorescence spectrum (43.5 nM Alexa Fluor 488-Adx) in 100 mM potassium phosphate (pH 7.4) (ex: 493 nm). Labeling efficiency was calculated to be ≥ 93%.

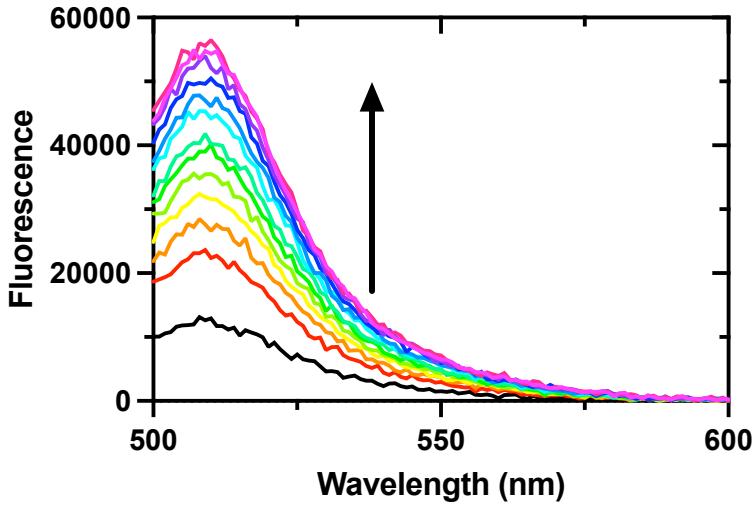

Figure 25. Representative spectra from titration of P450 27C1 with Alexa Fluor 488-Adx. Excitation of Alexa Fluor 488-Adx was at 493 nm. The fluorescence at the emission maximum increased with increasing concentrations of P450 27C1. The titration was performed in 100 mM potassium phosphate (pH 7.4) with 50 nM of Alexa Fluor 488-Adx and 0-0.29 µM (0, 0.0086, 0.017, 0.026, 0.034, 0.052, 0.069, 0.086, 0.12, 0.15, 0.19, 0.22, 0.29 µM) of P450 27C1.

The fluorescence of Alexa Fluor 488-Adx was linear over a large range (Figure 26) and labeling Adx with Alexa Fluor 488 did not negatively affect the electron transfer capabilities of Adx to P450 27C1 (Figure 27). While Adx has five cysteine residues, the labeling calculation and presence of a single Alexa Fluor 488 modification by proteomic analysis suggests only one cysteine is labeled (Figure 28).

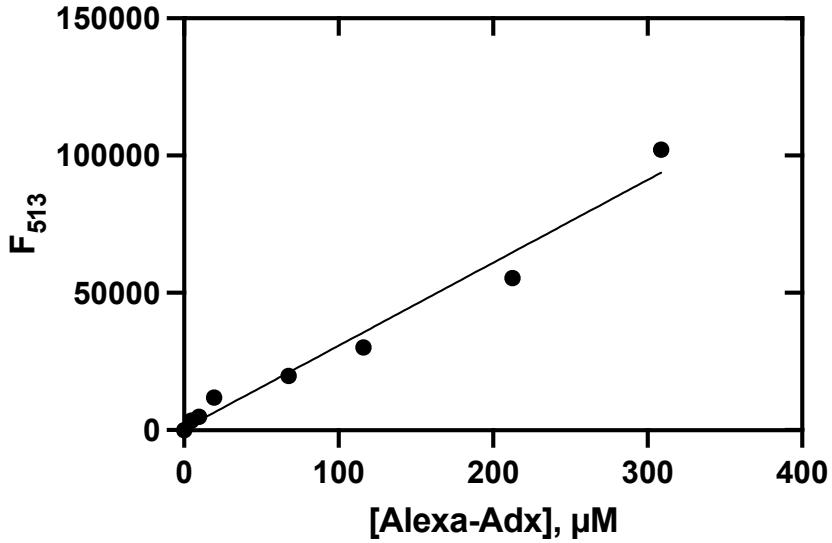

Figure 26. Linearity of fluorescence response of Alexa Fluor 488-Adx. The fluorescence emission intensity at 513 nm was extracted from full emission spectra measured as increasing concentrations of Alexa Fluor 488-Adx were titrated into the cuvette. Data was fit by linear regression in GraphPad Prism ($R^2 = 0.974$).

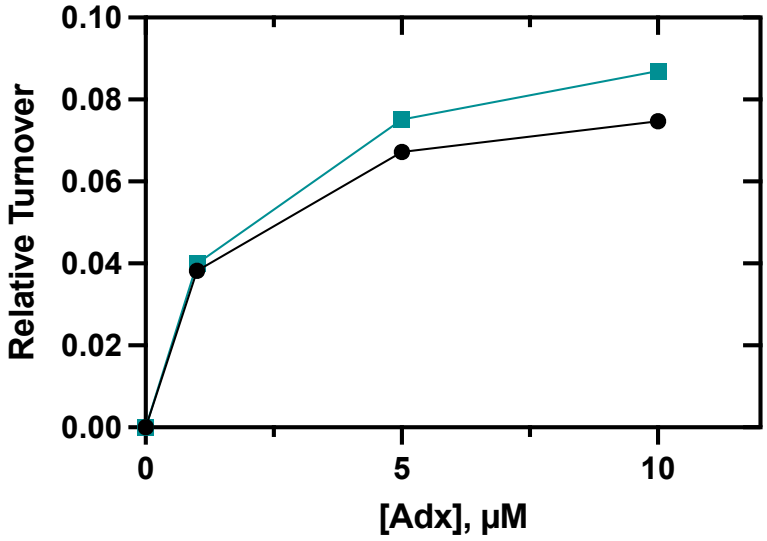

Figure 27. Stimulation of P450 27C1 activity by Adx and Alexa Fluor 488-Adx. P450 27C1 all-*trans* retinol desaturation assays were performed with increasing concentrations of unlabeled Adx (●) or Alexa Fluor 488-Adx (■). Points represent data from single assays. Samples were analyzed by UPLC-UV.

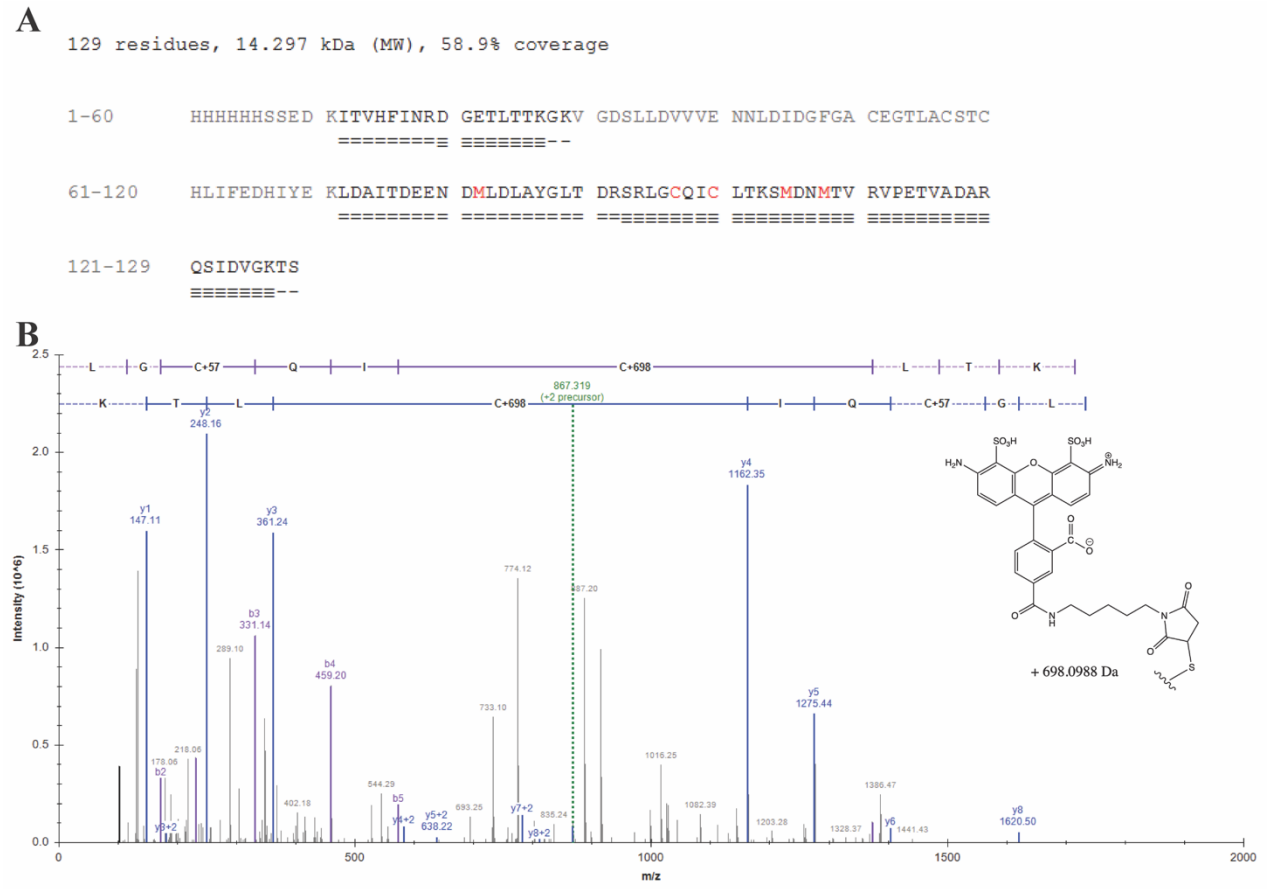

Figure 28. Proteomic analysis of the site of Alexa Fluor 488 labeling. *A*, Sequence coverage of recombinant human Adx following proteomic analysis of in-gel trypsin digest. *B*, MS/MS spectrum of peptide LGCQICLTQ containing the Alexa Fluor 488 label. Cys-100 has the Alexa Fluor 488 modification.

4.2.4 Alexa Fluor 488-Adx binds tightly to P450 27C1 and AdR

Fluorescence spectroscopy titrations were used to measure the dissociation constant of P450 27C1 and AdR with Adx. Varying concentrations of potassium phosphate were used to assess the ionic strength dependence of each interaction. At lower concentrations of potassium phosphate, P450 precipitated from solution causing Rayleigh scattering which prevented the measurement of K_d values (see spectra in Figure A4). The K_d of P450 27C1 with Adx ranged from 12-22 nM and the K_d of AdR with Adx ranged from 19-90 nM (Figure 29, Table 6). While a larger effect was

observed with AdR, the binding affinity for Adx with both proteins decreased with increasing ionic strength. Even at higher concentrations of potassium phosphate, these values indicate tight binding between Adx and P450 27C1 or AdR. The presence of all-*trans* retinol did not affect the binding affinity of P450 27C1 for Adx (Figure 30).

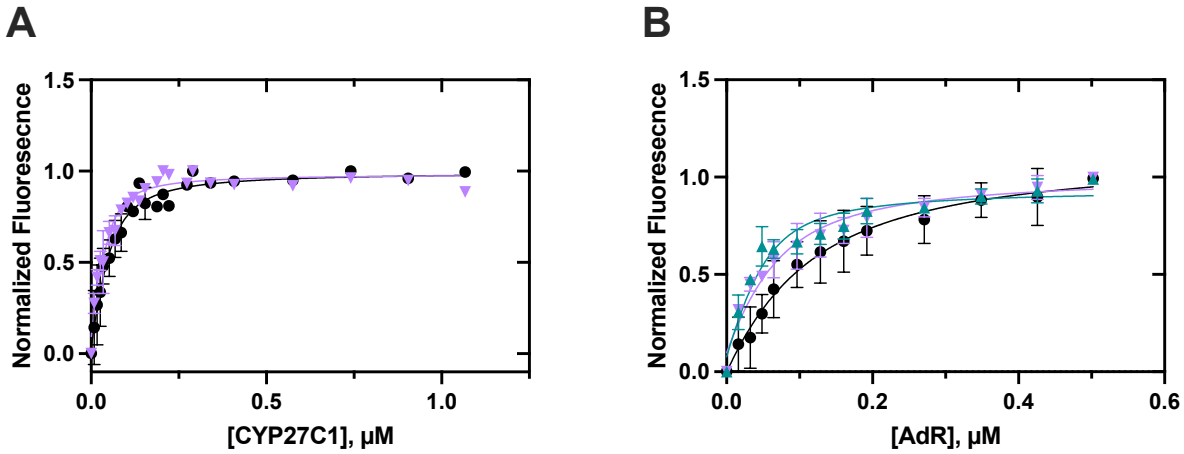

Figure 29. Fluorometric titration data for P450 27C1 and AdR equilibrium binding to Adx. Binding titrations were completed with: *A*, P450 27C1; *B*, AdR. Ionic strength was varied by changing the concentration of potassium phosphate buffer: 50 mM (▲), 100 mM (▼), 200 mM (●). At lower ionic strengths with P450 27C1, Raleigh scattering prevented binding measurements. Experiments were completed in triplicate and points are shown as means ± SD. Representative spectra are shown in Figure A4.

Table 6. Dissociation constants for P450 27C1 and AdR with human Adx at varying ionic strengths.

[KPhos] (mM)	P450 27C1 K_d (nM)	AdR K_d (nM)
50	[a]	19 ± 5
100	12 ± 3	40 ± 10
200	22 ± 6	90 ± 30

Values are derived from fitting in Figure 29 from experiments completed in triplicate.

[a] Raleigh scattering prevented binding measurement.

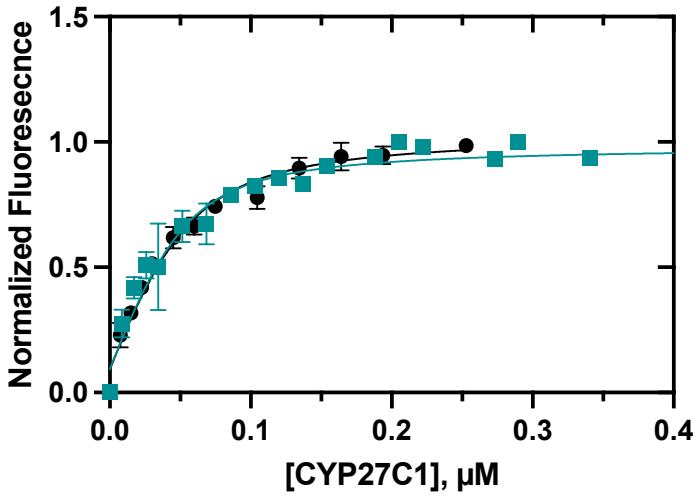

Figure 30. Lack of effect of all-*trans* retinol on the equilibrium binding of P450 27C1 to Adx. P450 27C1-Adx binding titrations were completed with (●) or without (■) all-*trans* retinol present. Data without all-*trans* retinol present is also shown in Figure 29 (only up to 0.4 µM shown here). Titrations were done in 100 mM potassium phosphate buffer (pH 7.4). The K_d value was 15 ± 3 nM with all-*trans* retinol and 22 ± 5 nM without. Data points represent results from triplicate experiments (show as means ± SD).

4.2.5 Effect of Adx on substrate binding by P450 27C1

With some other mitochondrial P450s, Adx has been shown to affect P450 substrate binding (99,169). To investigate this possibility with P450 27C1, substrate binding affinity was assessed with varying concentrations of Adx present (0 µM, equal molar, 10-fold excess, and 20-fold excess). P450 27C1 displays a Type I spectral change when binding all-*trans* retinol ((88), Figure 31). Dissociation constants were calculated from quadratic fits of this absorbance change plotted versus the substrate concentration (Figure 31, Table 7). The binding affinity for all-*trans* retinol did not notably vary in the presence of Adx; K_d values ranged from 10 ± 7 nM to 30 ± 20 nM. Variation in A_{max} values have previously been associated with changes in the amount of the P450 in solution that is able to bind substrate (99). No changes in A_{max} were observed across titrations with the addition of Adx, suggesting that the proportion of P450 27C1 that binds all-

trans retinol remains the same. At equilibrium, Adx did not appear to alter P450 27C1 substrate binding.

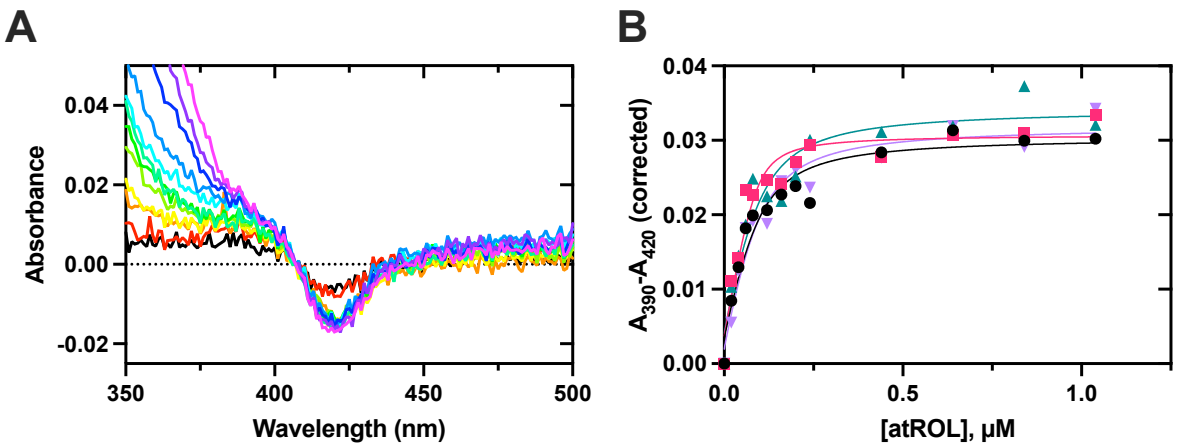

Figure 31. Lack of effect of Adx on the equilibrium binding of P450 27C1 to all-*trans* retinol. *A*, Representative all-*trans* retinol substrate binding spectra from titration with equal concentrations of P450 27C1 and Adx. With subsequent additions (indicated with different colors), the absorbance increased at 390 nm and the A_{420} decreased. Spectra were adjusted to 0 at the isobestic point (407 nm). *B*, Quadratic fits for calculation of K_d and A_{max} values for all-*trans* retinol binding to P450 27C1 in the presence of no Adx (●), equal molar Adx (■), 10-fold Adx (▲), or 20-fold Adx (▼).

Table 7. Equilibrium binding constants for P450 27C1 and all-*trans* retinol at varying concentrations of Adx.

Adx	K_d (nM)	A_{max}
No Adx	30 ± 10	0.027 ± 0.002
+ Equimolar Adx	10 ± 7	0.027 ± 0.002
+ 10-fold Adx	30 ± 20	0.030 ± 0.003
+ 20-fold Adx	30 ± 10	0.030 ± 0.002

Values are derived from fitting in Figure 31 from single titrations.

4.2.6 Characterization of the P450 27C1-Adx binding interface

No structural information is currently available describing the interaction between P450 27C1 and Adx. To identify the protein-protein interaction interface that exists between P450 27C1 and Adx, chemical cross-linking with EDC was utilized. Both unlabeled Adx and Alexa Fluor 488-Adx were used in reactions. In the absence of cross-linking, Adx and P450 27C1 displayed molecular weights of approximately 13 kDa and 50 kDa, respectively (Figure 32). Incubation of P450 27C1 and Adx resulted in the appearance of two new bands, at approximately 29 kDa and 62 kDa (labeled by arrows in Figure 32). The sizes of the cross-links are consistent with a P450 27C1-Adx (monomer) complex (62 kDa) and an Adx dimer (29 kDa). The presence of the Alexa Fluor 488 label did not negatively affect crosslinking with P450 27C1 (Figure 32, lane 7 vs. 9). Bands of interest were excised and in-gel trypsin digestion was performed. Peptides were analyzed by high-resolution mass spectrometry (HRMS) to identify proteins and cross-linked peptides within the bands of interest.

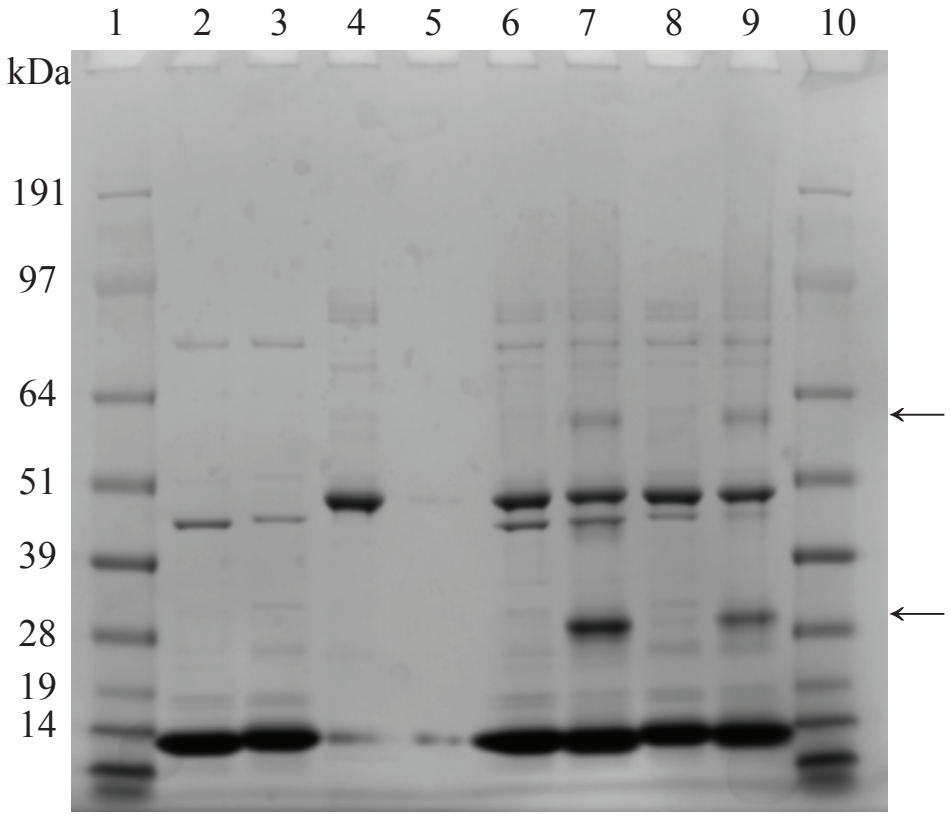

Figure 32. SDS-PAGE of P450 27C1 and Adx cross-links. Proteins in crosslinking reactions mixtures were separated on a 4-12% Bis-Tris gel with MOPS running buffer. SimplyBlue SafeStain was used for total protein staining. Lanes 1 and 10: SeeBlue Plus2 pre-stained protein ladder; lanes 2-4: Adx (2), Alexa Fluor 488-Adx (3), and P450 27C1 (4) proteins (no crosslinking); lanes 5: intentionally left blank; lanes 6 and 7: Adx and P450 27C1 (without (6) and with crosslinking (7)); lanes 8 and 9: Alexa Fluor 488-Adx and P450 27C1 (without (8) and with crosslinking (9)). Cross-linked proteins indicated by arrows were excised for proteomic analysis.

Analysis of the 62 kDa band showed peptides corresponding to both P450 27C1 and Adx. Many cross-linked peptides between P450 27C1 and Adx were identified by LC-MS/MS (Table A7, Table 8, Figure 33, Figure 34, Figure A5). The Lys-117, Glu-127, Glu-147, Lys-318, Lys-403, and Lys-478 residues of P450 27C1 and Asp-77, Glu-78, Asp-84, and Lys-127 residues of Adx were involved in cross-links in the identified peptides (Table 8, numbering according to recombinant protein sequences in Table A2). The interacting residues on both proteins are localized to a single surface of each protein (Figure 35). The 62 kDa band also contains three Adx-

Adx cross-links, but all of these cross-links involved Lys-127, part of the flexible C-terminal part of the protein, and not other Adx-Adx cross-links identified in the 29 kDa band (Table A8). These results further support the designation of the 62 kDa cross-link as a P450 27C1-Adx monomer complex as opposed to a P450 27C1-Adx dimer complex.

Table 8. Cross-linked residues between P450 27C1 and Adx.

P450 27C1	Adx
Lys-117	Asp-77, Glu-78, Asp-84
Glu-127	Lys-127
Glu-147	Lys-127
Lys-318	Glu-78, Asp-84
Lys-403	Asp-77, Asp-84
Lys-478	Asp-77, Asp-84

Results are from proteomic analysis performed on the 62 kDa band from P450 27C1 cross-linking with Adx (unlabeled). Numbering is based on sequence of recombinant proteins shown in Table A2. Representative peptide MS/MS information for identification is shown in Table A7, Figure 33, Figure 34, Figure A5.

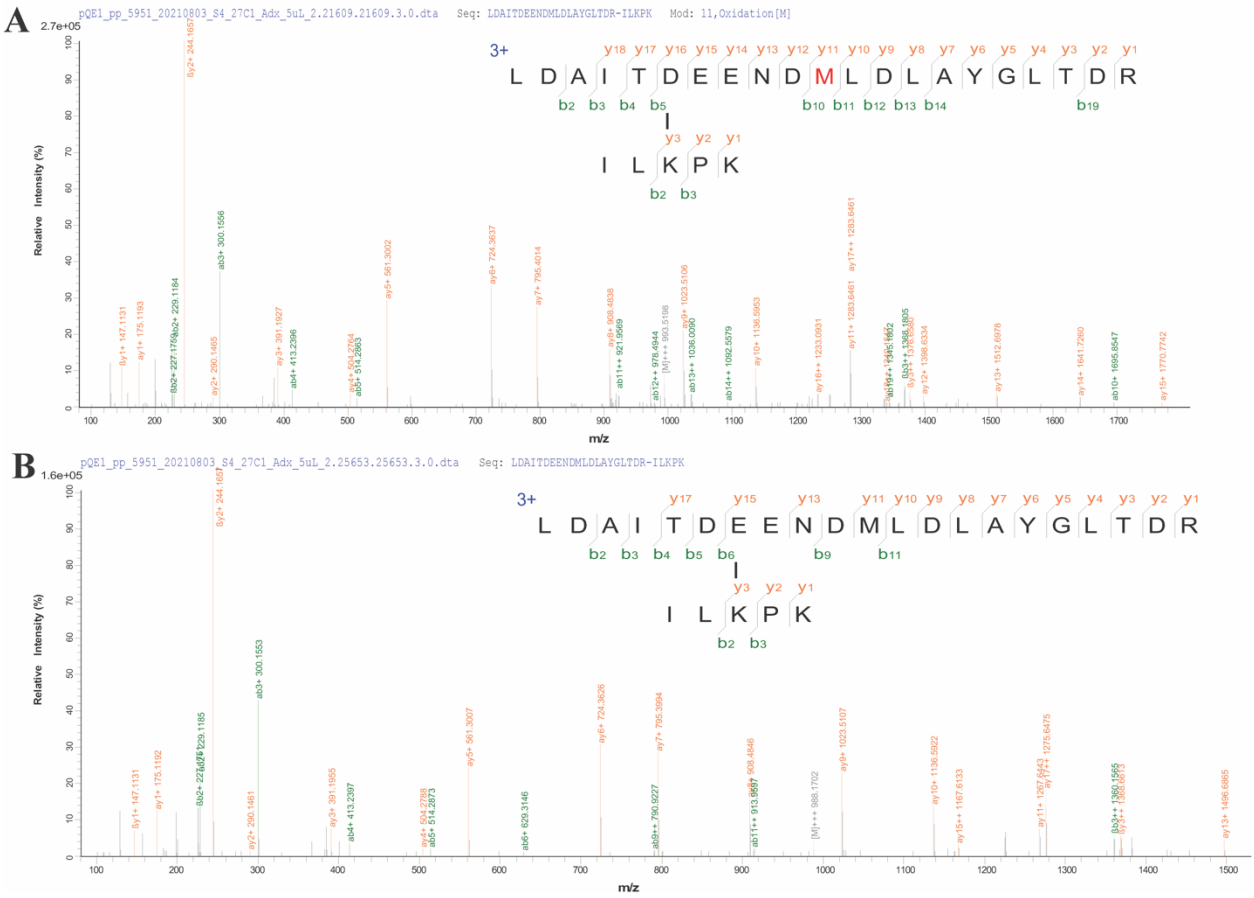

Figure 33. Representative fragmentation of P450 27C1-Adx cross-linked peptides from proximal binding site (cluster 4). MS/MS spectra with fragment assignment for cross-links observed between: *A*, Asp-77 of Adx and Lys-117 of P450 27C1; *B*, Glu-78 of Adx and Lys-117 of P450 27C1. Full peptide information is shown in Table A7.

Figure 34. Representative fragmentation of P450 27C1-Adx cross-linked peptides from distant binding site (cluster 3). *A*, Asp-77 of Adx and Lys-478 of P450 27C1; *B*, Asp-84 of Adx and Lys-318 Full peptide information is shown in Table A7.

HADDOCK software was used to generate P450 27C1-Adx complex models utilizing residues identified in cross-linking studies. HADDOCK clustered 89 structures into 11 clusters (44% of generated models). Energy values for clusters are shown in Figure A6. The best structures from the top 10 clusters were manually compared. The P450 27C1 molecule in each complex was aligned to visualize the range of Adx docking positions (Figure A7). The range of Adx orientations covers the range of P450 27C1 residues identified in cross-links. The best scoring structures from each cluster were aligned with two experimentally determined x-ray crystallography structures of mitochondrial P450-Adx fusion proteins (11A1, PDB: 3N9Y (158) and 11B2, PDB: 7M8I (99)).

The models from cluster 4 had low energy values and were the most similar to the fusion protein structures (Figure 35, Figure A8). Models from cluster 3 also had low energy values and several experimentally observed cross-links were fit well (Figure 35). Interactions between amino acids determined by cross-linking are shown for cluster 4 and 3 (MS/MS spectra in Figure 33 and Figure 34, respectively). The distance between the [2Fe-2S] cluster and the heme varied depending on the model. Distances were 26.1 Å and 44.8 Å for cluster 4 and 3, respectively.

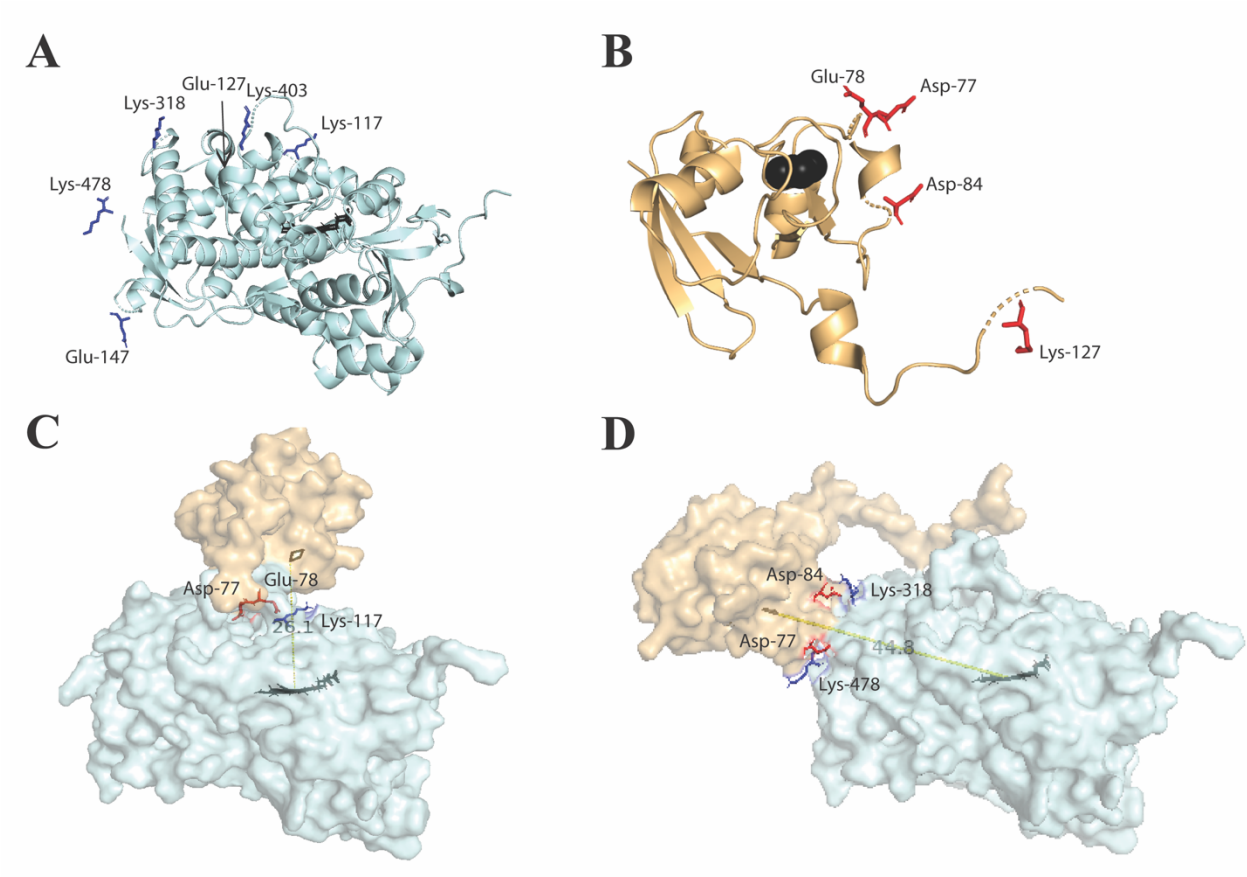

Figure 35. Model of P450 27C1-Adx interaction. Localization of P450 27C1 (*A*) and Adx (*B*) residues identified in cross-links. Residues are shown as sticks (red for Adx, blue for P450 27C1) and the rest of the structure is shown as cartoon (light orange for Adx, pale cyan for P450 27C1). *C-D*, Modeled P450 27C1-Adx complexes ((*C*), cluster 4; (*D*), cluster 3). Residues identified from cross-linking data at the interface are shown as sticks, the rest of the structure is shown as a transparent surface. The heme of the P450 and the [2Fe-2S] cluster of Adx are shown in black. The distance between the [2Fe-2S] cluster and the center of the heme was 26.1 Å in the cluster 3 model and 44.8 Å in the cluster 4 model (shown as dashed line).

4.3 Discussion

This study started with assessing how variations the species form of Adx used and the concentration of Adx used could affect mitochondrial P450-mediated catalysis. The first issue is whether using bovine or human Adx as the electron carrier in P450 reactions changes the observed reaction kinetics. In an ideal experimental setup, the concentration of Adx would be saturating and not be rate-limiting, so the most useful steady-state kinetic parameter to compare is k_{cat}. With P450 27C1, there was no different in k_{cat}, indicated that both forms of Adx are effective electron transporters (Figure 22).

With Adx and mitochondrial P450s, the primary methods reported to measure binding affinity are UV/Vis-difference titrations (163), surface plasmon resonance (SPR) (175), and titrations with fluorescently labeled proteins (176). In this work, two methods were utilized to measure the binding affinity between Adx and P450 27C1: MST and titrations with fluorescently labeled Adx. While not described in this thesis as it is outside of the scope, MST was performed with other mitochondrial P450s also (P450 11B2 and 27A1). With all P450s tested, the K_d values for Adx binding were low (< 200 nM). Other P450s are briefly discussed here to offer insight into the comparison of MST with other methods, as no other studies have assessed P450 27C1-Adx binding. This appears to be the first study utilizing MST with P450s. A direct comparison of measurements can be made for P450 11B2 and bovine Adx, which had a K_d value of 6 nM with MST and a reported K_d of 80 nM with SPR (177). The lower K_d value with MST in comparison with SPR suggests that free diffusion of the proteins may be important for optimal binding.

One concern with the MST work was that the labeling method utilized could interfere with the protein-protein interactions (a lysine reactive dye was used to label Adx, and there are many lysine residues). Because of this, another method where perturbation of the interaction would be

minimized was pursued. Adx has five cysteine residues. Four of these residues are involved with binding the [2Fe-2S] cluster, leaving only one available free cysteine for labeling (178). Because of this, we elected to label Adx with Cys-reactive fluorescence dyes. IAEDANS has previously been utilized to specifically label Adx at an individual cysteine residue to assess interactions with AdR and P450 11A1 (176). Specific labeling of Cys-95 (Cys-100 of our construct, Figure 28) of Adx was proposed in a study with 5-iodoacetamidofluorescein (5-IAF) (178), though binding affinities were not assessed in that work. Our group has recently utilized Alexa Fluor 488 C_5 maleimide (structure shown in Figure 24) for labeling b_5 (T70C mutant) to quantify interactions with a range of microsomal P450s (179,180). Acrylodan was originally utilized to label a homolog of this b_5 mutant (181). In the present study, we attempted to label Adx with acrylodan, IAEDANS, and Alexa Fluor 488 C_5 maleimide. While labeling with each dye was successful, we found that the Alexa Fluor 488 was the most effective for labeling Adx in detecting interactions with P450 27C1, in that it was the only dye that resulted in a strong fluorescent signal that was clearly altered by the addition of P450 27C1 (Figure 25, other data not shown). Like previous reports of Adx labeling with IAEDANS and 5-IAF (176,178), Alexa Fluor 488-Adx still efficiently supports P450 catalysis (Figure 27) and labeling presumably occurs at a single site (Figure 28). With the high fluorescence of the Alexa Fluor 488-Adx, very low concentrations of protein could be used (50 nM) which is important given the low K_d values between Adx and AdR/P450s. In the previous work with IAEDANS labeling, 0.5-1 μM of AEDANS-Adx was used and the K_d with AdR was reported to be 0.07 μM (176). This K_d value is in the range of values of what we determined with AdR and the Alexa Fluor 488-Adx (~20-90 nM, depending on ionic strength, Table 6), but is subject to higher error due to the high concentration of AEDANS-Adx used. The K_d determination for the interaction of AdR and Adx in this work utilized bovine AdR. A previous study has shown

that human Adx binds to human AdR 5-fold less tightly than human Adx binds to bovine AdR (182). While this work is predominantly focused on interactions with P450 27C1 and Adx (both human proteins), the studies with AdR are limited due to this apparent species difference. In comparison with MST results, the K_d values with Alexa Fluor 488-Adx were lower for P450 27C1 (12 nM versus 220 nM) but equal for AdR (both 40 nM) (Figure 23, Table 6). This points to some improvement in P450 27C1 binding to Adx with the single fluorescent label at Cys-100.

Interactions with Adx are driven by electrostatic interactions, generally making the complexes sensitive to changes in ionic strength. Consistent with previous reports, Adx binding affinity for AdR decreased with increasing ionic strength (Table 6) (153). Differences in Adx affinity for P450 27C1 were also noted (Table 6), though the range of ionic strengths investigated was limited due to precipitation of P450 27C1 at low ionic strengths (Figure A4). The interaction between P450 27C1 and Adx is not nearly as dependent on low ionic strengths as P450 11B1 and 11B2, which did not form cross-links with Adx at potassium phosphate concentrations above 20 mM (113).

The P450 27C1-Adx interaction interface was modeled utilizing data from cross-linking mass spectrometry. While there are many residues of P450 27C1 identified in cross-linked peptides that cover a large surface across the protein (Figure 35), the interactions do appear specific, in that there are many other lysine residues on the surface of P450 27C1 that were not detected in cross-links. While previously identified large interfaces have been used to suggest the interaction of an Adx dimer (100), we do not believe that our crosslinking results are consistent with that model, given the apparent molecular weight on SDS-PAGE (Figure 32) and the lack of Adx-Adx cross-linked peptides in the P450-Adx crosslink band (Table A8).

The cross-links identified cannot be well explained by any single model of a P450 27C1-Adx complex. The presence of multiple P450-Adx protein conformations has been proposed before (183). The first model illustrated involves interactions between Asp-77 and Glu-78 of Adx and Lys-117 of P450 27C1 (Figure 33, Figure 35, Table 8) This complex has Adx positioned similarly to the previously published P450-Adx fusion structures (Figure A8). Typically, the interaction with Adx at this position involves two lysine residues of the K-helix. In P450 27C1, these two residues correspond to Arg-338 and Lys-342. Lys-342 was not found in any cross-linked peptides, which was surprising given its conserved role in Adx binding (Figure 36). The distance between the [2Fe-2S] cluster and the heme in this model is 26.1 Å, further than in the two P450-Adx fusion structures (17.4 Å for 11A1, 17.8 Å for 11B2) (99,158), but still in line with distance constraints for productive electron transfer (184). It is possible that the model we have generated from docking is representative of an initial recognition structure driven by electrostatic interactions, and that the Adx could reposition to shorten the distance between the [2Fe-2S] cluster and the heme as previously proposed by Strushkevich *et al.* (158). We believe that could be the case, given that structural model generated from 11B2-Adx crosslink data also resulted in a longer [2Fe-2S] cluster to heme distance (24.4 Å) than what was later observed in the 11B2-Adx fusion protein structure (17.8 Å) (99,113). Alternatively, if this is the structure associated with electron transfer, the increased distance may contribute to the lack of spectral perturbation of P450 27C1 by Adx, as observed with P450 11A1 (91,163) and the slower rate of reduction of P450 27C1 (0.35 s^{-1}) in comparison to 11A1 (2.0 s^{-1}) (91,185).

Many other model clusters are focused away from the traditional Adx binding site. The most favorable scoring model of this type of interaction involves Asp-77 and Asp-84 of Adx interacting with Lys-478 and Lys-318 of P450 27C1, respectively (Figure 34, Figure 35, Table 8).

Interactions with residues in these regions have not been identified with other mitochondrial P450s (Figure 36). P450 27C1 is the only mitochondrial P450 with multiple positively charged residues here, and this may allow for P450 27C1 to bind Adx at a unique interface. Like P450 27A1, the K_d value for binding between P450 27C1 and Adx is very low. Pikuleva *et al.* demonstrated that this was due to Arg-418 of P450 27A1 also being involved with Adx binding (183). It was proposed that there may be additional binding sites for Adx outside of the common site for P450s with high affinity for Adx. Prior to identification of P450 27C1, this residue was thought to be specific to P450 27A1 as it is not present other mitochondrial P450s, including P450 family member 27B1 (105). P450 27C1 also has this arginine residue (Arg-402). Lys-403 is the subsequent amino acid in P450 27C1 and it was detected in cross-links with Adx (Table 8, Table A7). Thus, as in P450 27A1, Arg-402 of P450 27C1 and the region surround it may serve as an additional binding site for Adx. Given the distance between the [2Fe-2S] cluster and the heme with these other binding sites, they are not likely involved in electron transfer. The functional relevance of these other binding sites is unknown, but Adx binding to these sites may lead to allosteric effects on the P450 activity (discussed below).

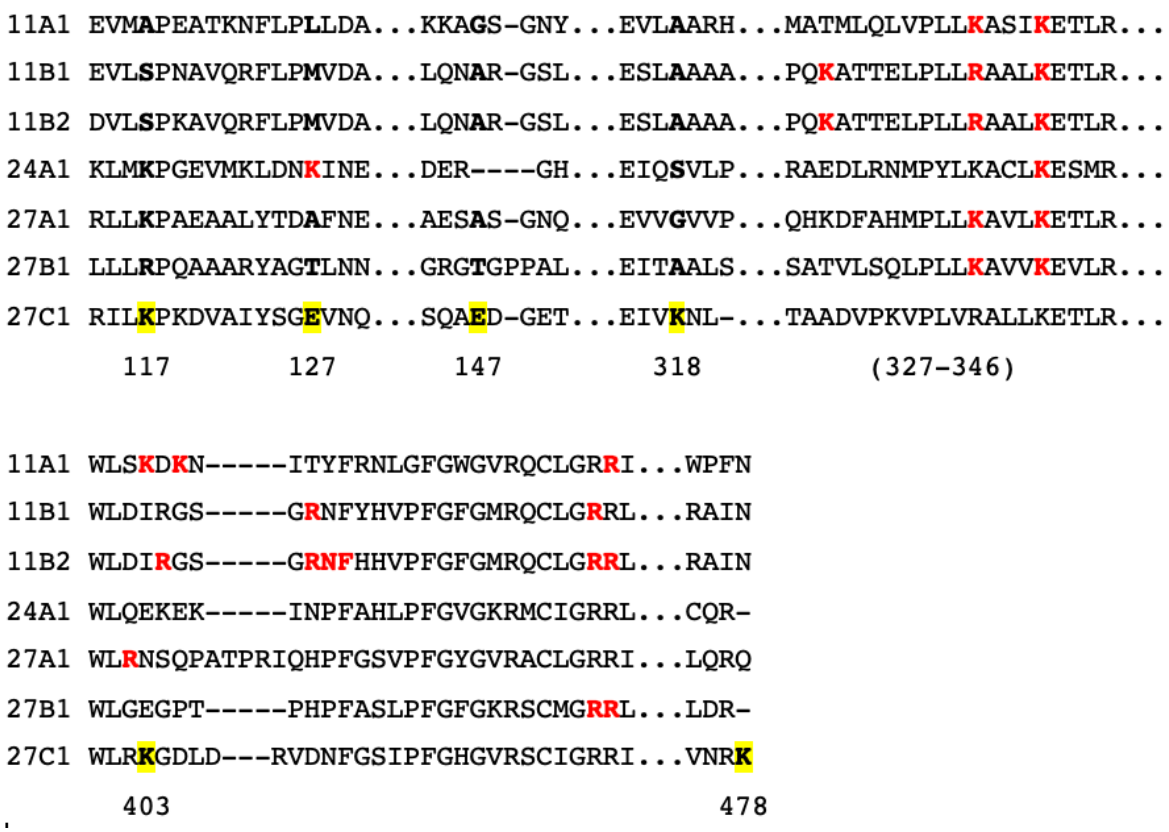

Figure 36. Comparison of mitochondrial P450 sequences. Sequences for the human mitochondrial P450s from UniProt (186) were aligned using the Clustal Omega program (131). Gaps in alignments are shown as dashes (-) and portions of sequences are omitted by ellipses (...). Relevant numbering of the recombinant P450 27C1 sequence is shown below. The P450 27C1 residues identified in cross-links are bolded and highlighted in yellow. The corresponding aligned residues from other mitochondrial P450s are bolded. Residues that have been implicated in interactions with Adx in other P450s are bolded and shown in red (99,105,113,183,187-190). Note that some of the cited work utilized species homologs of the P450s.

For the mechanism of electron transfer, our data is most supportive of the shuttle mechanism (153,160). The lack of Adx-Adx crosslinks suggests that an Adx dimer does not interact with P450 27C1, which would be required for the proposed quaternary structure (164). Additionally, the interface of Adx that interacts with P450 27C1 is the same as what interacts with AdR (191), preventing the possibility of Adx to interact with both AdR and the P450 at the same time. One potential area of concern with the shuttle mechanism and the measured K_d values is that

Adx appears to bind preferentially to the P450 over AdR (Table 6), and that binding of oxidized Adx to P450 27C1 may prevent the binding of reduced Adx. These studies utilized oxidized Adx, so binding to AdR and reduction is necessary before productive electron transfer to the P450. It is possible that reduced Adx would have a different binding affinity with P450 27C1, allowing it to dissociate any bound oxidized Adx. Adx structural changes upon reduction have been observed (149), so this is not outside of the realm of possibility. As far as preferential binding of Adx to the P450 over AdR, the respective concentrations of AdR and P450 27C1 within the system are also important to consider. P450 27C1 is expressed in the skin and has been quantified (91), but the concentrations of Adx and AdR within the skin are currently unknown to our knowledge. The difference in binding affinity may be important to facilitate P450 27C1 reduction if AdR is present at much higher concentrations than P450 27C1.

Given the presence of multiple Adx binding sites on P450 27C1, some of which do not seem conducive for productive electron transfer, Adx binding to P450 27C1 may play an allosteric role in the enzyme's activity. A potential allosteric role of Adx on P450 substrate binding has been proposed for other mitochondrial P450s. The potential for Adx binding to stimulate P450 27C1 substrate binding was assessed by equilibrium titrations (Figure 29, Table 6), but no differences in equilibrium substrate binding were observed. Given the low K_d for all-*trans* retinol binding to P450 27C1, it may be possible that there are minor changes in binding affinity that are not detected due to the concentration of P450 necessary for these measurements. The physiological relevance of assessing these changes may be limited though, as retinoid metabolizers like P450 27C1 are thought to receive their substrates from cellular retinoid-binding proteins *in vivo*, and I have provided *in vitro* evidence for such interactions with these binding proteins (see Chapter 5). There was also no difference in Adx binding to P450 27C1 when substrate was present (Figure 30). There

are other potential allosteric effects of Adx binding that have been described that were not assessed in this study (i.e., substrate positioning within the active site), so Adx allosteric regulation with P450 27C1 cannot be completely ruled out.

This work provides a basis for understanding the interaction between P450 27C1 and Adx, although much remains unknown. Cross-linking mass spectrometry has some limitations, and complementary methods would help refine models for the P450 27C1-Adx interaction. The protein-protein interaction modeling was also performed with the P450 27C1 AlphaFold structure. Modeling the interaction could be improved with the description of a P450 27C1 crystal structure. The validation and assessment of the respective contribution of each P450 27C1 residue/interface to the interaction with Adx could be addressed through site-directed mutagenesis. Utilizing EDC cross-linking to identify interactions between P450 27C1 and Adx limited our study to focus on interactions between primary amines and carboxyl groups, and residues may interact that were not detected in our study. Additionally, other components may alter the interaction between P450 27C1 and Adx. For example, phospholipids can sometimes alter P450-redox partner protein binding affinity (96), though we have previously shown that this P450 27C1 construct does not require lipids for catalysis (91). In this work, we focused on characterizing interactions with oxidized, non-modified Adx. It is possible that reduced Adx may have a different affinity for P450 27C1 or interact with it differently, in light of conformational changes that can occur when Adx is reduced (192). There are also reports of Adx post-translational modifications affecting binding with P450s (193).

4.4 Conclusion

The goal of this work was to characterize the P450 27C1-Adx complex and to investigate potential allosteric effects of Adx binding to P450 27C1. Both bovine and human Adx are efficient in supporting P450 27C1-mediated catalysis. Adx binds to P450 27C1 with very high affinity even at higher ionic strengths. This tight binding may be due to the increased number of contacts formed between P450 27C1 and Adx identified by cross-linking mass spectrometry. No significant Adx allosteric effect on P450 27C1 all-*trans* retinol substrate binding was observed. Overall, the interaction between P450 27C1 and Adx appears to be different than what has been observed with other mitochondrial P450s, supporting the conclusion that interactions between P450s and Adx are P450-specific. *In vivo*, differences in P450-Adx binding affinity may serve an important function in partitioning Adx-mediated electron transfer among multiple P450s. For example, if two mitochondrial P450s are expressed in the same tissue at different concentrations, a higher Adx binding affinity with the lower expression P450 may allow it to compete with a more highly expressed P450 with lower Adx binding affinity as proposed by Pikuleva *et al.* (183). The physiological importance of multiple Adx-P450 binding sites has not been directly elucidated *in vivo*, but they may be important for allosteric modulation of P450 function (i.e., substrate binding, regioselectivity, etc.). Additionally, the differences in P450-Adx binding modes has previously been proposed as a potential avenue for selective drug design, as molecules tailored to the distinct components of the Adx-P450 interface could prevent Adx binding and selectively inhibit the P450 (99).

Chapter 5. Cellular retinoid-binding proteins transfer retinoids to P450 27C1 for desaturation

This chapter is adapted from work published in the Journal of Biological Chemistry and has been reproduced with the permission of the publisher.

Glass, S.M. and Guengerich, F.P. (2021) "Cellular retinoid-binding proteins transfer retinoids to human cytochrome P450 27C1 for desaturation." *J. Biol. Chem*. 297 (4), 101142.

5.1 Introduction

In vivo, all-*trans* retinol can be sequentially metabolized by dehydrogenases to form all-*trans* retinaldehyde and all-*trans* retinoic acid, the biologically active form of retinoids in the cell (retinoid metabolism is summarized in Figure 3). In cells, there exist two types of retinoid-binding proteins, CRBPs and CRABPs. These small proteins are members of the intracellular lipid-binding protein (iLBP) superfamily, which bind hydrophobic ligands within an internal β-barrel cavity (194). In humans, there are four isoforms of CRBP that bind all-*trans* retinol and all-*trans* retinaldehyde and two isoforms of CRABP that bind all-*trans* retinoic acid (21). Since retinoids bind to these proteins tightly, and retinoid-binding proteins are generally expressed in concentrations that exceed their ligands, it is expected that little to no free all-*trans* retinoids exist within the cell (21). Cellular retinoid-binding proteins mediate retinoid function and metabolism within the cell by delivering retinoids specifically to receptors and metabolic enzymes. Additionally, the ratio of apo-CRBP (without retinoid bound) to holo-CRBP (with retinoid bound) has been shown to regulate retinoid metabolism within the cell. The most well studied example of this is in the formation and breakdown of retinyl esters, the storage form of retinoids. LRAT catalyzes the esterification of fatty acyl groups to the terminal hydroxyl group of all-*trans* retinol. All-*trans* retinol can be released from retinyl esters through hydrolysis by REH. The activity of LRAT is inhibited by excess apo-CRBP-1 (37) and the activity of REH is stimulated (38), leading

to increased amounts of available all-*trans* retinol. This activity of apo-CRBPs is not thought to be due to retinoid-binding capabilities, given that chemically modified CRBP-1 that can no longer bind all-*trans* retinol still inhibits LRAT (37). This apo:holo-CRBP regulation is thought to provide a mechanism to control retinoid availability within the cell (21).

The ability of P450s to interact with retinoid-binding proteins has previously been illustrated with P450 26B1 and 26C1, which can utilize all-*trans* retinoic acid bound to CRABP-1 or CRABP-2 (holo-CRABPs) as substrates (31,32). Direct channeling of all-*trans* retinoic acid from holo-CRABPs to CYP26s has been proposed. Excess apo-CRABPs were also shown to inhibit P450 26B1 and 26C1 metabolism and it was proposed that this was through allosteric modulation or inhibition, not through retinoid sequestration or competition for binding to the P450. Notably, P450s 3A4 and 2C8, P450s that had been shown to metabolize free all-*trans* retinoic acid *in vitro*, do not utilize holo-CRABPs as substrates (31), suggesting that this interaction is P450 specific and that not all P450s identified as *in vitro* retinoid metabolizers may be as relevant for retinoid metabolism *in vivo.*

P450 27C1 was recently characterized as an all-*trans* retinoid desaturase (Figure 4) expressed in the skin (88,91). Previous studies that identified and characterized the ability of P450 27C1 to convert all-*trans* retinoids to 3,4-dehydroretinoids utilized a reconstituted *in vitro* system with free retinoids. Whether or not P450 27C1 is able to accept retinoid substrates from cellular retinoid-binding proteins is currently unknown. 3,4-Dehydroretinoid levels have been correlated with levels of cellular retinoid-binding proteins, but the role of these proteins in 3,4-dehydroretinoid formation is unknown (69,195). Potential regulation of 3,4-dehydroretinoid formation by excess apo-CRBPs has also not been assessed.

In this work, we addressed the hypothesis that human P450 27C1 interacts with three cellular retinoid-binding proteins expressed in the skin (23,25)—CRBP-1, CRABP-1, and CRABP-2—to directly receive retinoid substrates (channeling) or if ligand dissociation from the retinoid-binding protein is required as would be predicted by the free ligand model (Figure 37). Channeling in this case refers to the direct transfer of retinoid from the holo-cellular retinoid-binding protein to the P450 without free diffusion into the bulk solution. *In vitro* steady-state kinetic experiments and isotope dilution channeling assays were performed with purified recombinant P450 27C1 and cellular retinoid-binding proteins to distinguish between these two models. These interactions are further characterized through substrate binding assays and mutagenesis.

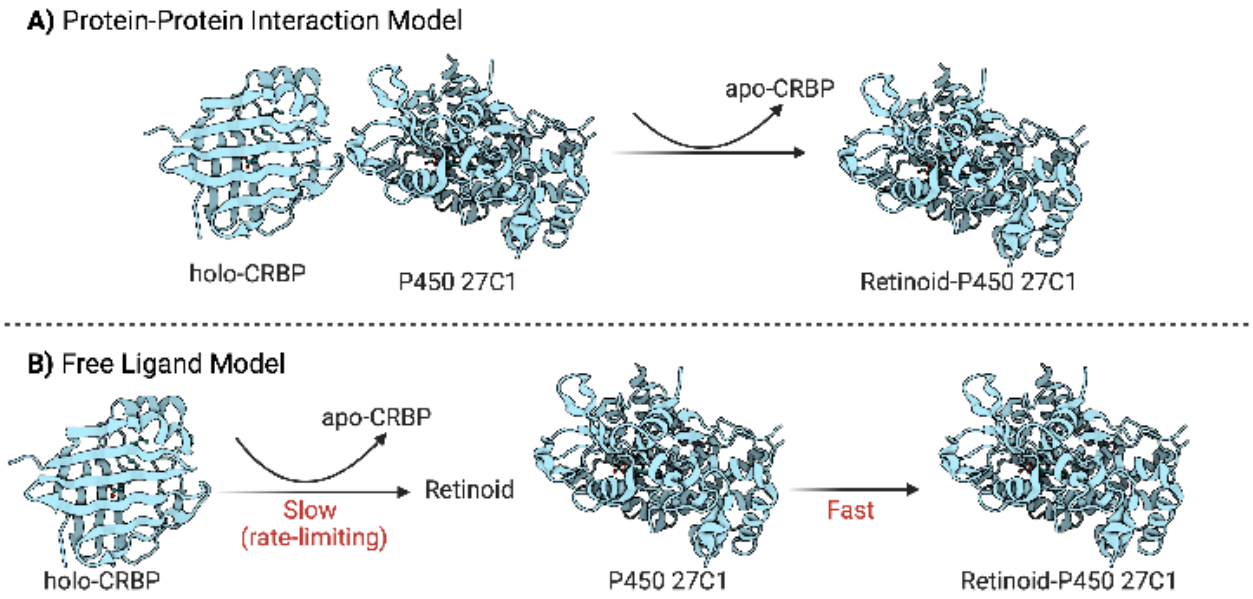

Figure 37. Potential mechanisms of retinoid transfer from holo-CRBPs to P450 27C1. *A*, Protein-protein interaction model: holo-CRBP interacts directly with P450 27C1 and transfers retinoid substrate. *B*, Free ligand hypothesis model (indirect transfer): retinoid dissociates from holo-CRBP, and free retinoid can then bind to P450 27C1. Figure created in BioRender.com.

5.2 Results

5.2.1 Assessing holo-CRBPs as substrates for P450 27C1 retinoid desaturation

To determine if P450 27C1 can directly accept retinoid substrates from cellular retinoid-binding proteins, P450 27C1 steady-state kinetics assays were performed with holo-CRBPs (atROL-CRBP-1, atRAL-CRBP-1, atRA-CRABP-1, and atRA-CRABP-2) prepared with a retinoid:CRBP ratio of 1:1. Reactions were run with the free substrates in parallel. Values for the k_{cat} and k_{cat}/K_m for the reactions were calculated from hyperbolic fits to the data for the rate of dehydroretinoid formation against substrate concentration (free retinoid, or holo-CRBP) (Figure 38, Table 9). For atROL-CRBP-1 and atRAL-CRBP-1, the specificity constant (k_{cat}/K_m) was similar to the respective free retinoids while the k_{cat} was slightly lower (68% and 74% of the free retinoid for atROL-CRBP-1 and atRAL-CRBP-1, respectively), and the K_m values were not different. For atRA-CRABP-2, the k_{cat}/K_m was 5-fold lower, due to a 36% decrease in k_{cat} and a 3-fold increase in K_m. For atRA-CRABP-1, these changes were even more substantial: the k_{cat}/K_m was decreased 65-fold, k_{cat} was decreased 10-fold, and K_m was increased 7.5-fold.

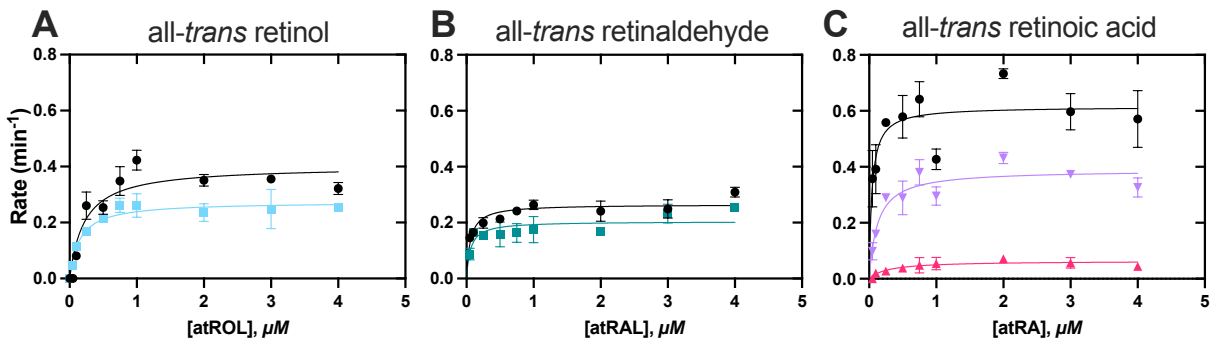

Figure 38. Effects of CRBPs on P450 27C1 retinoid desaturation. Steady-state kinetics of 3,4-dehydroretinoid formation from: *A*, all-*trans* retinol bound to CRBP-1 (▫); *B*, all-*trans* retinaldehyde bound to CRBP-1 (■); *C*, all-*trans* retinoic acid bound to CRABP-1 (▲) or CRABP-2 (▼) or as a free substrate (●). Reactions were done in duplicate and points are shown as means ± SD (range). Samples were analyzed by UPLC-UV.

Table 9. Kinetic parameters of retinoid desaturation with holo-CRBP or free retinoid by P450 27C1.

Substrate	K_m (μM)	k_{cat} (min^{-1})	k_{cat}/K_m ($\mu M^{-1}\ min^{-1}$)
atROL	0.22 ± 0.06	0.40 ± 0.03	1.8 ± 0.5
atROL-CRBP-1	0.15 ± 0.03	0.27 ± 0.01	1.9 ± 0.4
atRAL	0.06 ± 0.01	0.27 ± 0.01	5 ± 1
atRAL-CRBP-1	0.06 ± 0.02	0.20 ± 0.01	4 ± 1
atRA	0.04 ± 0.02	0.61 ± 0.03	15 ± 5
atRA-CRABP-1	0.3 ± 0.1	0.064 ± 0.008	0.23 ± 0.09
atRA-CRABP-2	0.12 ± 0.03	0.39 ± 0.02	3.1 ± 0.7

Results are from experiments done in duplicate. Parameters were estimated using a hyperbolic fit in GraphPad Prism that solved for k_{cat} and k_{cat}/K_m directly.

To determine whether the amount of desaturation that occurred in the reactions with the holo-CRBPs as substrates was due to channeling or only metabolism of the free retinoid available in solution, kinetic values were calculated based on the amount of free substrate that would be present given the reported binding affinity of the CRBPs for retinoids (Figure 39). For atROL-CRBP-1, atRAL-CRBP-1, and atRA-CRABP-2, the amount of product formed was higher than

what would be expected if P450 27C1 was only able to oxidize the free retinoid in reaction. For atRA-CRABP-1, the amount of 3,4-dehydroretinoic acid formed does not exceed the free ligand prediction. These steady-state kinetic results suggest that atROL-CRBP-1, atRAL-CRBP-1, and atRA-CRABP-2 channel retinoids to P450 27C1, but atRA-CRABP-1 does not.

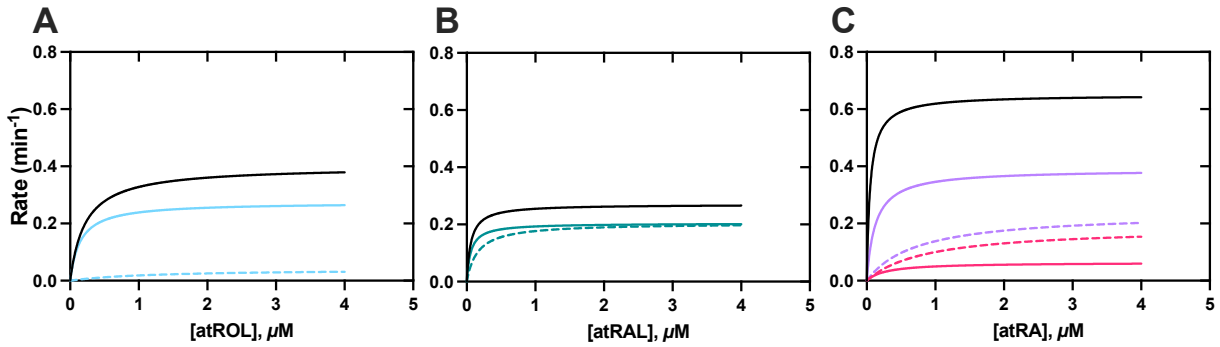

Figure 39. Calculated product formation in steady-state kinetic assays under the free ligand hypothesis model. Observed and modeled steady-state kinetics of 3,4-dehydroretinoid formation: *A*, all-*trans* retinol bound to CRBP-1 (—); *B*, all-*trans* retinaldehyde bound to CRBP-1 (—); *C*, all-*trans* retinoic acid bound to CRABP-1 (—) or CRABP-2 (—) or as a free substrate (—). Fits from experimental data (Figure 38) are shown as solid lines. Calculated product formation under the free ligand hypothesis with retinoid binding proteins is shown as dashed lines.

5.2.2 Direct channeling of retinoids from holo-CRBPs to P450 27C1

Isotope dilution experiments were performed to examine the differences in all-*trans* retinoic acid delivery to P450 27C1 by CRABP-1 and CRABP-2. In these assays, free d_5-all-*trans* retinoic acid was added along with an equal concentration of a holo-CRABP with d_0-all-trans retinoic acid bound. If no channeling of retinoid to the P450 occurs, dissociation from the CRABP is required and the product formed from the free retinoid (added to the reaction) should be much higher than the amount of product formed from the retinoid bound to the CRABP. Conversely, if channeling occurs, the amount of product formed from each retinoid should be similar.

With CRABP-1 (Figure 40), the amount of product formed from the free all-*trans* retinoic acid was much higher than from the holo-CRABP. Notably, the ratio of free:bound product formation also decreased over time, which would be expected as the retinoid originally bound to the CRABP dissociated and exchanged with the retinoid in solution (Figure 40). With CRABP-2, the amount of product formed from both the free and bound retinoid was more similar, and the ratio of product formation remained largely the same over time (Figure 40). This result is consistent with what would be expected for direct retinoid delivery between the CRABP and the P450. Overall, the results from these isotope dilution channeling experiments support the differences in channeling observed in steady-state kinetic analyses with holo-CRABP-1 and holo-CRABP-2.

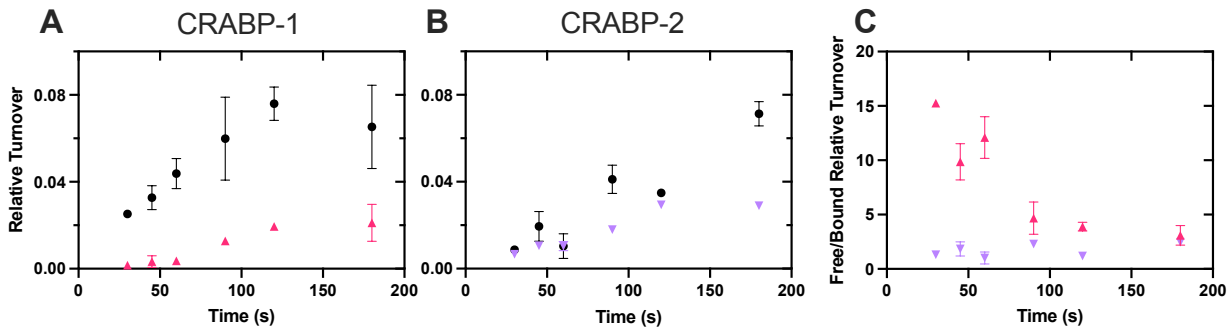

Figure 40. Differential channeling of all-*trans* retinoic acid from CRABPs to P450 27C1. Isotope dilution experiments with free d_5-all-*trans* retinoic acid and d_0-all-*trans* retinoic acid bound to: *A*, CRABP-1; *B*, CRABP-2. Relative product formation from the free retinoid (●) and the holo-CRABP (▲ CRABP-1 and ▼ CRABP-2) is shown in each panel. *C*, Ratio of free:bound product formation as a function of time for CRABP-1 (▲) and CRABP-2 (▼). Reactions were done in duplicate and points are shown as means ± SD (range). Samples were analyzed by LC-MS/MS.

5.2.3 Rate of retinoid transfer from holo-CRABPs to P450 27C1

Stopped-flow binding studies were performed to compare the rate of free retinoid-binding to P450 27C1 to the rate of retinoid transfer from holo-CRABPs to P450 27C1 (Figure 41). With

free all-*trans* retinoic acid, the k_{on} was 278 ± 5 μM^{-1} min^{-1} (i.e., 4.6 × 10^6 M^{-1} s^{-1}). The transfer of retinoids from holo-CRABPs to P450 27C1 was much slower, as evidenced by the time scale required to saturate P450 27C1 binding (Figure 41*B*).

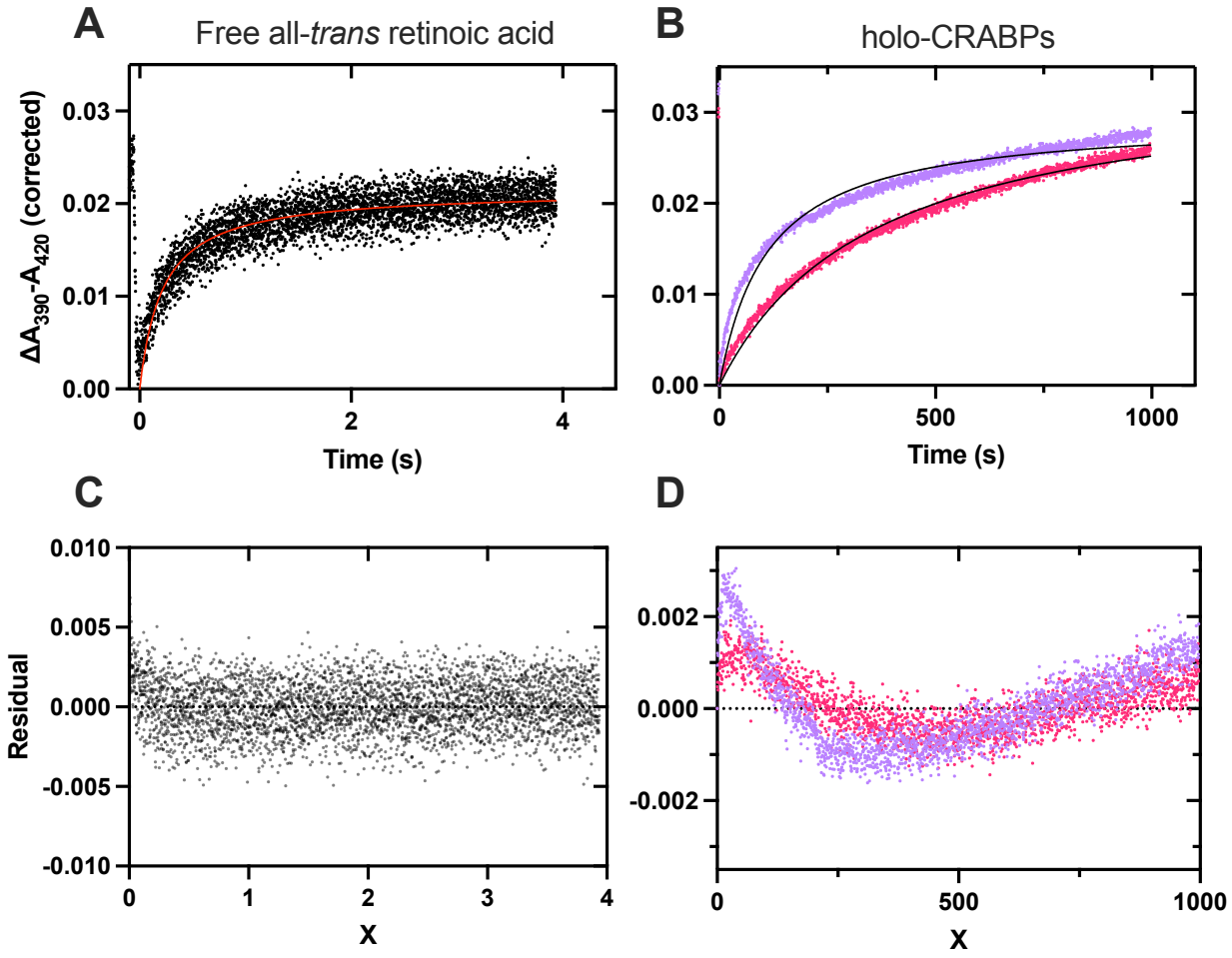

Figure 41. Stopped-flow mixing transients of all-*trans* retinoic acid substrate mixing with P450 27C1. P450 27C1 (1 μM, final) was mixed with: *A*, free (●); *B*, CRABP-1-bound (●) or CRABP-2 (●) bound all-*trans* retinoic acid (all 1 μM, final) in 200 mM potassium phosphate (pH 7.4). *C*, residuals plot for panel *A*. *D*, residuals plot for panel *B*. Free all-*trans* retinoic acid data is an average of 6 replicate shots, holo-CRABP data is from a single shot. The line in each panel is a single-exponential fit to the data (see Experimental procedures). Apparent k_{on} values: free all-*trans* retinoic acid, 278 ± 5 $\mu M^{-1}min^{-1}$; holo-CRABP-1, 0.169 ± 0.001 $\mu M^{-1}min^{-1}$; holo-CRABP-2, 0.539 ± 0.005 $\mu M^{-1}min^{-1}$.

The patterns with the CRABP-1 and CRABP-2 retinoic acid complexes were different. The CRABP-2 complex showed a distinctive multiphasic behavior (Figure 42*A*, *B*). The rates with the complexes were measured with varying concentrations of P450 27C1, and as expected the amplitude of the final P450-retinoic acid complex increased with the P450 concentration in both cases. With the CRABP-1 complex, the plots could be fit with single exponentials of 0.0020 to 0.0034 s^{-1}, which are very close to the reported CRABP-1 k_{off} rate in the literature (Table A5, (196)). The plots of the CRABP-2 data were fit much better with biexponential fits (Figure 42*C*, *D*). The goodness of fit with the single exponential is illustrated by the residuals plot in Figure 41*D*. The fast phase, which accounted for 25-38% of the reaction, was much faster than the reported CRABP-2 k_{off} rate (196) but much slower than the binding of free retinoic acid by P450 27C1 (Figure 41*A*). We interpreted the equilibria in the context of the scheme in Figure 42*E*. The CRABP-1 system was dominated by the k_{off} rate (0.0020 to 0.0034 s^{-1}). For the CRABP-2 system, the equilibrium was more complex, as indicated by the biphasic behavior at all P450 concentrations. This was interpreted as a faster conversion to a P450-CRABP-2-retinoic acid ternary complex, which then undergoes a slower rearrangement to a complex in which the retinoic acid has been delivered to the P450 active site to produce the Type I spectral change (observable by the ΔA_{390}-A_{420} difference). However, I did not have enough boundary conditions to further model the individual steps in this complex system.

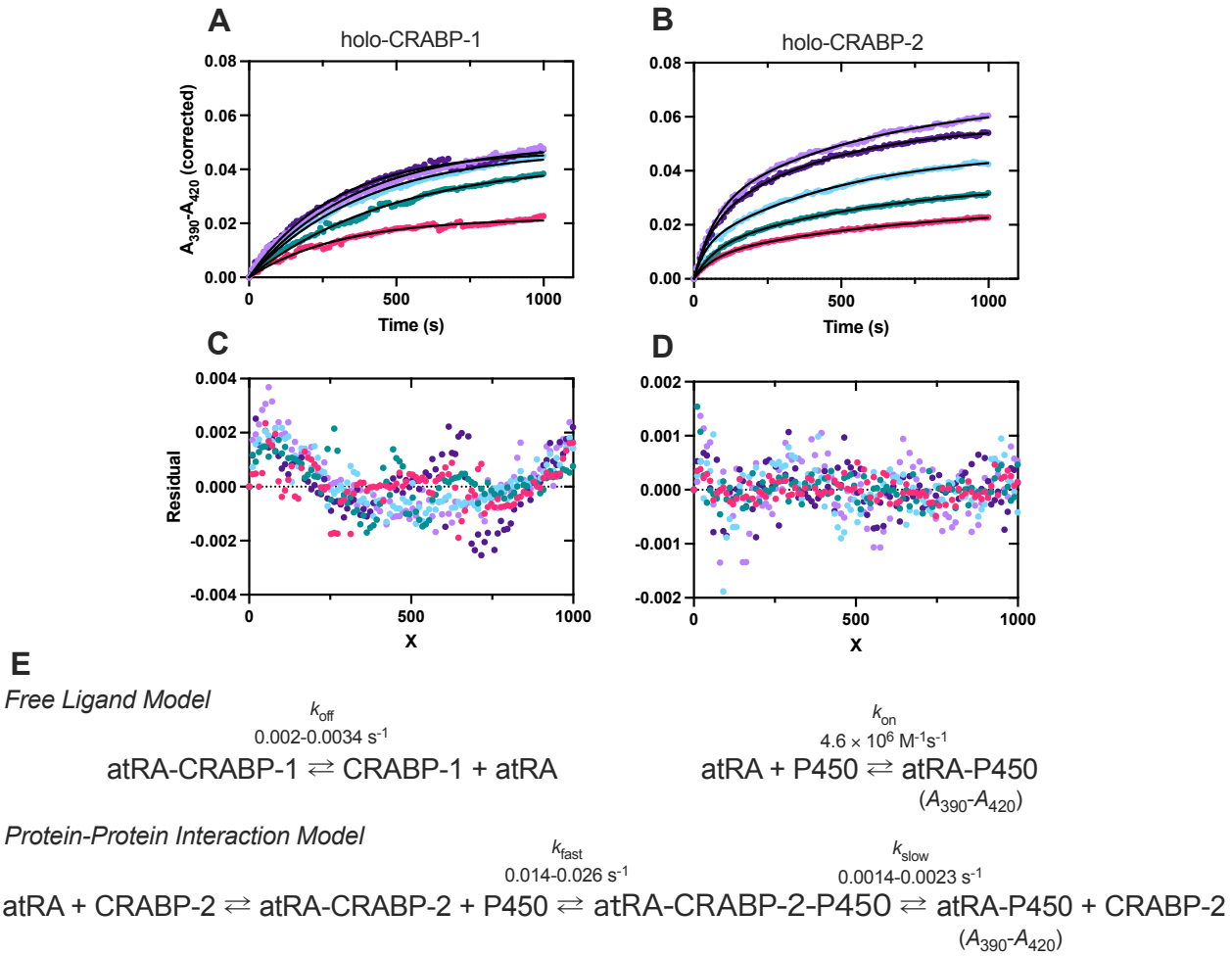

Figure 42. All-*trans* retinoic acid transfer rate dependence on P450 27C1 concentration. *A*, CRABP-1 fits. P450 27C1 concentration was varied (1-5 μM), and the data were fit to a single exponential, with rates varying from 0.0025 to 0.0034 s^{-1}. *B*, residuals plot for panel *A*. *C*, CRABP-2 fits. The P450 27C1 concentration was varied (1-5 μM), and the data were fit to a biexponential equation, with rates of the fast phase (25-38% of the reaction) varying from 0.014 to 0.026 s^{-1}. *D*, residuals plot for panel *C*. *E*, Scheme of proposed equilibria involved in the reactions.

5.2.4 Attempts to identify the P450 27C1-CRABP interaction interface

Cross-linking experiments were performed in attempt to characterize potential P450:CRABP complex formation. No cross-links were formed between P450 27C1 and apo- or holo-CRABPs (Figure 43), although a cross-link of P450 27C1 and Adx was detected under these conditions. Because of this, no downstream applications (i.e., in-gel digestion and LC-MS/MS

analysis) could be used to identify potential residues that mediated the P450 27C1:CRABP interaction.

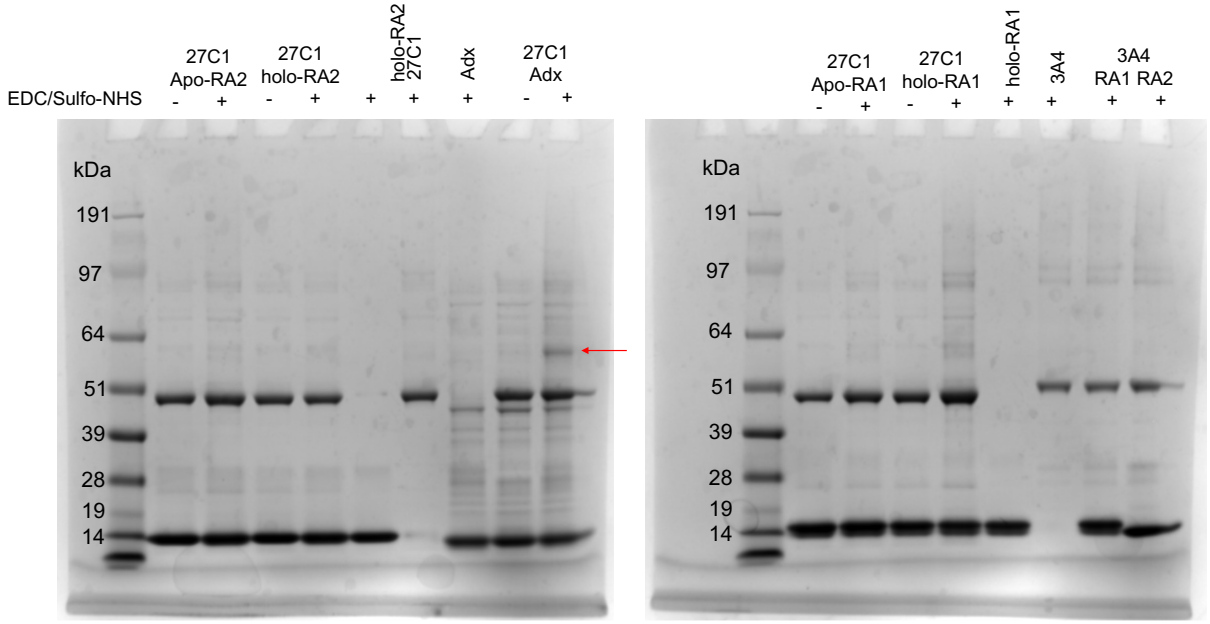

Figure 43. SDS-PAGE of EDC crosslinking of P450 27C1 with CRABPs. Crosslinking reactions were loaded in each lane as labeled. Incubations were performed with and without crosslinking reagents added. Controls with P450 27C1 and Adx (positive control) and P450 3A4 with holo-CRABPs (negative control) were also performed. Crosslink formed between P450 27C1 and Adx is labeled with a red arrow.

CRABP sequences and holo-CRABP structures were compared with one another to identify residues that may allow for differential interactions with P450 27C1 (Figure 44). There was one predominant area, the residues surrounding the entrance to the ligand binding site, where differences between the two structures were noted. To determine if these residues were key in mediating the interaction with P450 27C1, two mutant CRABPs were made, where the residues of one protein were swapped with the residues from the other. Steady-state kinetics assays with these holo-CRABP mutants (CRABP-1 Q75E/P81K/K102E and CRABP-2 E75Q/K81P/E102K) were performed, but the results were similar to those observed for the wild-type proteins (Figure 45).

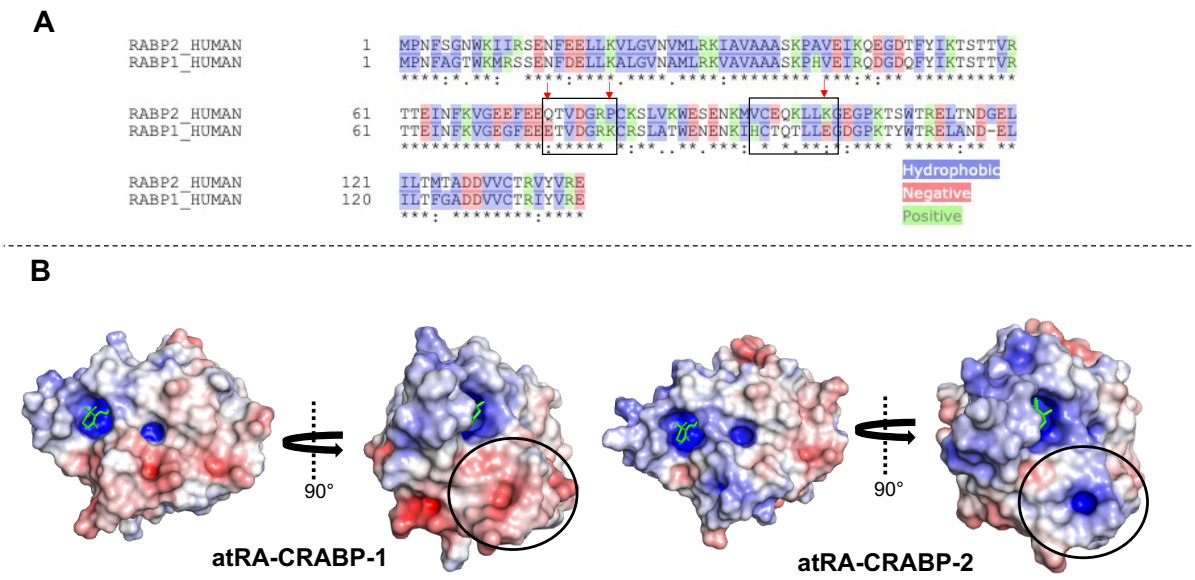

Figure 44. Sequence alignment and structural comparison of CRABP-1 and CRABP-2. *A*, Sequences for human CRABP-1 and CRABP-2 were aligned in UniProt with the Clustal Omega program (131). The proteins have 106 identical positions (77%) and 21 additional similar positions. Major regions of dissimilarity are boxed. Residues selected for mutagenesis are labeled with red arrows. **(***B*, The electrostatic potential of the holo-CRABP-1 (PDB: 1CBR) and holo-CRABP-2 (PDB: 1CBS) proteins (133) surface was visualized with the APBS plugin (132) in PyMOL (130). The major difference is circled, this corresponds to the boxed residues in panel *A*.

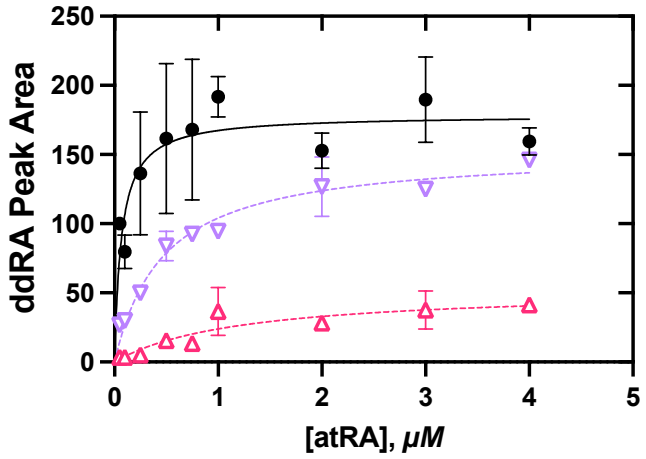

Figure 45. Effects of CRABP mutants on P450 27C1 all-*trans* retinoic acid desaturation. Steady-state kinetics of 3,4-dehydroretinoic acid formation from free all-*trans* retinoic acid (●), holo-CRABP-1 Q75E/P81K/K102E (△), and holo-CRABP-2 E75Q/K81P/E102K (▽). Reactions were done in duplicate and points are shown as means ± SD (range). Samples were analyzed by UPLC-UV.

5.2.5 Effects of apo-CRBPs on P450 27C1 activity

In order to examine the potential regulation of P450 27C1 activity by apo-CRBPs, reactions were performed with each retinoid and the respective retinoid-binding protein (Figure 46). All-*trans* retinol desaturation was inhibited by excess apo-CRBP-1, but this inhibition plateaued (Figure 46*A*). No inhibition was observed for all-*trans* retinaldehyde desaturation (Figure 46*B*), and all-*trans* retinoic acid desaturation was inhibited by both apo-CRABP-1 and apo-CRABP-2 with no product formation at a >2-fold molar excess of apo-CRABP (Figure 46*C*). K_i values calculated for inhibition of desaturation of all-*trans* retinol by apo-CRBP-1 or all-*trans* retinoic acid by apo-CRABPs ranged from 0.025 – 0.21 µM (Table 10).

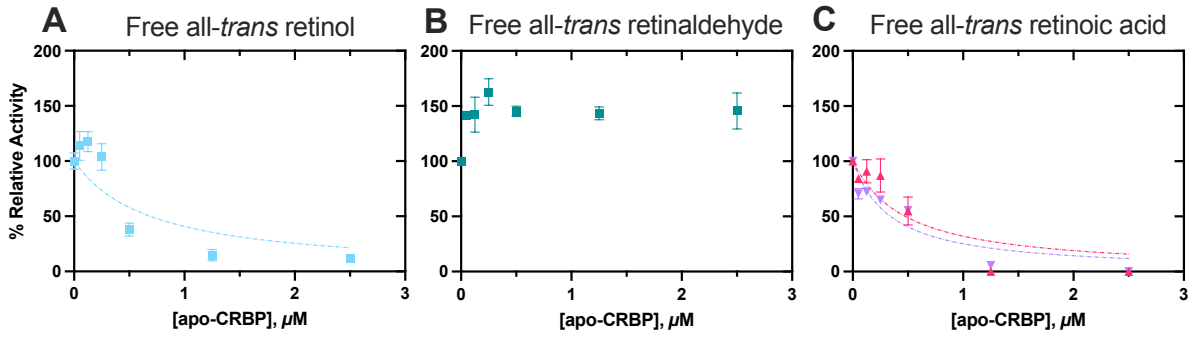

Figure 46. Effect of excess apo-CRBPs on 3,4-dehydroretinoid formation by P450 27C1. Incubations with excess apo-CRBPs were performed with: *A,* all-*trans* retinol; *B*, all-*trans* retinaldehyde; *C*, all-*trans* retinoic acid (0.5 µM, added as free substrate). Reactions contained apo-CRBP-1 (▫,▪), apo-CRABP-1 (▲), or apo-CRABP-2 (▼) up to 5 × the concentration of the retinoid in the reaction (0.05-2.5 µM, final). Reactions were done in duplicate and points are shown as means ± SD (range). Activity is relative to a point that did not contain apo-CRBP. Samples were analyzed by UPLC-UV.

Table 10. Inhibition of P450 27C1 retinoid desaturation by excess apo-CRBPs.

Retinoid	Apo-CRBP	K_i (μM)
atROL	CRBP-1	0.21 ± 0.08
atRAL	CRBP-1	N.D.[a]
atRA	CRABP-1	0.03 ± 0.01
	CRABP-2	0.025 ± 0.005

Results are from experiments done in duplicate. Parameters were estimated using the Morrison K_i equation in GraphPad Prism with data from Figure 46.

[a] No inhibition was observed with excess apo-CRBP-1 with all-*trans* retinaldehyde.

Similar to steady-state kinetics results, to determine whether the amount of desaturation that occurred in the reactions with excess apo-CRBP was due to substrate sequestration, kinetic values were calculated based on the amount of free substrate that would be present given the reported binding affinity of the CRBPs for retinoids (Table A5, Figure 47). Generally, the amount of product formed was higher than what would be expected if P450 27C1 was only able to oxidize the free retinoid in reaction. This further supports retinoid delivery from CRBPs to P450 27C1.

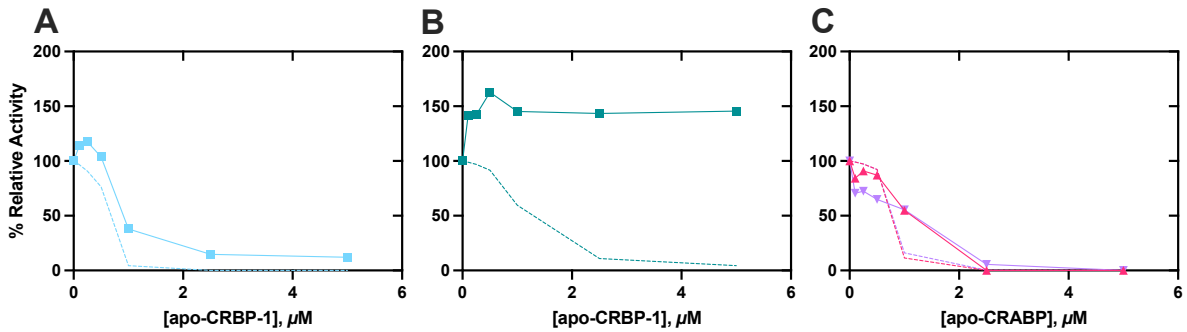

Figure 47. Calculated product formation in excess apo-CRBP assays under the free ligand hypothesis model. Observed and modeled inhibition of P450 27C1 desaturation reactions with: *A*, all-*trans* retinol with apo-CRBP-1 (—); *B*, all-*trans* retinaldehyde with apo-CRBP-1 (—); *C*, all-*trans* retinoic acid with apo-CRABP-1 (—) and apo-CRABP-2 (—). Experimental results (Figure 46) are shown as solid lines. Calculated product formation under the free ligand hypothesis with retinoid binding proteins is shown as dashed lines.

To determine if apo-CRBPs were general inhibitors of P450 27C1 desaturation or if apo-CRBPs could compete with holo-CRBPs for binding to P450 27C1, apo-CRPB inhibition assays were completed with CRBPs that did not bind the retinoid in the reaction (i.e. CRABPs with atROL and atRAL, CRBP-1 with atRA) (Figure 48). Reactions that were initiated with free substrate were designed to examine the general capacity for apo-CRBPs to inhibit desaturation (Figure 48*A*-*C*). Reactions initiated with holo-CRBPs were done to measure the potential for apo-CRBPs to compete for binding (Figure 48*D*-*F*). No inhibition was observed unless the apo-CRBP was able to bind the retinoid in the reaction.

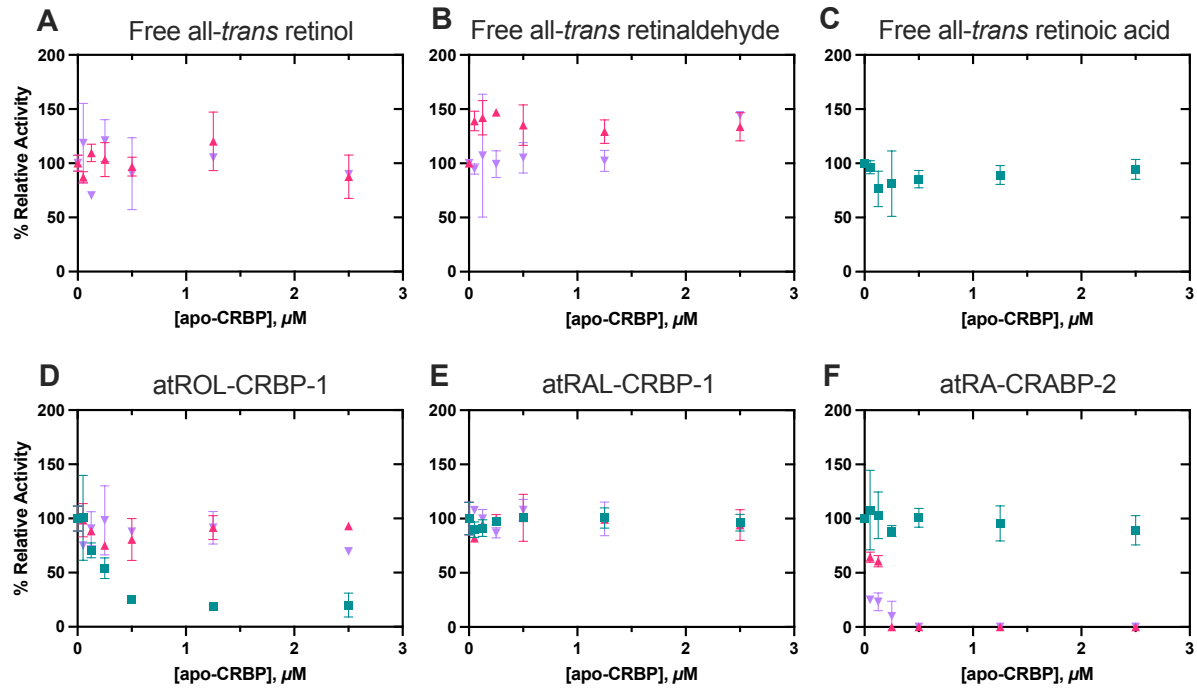

Figure 48. apo-CRBP inhibition of P450 27C1 does not occur through general allosteric modulation or competition with holo-CRBPs. Incubations with excess apo-CRBPs were performed with free substrate (0.5 μM): *A*, all-*trans* retinol; *B*, all-*trans* retinaldehyde; *C*, all-*trans* retinoic acid; or with holo-CRBP (0.5 μM): *D*, atROL-CRBP-1; *E,* atRAL-CRBP-1; *F*, atRA-CRABP-2. Reactions contained apo-CRBP-1 (■), apo-CRABP-1 (▲), or apo-CRABP-2 (▼) up to 5× the concentration of the retinoid in the reaction (0.05-2.5 μM, final). Reactions were done in duplicate and points are shown as means ± SD (range). Activity is relative to a point that did not contain apo-CRBP. Samples were analyzed by UPLC-UV.

5.3 Discussion

P450 27C1 has been identified as a retinoid desaturase (87,88). In fish and amphibians, the retinoid desaturase activity of P450 27C1 has an important physiological role in red-shifting photoreceptor sensitivity and allowing these organisms being able to see longer wavelength light (87). Human P450 27C1 performs the same reactions *in vitro* (88) and its localization to the skin has been identified (91), but the contribution of human P450 27C1 to retinoid desaturation *in vivo* has not been determined. The function of dehydroretinoids within the skin, where they constitute approximately ¼ of the retinoid pool (16), is also not well understood. In this work, we sought to

assess the potential contribution of P450 27C1 to retinoid desaturation *in vivo* and provide additional insight into the regulation and formation of dehydroretinoids, in the context of individual retinoid-binding proteins.

P450 27C1 is able to interact with holo-CRBP-1 and holo-CRABP-2 to receive all-*trans* retinoid substrates for metabolism. Based on the steady-state kinetics of product formation (Figure 38) and isotope dilution experiments (Figure 40), the observed patterns of product formation can only be explained by direct channeling of the retinoid substrate from the holo-binding protein to the P450 in that metabolism of only the free retinoid in the reaction would result in lower amounts of product formation (Figure 39). Catalytic assay results suggest that holo-CRABP-1 does not channel all-*trans* retinoic acid to P450 27C1 (Figure 38, Figure 40). Rates of all-*trans* retinoic acid transfer from the holo-CRABPs to P450 27C1 also support the conclusion about channeling with CRABP-2 but not CRABP-1 (Figure 41, Figure 42). Within the context of retinoid metabolism in the skin, the lack of interaction between P450 27C1 and CRABP-1 likely does not negatively affect the potential contribution of P450 27C1 to retinoid desaturation. CRABP-2 is the predominant CRABP expressed in the skin, and some reports describe little to no expression of CRABP-1 (22,23). P450 27C1 therefore could access most, if not all, of the all-*trans* retinoids present in the skin.

In all reactions with holo-CRBPs as substrate, the catalytic rate (k_{cat}) was decreased in comparison with the respective free substrates (Table 9). Previous studies have proposed that the decrease in catalytic rate observed with holo-retinoid-binding proteins is due to the rate of retinoid transfer from the binding protein to metabolic enzyme becoming rate-limiting in the reaction (21). To our knowledge, this has been proposed, but rates of transfer have not been determined. Given that substrate binding to P450s is readily observable and that we have previously determined the

rates of several steps of the P450 27C1 catalytic cycle (Figure 50) (91), we addressed the question of whether retinoid transfer became rate-limiting for P450 27C1 through UV-vis spectroscopy (Figure 41, Figure 42). The apparent k_{on} values of retinoid transfer from holo-CRABPs to P450 27C1 are much slower than the rate of free retinoid-binding (Figure 41). Additionally, these rates are on the same order of the observed k_{cat} for the reaction (Table 9), suggesting that retinoid transfer may be rate limiting. Additionally, no kinetic burst with holo-CRBPs was observed (Figure 49), as in the case with free all-*trans*-retinol as a substrate (91), indicating that a step following product formation did not become rate-limiting (i.e. step 9 in Figure 50).

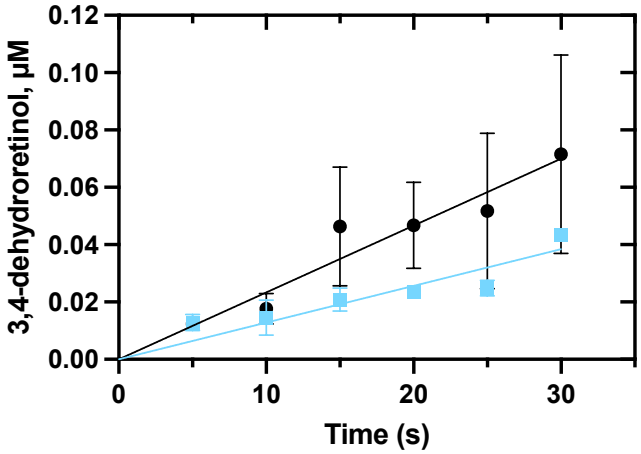

Figure 49. Lack of kinetic burst of product formation by P450 27C1 from free all-*trans* retinol or holo-CRBP-1. Time course assay of all-*trans* retinol desaturation with linear extrapolation to time 0. Reactions contained 0.02 µM P450 27C1. The curves represent the fit to the equation $y = A(1-e^{-kp*t}) + k_{ss}*t$, where A represents the burst amplitude, k_p represents the first-order rate of the pre-steady-state burst, and k_{ss} represents the steady-state rate. The best-fit values for A and k_p were 0 with both free atROL (●) and holo-CRBP-1 (■), indicating a lack of burst kinetics.

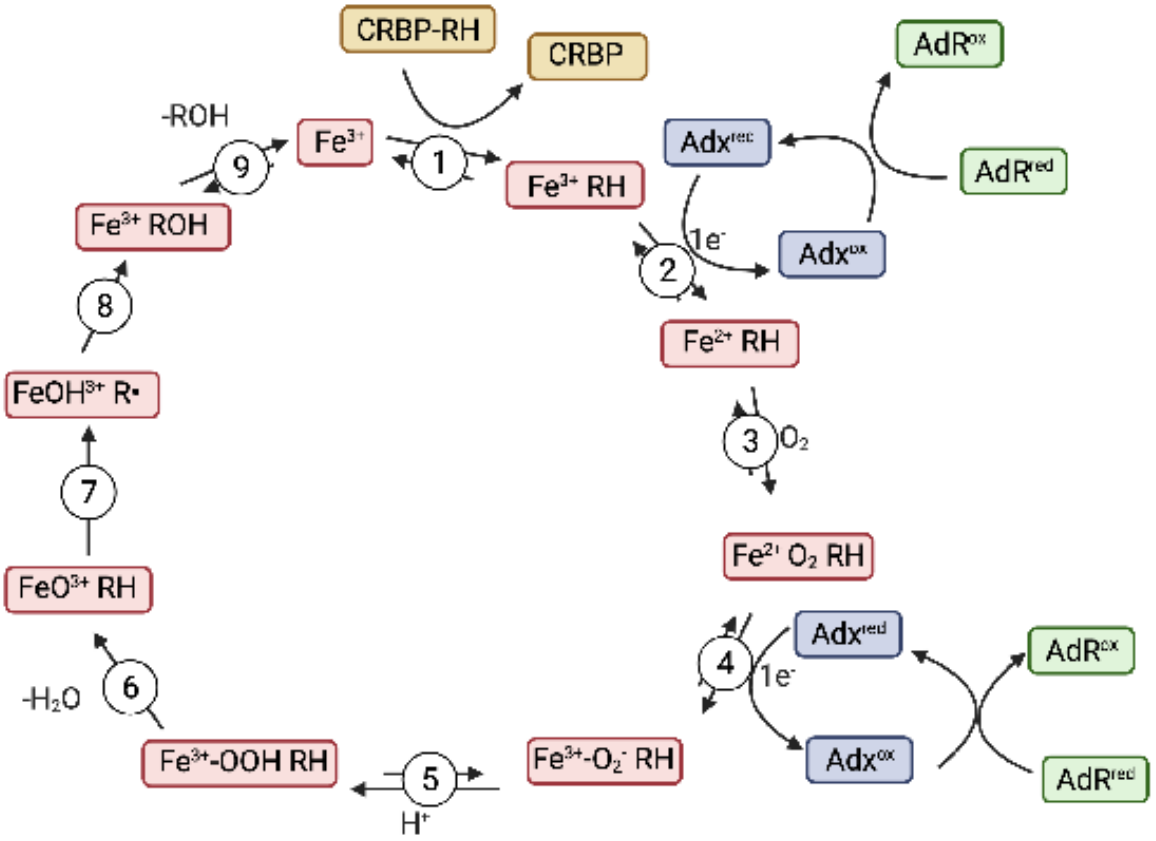

Figure 50. Proposed catalytic cycle for P450 27C1 with CRBPs. Steps are indicated with numbers. Rates for steps 1 (with free retinoid binding), 2, 7, and 9 were previously measured, and steps 2 (reduction by Adx) and 7 (hydrogen abstraction) were determined to be partially rate limiting (91). With holo-CRBPs, step 1 (retinoid transfer) becomes rate-limiting, leading to the observed decreases in k_{cat}. Figure created in BioRender.com.

We observed specificity in the interaction of cellular retinoid-binding proteins with P450 27C1. P450 27C1 can accept retinoid substrates from holo-CRBP-1 and holo-CRABP-2 but not holo-CRABP-1. There are minor differences between the two CRABP proteins studied (77% identity, 93% similarity, Figure 44), and attempts were made to identify the potential P450:CRABP interaction interface. Interactions between holo-CRBPs and retinoid-receiving proteins are often transient and have been difficult to detect (197-199). Cross-linking was selected as a potential experimental method to trap the proteins together for structural characterization. The

approach has previously been used to study interactions between P450s and their catalytic redox partners. EDC is often used due to the presence of primary amines on the proximal P450 surface and abundance of carboxylic groups on the redox partner surface (113,174,200,201). CRABPs, like NADPH-P450 reductase, cytochrome b_5, and Adx, also have many carboxylic acid groups on their surfaces, so a similar cross-linking approach was utilized. While P450 27C1 was able to form cross-links with Adx, as expected, no cross-links were detected between P450 27C1 and CRABPs (Figure 43). Lack of chemical cross-linking has also previously been reported with CRABP-2 and RAR (196). This was attributed to the transient nature of the interaction between the two proteins. We believe that the interaction between P450 27C1 and the cellular retinoid-binding proteins may also be transient. Other efforts (gel filtration, UV-visible spectroscopy, zonal elution chromatography) were made to observe physical binding but were unsuccessful (data not shown).

Accordingly, mutagenesis was performed solely on the basis of a holo-CRABP structure comparison (Figure 44). Three residues—amino acids 75, 81, and 102—were selected for mutagenesis. Notably, these mutations to CRABPs have been made previously to identify the region of CRABP-2 that mediates the interaction with the retinoic acid receptor (RAR) (197). As in the case of P450 27C1, holo-CRABP-2 can transfer all-*trans* retinoic acid to RAR but holo-CRABP-1 cannot. In the case of RAR, it was found that these three residues were necessary and sufficient to mediate the interaction of CRABPs with RAR. CRABP-1, with the corresponding residues from CRABP-2 (Glu-75, Lys-81, Glu-102), was able to transfer all-*trans* retinoic acid to RAR; CRABP-2 with the corresponding residues from CRABP-1 (Gln-75, Pro-81, Lys-102) was no longer able to. With P450 27C1, this did not occur. Steady-state kinetic analyses with these two mutant proteins resembled that of the WT proteins (Figure 45). These results suggest that different (or additional) residues are required to mediate the interactions of CRABPs with P450 27C1 in

comparison with RAR. The molecular basis for the functional difference between CRABP-1 and CRABP-2 in delivery of all-*trans* retinoic acid to P450 27C1 remains unknown.

Regulation of P450 27C1 activity by apo-CRBPs was also assessed (Figure 46). The effects of apo-CRBPs on P450 27C1 retinoid desaturation was substrate dependent, with the amount of inhibition varying from 0-100%. Previously, the plateau in inhibition after the ratio of binding protein:retinoid exceeded 1, as observed with P450 27C1 and all-*trans* retinol desaturation with excess apo-CRBP-1, was proposed to indicate allosteric modulation or inhibition of P450-mediated retinoid metabolism (32). For apo-CRABPs, the K_i values were less than the K_m for the reactions of P450 27C1 with the holo-CRABPs. This has previously been suggested to be due to differential recognition of apo-and holo-binding proteins by metabolic enzymes (37). If this was the case with P450 27C1, apo-cellular retinoid-binding proteins may inhibit desaturation even if they do not bind the retinoids present in the reaction (i.e., apo-CRABPs should inhibit all-*trans* retinol and retinaldehyde desaturation and apo-CRBP should inhibit all-*trans* retinoic acid desaturation). To examine this possibility, additional assays were done with excess apo-CRBPs that did not bind the retinoid in the reaction (Figure 48*A*-*C*). No inhibition was observed in any of these conditions, suggesting that apo-CRBPs do not cause P450 27C1 inhibition through allosteric modulation. The possibility of apo-CRBPs competing with holo-CRBPs for binding to P450 27C1 was also considered. To address this, holo-CRBP-1 or holo-CRABP-2 was used to initiate reactions containing excess apo-CRBPs. Again, no inhibition was observed with each apo-CRBPs unless it could bind the retinoid in the reaction. Of note, the activity observed with increasing concentrations of apo-CRBP-1 supports our conclusion about the interaction of holo-CRBP-1 with P450 27C1, as the amount of product formed in these assays surpasses what would be predicted by the free ligand model (Figure 47*A*-*B*). With all-*trans* retinaldehyde, where the steady-state

kinetics of product formation do not appear largely different from the free ligand prediction (Figure 39*B*) due to the low K_m of retinoid desaturation and relatively high K_d of binding to CRBP-1 (Table A5), apo-CRBP-1 inhibition results provide additional support for substrate channeling.

Some results from this study were surprising and are still not fully understood. While not unprecedented (i.e., RAR specificity (196)), given the similarity of CRABP-1 and CRABP-2 and the ability of both proteins to interact with the CYP26 enzymes (31,32), the difference observed in the CRABP interaction with P450 27C1 was unexpected. Despite our efforts, the basis of the difference in specificity remains unknown. Additionally, the mechanism by which apo-cellular retinoid-binding proteins inhibit P450 27C1 desaturation is unclear. Previous work has suggested that the retinoid-binding ability of the protein was not required, and that inhibition may occur through allosteric modulation or competition with holo-binding proteins. Our results suggest that these two mechanisms do not generally occur with P450 27C1, but our results are consistent with the hypothesis that inhibition does not occur purely through retinoid sequestration (as would be predicted by the free ligand model, Figure 47). Also of note, there is a lack of inhibition with all-*trans* retinaldehyde (Figure 46, Figure 48). One possibility is that the interaction interface between P450 27C1 and each holo-CRBP is different, and that only the corresponding apo-CRBP can bind to the same site as the holo-CRBP. Alternatively, apo-CRBPs could specifically interact with the corresponding holo-CRBP and prevent transfer to P450 27C1. Without additional evidence, we cannot prove an alternate mechanism of apo-CRBP inhibition.

To our knowledge, this is the first study characterizing the interactions of a mitochondrial retinoid metabolizing enzyme with cellular retinoid-binding proteins. The mitochondrial localization of P450 27C1 is based on its requirement of Adx and AdR for catalysis (88) and the presence of a putative mitochondrial translocation sequence (91). Previous work of this nature has

focused on interactions with proteins that are generally expressed in the endoplasmic reticulum (CYP26 enzymes (31,32), retinol dehydrogenases (202), retinaldehyde dehydrogenases (203), lecithin retinol acyltransferase (37)), cytosol (retinaldehyde dehydrogenase (204)), or nucleus (RAR (196)). Cellular retinoid-binding proteins are soluble proteins and largely considered cytoplasmic, but it is well known that they can localize to other areas within the cell (i.e. nucleus, ER-associated). Some studies have suggested that retinoid-binding proteins may also localize to the mitochondria. CRBP-1 has been shown to co-localize with mitochondrial markers in cell immunofluorescence studies (205), and CRBP and CRABP have previously been shown to co-sediment with mitochondria (206,207). The localization of retinoid-binding proteins within the mitochondria is currently unknown, but potential presence within the intermembrane space has been proposed (207). Mitochondrial P450s are cytoplasmically-synthesized and then are generally thought to be inserted into the inner membrane of the mitochondria after cleavage, with the protein residing in the intermembrane space (97), thus potentially co-localizing with CRBPs. The mechanism of cellular retinoid-binding protein localization to the mitochondria has not been characterized. Some studies have shown that cellular retinoid-binding proteins can become post-translationally modified when localizing to different subcellular areas (e.g. nuclear localization of CRABP-2 following SUMOylation (208)). No modifications have been identified with mitochondria-localized cellular retinoid-binding proteins, but if they are present, these may affect the interaction with P450 27C1 *in vivo*.

The majority of retinoid metabolizing enzymes are localized to the endoplasmic reticulum. Outside of P450 27C1, the only mitochondrial retinoid metabolizing enzyme that has been identified to our knowledge is retinol dehydrogenase 13 (RDH13), which catalyzes the reduction of all-*trans* retinaldehyde (209). Like mitochondrial P450s, RDH13 is associated with the inner

mitochondrial membrane, facing the intermembrane space. The ability of RDH13 to interact with retinoid-binding proteins has not been assessed. Some isoforms of RAR have even been found in mitochondria (210) and direct RAR regulation of mitochondrial transcription has been proposed (211). Although mitochondria have historically not been considered to have roles in retinoid function or metabolism, the presence of retinoid-binding proteins, RARs, and metabolic enzymes suggests a potential unknown biological importance of retinoids in mitochondrial function or the mitochondria in retinoid metabolism.

The ability of P450s to interact with cellular retinoid-binding proteins to receive substrates raises interesting questions about the potential for other P450-shuttle protein interactions. CRBPs and CRABPs are members of the iLBP family of proteins. Within this family is also the fatty acid-binding proteins (FABPs). Like retinoid-binding proteins, FABPs can directly interact with nuclear receptors (peroxisome proliferator activated receptors (PPARs)) (212-214) and some metabolic enzymes (hormone-sensitive lipase) (215). Many P450s oxidize fatty acids (148), but to our knowledge, potential interactions between P450s and FABPs have not been investigated. These shuttle proteins may have the potential to directly interact with P450s and regulate metabolism *in vivo*. Alternatively, they may sequester ligands from P450s that have been identified as metabolic enzymes *in vitro*, limiting the contributions of these P450s to *in vivo* metabolism.

5.4 Conclusions

In summary, both holo-CRBP-1 and holo-CRABP-2 appear to directly channel retinoid ligands to P450 27C1. The rate of the P450 27C1 desaturation reaction when utilizing these holo-CRBPs as substrates is limited by the rate of retinoid transfer from the binding protein to the P450.

Additionally, P450 27C1 activity can be regulated by concentrations of apo-CRBPs; increasing the concentrations of these apo-CRBPs typically inhibits P450 27C1 desaturation. The ability of P450 27C1 to interact with cellular retinoid-binding proteins supports its identification as an *in vivo* retinoid desaturase.

Chapter 6. Physiological role of P450 27C1 and 3,4-dehydroretinoids in the skin

6.1 Introduction

The function of P450 27C1 within the skin is unknown. In Chapter 3, P450 27C1 was localized to keratinocytes, so keratinocytes are the ideal cell type to study the physiological function of P450 27C1. Work in Chapter 3 utilized primary keratinocytes to illustrate localization, but primary cells have a limited life span in culture. Primary keratinocytes are also prone to undergo terminal differentiation. Because of this, immortalized keratinocytes are an attractive alternative for a model system. Very few immortalized keratinocyte cell lines are available. The most commonly used is the HaCaT line, which is spontaneously immortalized human keratinocyte cell line. These cells differentiate in response to stimuli like primary keratinocytes (216), but studies have shown that some transcription patterns are abnormal (217,218) and the cells are aneuploid (217). In 2000, the N/TERT lines were developed (N/TERT-1, N/TERT-2G) by transduction with telomerase reverse transcriptase (134). These cells lack a cell cycle control mechanism (pRB/$p16^{INK4a}$) but differentiate normally and are considered a better model for primary keratinocytes (219). RNA-sequencing analyses of N/TERT-2G cells also show the presence of *CYP27C1* transcripts (personal communication). Because of this, N/TERT-2G cells were pursued as a potential system to study P450 27C1 function. To determine the function of P450 27C1, N/TERT-2G *CYP27C1* KO cell lines were generated (by the University of Michigan Skin Biology and Disease Resource-based Center) to be compared with WT cells by RNA-sequencing.

The function of 3,4-dehydroretinoids within the cell is unknown. Like all-*trans* retinoic acid, 3,4-dehydroretinoic can bind to RARs/RXRs (56,63), but few, if any, differentially regulated

genes have been identified (64,65). Some studies have proposed that 3,4-dehydroretinoids are more stable than all-*trans* retinoids when exposed to UV light (65,66). To date, 3,4-dehydroretinoids serving as a potential "storage reserve" for all-*trans* retinoids following UV exposure is the only unique proposed function for 3,4-dehydroretinoids in the skin. We hypothesize that 3,4-dehydroretinoids may also be more metabolically stable than all-*trans* retinoids. All-*trans* retinoic acid is the active form of retinoids within the cell, and it is catabolized through oxidation by cytochrome P450s. Many cytochrome P450s (e.g. P450 3A4, 2C8, 2C9, 1A1, 4A11) have been shown to metabolize retinoids *in vitro* (220), but the CYP26s are believed to be the major enzymes responsible for clearing all-*trans* retinoic acid (221). Unlike P450 27C1, the CYP26s are present in many tissues throughout the body. The primary metabolite formed from all-*trans* retinoic acid is all-*trans* 4-hydroxyretinoic acid. All-*trans* 4-oxoretinoic acid and all-*trans* 18-hydroxyretinoic acid along with secondary metabolites have also been observed (221). 3,4-Dehydroretinoids have a double bond at the all-*trans* retinoic acid site of catabolism (position 4, Figure 1). While not mechanistically impossible, this may prevent the CYP26 enzymes from hydroxylating 3,4-dehydroretinoids at this position. The activity of the CYP26s with 3,4-dehydroretinoic acid has not been tested, though one study reported that P450 26C1 cannot metabolize 3,4-dehydroretinol (32).

In this work, N/TERT-2G lines were assessed for P450 27C1 expression and 3,4-dehydroretinoid formation. 3,4-Dehydroretinoids levels in cultured keratinocytes have been reported to be dependent on the differentiation status of the cells (54). Studies were pursued here with calcium-induced differentiation to directly assess effects of differentiation of P450 27C1 expression. Additionally, metabolic stability is explored as a potential function of 3,4-dehydroretinoids.

6.2 Results

6.2.1 P450 27C1 expression and 3,4-dehydroretinoid formation in N/TERT cell lines

WT, CRISPR Cas9 KO control, and two *CYP27C1* KO N/TERT-2G cell lines were grown as monolayer cultures in serum-free media with both low (0.3 mM) and high (2.0 mM) calcium. From a general morphology perspective, all cells appeared normal and differentiated as expected with calcium treatment (Figure 51).

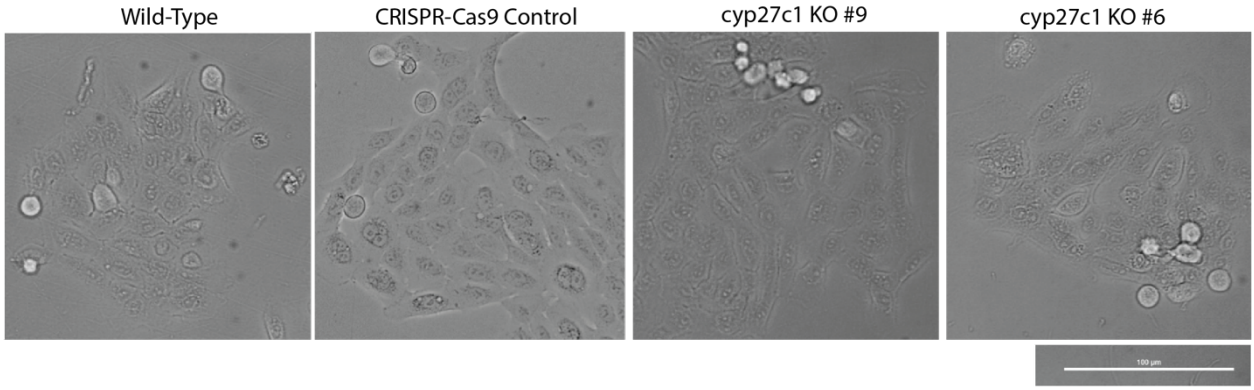

Figure 51. Morphology of N/TERT-2G cell lines. Cells shown were grown in keratinocyte SFM with 0.3 mM calcium. Cells were imaged in plastic culture dishes with a Nikon AZ100 at 20X magnification by Dr. Jenny Schafer. Scale bar is for 100 µm.

For validation of the *CYP27C1* KO (previously confirmed by sequencing) and to select optimum conditions to study P450 27C1, immunoblotting was performed with cells grown in low calcium (undifferentiated) or in high calcium media for 2 or 6 days (differentiating conditions). P450 27C1 did not seem to be present in any of the cell lines or media conditions (Figure 52). There is a weak immunoreactive band in the most differentiated keratinocytes around the expected size of P450 27C1, but it is present in both KO cell lines.

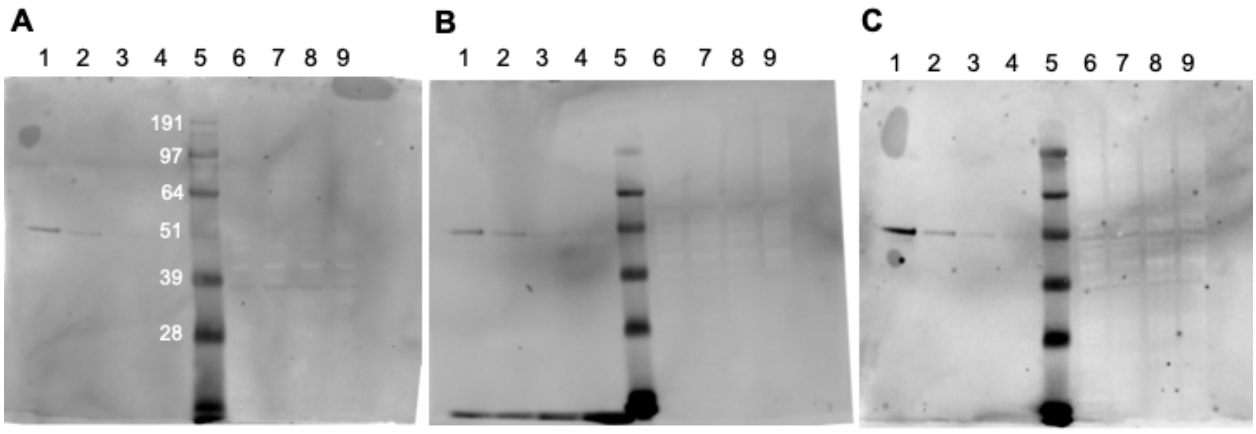

Figure 52. Immunoblot of P450 27C1 expression in N/TERT cell lines. *A*, 0.3 mM calcium; *B*, 2.0 mM calcium for 2 days; *C,* 2.0 mM calcium for 6 days. Each lysate lane contains 20 µg of total protein as determined by BCA assay. Purified recombinant P450 27C1 is shown as a control. Lanes: 1-4, purified recombinant P450 27C1 (0.5, 0.25, 0.1, 0.05 pmol); 5, ladder; 6, WT; 7, CRISPR Cas9 control; 8, *CYP27C1* KO #6; 9, *CYP27C1* KO #9. Molecular weight markers are labeled in panel *A*.

The N/TERT-2G lines were also assessed for biosynthesis of 3,4-dehydroretinoids utilizing an *in vitro* system with cell lysates as previously described (65). For analysis of 3,4-dehydroretinoid formation in N/TERT-2G lysates, extracts were treated with ethanolic KOH to liberate retinols from retinyl esters. Because hydrolysis is required for analysis, retinoids from these reactions were analyzed in two parts: retinoid alcohol and retinoic acids. Extractions of the ethanolic KOH mixture results in only retinoid alcohols and the sample is acidified for retrieval of retinoid acids. WT N/TERT-2G lysates incubated with all-*trans* retinol were unable to form 3,4-dehydroretinoids (either 3,4-dehydroretinol or 3,4-dehydroretinoic acid) (Figure 53). This is not due to a general lack of activity in these lysates, as all-*trans* retinoic acid was formed in the incubations. As expected given the serum-free media conditions, cells did not naturally contain retinoids. The other N/TERT-2G cell lines (the CRISPR Cas9 control and both KO) were also

assessed for their ability to form 3,4-dehydroretinoids, but 3,4-dehydroretinoids were not detected, similar to the WT cells (Figure 54).

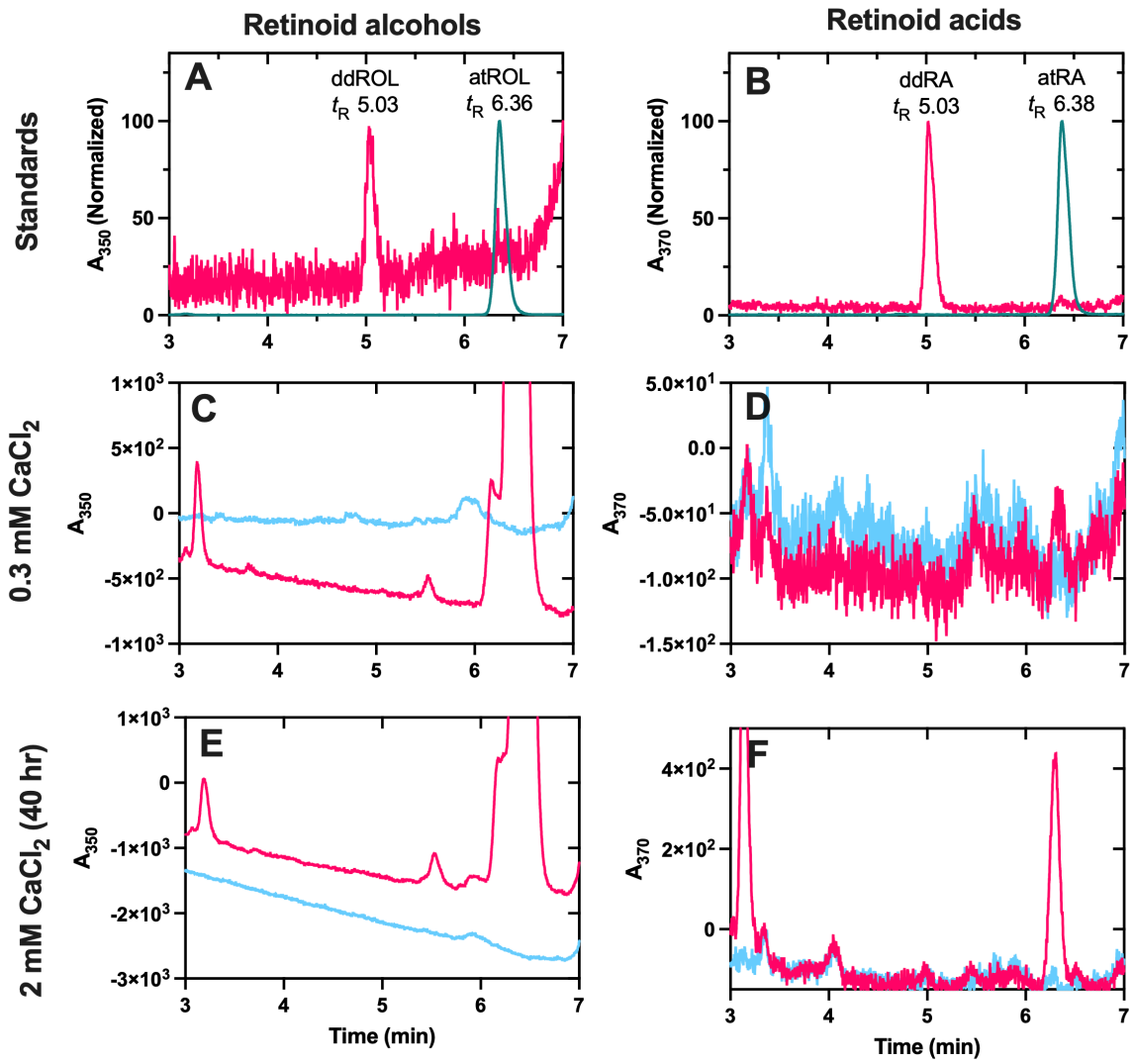

Figure 53. Assessing 3,4-dehydroretinoid formation in wild-type N/TERT-2G cells. Standards for 3,4-dehydroretinoids and all-*trans* retinoids are shown in panel *A* (alcohols) and *B* (acids). Reactions were performed with 10 µM all-*trans* retinol (–) or ethanol vehicle control (–) for 1 hr with cell grown in low calcium media (*C*, *D*) or high calcium media for 2 days (*E*, *F*). Samples were analyzed by UPLC-UV.

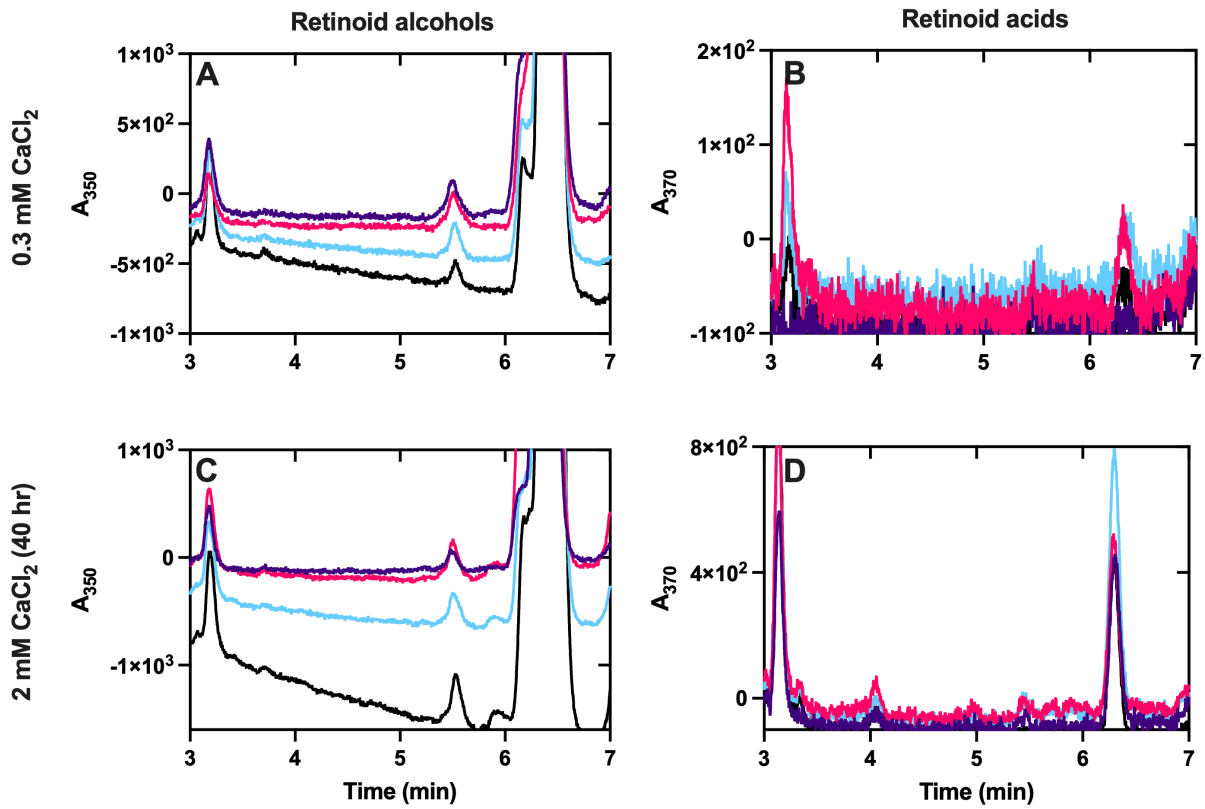

Figure 54. Comparison of all-*trans* retinol metabolism in N/TERT-2G cell lines. Reactions were performed with 10 µM all-*trans* retinol with WT (–), CRISPR Cas9 control (–), *CYP27C1* KO #6 (–), and *CYP27C1* KO #9 (–) cells grown in low calcium media (*A*, *B*) or high calcium media for 2 days (*C*, *D*). Samples were analyzed by UPLC-UV.

6.2.2 Resistance of 3,4-dehydroretinoids to CYP26-mediated catabolism

The ability of P450s to form all-*trans* 4-hydroxyretinoic acid and all-*trans* 4-oxoretinoic acid from all-*trans* retinoic acid and 3,4-dehydroretinoic acid was assessed in HLMs (Figure 55). HLMs contain many P450s including the CYP26s that are responsible for catabolism of all-*trans* retinoic acid *in vivo*. Incubation with all-*trans* retinoic acid resulted in three major peaks, two of which were identified by co-elution with reference standards to be all-*trans* 4-hydroxy and 4-oxo-retinoic acid. Incubation with 3,4-dehydroretinoic acid resulted in no P450-mediated metabolites as evidenced by the comparison with the no NADPH control. To assess the relative contribution

of the CYP26s to all observed P450-mediated metabolism, reactions were also performed with ketoconazole (a general P450 inhibitor) and R115866 (a CYP26-specific inhibitor). Incubations with both ketoconazole and R115866 resulted in significant inhibition of all-*trans* retinoic acid metabolism. Similarity between metabolite peak areas from incubations with both inhibitors indicates that this metabolism is predominantly CYP26-mediated.

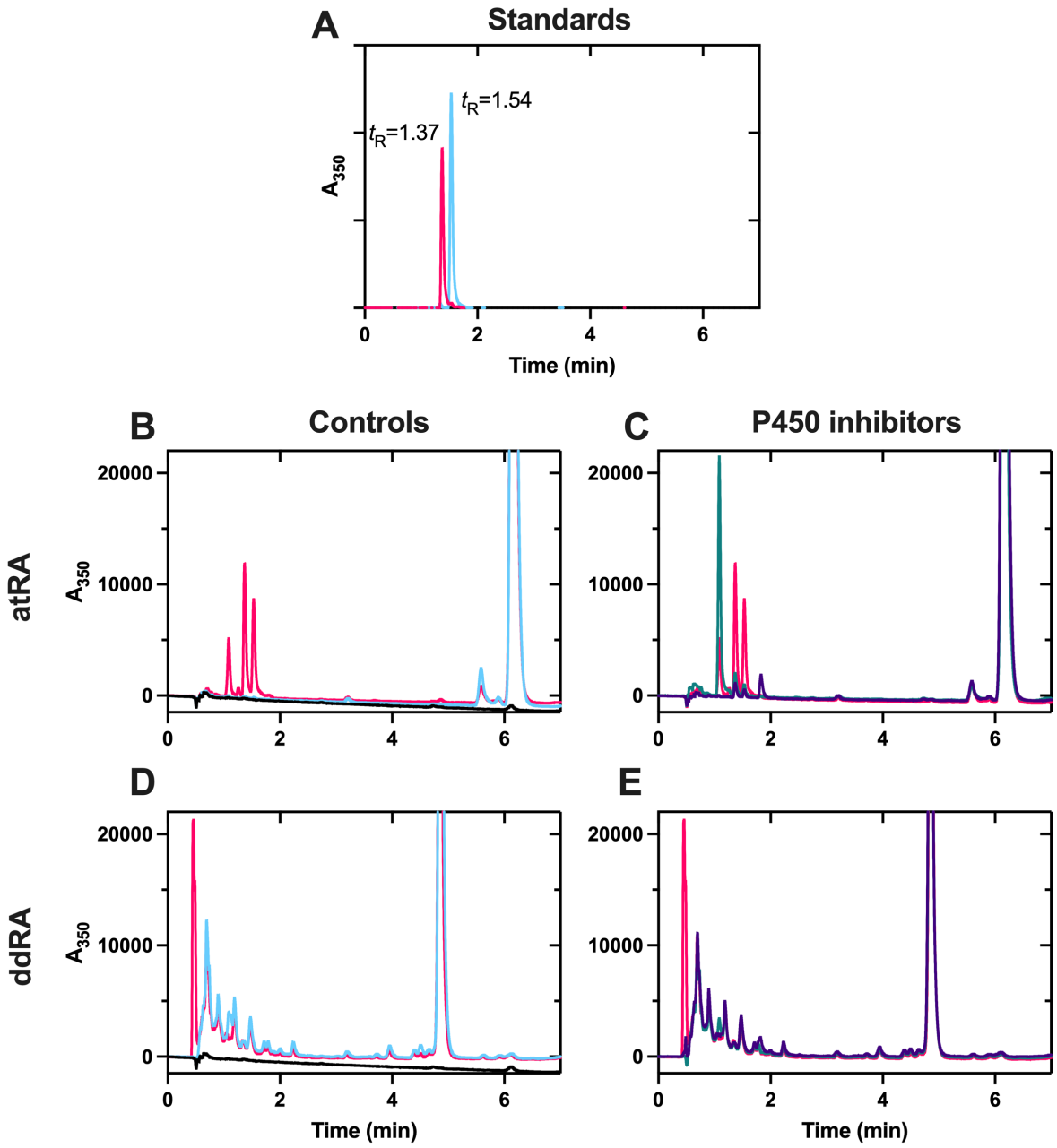

Figure 55. Comparison of all-*trans* retinoic acid and 3,4-dehydroretinoic acid catabolism. Metabolism of all-*trans* retinoic acid (*B*, *C*) and 3,4-dehydroretinoic acid (*D*, *E*) in HLM (–). Panels *B* and *D* show comparisons with control reactions performed without NADPH (–) or without retinoid (–, ethanol vehicle control). Panels *C* and *E* show comparisons with reactions performed in the presence of ketoconazole (–, general P450 inhibitor) or R115866 (–, CYP26-specific inhibitor). Standards for major catabolic products all-*trans* 4-hydroxyretinoic acid (–, 4-OH-RA) and all-*trans* 4-oxoretinoic acid (–, 4-oxo-RA) are shown in panel *A*. Samples were analyzed by UPLC-UV.

6.3 Discussion

The function of P450 27C1 (and 3,4-dehydroretinoids) within the skin is unknown. To address this, I opted to pursue the generation of a *CYP27C1* KO cell line. P450 27C1 was found to be expressed in primary keratinocytes (Chapter 3) so N/TERT-2G cells, an immortalized keratinocyte cell line, were selected for this purpose as they are generally considered the best comparison with primary cells (219). With these N/TERT-2G cells, I had planned on performing RNA-sequencing to compare the WT, CRISPR Cas9 control, and two *CYP27C1* KO lines with and without all-*trans* retinoid or 3,4-dehydroretinoid treatment.

Successful KO of *CYP27C1* was verified by sequencing (Figure A2) but immunoblot analysis of both control cell lines (WT and the CRISPR Cas9 control) show that these cells do not express P450 27C1 in the undifferentiated or differentiated state (Figure 52). The lack of P450 27C1 in immunoblotting prevented validation of the *CYP27C1* KO on the protein level. These cells do also not appear to be able to form 3,4-dehydroretinoids from all-*trans* retinol (Figure 53, Figure 54). While the lack of P450 27C1 expression in the N/TERT-2G line did end up making these immortalized keratinocytes a poor choice for a *CYP27C1* KO to assess the protein's function, there are still useful insights that can be gained from this work. First, there is no detectable 3,4-dehydroretinoid formation in *in vitro* assays with these cells which does provide some support of the assignment of P450 27C1 as the potentially sole retinoid desaturase in the skin. Additionally, this N/TERT-2G cell line was initially utilized due to the amenability to modification in comparison with primary keratinocytes. While in this case, that was utilized to perform a CRISPR/Cas9 KO, it could also potentially be used as a system to express P450 27C1. This would be more informative than expressing P450 27C1 in a cell type that P450 27C1 is not typically present in *in vivo* (e.g. HEK293 or COS cells). A difference in P450 27C1 expression or 3,4-

dehydroretinoid formation within different keratinocyte cell lines is not unprecedented. Previous work by Tafrova *et al.* tested a variety of keratinocyte cell lines for their ability to convert all-*trans* retinol to 3,4-dehydroretinol. Four cell lines (two normal human epidermal keratinocyte lines (NHEK) and two squamous cell carcinoma cell (SCC) lines) were screened (106). The SCC lines had a higher percentage of 3,4-dehydroretinoids than the NHEK. The two SCC cell lines were also different - one had 2.5 times the amount of 3,4-dehydroretinyl esters than the other. HaCaT cells and N/TERT cell lines were not tested, and to my knowledge no studies have reported 3,4-dehydroretinoid levels or biosynthetic capacities in these cell lines. It may also be possible that P450 27C1 is expressed in N/TERT-2G cells, but only in conditions that were not tested here. Additional analyses of P450 27C1 expression could be performed by PCR (to see if *CYP27C1* transcripts are present in any of the cell lines) or proteomics (for more sensitivity and to rule out any potential problems with immunoblotting).

The ability of the CYP26 enzymes to form all-*trans* 4-hydroxy and 4-oxoretinoic acid from 3,4-dehydroretinoic acid was assessed in HLMs. HLMs were utilized as they contain the CYP26 enzymes, though this is not the most direct (i.e. studies with recombinant proteins) or physiologically relevant system (i.e. skin cell based system) to study 3,4-dehydroretinoid metabolism by the CYP26 enzymes. Unlike all-*trans* retinoic acid, incubations with 3,4-dehydroretinoic acid do not result in the significant formation of 4-oxygenated retinoic acid (Figure 55). Additional work is necessary to prove that 3,4-dehydroretinoids are overall more metabolically stable. A time course assay to measure the quantity of remaining 3,4-dehydroretinoic acid would more directly assess this, as there could be products outside of 4-oxygenated retinoic acid formed that are not being accounted for.

6.4 Conclusions

The N/TERT-2G immortalized keratinocyte cell line does not appear to express P450 27C1 or form 3,4-dehydroretinoids *in vitro*. The lack of CYP26-mediated catabolism of 3,4-dehydroretinoic acid suggests a previously undescribed function of 3,4-dehydroretinoids *in vivo*. 3,4-Dehydroretinoids may serve as a more stable retinoid source within the cell, even outside of exposure to UV light.

Chapter 7. Conclusions and Future Directions

7.1 Summary of Work

3,4-Dehydroretinoids were first identified in the skin in 1980 (48) but the enzyme responsible for their formation has not been identified. Evidence in the literature supports a mitochondrial P450 being responsible for this activity – subcellular fractions containing mitochondria are able to generate 3,4-dehydroretinoids and their formation is stimulated by NADPH (utilized by P450 redox partners) and inhibited by ketoconazole (a general P450 inhibitor) (65,67,106). Human P450 27C1 is a mitochondrial P450 based in its requirements of AdR and Adx for catalysis and catalyzes the desaturation of all-*trans* retinoids *in vitro* (88). P450 27C1 expression is also enriched in the skin (91). Given these facts, P450 27C1 is hypothesized to be the enzyme responsible for 3,4-dehydroretinoid formation in the skin. The overall goal of this work was to test this hypothesis and to further characterize P450 27C1 to provide a better understanding of the formation of dehydroretinoids in the skin. Towards this goal, I have worked on four projects related to P450 27C1.

In Chapter 3, the localization and quantification of P450 27C1 within the skin was assessed. By tissue immunofluorescence and immunoblotting, P450 27C1 appears to be specifically expressed in keratinocytes of the epidermis. This is consistent with what is known about 3,4-dehydroretinoid formation, as this activity is generally associated with keratinocytes (54). A QconCAT was generated to enable simultaneous quantification of P450 27C1 and the P450 redox partners through a targeted mass spectrometry-based approach.

For Chapter 4, interactions between P450 27C1 and Adx, the protein that directly delivers electrons to mitochondrial P450s for catalysis, were assessed. Two methods, MST and fluorescence titrations, were utilized to measure the binding affinity between P450 27C1 and Adx.

Both methods illustrated low nM affinity. This study is also the first reported use of MST with P450s. For fluorescence titration-based assay development, multiple labeling methods were tested and Alexa Fluor 488-Adx ended up being the best for measuring interactions with P450 27C1. Compared to other reported methods of measuring binding affinities between mitochondrial P450s and Adx, titrations with Alexa Fluor 488-Adx have many benefits: 1) both proteins are free in solution (in contrast to SPR), 2) Adx can be selectively labeled at a single site, minimizing interference with the protein-protein interactions, and 3) very low concentrations of Alexa Fluor 488-Adx can be utilized in the assay, enabling more accurate measurements of low nM affinities. The characterization of this labeling technique can enable use of this method with other mitochondrial P450s. It was also found that Adx and P450 27C1 substrate binding is not allosterically coupled, unlike some other mitochondrial P450s (99,169). In cross-linking mass spectrometry analysis, P450 27C1 was found to form many contacts with Adx, some of which have not been identified with other mitochondrial P450s, which could lead to the observed high affinity and stability of the interaction.

Chapter 5 assessed the ability of P450 27C1 to interact with cellular retinoid binding protein *in vitro*. Interactions with these binding proteins are considered a defining characteristic for physiologically relevant enzymes in retinoid metabolism (21). Catalytic assays and analysis of retinoid transfer rates were utilized to characterize the interactions between P450 27C1 and CRBP-1, CRABP-1, and CRABP-2. While the interaction could not be illustrated with a biophysical technique, kinetic analyses illustrate that P450 27C1 directly interacts with CRBP-1 and CRABP-2 to receive retinoid substrates. Surprisingly, P450 27C1 interacts with CRABP-2 but not CRABP-1. The other major retinoid-metabolizing P450s, the CYP26s, do not appear to have this specificity (31,32). P450 27C1 activity can also be affected by the amount of apo-CRBP present. This may

represent a mechanism to control 3,4-dehydroretinoid formation *in vivo*, as proposed with other enzymes (LRAT, REH, CYP26s). This is also the first study illustrating the interaction between CRBPs and a mitochondrial retinoid metabolizing enzyme. Overall, the ability of P450 27C1 to interact with CRBPs supports its designation as a physiologically relevant retinoid desaturase.

Lastly, in Chapter 6, the function of P450 27C1 and 3,4-dehydroretinoids within keratinocytes was investigated. Unfortunately, the N/TERT-2G cells selected to study P450 27C1 function (and generate KOs) do not appear to express P450 27C1 in the conditions tested. It is worth noting that N/TERT-2G cells lack the *in vitro* biosynthetic capabilities to form 3,4-dehydroretinoids that has been observed with other keratinocyte cell lines (106), though it is hard to make any conclusions given the absence of evidence of P450 27C1 expression in these other cell lines. CYP26-mediated catabolism of 3,4-dehydroretinoic acid was also assessed utilizing a HLM system. In comparison to all-*trans* retinoic acid, 3,4-dehydroretinoic acid seems to be resistant to 4-oxidation. The lack of P450-mediated catabolism of 3,4-dehydroretinoids may lead to 3,4-dehydroretinoids being a more metabolically stable source of retinoids within the cell.

7.2 Future Directions

While results from these studies have provided a better understanding of human P450 27C1, much remains unknown. I have outlined six major questions below that, if investigated, would increase the understanding of P450 27C1 function *in vivo*.

1. Do 3,4-dehydroretinoid levels correlate with P450 27C1 expression? As reviewed in Chapter 1, there are many skin conditions that are associated with altered levels of 3,4-dehydroretinoids. It is unknown if this is causative or correlative, and the mechanism leading to these changes in retinoid concentrations is also unknown. Changes in P450 27C1

expression levels may contribute to these aberrant retinoid levels. No studies have measured both the concentration of 3,4-dehydroretinoids and the level of P450 27C1 within the same sample. This may be logistically challenging with tissue, given that human skin tissue is typically obtained from waste tissue generated in surgical procedures while tissue should be harvested under yellow light to maintain the retinoids within the sample. Sample collection under regular white lights leads to isomerization and degradation of retinoids (52). Levels of P450 27C1 could be quantified in cultured cells and 3,4-dehydroretinoid biosynthesis could be measured. The generation of the QconCAT in this work (Chapter 3) could enable measurement of the concentration of P450 27C1 and 3,4-dehydroretinoid biosynthesis could be assessed utilizing the *in vitro* assays with cell lysates illustrated in Chapter 6.

2. How is P450 27C1 expression regulated? Multiple conditions have been shown to affect the formation of 3,4-dehydroretinoids. Keratinocytes exposed to UVA/B light show more rapid desaturation of all-*trans* retinol to 3,4-dehydroretinol, suggesting that UV light may induce desaturase activity (65). Also, epidermal levels of all-*trans* retinol are increased and 3,4-dehydroretinol are decreased following treatment with 13-*cis* retinoic acid or all-*trans* retinoic acid (67). P450 27C1 may be a target gene that is altered by retinoid induced RAR/RXR binding. Notably, data mined from a variety of databases have suggested the presence of RARα, RXRα, and RXRβ transcription factor binding sites in a *CYP27C1* enhancer (GH ID: GH02J128177), RXRα in another promoter/enhancer (GH ID: GH02J127883), and RXRα and RXRβ in a third promoter/enhancer (RH02J127525) (https://www.genecards.org/cgi-bin/carddisp.pl?gene=CYP27C1). Potential RAREs/RXREs could be identified and validated utilizing a series of promoter constructs

as previously described (222,223). Expression of P450 27C1 in fish and amphibians is induced by thyroid hormone (87). It is unknown if this also occurs in humans.

3. How does P450 27C1 interact with CRBPs? In Chapter 5, I illustrated that P450 27C1 interacts with CRBP-1 and CRABP-2, but not CRABP-1. Mutagenesis was attempted to identify the cause of specificity in the interaction with the two CRABPs, but results were inconclusive. The molecular basis for the difference in the interaction with P450 27C1 remains unknown but could be addressed through structural or additional mutagenesis studies. Apo-CRBPs also inhibit P450 27C1-mediated retinoid desaturation (but not with all-*trans* retinaldehyde). The mechanism for this inhibition is unknown, as it does not appear to be consistent with the mechanisms already proposed (allosteric modulation, competition with holo-CRBPs for binding). The mechanism for this inhibition may represent a novel mechanism of metabolic control of retinoids within the cell. Additionally, this work focused on characterizing potential interactions with CRBPs that have been localized to the skin. Humans contain four other retinoid binding proteins, CRBP-2, CRBP-3, CRBP-4, and FABP-5 (21). While P450 27C1 was shown to be expressed in the skin and not the liver or kidney, it may be expressed in other tissues as well and these tissues may have different expression patterns of retinoid binding proteins. Also, CRBPs are generally considered cytoplasmic, but there is some evidence that they can localize to the mitochondria (205-207). The mechanism of cellular retinoid-binding protein localization to the mitochondria is unknown, and this localization has not been illustrated directly in keratinocytes. Direct assessment of P450 27C1 and CRBP co-localization within the cell would provide evidence that these proteins could interact *in vivo*.

4. What are the proteoforms of P450 27C1 and are the differences functionally relevant? Two proteoforms of P450 27C1 were originally described in human skin (Figure 5). Proteomic analyses suggests that the larger proteoform is the full-length P450 27C1 and the smaller proteoform is an N-terminal truncation (91). The smaller proteoform is similar in size and sequence to the recombinant human P450 27C1 construct, so this is presumably a catalytically-active form. It is unknown if the larger proteoform is active. The exact site of cleavage and localization of the two proteoforms within the cell also remains unknown. Since mitochondrial P450s are cytoplasmically synthesized and then cleaved after insertion to the mitochondrial membrane, the larger proteoform potentially corresponds to the newly synthesized P450 27C1 and the smaller proteoform is what is present in the mitochondria. This has not yet been directly illustrated. In this work, additional immunoreactive bands for P450 27C1 were detected in primary keratinocytes. The sizes were similar to what was observed in the skin, but there were two "full-length" and two "truncated" bands. This may indicate that P450 27C1 may have additional post-translational modifications. Post-translational modification of P450s is a generally understudied area, especially from the functional standpoint. Work with other mitochondrial P450s have shown that phosphorylation of the P450 mediates import into the mitochondria and strengthens the interaction with Adx (145). A similar process could occur with P450 27C1.
5. Are there any genes that are differentially regulated by 3,4-dehydroretinoids in comparison with all-*trans* retinoids? Previous studies that compared gene expression following treatment with both all-*trans* retinoids and 3,4-dehydroretinoids utilized array analyses (64,65). Few differences were observed. No studies have performed RNA sequencing to assess full transcriptome changes with 3,4-dehydroretinoid treatment, so there may be

additional differentially regulated genes. Identification of differences in gene expression following all-t*rans* retinoid and 3,4-dehydroretinoid treatment would shed light on the function of 3,4-dehydroretinoids. This question may not be straightforward, as it may be possible that 3,4-dehydroretinoids play an important role in certain conditions (e.g. with UV response) but a redundant role in others. Understanding the function of 3,4-dehydoretinoids would provide insight into the potential effects of altered dehydroretinoids levels observed in a variety of hyperproliferative skin conditions as discussed in Chapter 1.

6. Is P450 27C1 expressed in other tissues? Do 3,4-dehydroretinoids have functions outside of the skin? This work focuses on the characterization of P450 27C1 within the skin (though some of the *in vitro* work in Chapters 4 and 5 would be broadly applicable to P450 27C1). 3,4-Dehydroretinoids are generally associated with the skin, but a few studies have noted their presence elsewhere, specifically in embryos and fetuses (49,50). Some datasets in the Human Protein Atlas also suggest that P450 27C1 may be expressed in female reproductive tissues (https://www.proteinatlas.org/ENSG00000186684-CYP27C1/tissue) (92). 3,4-Dehydroretinoids are known to be morphogenetic in other species (84,85), but potential roles in human development are unknown.

PUBLICATIONS

Glass, S.M., Webb, S.N., Guengerich, F.P. (2021) "Binding of cytochrome P450 27C1, a retinoid desaturase, to its accessory protein adrenodoxin." (Submitted, in revision)

Glass, S.M. and Guengerich, F.P (2021) "Cellular retinoid binding proteins transfer retinoids to P450 27C1 for desaturation". *J. Biol. Chem.* 297 (4), 101142

Glass, S.M., Reddish, M.J., Child, S.A., Wilkey, C.J., Stec, D.F., Guengerich, F.P. (2020) "Characterization of human adrenal cytochrome P450 11B2 products of progesterone and androstenedione oxidation". *J. Steroid. Biochem. Mol. Biol.* **208**, 105787

Child, S.A. *, Reddish, M.J. *, **Glass, S.M.***, Goldfarb, M.H., Barckhausen, I.R., Guengerich, F.P. (2020) "Functional interactions of adrenodoxin with several human mitochondrial P450 enzymes". *Arch. Biochem. Biophys.* **694**, 108596 (* Contributed equally)

Guengerich, F.P., Wilkey, C.J., **Glass, S.M.**, Reddish, M.J. (2019) "Conformational selection has a dominant role in binding of steroid substrates and other ligands to human cytochrome P450 17A1". *J. Biol. Chem.* **294,** 10028-10041 (Editors' Pick)

Albertolle, M.E., **Glass, S.M.,** Trefts, E., Guengerich, F.P. (2019) "Isotopic tagging of oxidized and reduced cysteines (iTORC) for detecting and quantifying sulfenic acids, disulfides, and free thiols in cells". *J. Biol. Chem.* **294**, 6522-6530

References:

1. (1983) NOMENCLATURE OF RETINOIDS. *Pure Appl Chem* **55**, 721-726

2. Harrison, E. H. (2005) Mechanisms of digestion and absorption of dietary vitamin A. *Annu Rev Nutr* **25**, 87-103

3. Goodman, D. S., Blomstrand, R., Werner, B., Huang, H. S., and Shiratori, T. (1966) The intestinal absorption and metabolism of vitamin A and beta-carotene in man. *J Clin Invest* **45**, 1615-1623

4. Blomhoff, R., Helgerud, P., Rasmussen, M., Berg, T., and Norum, K. R. (1982) In vivo uptake of chylomicron [3H]retinyl ester by rat liver: evidence for retinol transfer from parenchymal to nonparenchymal cells. *Proc Natl Acad Sci U S A* **79**, 7326-7330

5. Kanai, M., Raz, A., and Goodman, D. S. (1968) Retinol-binding protein: the transport protein for vitamin A in human plasma. *J Clin Invest* **47**, 2025-2044

6. Ronne, H., Ocklind, C., Wiman, K., Rask, L., Obrink, B., and Peterson, P. A. (1983) Ligand-dependent regulation of intracellular protein transport: effect of vitamin a on the secretion of the retinol-binding protein. *J Cell Biol* **96**, 907-910

7. Blomhoff, R., Rasmussen, M., Nilsson, A., Norum, K. R., Berg, T., Blaner, W. S., Kato, M., Mertz, J. R., Goodman, D. S., Eriksson, U., and et al. (1985) Hepatic retinol metabolism. Distribution of retinoids, enzymes, and binding proteins in isolated rat liver cells. *J Biol Chem* **260**, 13560-13565

8. Peterson, P. A. (1971) Studies on the interaction between prealbumin, retinol-binding protein, and vitamin A. *J Biol Chem* **246**, 44-49

9. Blomhoff, R., and Blomhoff, H. K. (2006) Overview of retinoid metabolism and function. *J Neurobio* **66**, 606-630

10. Balmer, J. E., and Blomhoff, R. (2002) Gene expression regulation by retinoic acid. *J Lipid Res* **43**, 1773-1808

11. Wolbach, S. B., and Howe, P. R. (1925) Tissue changes following depreivation of fat-soluble A vitamin. *J Exp Med* **42**, 753-777

12. Yuspa, S. H., Kilkenny, A. E., Steinert, P. M., and Roop, D. R. (1989) Expression of murine epidermal differentiation markers is tightly regulated by restricted extracellular calcium concentrations in vitro. *J Cell Biol* **109**, 1207-1217

13. Elias, P. M., Ahn, S. K., Denda, M., Brown, B. E., Crumrine, D., Kimutai, L. K., Kömüves, L., Lee, S. H., and Feingold, K. R. (2002) Modulations in epidermal calcium regulate the expression of differentiation-specific markers. *J Invest Dermatol* **119**, 1128-1136

14. Kawaguchi, R., Yu, J., Honda, J., Hu, J., Whitelegge, J., Ping, P., Wiita, P., Bok, D., and Sun, H. (2007) A membrane receptor for retinol binding protein mediates cellular uptake of vitamin A. *Science* **315**, 820-825

15. Lehman, P. A., and Malany, A. M. (1989) Evidence for percutaneous absorption of isotretinoin from the photo-isomerization of topical tretinoin. *J Invest Dermatol* **93**, 595-599

16. Vahlquist, A., Lee, J. B., Michaëlsson, G., and Rollman, O. (1982) Vitamin A in human skin: II concentrations of carotene, retinol and dehydroretinol in various components of normal skin. *J Invest Dermatol* **79**, 94-97

17. Siegenthaler, G., Saurat, J. H., and Ponec, M. (1990) Retinol and retinal metabolism. Relationship to the state of differentiation of cultured human keratinocytes. *Biochem J* **268**, 371-378

18. Canada, F. J., Law, W. C., Rando, R. R., Yamamoto, T., Derguini, F., and Nakanishi, K. (1990) Substrate specificities and mechanism in the enzymic processing of vitamin A into 11-*cis*-retinol. *Biochemistry* **29**, 9690-9697

19. El Akawi, Z., and Napoli, J. L. (1994) Rat liver cytosolic retinal dehydrogenase: comparison of 13-*cis*-, 9-*cis*-, and all-*trans*-retinal as substrates and effects of cellular retinoid-binding proteins and retinoic acid on activity. *Biochemistry* **33**, 1938-1943

20. Roos, T. C., Jugert, F. K., Merk, H. F., and Bickers, D. R. (1998) Retinoid metabolism in the skin. *Pharmacol Rev* **50**, 315

21. Napoli, J. L. (2017) Cellular retinoid binding-proteins, CRBP, CRABP, FABP5: effects on retinoid metabolism, function and related diseases. *Pharmacol Ther* **173**, 19-33

22. Aström, A., Tavakkol, A., Pettersson, U., Cromie, M., Elder, J. T., and Voorhees, J. J. (1991) Molecular cloning of two human cellular retinoic acid-binding proteins (CRABP). Retinoic acid-induced expression of CRABP-II but not CRABP-I in adult human skin in vivo and in skin fibroblasts in vitro. *J Biol Chem* **266**, 17662-17666

23. Eller, M. S., Oleksiak, M. F., McQuaid, T. J., McAfee, S. G., and Gilchrest, B. A. (1992) The molecular cloning and expression of two CRABP cDNAs from human skin. *Exp Cell Res* **198**, 328-336

24. Sanquer, S., and Gilchrest, B. A. (1994) Characterization of human cellular retinoic acid-binding proteins-I and -II: ligand binding affinities and distribution in skin. *Arch Biochem Biophys* **311**, 86-94

25. Siegenthaler, G., Saurat, J. H., Morin, C., and Hotz, R. (1984) Cellular retinol- and retinoic acid-binding proteins in the epidermis and dermis of normal human skin. *Br J Dermatol* **111**, 647-654

26. Pavez Loriè, E., Li, H., Vahlquist, A., and Törmä, H. (2009) The involvement of cytochrome P450 (CYP) 26 in the retinoic acid metabolism of human epidermal keratinocytes. *Biochim Biophys Acta* **1791**, 220-228

27. Ross, A. C., and Zolfaghari, R. (2011) Cytochrome P450s in the regulation of cellular retinoic acid metabolism. *Annual Rev Nutr* **31**, 65-87

28. Heise, R., Mey, J., Neis, M. M., Marquardt, Y., Joussen, S., Ott, H., Wiederholt, T., Kurschat, P., Megahed, M., Bickers, D. R., Merk, H. F., and Baron, J. M. (2006) Skin retinoid concentrations are modulated by CYP26AI expression restricted to basal keratinocytes in normal human skin and differentiated 3D skin models. *J Invest Dermatol* **126**, 2473-2480

29. Kurashima, Y., Amiya, T., Fujisawa, K., Shibata, N., Suzuki, Y., Kogure, Y., Hashimoto, E., Otsuka, A., Kabashima, K., Sato, S., Sato, T., Kubo, M., Akira, S., Miyake, K., Kunisawa, J., and Kiyono, H. (2014) The enzyme CYP26B1 mediates inhibition of mast cell activation by fibroblasts to maintain skin-barrier homeostasis. *Immunity* **40**, 530-541

30. Taimi, M., Helvig, C., Wisniewski, J., Ramshaw, H., White, J., Amad, M. a., Korczak, B., and Petkovich, M. (2004) A novel human cytochrome P450, CYP26C1, involved in metabolism of 9-*cis* and all-*trans* isomers of retinoic acid. *J Biol Chem* **279**, 77-85

31. Nelson, C. H., Peng, C. C., Lutz, J. D., Yeung, C. K., Zelter, A., and Isoherranen, N. (2016) Direct protein-protein interactions and substrate channeling between cellular retinoic acid binding proteins and CYP26B1. *FEBS Lett* **590**, 2527-2535

32. Zhong, G., Ortiz, D., Zelter, A., Nath, A., and Isoherranen, N. (2018) CYP26C1 is a hydroxylase of multiple active retinoids and interacts with cellular retinoic acid binding proteins. *Mol Pharmacol* **93**, 489-503

33. Blaner, W. S., and Li, Y. (2015) Vitamin A metabolism, storage and tissue delivery mechanisms. *The Retinoids: Biology, Biochemistry, and Disease; Dolle, P., Niederreither, K., Eds*, 1-34

34. Kurlandsky, S. B., Duell, E. A., Kang, S., Voorhees, J. J., and Fisher, G. J. (1996) Auto-regulation of retinoic acid biosynthesis through regulation of retinol esterification in human keratinocytes. *J Biol Chem* **271**, 15346-15352

35. Törmä, H., and Vahlquist, A. (1987) Retinol esterification by mouse epidermal microsomes: evidence for Acyl-CoA:retinol acyltransferase activity. *J Invest Dermatol* **88**, 398-402

36. Randolph, R. K., and Simon, M. (1996) All-*trans*-retinoic acid regulates retinol and 3,4-didehydroretinol metabolism in cultured human epidermal keratinocytes. *J Invest Dermatol* **106**, 168-175

37. Herr, F. M., and Ong, D. E. (1992) Differential interaction of lecithin-retinol acyltransferase with cellular retinol binding proteins. *Biochemistry* **31**, 6748-6755

38. Boerman, M. H., and Napoli, J. L. (1991) Cholate-independent retinyl ester hydrolysis. Stimulation by Apo-cellular retinol-binding protein. *J Biol Chem* **266**, 22273-22278

39. Lee, D.-D., Stojadinovic, O., Krzyzanowska, A., Vouthounis, C., Blumenberg, M., and Tomic-Canic, M. (2009) Retinoid-responsive transcriptional changes in epidermal keratinocytes. *J Cell Physiol* **220**, 427-439

40. Xiao, J.-H., Durand, B., Chambon, P., and Voorhees, J. J. (1995) Endogenous retinoic acid receptor (RAR)-retinoid X receptor (RXR) heterodimers are the major functional forms regulating retinoid-responsive elements in adult human keratinocytes. *J Biol Chem* **270**, 3001-3011

41. Connor, M. J., Ashton, R. E., and Lowe, N. J. (1986) A comparative study of the induction of epidermal hyperplasia by natural and synthetic retinoids. *J Pharmacol Exp Ther* **237**, 31-35

42. Zasada, M., and Budzisz, E. (2019) Retinoids: active molecules influencing skin structure formation in cosmetic and dermatological treatments. *Postepy Dermatol Alergol* **36**, 392-397

43. Varani, J., Warner, R. L., Gharaee-Kermani, M., Phan, S. H., Kang, S., Chung, J. H., Wang, Z. Q., Datta, S. C., Fisher, G. J., and Voorhees, J. J. (2000) Vitamin A antagonizes decreased cell growth and elevated collagen-degrading matrix metalloproteinases and stimulates collagen accumulation in naturally aged human skin. *J Invest Dermatol* **114**, 480-486

44. Afifi, T., de Gannes, G., Huang, C., and Zhou, Y. (2005) Topical therapies for psoriasis: evidence-based review. *Can Fam Physician* **51**, 519-525

45. Futoryan, T., and Gilchrest, B. A. (1994) Retinoids and the skin. *Nutr Rev* **52**, 299-310

46. Mukherjee, S., Date, A., Patravale, V., Korting, H. C., Roeder, A., and Weindl, G. (2006) Retinoids in the treatment of skin aging: an overview of clinical efficacy and safety. *Clin Interv Aging* **1**, 327-348

47. Balkrishnan, R., Bhosle, M. J., Camacho, F., Fleischer, A. B., and Feldman, S. R. (2010) Prescribing patterns for topical retinoids: analyses of 15 years of data from the national ambulatory medical care survey. *J Dermatolog Treat* **21**, 193-200

48. Vahlquist, A. (1980) The identification of dehydroretinol (vitamin A2) in human skin. *Experientia* **36**, 317-318

49. Kraft, J. C., Shepard, T., and Juchau, M. R. (1993) Tissue levels of retinoids in human embryos/fetuses. *Reprod Toxicol* **7**, 11-15

50. Sass, J. O. (1994) 3,4-didehydroretinol may be present in human embryos/fetuses. *Reprod Toxicol* **8**, 191

51. Barua, A. B., and Olson, J. A. (1998) Reversed-phase gradient high-performance liquid chromatographic procedure for simultaneous analysis of very polar to nonpolar retinoids, carotenoids and tocopherols in animal and plant samples. *J Chromatogr B Biomed Appl* **707**, 69-79

52. Kane, M. A., and Napoli, J. L. (2010) Quantification of endogenous retinoids. *Methods Mol Biol* **652**, 1-54

53. Törmä, H., and Vahlquist, A. (1985) Biosynthesis of 3-dehydroretinol (vitamin A2) from all-*trans*-retinol (Vitamin A1) in human epidermis. *J Invest Dermatol* **85**, 498-500

54. Rollman, O., Wood, E. J., Olsson, M. J., and Cunliffe, W. J. (1993) Biosynthesis of 3,4-didehydroretinol from retinol by human skin keratinocytes in culture. *Biochem J* **293 (Pt 3)**, 675-682

55. Rosdahl, I., Andersson, E., Kågedal, B., and Törmä, H. (1997) Vitamin A metabolism and mRNA expression of retinoid-binding protein and receptor genes in human epidermal melanocytes and melanoma cells. *Melanoma Res* **7**(4), 267-274

56. Törmä, H., Asselineau, D., Andersson, E., Martin, B., Reiniche, P., Chambon, P., Shroot, B., Darmon, M., and Vahlquist, A. (1994) Biologic activities of retinoic acid and 3,4-didehydroretinoic acid in human keratinocytes are similar and correlate with receptor affinities and transactivation properties. *J Invest Dermatol* **102**, 49-54

57. Fiorella, P. D., Giguère, V., and Napoli, J. L. (1993) Expression of cellular retinoic acid-binding protein (type II) in *Escherichia coli*. Characterization and comparison to cellular retinoic acid-binding protein (type I). *J Biol Chem* **268**, 21545-21552

58. MacDonald, P. N., and Ong, D. E. (1987) Binding specificities of cellular retinol-binding protein and cellular retinol-binding protein, type II. *J Biol Chem* **262**, 10550-10556

59. Lee, S.-A., Belyaeva, O. V., Wu, L., and Kedishvili, N. Y. (2011) Retinol dehydrogenase 10 but not retinol/sterol dehydrogenase(s) regulates the expression of retinoic acid-responsive genes in human transgenic skin raft culture. *J Biol Chem* **286**, 13550-13560

60. Bamji, M. S., Mahadevan, S., Lakshmanan, M. R., and Murthy, S. K. (1962) Oxidation of vitamin A1 and vitamin A2 aldehydes to the corresponding acids by enzymes from pig and rat livers. *Nature* **196**, 672-673

61. Lakshmanan, M. R., Vaidyanathan, C. S., and Cama, H. R. (1964) Oxidation of vitamin A1 aldehyde and vitamin A2 aldehyde to the corresponding acids by aldehyde oxidase from different species. *Biochem J* **90**, 569-573

62. Allenby, G., Bocquel, M. T., Saunders, M., Kazmer, S., Speck, J., Rosenberger, M., Lovey, A., Kastner, P., Grippo, J. F., Chambon, P. (1993) Retinoic acid receptors and retinoid X receptors: interactions with endogenous retinoic acids. *Proc Natl Acad Sci U S A* **90**, 30-34

63. Sani, B. P., Venepally, P. R., and Levin, A. A. (1997) Didehydroretinoic acid: Retinoid receptor-mediated transcriptional activation and binding properties. *Biochem Pharmacol* **53**, 1049-1053

64. Törmä, H., Bergström, A., Ghiasifarahani, G., and Berne, B. (2014) The effect of two endogenous retinoids on the mRNA expression profile in human primary keratinocytes, focusing on genes causing autosomal recessive congenital ichthyosis. *Arch Dermatol Res* **306**, 739-747

65. Tafrova, J. I., Pinkas-Sarafova, A., Stolarzewicz, E., Parker, K. A., and Simon, M. (2012) UVA/B exposure promotes the biosynthesis of dehydroretinol in cultured human keratinocytes. *Mol Cell Biochem* **364**, 351-361

66. Andersson, E., Rosdahl, I., Törmä, H., and Vahlquist, A. (1999) Ultraviolet irradiation depletes cellular retinol and alters the metabolism of retinoic acid in cultured human keratinocytes and melanocytes. *Melanoma Res* **9**, 339-346

67. Törmä, H., Stenström, E., Andersson, E., and Vahlquist, A. (1991) Synthetic retinoids affect differently the epidermal synthesis of 3,4-didehydroretinol. *Skin Pharmacol Phys* **4**, 246-253

68. Rollman, O., and Vahlquist, A. (1981) Cutaneous vitamin A levels in seborrheic keratosis, actinic keratosis, and basal cell carcinoma. *Arch Dermatol Res* **270**, 193-196

69. Vahlquist, A., Andersson, E., Coble, B. I., Rollman, O., and Törmä, H. (1996) Increased concentrations of 3,4-didehydroretinol and retinoic acid-binding protein (CRABPII) in human squamous cell carcinoma and keratoacanthoma but not in basal cell carcinoma of the skin. *J Invest Dermatol* **106**, 1070-1074

70. Rollman, O., and Vahlquist, A. (1985) Psoriasis and vitamin A. *Arch Dermatol Res* **278**, 17-24

71. Vahlquist, A., Lee, J. B., and Michaëlsson, G. (1982) Darier's disease and vitamin A: concentrations of retinoids in serum and epidermis of untreated patients. *Arch Dermatol* **118**, 389-392

72. Rollman, O. L. A., and Vahlquist, A. (1985) Vitamin A in skin and serum—studies of acne vulgaris, atopic dermatitis, ichthyosis vulgaris and lichen planus. *B J Dermatol* **113**, 405-413

73. Berne, B., Vahlquist, A., Fischer, T., Danielson, B. G., and Berne, C. (1984) UV treatment of uraemic pruritus reduces the vitamin A content of the skin. *Eur J Clin Invest* **14**, 203-206

74. Köttgen, E., and Abelsdorff, G. (1896) Absorption und Zersetzung des Sehpurpurs bei den Wirbeltieren. *Z. Psychol. Physiol. Sinnesorg* **12**, 161-184

75. Kühne, W., and Sewall, H. (1880) *Zur Physiologie des Sehepithels, insbesondere der Fische*, Carl Winter's Universitätbuchhandlung

76. Corbo, J. C. (2021) Vitamin A1/A2 chromophore exchange: its role in spectral tuning and visual plasticity. *Dev Bio* **475**, 145-155

77. Röll, B., Amons, R., and de Jong, W. W. (1996) Vitamin A2 bound to cellular retinol-binding protein as ultraviolet filter in the eye lens of the gecko *Lygodactylus picturatus*. *J Biol Chem* **271**, 10437-10440

78. Howell, J. M., Thompson, J. N., and Pitt, G. A. (1967) Reproduction and vision in rats maintained on a retinol-free diet containing 3-dehydroretinol (vitamin A2). *B J Nutr* **21**, 373-376

79. Wilson, T. C. M., and Pitt, G. A. J. (1986) 3,4-Didehydroretinol (vitamin A2) has vitamin A activity in the rat without conversion to retinol. *Biochem Soc Trans* **14**, 950-950

80. Gillam, A. E. (1938) The vitamin A(1) and A(2) contents of mammalian and other animal livers. *Biochem J* **32**, 1496-1500

81. Müller, K., Raila, J., Altenkamp, R., Schmidt, D., Dietrich, R., Hurtienne, A., Wink, M., Krone, O., Brunnberg, L., and Schweigert, F. J. (2012) Concentrations of retinol, 3,4-didehydroretinol, and retinyl esters in plasma of free-ranging birds of prey. *J Anim Phys Anim Nutr* **96**, 1044-1053

82. Törmä, H., and Vahlquist, A. (1988) Identification of 3-dehydroretinol (vitamin A2) in mouse liver. *Biochim Biophys Acta Lipids Lipid Metab* **961**, 177-182

83. Budowski, P., and Gross, J. (1965) Conversion of carotenoids to 3-dehydroretinol (vitamin A2) in the mouse. *Nature* **206**, 1254-1255

84. Maden, M., Sonneveld, E., van der Saag, P. T., and Gale, E. (1998) The distribution of endogenous retinoic acid in the chick embryo: implications for developmental mechanisms. *Development* **125**, 4133-4144

85. Thaller, C., and Eichele, G. (1990) Isolation of 3,4-didehydroretinoic acid, a novel morphogenetic signal in the chick wing bud. *Nature* **345**, 815-819

86. Plack, P. A., and Kon, S. K. (1961) A comparative survey of the distribution of vitamin A aldehyde in eggs. *Biochem J* **81**, 561-570

87. Enright, J.M., Toomey, M.B., Sato, S.-Y., Temple, S.E., Allen, James R., Fujiwara, R., Kramlinger, V.M., Nagy, L.D., Johnson, K.M., Xiao, Y., How, M.J., Johnson, S.L., Roberts, N.W., Kefalov, V.J., Guengerich, F. P., and Corbo, J.C. (2015) Cyp27c1 Red-Shifts the Spectral Sensitivity of Photoreceptors by Converting Vitamin A1 into A2. *Curr Biol* **25**, 3048-3057

88. Kramlinger, V. M., Nagy, L. D., Fujiwara, R., Johnson, K. M., Phan, T. T., Xiao, Y., Enright, J. M., Toomey, M. B., Corbo, J. C., and Guengerich, F. P. (2016) Human cytochrome P450 27C1 catalyzes 3,4-desaturation of retinoids. *FEBS Lett* **590**, 1304-1312

89. Nelson, D. R., Zeldin, D. C., Hoffman, S. M., Maltais, L. J., Wain, H. M., and Nebert, D. W. (2004) Comparison of cytochrome P450 (CYP) genes from the mouse and human genomes, including nomenclature recommendations for genes, pseudogenes and alternative-splice variants. *Pharmacogenetics* **14**, 1-18

90. Wu, Z. L., Bartleson, C. J., Ham, A. J., and Guengerich, F. P. (2006) Heterologous expression, purification, and properties of human cytochrome P450 27C1. *Arch Biochem Biophys* **445**, 138-146

91. Johnson, K. M., Phan, T. T. N., Albertolle, M. E., and Guengerich, F. P. (2017) Human mitochondrial cytochrome P450 27C1 is localized in skin and preferentially desaturates *trans*-retinol to 3,4-dehydroretinol. *J Biol Chem* **292**, 13672-13687

92. Uhlén, M., Fagerberg, L., Hallström Björn, M., Lindskog, C., Oksvold, P., Mardinoglu, A., Sivertsson, Å., Kampf, C., Sjöstedt, E., Asplund, A., Olsson, I., Edlund, K., Lundberg, E., Navani, S., Szigyarto Cristina, A.-K., Odeberg, J., Djureinovic, D., Takanen Jenny, O., Hober, S., Alm, T., Edqvist, P.-H., Berling, H., Tegel, H., Mulder, J., Rockberg, J., Nilsson, P., Schwenk Jochen, M., Hamsten, M., von Feilitzen, K., Forsberg, M., Persson, L., Johansson, F., Zwahlen, M., von Heijne, G., Nielsen, J., and Pontén, F. (2015) Tissue-based map of the human proteome. *Science* **347**, 1260419

93. Omura, T., and Sato, R. (1962) A new cytochrome in liver microsomes. *J Biol Chem* **237**, PC1375-PC1376

94. Nelson, D. R. (2006) Cytochrome P450 Nomenclature, 2004. in *Cytochrome P450 Protocols* (Phillips, I. R., and Shephard, E. A. eds.), Humana Press, Totowa, NJ. pp 1-10

95. Guengerich, F. P. (2021) Drug Metabolism: Cytochrome P450. in *Reference Module in Biomedical Sciences*, Elsevier. (In press)

96. Hlavica, P. (2015) Mechanistic Basis of Electron Transfer to Cytochromes P450 by Natural Redox Partners and Artificial Donor Constructs. in *Monooxygenase, Peroxidase and Peroxygenase Properties and Mechanisms of Cytochrome P450* (Hrycay, E. G., and Bandiera, S. M. eds.), Springer International Publishing, Cham. pp 247-297

97. Omura, T. (2006) Mitochondrial P450s. *Chem Biol Interact* **163**, 86-93

98. Auchus, R. J., Lee, T. C., and Miller, W. L. (1998) Cytochrome b_5 augments the 17,20-lyase activity of human P450c17 without direct electron transfer. *J Biol Chem* **273**, 3158-3165

99. Brixius-Anderko, S., and Scott, E. E. (2021) Structural and functional insights into aldosterone synthase interaction with its redox partner protein adrenodoxin. *J Biol Chem* **296**, 100794

100. Estrada, D. F. (2018) The cytochrome P450 24A1 interaction with adrenodoxin relies on multiple recognition sites that vary among species. *J Biol Chem* **293**, 4167-4179

101. Guengerich, F. P., Wilkey, C. J., Glass, S. M., and Reddish, M. J. (2019) Conformational selection dominates binding of steroids to human cytochrome P450 17A1. *J Biol Chem* **294**, 10028-10041

102. Hartfield, K. A., Stout, C. D., and Annalora, A. J. (2013) The novel purification and biochemical characterization of a reversible CYP24A1:adrenodoxin complex. *J Steroid Biochem Mol Biol* **136**, 47-53

103. Porter, T. D. (2002) The roles of cytochrome b_5 in cytochrome P450 reactions. *J Biochem Mol Toxicol* **16**, 311-316

104. Reddish, M. J., and Guengerich, F. P. (2019) Human cytochrome P450 11B2 produces aldosterone by a processive mechanism due to the lactol form of the intermediate 18-hydroxycorticosterone. *J Biol Chem* **294**, 12975-12991

105. Urushino, N., Yamamoto, K., Kagawa, N., Ikushiro, S., Kamakura, M., Yamada, S., Kato, S., Inouye, K., and Sakaki, T. (2006) Interaction between mitochondrial CYP27B1 and adrenodoxin: role of arginine 458 of mouse CYP27B1. *Biochemistry* **45**, 4405-4412

106. Tafrova, J. I. (2008) Conversion of vitamin A1 to vitamin A2 and its involvement in the response of cultured human keratinocytes to UV irradiation. Ph.D., State University of New York at Stony Brook

107. Atkinson, P. H., and Summers, D. F. (1971) Purification and properties of HeLa cell plasma membranes. *J Biol Chem* **246**, 5162-5175

108. DePierre, J. W., and Karnovsky, M. L. (1973) Plasma membranes of mammalian cells: a review of methods for their characterization and isolation. *J Cell Biol* **56**, 275-303

109. Barua, A. B., and Furr, H. C. (1998) Properties of Retinoids. in *Retinoid Protocols* (Redfern, C. P. F. ed.), Humana Press, Totowa, NJ. pp 3-28

110. Omura, T., and Sato, R. (1964) The carbon monoxide-binding pigment of livermicrosomes I. Evidence for its hemoprotein nature. *J Biol Chem* **239**, 2370-2378

111. Palin, M. F., Berthiaume, L., Lehoux, J. G., Waterman, M. R., and Sygusch, J. (1992) Direct expression of mature bovine adrenodoxin in *Escherichia coli*. *Arch Biochem Biophys* **295**, 126-131

112. Sagara, Y., Wada, A., Takata, Y., Waterman, M. R., Sekimizu, K., and Horiuchi, T. (1993) Direct expression of adrenodoxin reductase in *Escherichia coli* and the functional characterization. *Biol Pharm Bull* **16**, 627-630

113. Peng, H. M., and Auchus, R. J. (2017) Molecular recognition in mitochondrial cytochromes P450 that catalyze the terminal steps of corticosteroid biosynthesis. *Biochemistry* **56**, 2282-2293

114. Kimura, T. (1968) Biochemical aspects of iron-sulfur linkage in non-heme iron protein, with special reference to "Adrenodoxin". in *Structure and Bonding*, Springer, Berlin, Heidelberg

115. Silvaroli, J. A., Arne, J. M., Chelstowska, S., Kiser, P. D., Banerjee, S., and Golczak, M. (2016) Ligand binding induces conformational changes in human cellular retinol-binding protein 1 (CRBP1) revealed by atomic resolution crystal structures. *J Biol Chem* **291**, 8528-8540

116. Eyers, C. E., Lawless, C., Wedge, D. C., Lau, K. W., Gaskell, S. J., and Hubbard, S. J. (2011) CONSeQuence: prediction of reference peptides for absolute quantitative proteomics using consensus machine learning approaches. *Mol Cell Proteomics* **10**, M110.003384-M003110.003384

117. Russell, M. R., Achour, B., McKenzie, E. A., Lopez, R., Harwood, M. D., Rostami-Hodjegan, A., and Barber, J. (2013) Alternative fusion protein strategies to express recalcitrant QconCAT proteins for quantitative proteomics of human drug metabolizing enzymes and transporters. *J Proteome Res* **12**, 5934-5942

118. Johnson, K. A. (2019) New standards for collecting and fitting steady state kinetic data. *Beilstein J Org Chem* **15**, 16-29

119. Shevchenko, A., Tomas, H., Havli, J., Olsen, J. V., and Mann, M. (2006) In-gel digestion for mass spectrometric characterization of proteins and proteomes. *Nat Prot* **1**, 2856-2860

120. Wiśniewski, J. R., Zougman, A., Nagaraj, N., and Mann, M. (2009) Universal sample preparation method for proteome analysis. *Nat Meth* **6**, 359-362

121. Tabb, D. L., Fernando, C. G., and Chambers, M. C. (2007) MyriMatch: highly accurate tandem mass spectral peptide identification by multivariate hypergeometric analysis. *J Proteome Res* **6**, 654-661

122. Holman, J. D., Ma, Z. Q., and Tabb, D. L. (2012) Identifying proteomic LC-MS/MS data sets with Bumbershoot and IDPicker. *Curr Protoc Bioinformatics* **Chapter 13**, Unit13.17

123. Pino, L. K., Searle, B. C., Bollinger, J. G., Nunn, B., MacLean, B., and MacCoss, M. J. (2020) The Skyline ecosystem: informatics for quantitative mass spectrometry proteomics. *Mass Spectrom Rev* **39**, 229-244

124. Chen, Z.-L., Meng, J.-M., Cao, Y., Yin, J.-L., Fang, R.-Q., Fan, S.-B., Liu, C., Zeng, W.-F., Ding, Y.-H., Tan, D., Wu, L., Zhou, W.-J., Chi, H., Sun, R.-X., Dong, M.-Q., and He, S.-M. (2019) A high-speed search engine pLink 2 with systematic evaluation for proteome-scale identification of cross-linked peptides. *Nat Commun* **10**, 3404

125. Jones, J. W., Pierzchalski, K., Yu, J., and Kane, M. A. (2015) Use of fast HPLC multiple reaction monitoring cubed for endogenous retinoic acid quantification in complex matrices. *Anal Chem* **87**, 3222-3230

126. Jumper, J., Evans, R., Pritzel, A., Green, T., Figurnov, M., Ronneberger, O., Tunyasuvunakool, K., Bates, R., Žídek, A., Potapenko, A., Bridgland, A., Meyer, C., Kohl, S. A. A., Ballard, A. J., Cowie, A., Romera-Paredes, B., Nikolov, S., Jain, R., Adler, J., Back, T., Petersen, S., Reiman, D., Clancy, E., Zielinski, M., Steinegger, M., Pacholska, M., Berghammer, T., Bodenstein, S., Silver, D., Vinyals, O., Senior, A. W., Kavukcuoglu, K., Kohli, P., and Hassabis, D. (2021) Highly accurate protein structure prediction with AlphaFold. *Nature* **596,** 583-589

127. Chaikuad, A., Johansson, C., Krojer, T., Yue, W.W., Phillips, C., Bray, J.E., Pike, A.C.W., Muniz, J.R.C., Vollmar, M., Weigelt, J., Arrowsmith, C.H., Edwards, A.M., Bountra, C., Kavanagh, K., Oppermann, U. (2010) Crystal structure of human ferredoxin-1 (FDX1) in complex with iron-sulfur cluster. 2010-11-03 Ed., Protein Data Bank 3P1M

128. Honorato, R. V., Koukos, P. I., Jiménez-García, B., Tsaregorodtsev, A., Verlato, M., Giachetti, A., Rosato, A., and Bonvin, A. M. J. J. (2021) Structural biology in the clouds: the WeNMR-EOSC ecosystem. *Front Mol Biosci* **8,** 729513

129. van Zundert, G. C. P., Rodrigues, J. P. G. L. M., Trellet, M., Schmitz, C., Kastritis, P. L., Karaca, E., Melquiond, A. S. J., van Dijk, M., de Vries, S. J., and Bonvin, A. M. J. J. (2016) The HADDOCK2.2 Web Server: user-friendly integrative modeling of biomolecular complexes. *J Mol Biol* **428**, 720-725

130. (2015) The PyMOL Molecular Graphics System. 2.0 Ed., Schrodinger, LLC

131. Sievers, F., Wilm, A., Dineen, D., Gibson, T. J., Karplus, K., Li, W., Lopez, R., McWilliam, H., Remmert, M., Söding, J., Thompson, J. D., and Higgins, D. G. (2011) Fast, scalable generation of high-quality protein multiple sequence alignments using Clustal Omega. *Mol Syst Biol* **7**, 539

132. Baker, N. A., Sept, D., Joseph, S., Holst, M. J., and McCammon, J. A. (2001) Electrostatics of nanosystems: Application to microtubules and the ribosome. *Proc Natl Acad Sci USA* **98**, 10037

133. Kleywegt, G. J., Bergfors, T., Senn, H., Le Motte, P., Gsell, B., Shudo, K., and Jones, T. A. (1994) Crystal structures of cellular retinoic acid binding proteins I and II in complex with all-*trans*-retinoic acid and a synthetic retinoid. *Structure* **2**, 1241-1258

134. Dickson, M. A., Hahn, W. C., Ino, Y., Ronfard, V., Wu, J. Y., Weinberg, R. A., Louis, D. N., Li, F. P., and Rheinwald, J. G. (2000) Human keratinocytes that express hTERT and also bypass a p16(INK4a)-enforced mechanism that limits life span become immortal yet retain normal growth and differentiation characteristics. *Mol Cell Biol* **20**, 1436-1447

135. Sarkar, M. K., Hile, G. A., Tsoi, L. C., Xing, X., Liu, J., Liang, Y., Berthier, C. C., Swindell, W. R., Patrick, M. T., Shao, S., Tsou, P.-S., Uppala, R., Beamer, M. A.,

Srivastava, A., Bielas, S. L., Harms, P. W., Getsios, S., Elder, J. T., Voorhees, J. J., Gudjonsson, J. E., and Kahlenberg, J. M. (2018) Photosensitivity and type I IFN responses in cutaneous lupus are driven by epidermal-derived interferon kappa. *Ann Rheum Dis* **77**, 1653

136. Koller, A., and Wätzig, H. (2005) Precision and variance components in quantitative gel electrophoresis. *Electrophoresis* **26**, 2470-2475

137. Pillai-Kastoori, L., Schutz-Geschwender, A. R., and Harford, J. A. (2020) A systematic approach to quantitative Western blot analysis. *Anal Biochem* **593**, 113608

138. Pratt, J. M., Simpson, D. M., Doherty, M. K., Rivers, J., Gaskell, S. J., and Beynon, R. J. (2006) Multiplexed absolute quantification for proteomics using concatenated signature peptides encoded by QconCAT genes. *Nat Protoc* **1**, 1029-1043

139. Achour, B., Russell, M. R., Barber, J., and Rostami-Hodjegan, A. (2014) Simultaneous quantification of the abundance of several cytochrome P450 and uridine 5'-diphospho-glucuronosyltransferase enzymes in human liver microsomes using multiplexed targeted proteomics. *Drug Metab Dispos* **42**, 500-510

140. Dyring-Andersen, B., Løvendorf, M. B., Coscia, F., Santos, A., Møller, L. B. P., Colaço, A. R., Niu, L., Bzorek, M., Doll, S., Andersen, J. L., Clark, R. A., Skov, L., Teunissen, M. B. M., and Mann, M. (2020) Spatially and cell-type resolved quantitative proteomic atlas of healthy human skin. *Nat Commun* **11**, 5587

141. Edqvist, P.-H. D., Fagerberg, L., Hallström, B. M., Danielsson, A., Edlund, K., Uhlén, M., and Pontén, F. (2015) Expression of human skin-specific genes defined by transcriptomics and antibody-based profiling. *J Histochem Cytochem* **63**, 129-141

142. Fisher, G. J., and Voorhees, J. J. (1996) Molecular mechanisms of retinoid actions in skin. *FASEB J* **10**, 1002-1013

143. Howe, K. L., Achuthan, P., Allen, J., Allen, J., Alvarez-Jarreta, J., Amode, M. R., Armean, I. M., Azov, A. G., Bennett, R., Bhai, J., Billis, K., Boddu, S., Charkhchi, M., Cummins, C., Da Rin Fioretto, L., Davidson, C., Dodiya, K., El Houdaigui, B., Fatima, R., Gall, A., Garcia Giron, C., Grego, T., Guijarro-Clarke, C., Haggerty, L., Hemrom, A., Hourlier, T., Izuogu, O. G., Juettemann, T., Kaikala, V., Kay, M., Lavidas, I., Le, T., Lemos, D., Gonzalez Martinez, J., Marugán, J. C., Maurel, T., McMahon, A. C., Mohanan, S., Moore, B., Muffato, M., Oheh, D. N., Paraschas, D., Parker, A., Parton, A., Prosovetskaia, I., Sakthivel, M. P., Salam, Ahamed I A., Schmitt, B. M., Schuilenburg, H., Sheppard, D., Steed, E., Szpak, M., Szuba, M., Taylor, K., Thormann, A., Threadgold, G., Walts, B., Winterbottom, A., Chakiachvili, M., Chaubal, A., De Silva, N., Flint, B., Frankish, A., Hunt, S. E., Iisley, G. R., Langridge, N., Loveland, J. E., Martin, F. J., Mudge, J. M., Morales, J., Perry, E., Ruffier, M., Tate, J., Thybert, D., Trevanion, S. J., Cunningham, F., Yates, A. D., Zerbino, D. R., and Flicek, P. (2021) Ensembl 2021. *Nucl Acids Res* **49**, D884-D891

144. Stram, A. R., and Payne, R. M. (2016) Post-translational modifications in mitochondria: protein signaling in the powerhouse. *Cell Mol Life Sci* **73**, 4063-4073

145. Aguiar, M., Masse, R., and Gibbs, B. F. (2005) Regulation of cytochrome P450 by posttranslational modification. *Drug Metab Rev* **37**, 379-404

146. Couto, N., Newton, J. R. A., Russo, C., Karunakaran, E., Achour, B., Al-Majdoub, Z. M., Sidaway, J., Rostami-Hodjegan, A., Clench, M. R., and Barber, J. (2021) Label-free quantitative proteomics and substrate-based mass spectrometry imaging of xenobiotic metabolizing enzymes in *ex vivo* human skin and a human living skin equivalent model. *Drug Metab Dispos* **49**, 39

147. Baron, J. M., Wiederholt, T., Heise, R., Merk, H. F., and Bickers, D. R. (2008) Expression and function of cytochrome P450-dependent enzymes in human skin cells. *Curr Med Chem* **15**, 2258-2264

148. Guengerich, F. P. (2015) Human cytochrome P450 enzymes. in *Cytochrome P450: Structure, Mechanism, and Biochemistry* (Ortiz de Montellano, P. R. ed.), Springer International Publishing, Cham. pp 523-785

149. Beilke, D., Weiss, R., Löhr, F., Pristovšek, P., Hannemann, F., Bernhardt, R., and Rüterjans, H. (2002) A new electron transport mechanism in mitochondrial steroid hydroxylase systems based on structural changes upon the reduction of adrenodoxin. *Biochemistry* **41**, 7969-7978

150. Chu, J. W., and Kimura, T. (1973) Studies on adrenal steroid hydroxylases. Molecular and catalytic properties of adrenodoxin reductase (a flavoprotein). *J Biol Chem* **248**, 2089-2094

151. Katagiri, M., Takikawa, O., Sato, H., and Suhara, K. (1977) Formation of a cytochrome P-450scc-adrenodoxin complex. *Biochem Biophys Res Commun* **77**, 804-809

152. Lambeth, J. D., and Kamin, H. (1977) Adrenodoxin reductase and adrenodoxin. Mechanisms of reduction of ferricyanide and cytochrome *c*. *J Biol Chem* **252**, 2908-2917

153. Lambeth, J. D., Seybert, D. W., and Kamin, H. (1979) Ionic effects on adrenal steroidogenic electron transport. The role of adrenodoxin as an electron shuttle. *J Biol Chem* **254**, 7255-7264

154. Peng, H. M., Barlow, C., and Auchus, R. J. (2018) Catalytic modulation of human cytochromes P450 17A1 and P450 11B2 by phospholipid. *J Steroid Biochem Mol Biol* **181**, 63-72

155. Strushkevich, N., Gilep, A. A., Shen, L., Arrowsmith, C. H., Edwards, A. M., Usanov, S. A., and Park, H. W. (2013) Structural insights into aldosterone synthase substrate specificity and targeted inhibition. *Mol Endocrinol* **27**, 315-324

156. Hobler, A., Kagawa, N., Hutter, M. C., Hartmann, M. F., Wudy, S. A., Hannemann, F., and Bernhardt, R. (2012) Human aldosterone synthase: Recombinant expression in *E. coli*

and purification enables a detailed biochemical analysis of the protein on the molecular level. *J Steroid Biochem Mol Biol* **132**, 57-65

157. Yablokov, E. O., Sushko, T. A., Ershov, P. V., Florinskaya, A. V., Gnedenko, O. V., Shkel, T. V., Grabovec, I. P., Strushkevich, N. V., Kaluzhskiy, L. A., Usanov, S. A., Gilep, A. A., and Ivanov, A. S. (2019) A large-scale comparative analysis of affinity, thermodynamics and functional characteristics of interactions of twelve cytochrome P450 isoforms and their redox partners. *Biochimie* **162**, 156-166

158. Strushkevich, N., MacKenzie, F., Cherkesova, T., Grabovec, I., Usanov, S., and Park, H.-W. (2011) Structural basis for pregnenolone biosynthesis by the mitochondrial monooxygenase system. *Proc Natl Acad Sci U S A* **108**, 10139-10143

159. Lambeth, J. D., and Kriengsiri, S. (1985) Cytochrome P-450scc-adrenodoxin interactions. Ionic effects on binding, and regulation of cytochrome reduction by bound steroid substrates. *J Biol Chem* **260**, 8810-8816

160. Lambeth, J. D., Seybert, D. W., Lancaster, J. R., Salerno, J. C., and Kamin, H. (1982) Steroidogenic electron transport in adrenal cortex mitochondria. *Mol Cell Biochem* **45**, 13-31

161. Jose, J., Bernhardt, R., and Hannemann, F. (2002) Cellular surface display of dimeric Adx and whole cell P450-mediated steroid synthesis on *E. coli*. *J Biotechnol* **95**, 257-268

162. Pikuleva, I. A., Tesh, K., Waterman, M. R., and Kim, Y. (2000) The tertiary structure of full-length bovine adrenodoxin suggests functional dimers. *Arch Biochem Biophys* **373**, 44-55

163. Kido, T., and Kimura, T. (1979) The formation of binary and ternary complexes of cytochrome P-450scc with adrenodoxin and adrenodoxin reductase.adrenodoxin complex. The implication in ACTH function. *J Biol Chem* **254**, 11806-11815

164. Hara, T., and Takeshima, M. (1994) Conclusive evidence of aquaternary cluster model for cholesterol side chain cleavagereaction catalyzed by cytochrome P-450scc. in *Cytochrome P-450: Biochemistry, Biophysics, and Molecular Biology* (Lechner, M. C. ed.), Libbey Eurotext, Paris. pp 417-420

165. Lambeth, J. D., Geren, L. M., and Millett, F. (1984) Adrenodoxin interaction with adrenodoxin reductase and cytochrome P-450scc. Cross-linking of protein complexes and effects of adrenodoxin modification by 1-ethyl-3-(3-dimethylaminopropyl)carbodiimide. *J Biol Chem* **259**, 10025-10029

166. Estrada, D. F., Skinner, A. L., Laurence, J. S., and Scott, E. E. (2014) Human cytochrome P450 17A1 conformational selection: modulation by ligand and cytochrome b_5. *J Biol Chem* **289**, 14310-14320

167. Ducharme, J., Sevrioukova, I. F., Thibodeaux, C. J., and Auclair, K. (2021) Structural dynamics of cytochrome P450 3A4 in the presence of substrates and cytochrome P450 reductase. *Biochemistry* **60**, 2259-2271

168. Zhang, C., Catucci, G., Di Nardo, G., and Gilardi, G. (2020) Effector role of cytochrome P450 reductase for androstenedione binding to human aromatase. *Int J Biol Macro* **164**, 510-517

169. Kumar, A., Wilderman, P. R., Tu, C., Shen, S., Qu, J., and Estrada, D. F. (2020) Evidence of allosteric coupling between substrate binding and Adx recognition in the vitamin D carbon-24 hydroxylase CYP24A1. *Biochemistry* **59**, 1537-1548

170. Kyte, J. (1995) *Mechanism in Protein Chemistry*, 1st ed., Garland

171. Yablokov, E. O., Sushko, T. A., Kaluzhskiy, L. A., Kavaleuski, A. A., Mezentsev, Y. V., Ershov, P. V., Gilep, A. A., Ivanov, A. S., and Strushkevich, N. V. (2021) Substrate-induced modulation of protein-protein interactions within human mitochondrial cytochrome P450-dependent system. *J Steroid Biochem Mol Biol* **208**, 105793

172. Lambeth, J. D., Seybert, D. W., and Kamin, H. (1980) Phospholipid vesicle-reconstituted cytochrome P-450SCC. Mutually facilitated binding of cholesterol and adrenodoxin. *J Biol Chem* **255**, 138-143

173. Tang, E. K. Y., Tieu, E. W., and Tuckey, R. C. (2012) Expression of human CYP27B1 in *Escherichia coli* and characterization in phospholipid vesicles. *FEBS J* **279**, 3749-3761

174. Kumar, A., and Estrada, D. F. (2019) Specificity of the redox complex between cytochrome P450 24A1 and adrenodoxin relies on carbon-25 hydroxylation of vitamin-D substrate. *Drug Metab Dispos* dmd.119.087759

175. Ershov, P. V., Yablokov E, O., Florinskaya, A. V., Mezentsev, Y. V., Kaluzhskiy, L., Tumilovich, A. M., Gilep, A., Usanov, S. A., and Ivanov A, S. (2019) SPR-based study of affinity of cytochrome P450s / redox partners interactions modulated by steroidal substrates. *J Steroid Biochem Mol Biol* **187**, 124-129

176. Tuls, J., Geren, L., Lambeth, J. D., and Millett, F. (1987) The use of a specific fluorescence probe to study the interaction of adrenodoxin with adrenodoxin reductase and cytochrome P-450scc. *J Biol Chem* **262**, 10020-10025

177. Child, S. A., Reddish, M. J., Glass, S. M., Goldfarb, M. H., Barckhausen, I. R., and Guengerich, F. P. (2020) Functional interactions of adrenodoxin with several human mitochondrial cytochrome P450 enzymes. *Arch Biochem Biophys* **694**, 108596

178. Cupp, J. R., and Vickery, L. E. (1988) Identification of free and [Fe2S2]-bound cysteine residues of adrenodoxin. *J Biol Chem* **263**, 17418-17421

179. Kim, D., Kim, V., McCarty, K. D., and Guengerich, F. P. (2021) Tight binding of cytochrome b_5 to cytochrome P450 17A1 is a critical feature of stimulation of C21 steroid lyase activity and androgen synthesis. *J Biol Chem* **296**

180. Kim, D., Kim, V., Tateishi, Y., and Guengerich, F. P. (2021) Cytochrome b_5 binds tightly to several human cytochrome P450 enzymes. *Drug Metab Dispos*, DMD-AR-2021-000475

181. Stayton, P. S., Fisher, M. T., and Sligar, S. G. (1988) Determination of cytochrome b_5 association reactions. Characterization of metmyoglobin and cytochrome P-450cam binding to genetically engineered cytochrome b_5. *J Biol Chem* **263**, 13544-13548

182. Tuckey, R. C., and Sadleir, J. (1999) The concentration of adrenodoxin reductase limits cytochrome P450scc activity in the human placenta. *Eur J Biochem* **263**, 319-325

183. Pikuleva, I. A., Cao, C., and Waterman, M. R. (1999) An additional electrostatic interaction between adrenodoxin and P450c27 (CYP27A1) results in tighter binding than between adrenodoxin and P450scc (CYP11A1). *J Biol Chem* **274**, 2045-2052

184. Chiliza, Z. E., Martínez-Oyanedel, J., and Syed, K. (2020) An overview of the factors playing a role in cytochrome P450 monooxygenase and ferredoxin interactions. *Biophys Rev* **12**, 1217-1222

185. Schiffler, B., Kiefer, M., Wilken, A., Hannemann, F., Adolph, H. W., and Bernhardt, R. (2001) The interaction of bovine adrenodoxin with CYP11A1 (cytochrome P450scc) and CYP11B1 (cytochrome P45011beta). Acceleration of reduction and substrate conversion by site-directed mutagenesis of adrenodoxin. *J Biol Chem* **276**, 36225-36232

186. The UniProt, C. (2021) UniProt: the universal protein knowledgebase in 2021. *Nucl Acids Res* **49**, D480-D489

187. Strushkevich, N. V., Azeva, T. N., Lepesheva, G. I., and Usanov, S. A. (2005) Role of positively charged residues Lys267, Lys270, and Arg411 of cytochrome P450scc (CYP11A1) in interaction with adrenodoxin. *Biochemistry (Moscow)* **70**, 664-671

188. Tuls, J., Geren, L., and Millett, F. (1989) Fluorescein isothiocyanate specifically modifies lysine 338 of cytochrome P-450scc and inhibits adrenodoxin binding. *J Biol Chem* **264**, 16421-16425

189. Usanov, S. A., Graham, S. E., Lepesheva, G. I., Azeva, T. N., Strushkevich, N. V., Gilep, A. A., Estabrook, R. W., and Peterson, J. A. (2002) Probing the interaction of bovine cytochrome P450scc (CYP11A1) with adrenodoxin: evaluating site-directed mutations by molecular modeling. *Biochemistry* **41**, 8310-8320

190. Wada, A., and Waterman, M. R. (1992) Identification by site-directed mutagenesis of two lysine residues in cholesterol side chain cleavage cytochrome P450 that are essential for adrenodoxin binding. *J Biol Chem* **267**, 22877-22882

191. Müller, J. J., Lapko, A., Bourenkov, G., Ruckpaul, K., and Heinemann, U. (2001) Adrenodoxin reductase-adrenodoxin complex structure suggests electron transfer path in steroid iosynthesis. *J Biol Chem* **276**, 2786-2789

192. Miura, S., and Ichikawa, Y. (1991) Conformational change of adrenodoxin induced by reduction of iron-sulfur cluster. Proton nuclear magnetic resonance study. *J Biol Chem* **266**, 6252-6258

193. Zöllner, A., Pasquinelli, M. A., Bernhardt, R., and Beratan, D. N. (2007) Protein phosphorylation and intermolecular electron transfer: a joint experimental and computational study of a hormone biosynthesis pathway. *J Am Chem Soc* **129**, 4206-4216

194. Bernlohr, D. A., Simpson, M. A., Hertzel, A. V., and Banaszak, L. J. (1997) Intracellular lipid-binding proteins and their genes. *Annu Rev Nutr* **17**, 277-303

195. Andersson, E., Björklind, C., Törmä, H., and Vahlquist, A. (1994) The metabolism of vitamin A to 3,4-didehydroretinol can be demonstrated in human keratinocytes, melanoma cells and HeLa cells, and is correlated to cellular retinoid-binding protein expression. *Biochim Biophys Acta* **1224**, 349-354

196. Dong, D., Ruuska, S. E., Levinthal, D. J., and Noy, N. (1999) Distinct roles for cellular retinoic acid-binding proteins I and II in regulating signaling by retinoic acid. *J Biol Chem* **274**, 23695-23698

197. Budhu, A., Gillilan, R., and Noy, N. (2001) Localization of the RAR interaction domain of cellular retinoic acid binding protein-II. *J Mol Biol* **305**, 939-949

198. Budhu, A. S., and Noy, N. (2002) Direct channeling of retinoic acid between cellular retinoic acid-binding protein II and retinoic acid receptor sensitizes mammary carcinoma cells to retinoic acid-induced growth arrest. *Mol Cell Biol* **22**, 2632-2641

199. Sjoelund, V., and Kaltashov, I. A. (2012) Modification of the zonal elution method for detection of transient protein–protein interactions involving ligand exchange. *Anal Chem* **84**, 4608-4612

200. Bumpus, N. N., and Hollenberg, P. F. (2010) Cross-linking of human cytochrome P450 2B6 to NADPH-cytochrome P450 reductase: Identification of a potential site of interaction. *J Inorg Biochem* **104**, 485-488

201. Gao, Q., Doneanu, C. E., Shaffer, S. A., Adman, E. T., Goodlett, D. R., and Nelson, S. D. (2006) Identification of the interactions between cytochrome P450 2E1 and cytochrome b_5 by mass spectrometry and site-directed mutagenesis. *J Biol Chem* **281**, 20404-20417

202. Lapshina, E. A., Belyaeva, O. V., Chumakova, O. V., and Kedishvili, N. Y. (2003) Differential recognition of the free versus bound retinol by human microsomal retinol/sterol dehydrogenases: characterization of the holo-CRBP dehydrogenase activity of RoDH-4. *Biochemistry* **42**, 776-784

203. Penzes, P., Wang, X., and Napoli, J. L. (1997) Enzymatic characteristics of retinal dehydrogenase type I expressed in *Escherichia coli*. *Biochim Biophys Acta* **1342**, 175-181

204. Posch, K. C., Burns, R. D., and Napoli, J. L. (1992) Biosynthesis of all-*trans*-retinoic acid from retinal. Recognition of retinal bound to cellular retinol binding protein (type I) as substrate by a purified cytosolic dehydrogenase. *J Biol Chem* **267**, 19676-19682

205. Jiang, W., and Napoli, J. L. (2012) Reorganization of cellular retinol-binding protein type 1 and lecithin:retinol acyltransferase during retinyl ester biosynthesis. *Biochim Biophys Acta* **1820**, 859-869

206. Adachi, N., Smith, J. E., Sklan, D., and Goodman, D. S. (1981) Radioimmunoassay studies of the tissue distribution and subcellular localization of cellular retinol-binding protein in rats. *J Biol Chem* **256**, 9471-9476

207. Ruff, S. J., and Ong, D. E. (2000) Cellular retinoic acid binding protein is associated with mitochondria. *FEBS Lett* **487**, 282-286

208. Majumdar, A., Petrescu, A. D., Xiong, Y., and Noy, N. (2011) Nuclear translocation of cellular retinoic acid-binding protein II is regulated by retinoic acid-controlled SUMOylation. *J Biol Chem* **286**, 42749-42757

209. Belyaeva, O. V., Korkina, O. V., Stetsenko, A. V., and Kedishvili, N. Y. (2008) Human retinol dehydrogenase 13 (RDH13) is a mitochondrial short-chain dehydrogenase/reductase with a retinaldehyde reductase activity. *FEBS J* **275**, 138-147

210. Everts, H. B., Claassen, D. O., Hermoyian, C. L., and Berdanier, C. D. (2002) Nutrient-gene interactions: dietary vitamin A and mitochondrial gene expression. *IUBMB Life* **53**, 295-301

211. Everts, H. B., and Berdanier, C. D. (2002) Regulation of Mitochondrial Gene Expression by Retinoids. *IUBMB Life* **54**, 45-49

212. Hostetler, H. A., McIntosh, A. L., Atshaves, B. P., Storey, S. M., Payne, H. R., Kier, A. B., and Schroeder, F. (2009) L-FABP directly interacts with PPARalpha in cultured primary hepatocytes. *J Lipid Res* **50**, 1663-1675

213. Tan, N.-S., Shaw Natacha, S., Vinckenbosch, N., Liu, P., Yasmin, R., Desvergne, B., Wahli, W., and Noy, N. (2002) Selective cooperation between fatty acid binding proteins and peroxisome proliferator-activated receptors in regulating transcription. *Mol Cell Biol* **22**, 5114-5127

214. Velkov, T. (2013) Interactions between human liver fatty acid binding protein and peroxisome proliferator activated receptor selective drugs. *PPAR Res* **2013**, 938401-938401

215. Jenkins-Kruchten, A. E., Bennaars-Eiden, A., Ross, J. R., Shen, W.-J., Kraemer, F. B., and Bernlohr, D. A. (2003) Fatty acid-binding protein-hormone-sensitive lipase interaction: fatty acid dependence on binding. *J Biol Chem* **278**, 47636-47643

216. Wilson, V. G. (2014) Growth and Differentiation of HaCaT Keratinocytes. in *Epidermal Cells: Methods and Protocols* (Turksen, K. ed.), Springer New York, New York, NY. pp 33-41

217. Boukamp, P., Petrussevska, R. T., Breitkreutz, D., Hornung, J., Markham, A., and Fusenig, N. E. (1988) Normal keratinization in a spontaneously immortalized aneuploid human keratinocyte cell line. *J Cell Biol* **106**, 761-771

218. Seo, M.-D., Kang, T. J., Lee, C. H., Lee, A.-Y., and Noh, M. (2012) HaCaT keratinocytes and primary epidermal keratinocytes have different transcriptional Profiles of Cornified envelope-associated genes to T helper cell cytokines. *Biomol Ther (Seoul)* **20**, 171-176

219. Smits, J. P. H., Niehues, H., Rikken, G., van Vlijmen-Willems, I. M. J. J., van de Zande, G. W. H. J. F., Zeeuwen, P. L. J. M., Schalkwijk, J., and van den Bogaard, E. H. (2017) Immortalized N/TERT keratinocytes as an alternative cell source in 3D human epidermal models. *Sci Rep* **7**, 11838

220. Marill, J., Cresteil, T., Lanotte, M., and Chabot, G. G. (2000) Identification of human cytochrome P450s involved in the formation of all-*trans*-retinoic acid principal metabolites. *Mol Pharmacol* **58**, 1341-1348

221. Thatcher, J. E., and Isoherranen, N. (2009) The role of CYP26 enzymes in retinoic acid clearance. *Expert Opin Drug Metab Toxicol* **5**, 875-886

222. Wang, Y., Bell, J. C., Keeney, D. S., and Strobel, H. W. (2010) Gene regulation of CYP4F11 in human keratinocyte HaCaT cells. *Drug Metab Dispos* **38**, 100-107

223. Zhang, Y., Zolfaghari, R., and Ross, A. C. (2010) Multiple retinoic acid response elements cooperate to enhance the inducibility of CYP26A1 gene expression in liver. *Gene* **464**, 32-43

224. Hubbard, R., Brown, P. K., and Bownds, D. (1971) Methodology of vitamin A and visual pigments. *Methods Enzymol* **243**, 615-653

225. Robeson, C. D., Cawley, J. D., Weisler, L., Stern, M. H., Eddinger, C. C., and Chechak, A. J. (1955) Chemistry of vitamin A. XXIV. The synthesis of geometric isomers of vitamin A via methyl β-methylglutaconate1. *J Am Chem Soc* **77**, 4111-4119

226. Rao, M. S., John, J., and Cama, H. R. (1972) Studies on vitamin A 2 : preparation, properties, metabolism and biological activity of 4-oxoretinoic acid. *Int J Vitam Nutr Res* **42**, 368-378

227. Planta, C. V., Schweiter, U., Chopard-dit-Jean, L., Rüegg, R., Kofler, M., and Isler, O. (1962) Synthesen in der Vitamin-A2-Reihe. 4. Mitteilung. Physikalische Eigenschaften

von isomeren Vitamin-A- und Vitamin-A2-Verbindungen. *Helvetica Chimica Acta* **45**, 548-561

228. Akhrem, A. A., Lapko, V. N., Lapko, A. G., Shkumatov, V. M., and Chashchin, V. L. (1979) Isolation, structural organization and mechanism of action of mitochondrial steroid hydroxylating systems. *Acta Biol Med Ger* **38**, 257-273

229. Gasteiger, E., Hoogland, C., Gattiker, A., Duvaud, S. e., Wilkins, M. R., Appel, R. D., and Bairoch, A. (2005) Protein identification and analysis tools on the ExPASy server. in *The Proteomics Protocols Handbook* (Walker, J. M. ed.), Humana Press, Totowa, NJ. pp 571-607

230. Ong, D. E. (1982) Purification and partial characterization of cellular retinol-binding protein from human liver. *Cancer Res* **42**, 1033-1037

231. Ong, D. E., and Chytil, F. (1978) Cellular retinoic acid-binding protein from rat testis. Purification and characterization. *J Biol Chem* **253**, 4551-4554

232. Folli, C., Calderone, V., Ottonello, S., Bolchi, A., Zanotti, G., Stoppini, M., and Berni, R. (2001) Identification, retinoid binding, and x-ray analysis of a human retinol-binding protein. *Proc Natl Acad Sci USA* **98**, 3710

233. Kane, M. A., Bright, F. V., and Napoli, J. L. (2011) Binding affinities of CRBPI and CRBPII for 9-*cis*-retinoids. *Biochim Biophys Acta* **1810**, 514-518

234. Noy, N., and Blaner, W. S. (1991) Interactions of retinol with binding proteins: studies with rat cellular retinol-binding protein and with rat retinol-binding protein. *Biochemistry* **30**, 6380-6386

235. Notredame, C., Higgins, D. G., and Heringa, J. (2000) T-Coffee: A novel method for fast and accurate multiple sequence alignment. *J Mol Biol* **302**, 205-217

APPENDIX

Table A1. Extinction coefficients of retinoids and proteins.

	λ_{max} (nm)	ε ($M^{-1}cm^{-1}$)	Reference
Retinoids[a]			
All-*trans* retinol (atROL)	325	52,770	(224)
All-*trans* retinaldehyde (atRAL)	383	42,880	(224)
All-*trans* retinoic acid (atRA)	350	45,300	(225)
All-*trans* 4-oxoretinoic acid	360	58,220	(226)
All-*trans* 4-hydroxyretinoic acid			
3,4-dehydroretinol (ddROL)	350	41,320	(227)
3,4-dehydroretinaldehyde (ddRAL)	401	41,450	(227)
3,4-dehydroretinoic acid (ddRA)	370	41,570	(227)
Proteins			
Cytochrome P450[b]	450	91,000	(110)
Adrenodoxin Reductase (AdR)	450	11,300	(228)
Adrenodoxin (Adx)	414	9,800	(114)
Apo-CRBP-1[c]	280	26,470	(229)
Apo-CRABP-1 [c]	280	20,970	(229)
Apo-CRABP-2 [c]	280	19,480	(229)
atROL-CRBP-1	350	59,200	(230)
atRAL-CRBP-1[d]	395	38,000	(58)
atRA-CRABP-1	350	50,000	(231)
atRA-CRABP-2 [d]	350	50,000	(57,231)

[a] Extinction coefficients for retinoids recorded in 100% ethanol, reviewed in (109). Representative spectra are shown in Figure 7.

[b] Extinction coefficient for reduced CO difference spectrum (Fe^{2+}•CO vs Fe^{2+}).

[c] Extinction coefficients for apo-retinoid binding proteins were calculated using Expasy ProtParam (229).

[d] There is no reported extinction coefficient for all-*trans* retinaldehyde binding to CRBP-1 or all-*trans* retinoic acid binding to CRABP-2, so the ones for CRBP-2 or CRABP-1 were used, respectively. CRBP-1 and CRBP-2 and CRABP-1 and CRABP-2 generally have similar binding properties with retinoids (57,58). This assumption has been made with other holo-CRBPs (232).

Formatte

Deleted:

Table A2. Translated amino acid constructs used for expression of P450 27C1 and human Adx.

Cytochrome P450 27C1

1	MAGPRSLAAM	PGPRTLANLA	EFFCRDGFSR	IHEIQQKHTR	40
41	EYGKIFKSHF	GPQFVVSIAD	RDMVAQVLRA	EGAAPQRANM	80
81	ESWREYRDLR	GRATGLISAE	GEQWLKMRSV	LRQRILKPKD	120
121	VAIYSGEVNQ	VIADLIKRIY	LLRSQAEDGE	TVTNVNDLFF	160
161	KYSMEGVATI	LYESRLGCLE	NSIPQLTVEY	IEALELMFSM	200
201	FKTSMYAGAI	PRWLRPFIPK	PWREFCRSWD	GLFKFSQIHV	240
241	DNKLRDIQYQ	MDRGRRVSGG	LLTYLFLSQA	LTLQEIYANV	280
281	TEMLLAGVDT	TSFTLSWTVY	LLARHPEVQQ	TVYREIVKNL	320
321	GERHVPTAAD	VPKVPLVRAL	LKETLRLFPV	LPGNGRVTQE	360
361	DLVIGGYLIP	KGTQLALCHY	ATSYQDENFP	RAKEFRPERW	400
401	LRKGDLDRVD	NFGSIPFGHG	VRSCIGRRIA	ELEIHLVVIQ	440
441	LLQHFEIKTS	SQTNAVHAKT	HGLLTPGGPI	HVRFVNRKHH	480
481	HHH				483

Adx

1	HHHHHHSSED	KITVHFINRD	GETLTTKGKV	GDSLLDVVVE	40
41	NNLDIDGFGA	CEGTLACSTC	HLIFEDHIYE	KLDAITDEEN	80
81	DMLDLAYGLT	DRSRLGCQIC	LTKSMDNMTV	RVPETVADAR	120
121	QSIDVGKTS				129

Residues identified in P450 27C1-Adx cross-links are highlighted in yellow.

Table A3. Translated amino acid constructs used for the expression of retinoid binding proteins.

CRBP-1:

1	MPVDFTGYWK	MLVNENFEEY	LRALDVNVAL	RKIANLLKPD	40
41	KEIVQDGDHM	IIRTLSTFRN	YIMDFQVGKE	FEEDLTGIDD	80
81	RKCMTTVSWD	GDKLQCVQKG	EKEGRGWTQW	IEGDELHLEM	120
121	RVEGVVCKQV	FKKVQHHHHH	H		141

CRABP-1 (WT):

1	MGSSHHHHHH	SSGLVPR**G**SH	MASMTGGQQM	GRGSAMPNFA	40
11	GTWKMRSSEN	FDELLKALGV	NAMLRKVAVA	AASKPHVEIR	80
81	QDGDQFYIKT	STTVRTTEIN	FKVGEGFEEE	TVDGRKCRSL	120
121	ATWENENKIH	CTQTLLEGDG	PKTYWTRELA	NDELILTFGA	160
161	DDVVCTRIYV	RE			172

CRABP-2 (WT):

1	MGSSHHHHHH	SSGLVPR**G**SH	MPNFSGNWKI	IRSENFEELL	40
41	KVLGVNVMLR	KIAVAAASKP	AVEIKQEGDT	FYIKTSTTVR	80
81	TTEINFKVGE	EFEEQTVDGR	PCKSLVKWES	ENKMVCEQKL	120
121	LKGEGPKTSW	TRELTNDGEL	ILTMTADDVV	CTRVYVRE	158

CRABP-1 (E75Q/K81P/E102K):

1	MGSSHHHHHH	SSGLVPR**G**SH	MASMTGGQQM	GRGSAMPNFA	40
41	GTWKMRSSEN	FDELLKALGV	NAMLRKVAVA	AASKPHVEIR	80
81	QDGDQFYIKT	STTVRTTEIN	FKVGEGFEEQ	TVDGRPCRSL	120
121	ATWENENKIH	CTQTLLKGDG	PKTYWTRELA	NDELILTFGA	160
161	DDVVCTRIYV	RE			172

CRABP-2 (Q75E/P81K/K102E):

1	MGSSHHHHHH	SSGLVPR**G**SH	MPNFSGNWKI	IRSENFEELL	40
41	KVLGVNVMLR	KIAVAAASKP	AVEIKQEGDT	FYIKTSTTVR	80
81	TTEINFKVGE	EFEEETVDGR	KCKSLVKWES	ENKMVCEQKL	120
121	LEGEGPKTSW	TRELTNDGEL	ILTMTADDVV	CTRVYVRE	158

The N-terminus of the CRABP proteins containing the His-tag is cleaved following thrombin digestion. The first amino acid after digestion is shown bolded and underlined. For CRABP mutants, numbering is for processed form, and mutations are shown in red.

Table A4. Codon-optimized QconCAT cDNA for expression in *E. coli* with NdeI and HindIII restriction sites.

TAAGCACATATGATGGCCGGCAAAAATTTAGGTTTCGGTTGGGGTGTTCGCAATTTT
CTGCCGCTGCTGGATGCAGTGAGCCGCTTAAATCCGGAGGTGCTGAGCCCGAATGC
CGTTCAACGTCATTTACAAGTTGAAACTTTAACCCAAGAAGATATCAAGCTGAATCC
GGACGTTCTGAGCCCGAAATACAATCTGGGCGGCCCGCGTTATGGCCCGATTTACAG
CGTGCGCGATTCTTTAGTTGATCTGGTGCCGTGGCTGAAAGAAAGTCTGGTTGCCGG
TCAGTGGCGTGCTTTAGCATTTGGCTGTGGTGCACGCGTGCCGGAAACCGTTGCCGA
TGCACGTTTAGGCTGCCAGATTTGTTTAACCAAATTTTTAGAGGAGCATCCGGGCGG
CGAAGAAGTTCTGCGCTACTATACTTTAGAGGAAATCCAGAAAACCGTGTGGCTGGT
GGGTCGCTTTGGTGTTGCCCCGGATCACCCGGAAGTGAAAAACCCGTTTCTGGCCGC
AGTGACCACCAATCGTTTCGCCGTGTTCGGTCTGGGCAATAAAAGCCAAGCTGAAG
ACGGCGAAACCGTGACCAACGTGAACGATTTATTCTTCAAGCATCCGGAAGTGCAG
CAAACCGTTTATCGCGGCGTTAACGACAACGAGGAAGGCTTCTTCAGCGCACGTCTG
GCCGCCGCCTTAGAACACCATCATCACCATCATTGAAAGCTTTAAGCA

Table A5. Binding affinities and rates of retinoid binding to cellular retinoid-binding proteins.

Retinoid	CRBP	K_d (nM)	k_{on} ($M^{-1}s^{-1}$)	k_{off} (min^{-1})	Reference
atROL	CRBP-1	3 ± 2	4.4×10^7	0.68 ± 0.069	(233,234)
atRAL	CRBP-1	9 ± 4	[a]	[a]	(233)
atRA	CRABP-1	0.06	$3.55 \pm 0.38 \times 10^9$	0.22 ± 0.01	(196)
	CRABP-2	0.13	$3.08 \pm 0.08 \times 10^9$	0.42 ± 0.05	(196)

[a] There are no reported k_{on} and k_{off} values for all-*trans* retinaldehyde binding to CRBP-1 to our knowledge.

Table A6. Peptides for the quantification of P450 27C1 and P450 redox partner by targeted proteomics method.

Protein	Peptide	Source	Precursor *m/z*	Charge
P450 27C1	SQAEDGETVTNVNDLFFK	Native	1007.4736	2
		Standard	1010.4837	2
	HPEVQQTVYR	Native	628.8227	2
		Standard	631.8328	2
AdR	TVWLVGR	Native	415.7478	2
		Standard	418.7579	2
	FGVAPDHPEVK	Native	598.3089	2
		Standard	601.3190	2
POR	NPFLAAVTTNR	Native	602.3277	2
		Standard	605.3377	2
	FAVFGLGNK	Native	476.7662	2
		Standard	476.7762	2
Adx	VPETVADAR	Native	479.2536	2
		Standard	482.2637	2
	LGCQICLTK	Native	592.7684	2
		Standard	595.7784	2
b_5	FLEEHPGGEEVLR	Native	756.3781	2
		Standard	759.3881	2
	YYTLEEIQK	Native	593.8032	2
		Standard	596.8132	2
Mod Glu-Fib	GVNDNEEGFFSAR	Native	721.3207	2
		Standard	724.3308	2

Table A7. P450 27C1-Adx cross-linked peptides.

Adx Peptide	Adx Residue	27C1 Peptide	27C1 Residue	*z*	*m/z*	Mass deviation (ppm)	Modifications
$_{72}$LDAITDEENDMLDLAYGLTDR$_{92}$	D77	$_{115}$ILKPK$_{119}$	K117	3	2962.5087	0.4928	-
				3	2978.5070	1.6089	M(ox)
$_{72}$LDAITDEENDMLDLAYGLTDR$_{92}$	D77	$_{403}$KGDLDR$_{408}$	K403	4	3067.4500	0.6452	-
$_{72}$LDAITDEENDMLDLAYGLTDR$_{92}$	D77	$_{478}$ KHHHHH$_{483}$	K478	4	3212.4830	0.6489	M(ox)
				4	3212.4805	0.1193	M(ox)
$_{72}$LDAITDEENDMLDLAYGLTDR$_{92}$	E78	$_{115}$ILKPK$_{119}$	K117	3	3962.5071	0.0550	-
$_{72}$LDAITDEENDMLDLAYGLTDR$_{92}$	E78	$_{315}$EIVKNLGER$_{323}$	K318	4	3421.6791	0.1254	-
$_{72}$LDAITDEENDMLDLAYGLTDR$_{92}$	D84	$_{115}$ILKPK$_{119}$	K117	3	2962.5087	0.4928	-
				3	2962.5088	0.5111	-
$_{72}$LDAITDEENDMLDLAYGLTDR$_{92}$	D84	$_{315}$EIVKNLGER$_{323}$	K318	4	3421.6867	2.0519	-
				4	3421.6857	2.0671	-
$_{72}$LDAITDEENDMLDLAYGLTDR$_{92}$	D84	$_{403}$KGDLDR$_{408}$	K403	3	3067.4546	0.8680	-
				4	3067.4583	2.0620	-
				4	3067.4584	2.1102	-
$_{72}$LDAITDEENDMLDLAYGLTDR$_{92}$	D84	$_{478}$ KHHHHH$_{483}$	K478	5	3196.4950	2.8244	-
				5	3212.4813	0.1037	M(ox)
$_{121}$QSIDVGKTS$_{129}$	K127	$_{120}$DVAIYSGEVNQVIADLIK$_{137}$	E127	3	2862.5105	0.5253	-
$_{121}$QSIDVGKTS$_{129}$	K127	$_{144}$ SQAEDGETVTNVNDLFFK$_{161}$	E147	3	2929.4085	0.9740	-

Underlined residues are cross-linked.

Table A8. Adx-Adx cross-linked peptides.

Adx Peptide	Adx Residue	27C1 Peptide	27C1 Residue	*z*	*m/z*	Mass deviation (ppm)	Modifications
$_{72}$LDAITDEENDMLDLAYGLTDR$_{92}$	D77	$_{115}$ILKPK$_{119}$	K117	3	2962.5087	0.4928	-
				3	2978.5070	1.6089	M(ox)
$_{72}$LDAITDEENDMLDLAYGLTDR$_{92}$	D77	$_{403}$KGDLDR$_{408}$	K403	4	3067.4500	0.6452	-
$_{72}$LDAITDEENDMLDLAYGLTDR$_{92}$	D77	$_{478}$ KHHHHH$_{483}$	K478	4	3212.4830	0.6489	M(ox)
				4	3212.4805	0.1193	M(ox)
$_{72}$LDAITDEENDMLDLAYGLTDR$_{92}$	E78	$_{115}$ILKPK$_{119}$	K117	3	3962.5071	0.0550	-
$_{72}$LDAITDEENDMLDLAYGLTDR$_{92}$	E78	$_{315}$EIVKNLGER$_{323}$	K318	4	3421.6791	0.1254	-
$_{72}$LDAITDEENDMLDLAYGLTDR$_{92}$	D84	$_{115}$ILKPK$_{119}$	K117	3	2962.5087	0.4928	-
				3	2962.5088	0.5111	-
$_{72}$LDAITDEENDMLDLAYGLTDR$_{92}$	D84	$_{315}$EIVKNLGER$_{323}$	K318	4	3421.6867	2.0519	-
				4	3421.6857	2.0671	-
$_{72}$LDAITDEENDMLDLAYGLTDR$_{92}$	D84	$_{403}$KGDLDR$_{408}$	K403	3	3067.4546	0.8680	-
				4	3067.4583	2.0620	-
				4	3067.4584	2.1102	-
$_{72}$LDAITDEENDMLDLAYGLTDR$_{92}$	D84	$_{478}$ KHHHHH$_{483}$	K478	5	3196.4950	2.8244	-
				5	3212.4813	0.1037	M(ox)
$_{121}$QSIDVGKTS$_{129}$	K127	$_{120}$DVAIYSGEVNQVIADLIK$_{137}$	E127	3	2862.5105	0.5253	-
$_{121}$QSIDVGKTS$_{129}$	K127	$_{144}$ SQAEDGETVTNVNDLFFK$_{161}$	E147	3	2929.4085	0.9740	-

Underlined residues are cross-linked.

```
Bovine     1 -----MSSEDKITVHFINRDGETLTTKGKIGDSLLDVVVQNNLDIDGFGACEGTLACSTC
Human      1 HHHHHHSSEDKITVHFINRDGETLTTKGKVGDSLLDVVVENNLDIDGFGACEGTLACSTC

Bovine    56 HLIFEQHIFEKLEAITDEENDMLDLAYGLTDRSRLGCQICLTKAMDNMTVRVPDAVSDAR
Human     61 HLIFEDHIYEKLDAITDEENDMLDLAYGLTDRSRLGCQICLTKSMDNMTVRVPETVADAR

Bovine   116 ESIDMGMNSSKIE
Human    121 QSIDVGKTS----
```

Figure A1. Comparison of expressed bovine and human Adx constructs. Constructs have 110 identical positions (82.7%) identity and 12 similar positions. Sequence alignment was performed with T-Coffee (235) and visualized by BoxShade.

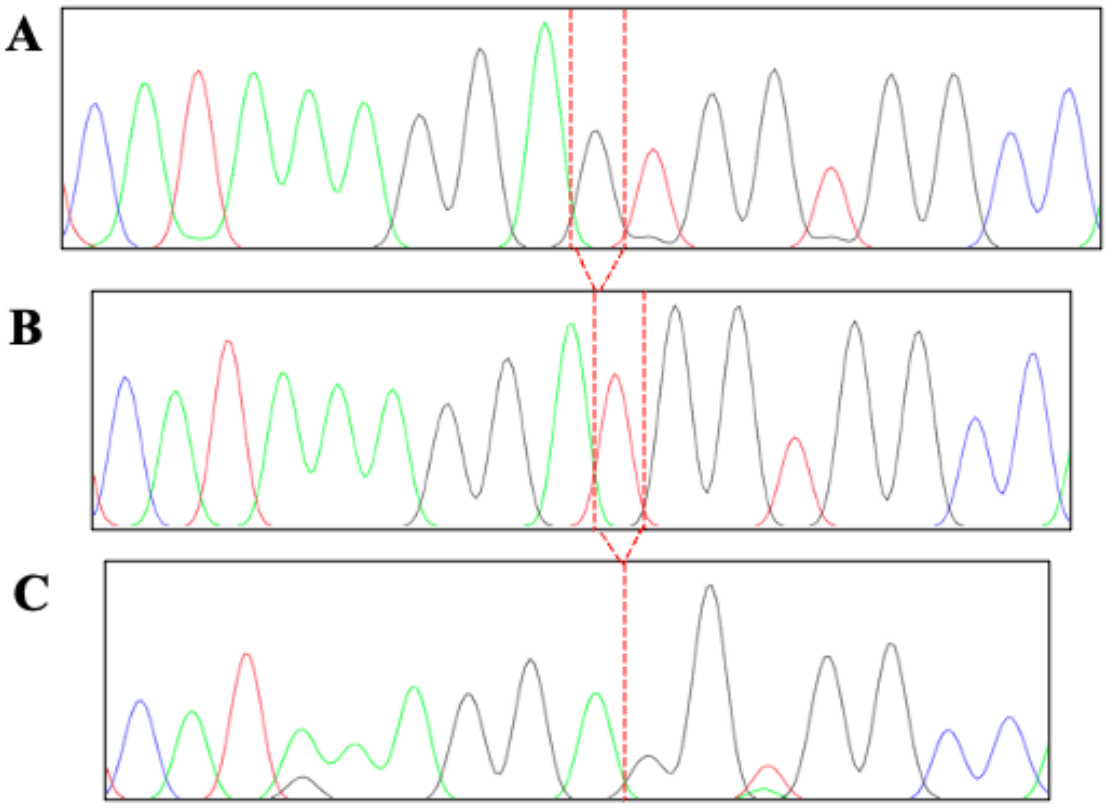

Figure A2. Sequencing chromatograms for CRISPR/Cas-9 *CYP27C1* KO N/TERT lines. *A*, Chromatogram showing a 1 nucleotide insertion (*CYP27C1* KO #9). *B,* Chromatogram for wild-type *CYP27C1*. *C*, Chromatogram showing a 1 nucleotide deletion (*CYP27C1* KO #6).

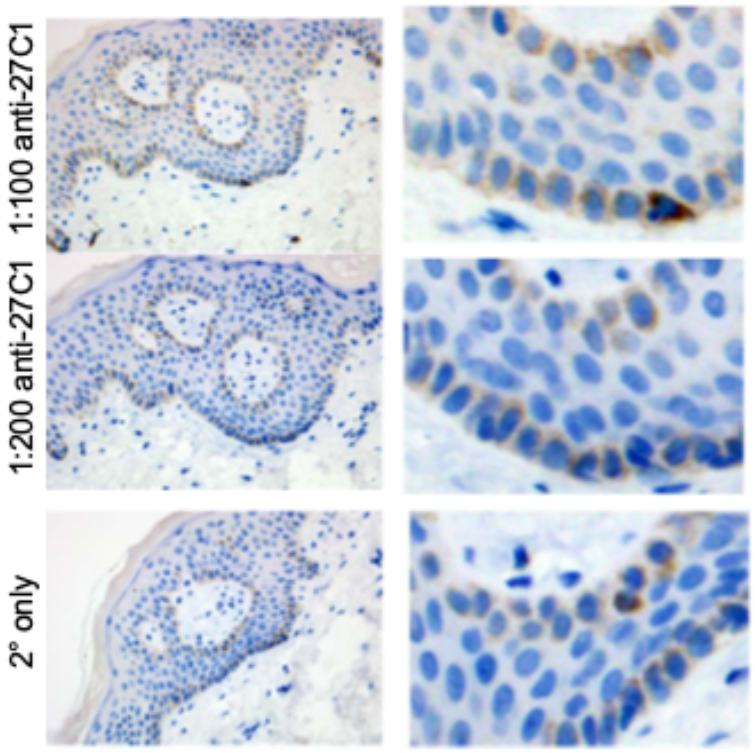

Figure A3. Immunohistochemistry for P450 27C1 in skin sections. Rows 1 and 2 show two different dilutions of anti-CYP27C1 utilized. Row 3 shows a secondary antibody only control. The second column is zoomed in to representative areas with signal.

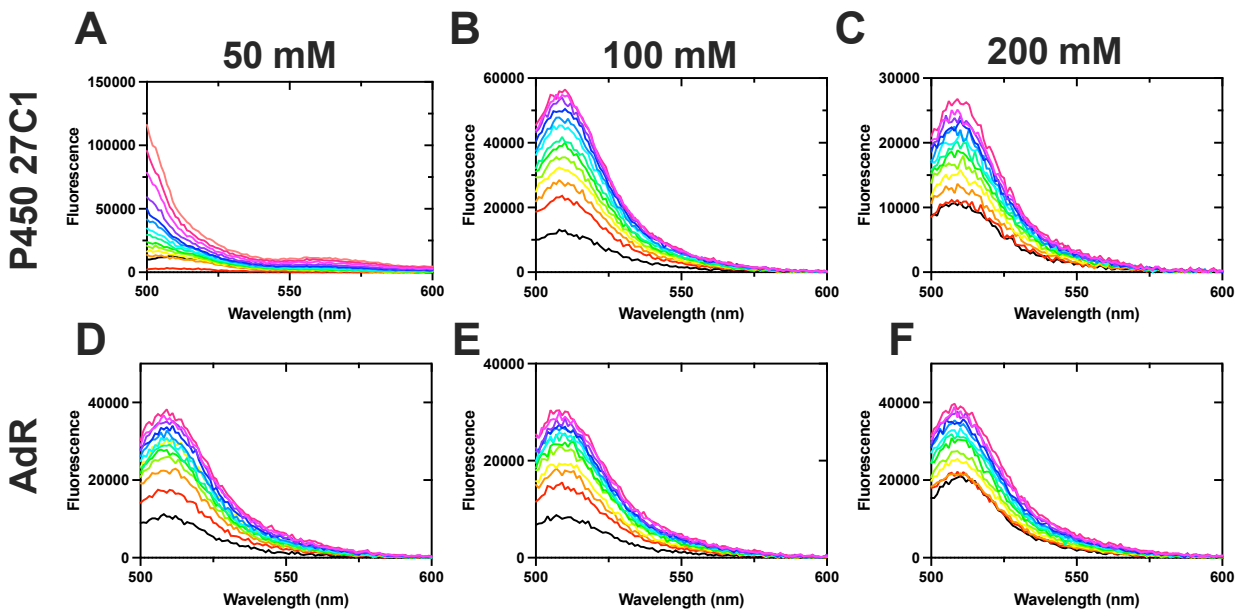

Figure A4. Representative spectra of Alexa Fluor 488-Adx titrations with P450 27C1 and AdR at varying ionic strengths. *A-C*, Titrations of P450 27C1 with Alexa Fluor 488-Adx at 50 mM (*A*), 100 mM (*B*), or 200 mM (*C*) potassium phosphate (pH 7.4). The fluorescence increased with increasing concentrations of P450 27C1, as shown with the colored spectra. See Figs. 2 and 3. The shift in the emission maximum in panel (*A*) is due to Rayleigh scattering caused by precipitation of P450 27C1 at lower ionic strength. Panel (*B*) is also shown in Figure 2. *D-F*, Titrations of AdR with Alexa Fluor 488-Adx at 50 mM (*D*), 100 mM (*E*), or 200 mM (*F*) potassium phosphate (pH 7.4).

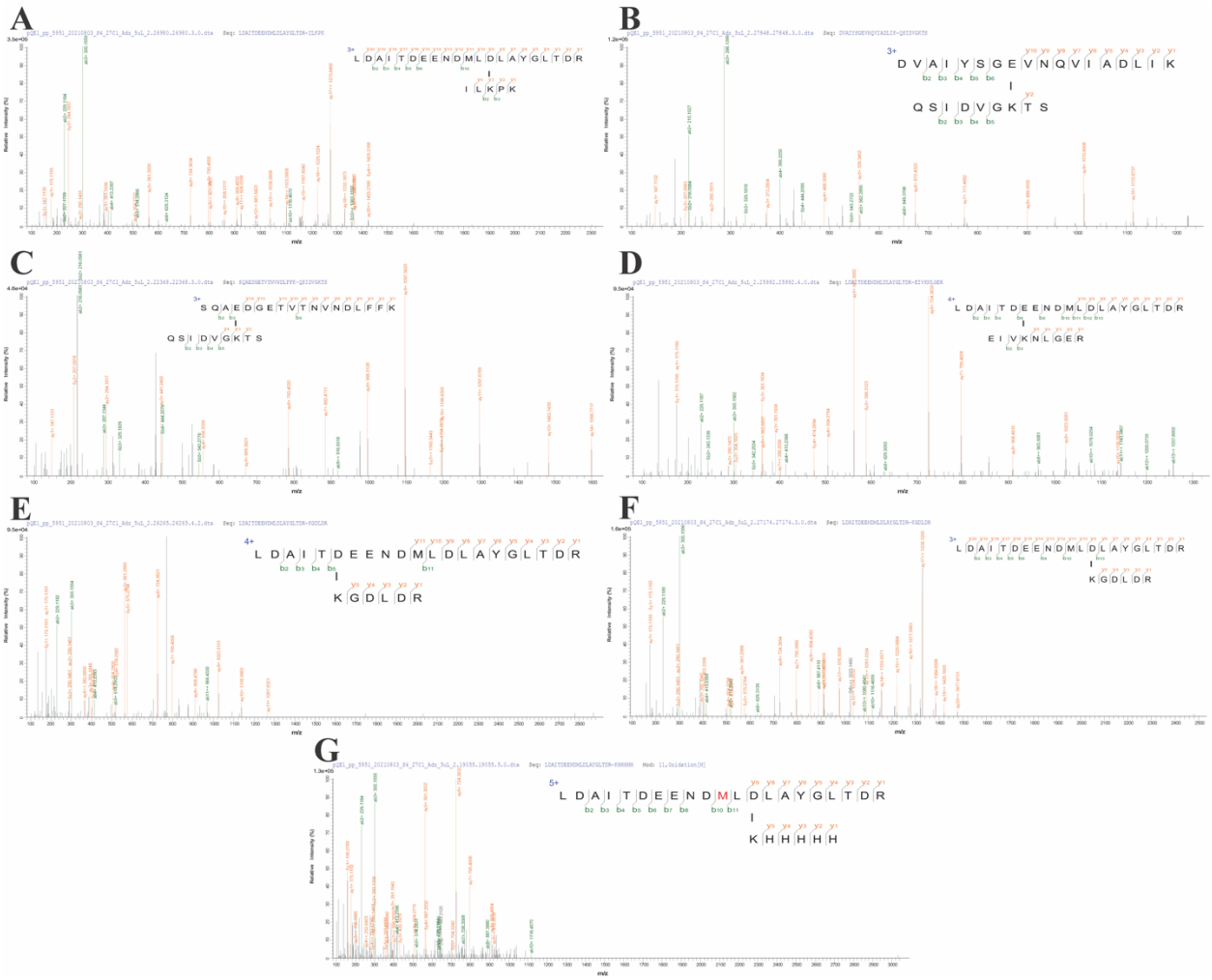

Figure A5. Representative fragmentation of additional identified P450 27C1-Adx cross-linked peptides. MS/MS spectra with fragment assignment for cross-links observed between: *A*, Asp-84 of Adx and Lys-117 of P450 27C1; *B*, Lys-127 of Adx and Glu-127 of P450 27C1; *C*, Lys-127 of Adx and Glu-147 of P450 27C1; *D*, Glu-78 of Adx and Lys-318 of P450 27C1; *E*, Asp-77 of Adx and Lys-403 of P450 27C1; *F*, Asp-84 of Adx and Lys-403 of P450 27C1; *G*, Asp-84 of Adx and Lys-478 of P450 27C1.

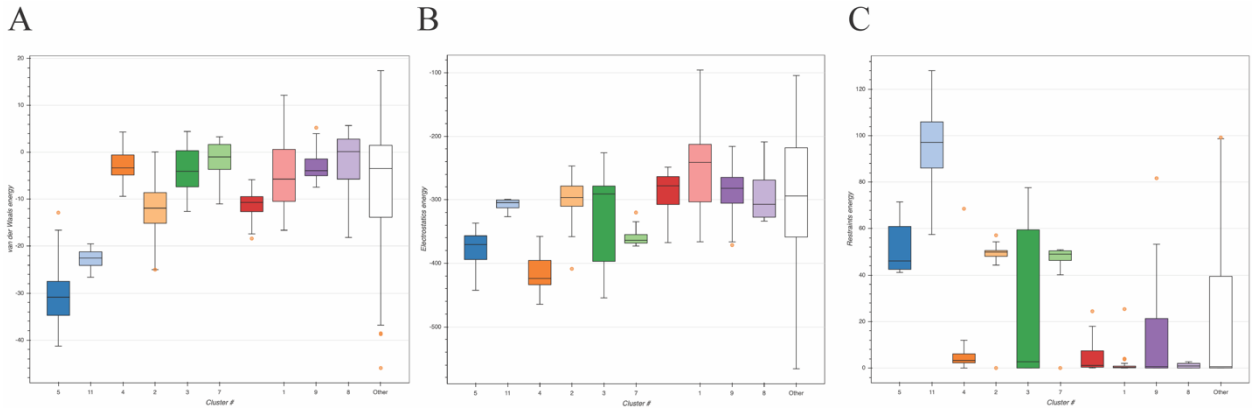

Figure A6. Energy values for HADDOCK model clusters. *A*, van der Waals energy; *B*, Electrostatic energy; *C*, Restraints violation energy. Lower energy values are more favorable. Cluster are listed across the x-axes of each plot in the following order: 5, 11, 4, 2, 3, 7, 10, 1, 9, 8, other models.

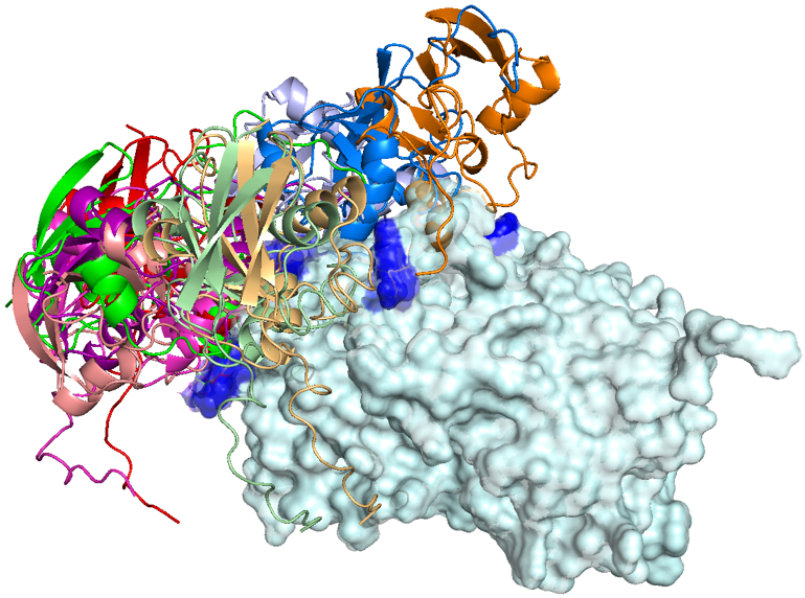

Figure A7. Visualization of Adx orientations in the modeled P450 27C1-Adx complexes. P450 27C1 structures from each cluster were aligned. P450 27C1 is shown as a surface in light cyan, with residues identified in cross-links shown in blue. Adx molecules from the top 10 clusters are shown as cartoons in colors corresponding to Figure A6.

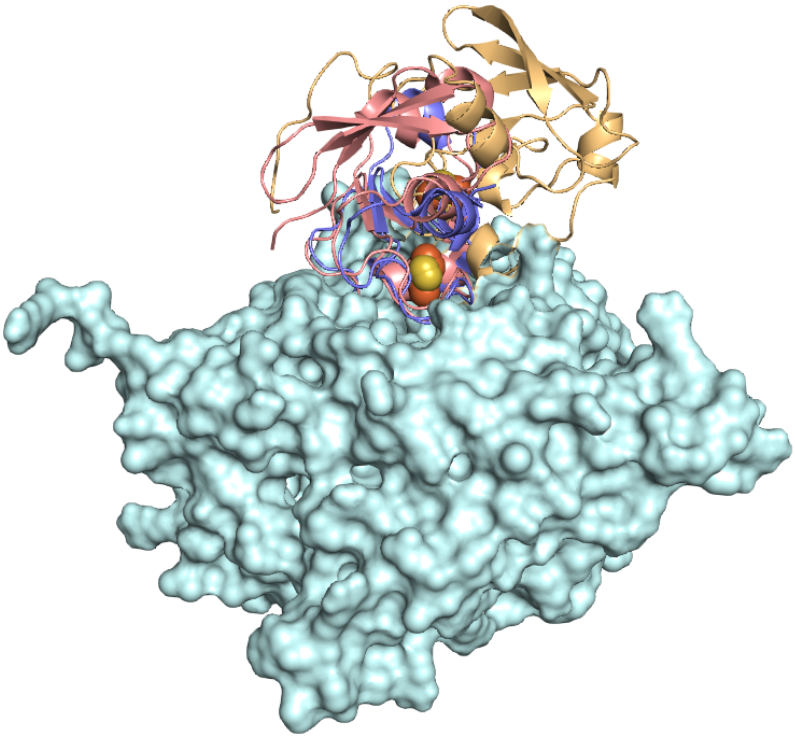

Figure A8. Comparison of the P450 27C1-Adx model (cluster 4) and the P450 11A1-Adx and P450 11B2-Adx fusion protein structures. The P450 of each structure was aligned and is shown as a pale cyan surface. The Adx for each structure is shown as a cartoon in light orange (27C1-Adx), pink (7M8I), and purple (3N9Y).